ESCUELA POLITÉCNICA NACIONAL

DEPARTAMENTO DE MATEMÁTICA

FOUR-DIMENSIONAL VARIATIONAL DATA ASSIMILATION: ANALYSIS IN SPACES OF LOW REGULARITY AND APPLICATION TO THE COVID-19 PANDEMIC

TRABAJO PREVIO A LA OBTENCIÓN DEL TÍTULO DE DOCTORA EN MATEMÁTICA APLICADA

TESIS

PAULA MONSERRATTE CASTRO CASTRO
paula.castro@epn.edu.ec

Director: JUAN CARLOS DE LOS REYES BUENO
juan.delosreyes@epn.edu.ec

Codirectora: IRA NEITZEL
neitzel@ins.uni-bonn.de

QUITO, ABRIL 2025

DECLARACIÓN

Yo, PAULA MONSERRATTE CASTRO CASTRO declaro bajo juramento que el trabajo aquí escrito es de mi autoría; que no ha sido previamente presentado para ningún grado o calificación profesional; y que he consultado las referencias bibliográficas que se incluyen en este documento.

A través de la presente declaración cedo mis derechos de propiedad intelectual, correspondientes a este trabajo, a la Escuela Politécnica Nacional, según lo establecido por la Ley de Propiedad Intelectual, por su reglamento y por la normatividad institucional vigente.

Paula Monserratte Castro Castro

CERTIFICACIÓN

We certify that the present work was developed by PAULA MONSERRATTE CASTRO CASTRO, under our supervision.

Juan Carlos De los Reyes Bueno
Director de Tesis

Ira Neitzel
Codirectora de Tesis

Paula Monserratte Castro Castro

ACKNOWLEDGMENTS

Developing this project has been one of the most challenging tasks I have ever faced; this would not have been possible without the support of many people to whom I would like to say *thank you!* First and foremost, I would like to express my deepest gratitude to my advisor, Juan Carlos De los Reyes, for his invaluable guidance throughout this journey. Thank you for all the knowledge you imparted and for your patience. I am proud of what I learned during my time working with Juan Carlos. Thank you for introducing me and some others to the research world.

My sincere thanks to Ira Neitzel for the fruitful discussions, her willingness to have online meetings in her afternoons (German time) when her workday had already ended, and for her patience during this process. I appreciate her hospitality during my research stays in Bonn.

I would also like to thank my colleagues at the Research Center on Mathematical Modeling (ModeMat), Tuomo Valkonen, Luis Miguel Torres, Sergio González, and Pedro Merino, who have advised and supported me over the years. Special thanks to Pedro for always keeping the door open for questions and discussions.

I am truly grateful for the opportunity to have been part of the Research Center on Mathematical Modeling. It has been an invaluable experience. My heartfelt thanks go to Juan Carlos, Luis Miguel, Pedro, and Sergio for dreaming of a place like ModeMat.

I am thankful to my current and former colleagues and friends, Sofía López, David Villacís, Evelyn Cueva, Myrian Guanoluiza, Kateryn Herrera, Andrés Miniguano, Franklin Vargas, Damián Cedeño, Diego Vargas, Gabriel Intriago, María Belén Moya, Felipe Guerra, Fernando Jiménez, and Felipe Fernández, for their constant willingness to help. I truly enjoyed working with all of you. Finally, I want to extend my heartfelt thanks to Estefi, Tati, and Ernesto for accompanying me, supporting me, and always believing in me.

This thesis was developed under the financial support of the projects: *Modelización matemática y control de fluidos magneto y eléctro-reológicos. Aplicación al control de amortiguadores sísmicos*, EPN-PIMI 16-04, and the project *Modelización de la propagación del SARS-CoV-2 en Ecuador*, MODEMAT-EPN PR-COVID19-20-01. I gratefully acknowledge the support of the Deutsche Forschungsgemeinschaft (DFG, German Research Foundation) through Collaborative Research Centre 1060 (SFB 1060). This funding enabled fruitful research stays at the University of Bonn that contributed to this thesis. Part of the numerical research of this thesis was conducted using the supercomputing infrastructure of the HPC-MODEMAT.

To my parents, Paulina and Carlos. To my sisters, brother, and niece, Samanta, Lesly, Carlos, and Lua

Contents

List of Figures

Abstract

This work addresses both the theoretical and practical aspects of variational data assimilation problems. On the theoretical side, given its wide range of applicability, variational data assimilation problems have been predominantly set in finite dimensions, with very few contributions dealing with the infinite dimensional setting and the theoretical study that they required. On the practical side, we investigate the applicability of variational data assimilation methods in fields beyond atmospheric and environmental sciences, where data assimilation has been traditionally used to estimate initial conditions in dynamical systems.

In the first part of this thesis, we analyze the four-dimensional variational data assimilation ($4D$-VAR) problem in spaces of low regularity with a cost function that incorporates pointwise spatial observations. The latter entails the need for continuous-in-space state variables. To address this, for an initial condition in a Lebesgue space $L^{\beta}(\Omega)$, we employ maximal parabolic regularity tools jointly with embedding results from real and complex interpolation spaces. These tools are first used to prove the well-posedness of the linear constraint case. Moreover, in the linear optimal control problem, the maximal parabolic regularity property of the operator is crucial for establishing the well-posedness of the adjoint equation, particularly because the right-hand side involves regular Borel measures arising from the pointwise spatial evaluations in the cost function.

The semilinear constraint case is more challenging. Beyond proving the well-posedness of the state equation —where the linear case results are crucial for enhancing solution regularity via a bootstrapping argument— it is necessary to study the differentiability properties of the control-to-state mapping to characterize the optimality system. The presence of non-linearities complicates the derivation of the first-order optimality conditions, particularly when analyzing the well-posedness of the adjoint equation. In fact, given a semilinear state constraint, the associated adjoint operator will be of non-autonomous type. Therefore, results on (autonomous) maximal parabolic regularity can not be applied. Consequently, the well-posedness of the adjoint equation must be established through a direct analysis of the equation itself.

In the second part of this thesis, we examine the applicability of variational data

assimilation methods to accurately estimate the evolution of the COVID-19 pandemic in Ecuador. This is accomplished by estimating key epidemiological parameters and the initial conditions of a compartmental SARS-CoV-2 propagation model under high-uncertainty conditions. We consider two different data sources: the official count of positive COVID-19 tests from the Ecuadorian Public Health Ministry and estimates of COVID-19-related deaths from the official mortality records of the Ecuadorian Civil Registry. A multimodel ensemble forecasting approach is employed, incorporating the reliability of the data to accurately capture the state of the pandemic.

Chapter 1

Introduction

In the first part of this thesis, we consider a 4D-VAR problem where the constraint is given first by a linear and then by a semilinear parabolic equation. Moreover, we impose low regularity on the problems' initial condition and pointwise evaluation in space for the state variable. To put our work in perspective, let us describe the data assimilation process.

In general terms, data assimilation aims to incorporate real observations into mathematical models to build the best approximation of a true (and unknown) state. The first application of variational data assimilation methods was presented in the seminal work of Le Dimet and Talagrand in [85]. The general finite dimensional formulation of the 4D-VAR problem has the form:

$$\begin{aligned}
&\min_{u} \ \frac{1}{2}\sum_{i=1}^{n} \left[H(y(t_i)) - z_o(t_i)\right]^T R_i^{-1} \left[H(y(t_i)) - z_o(t_i)\right] + \frac{1}{2}(u-u_b)^T B^{-1}(u-u_b) \\
&\text{subject to:} \\
&\qquad\qquad y(t_i) = M_i(y(t_0)) \qquad \text{(System model)}, \\
&\qquad\qquad y(t_0) = u \qquad\qquad\ \ \text{(Initial condition)},
\end{aligned} \tag{P}$$

where n is the number of instants t_i at which observations are taken, $z_o(t_i)$ represents the observations obtained at time t_i, and u_b is the background initial condition. For each $i = 1, \ldots, n$, R_i and B represent the error covariance matrices of the observations and the background error, respectively. The operator H maps the model state y to the observation space, enabling a comparison between the model's solution and the observations. The variable u represents the system's initial condition, which we aim to reconstruct. The operator M_i, which defines the system model, is typically a system of differential equations, which, depending on the application, could be non-linear. The first term of the cost functional in (2.26) represents a weighted difference between the observations and the model state affected by the observation operator, while the second

term is a weighted difference between the initial condition we aim to reconstruct and a known variable representing prior knowledge. The weights in both cases are given by the inverse of the error covariance matrices.

To fix ideas, let us specify the meaning of some of the aforementioned variables in the context of Numerical Weather Prediction (NWP). Here, u represents the initial condition of the atmosphere, and M_i models its behavior. The observations z_o can be retrieved from satellites, radars, and airport reports, among other sources. The operator H adapts its form depending on the type of observations.

Data assimilation has been used in many practical applications besides improving meteorological forecasts. Due to its widespread applicability, the analysis of 4D-VAR problems has predominantly occurred in finite dimensions rather than its infinite-dimensional counterpart. Concerning the study of the 4D-VAR problem in its infinite-dimensional setting, we mention again [85], where the variational assimilation of meteorological observations was proposed, and the most recent contribution by Le Dimet and co-authors [84], where a data assimilation problem of a simplified mathematical model describing a state of the atmosphere is posed and treated. These works explore the assimilation of meteorological observations using variational techniques, which involve calculating the adjoint system to determine the problem's gradient. One of the main challenges of this approach lies in studying the well-posedness of the problem and defining the functional analytical framework. To address these challenges, the authors assume that the state of the atmosphere belongs to a Hilbert space. Similarly, we mention the contribution of Shutyaev, in [113], where a more general setting of a variational data assimilation problem for quasi-linear evolution equations in Hilbert spaces was studied.

Some other contributions dealing with infinite-dimensional data assimilation for the atmospheric primitive-equations and ocean dynamical models are [2, 79]. In [79], the author imposes a stronger norm for the background error or additional pointwise box constraints on the control variable in order to guarantee the well-posedness of the data assimilation problem's state equation. In [2], the authors used a cost functional based on the L^2- norm and showed the existence of minimizers. However, as an assumption, the observational data is considered in the whole domain. Likewise, the well-posedness of the data assimilation problem constraint considering the continuity in the space variable was studied in [29], where the authors considered an initial condition in a more regular space, such as $H_0^1(\Omega)$. However, imposing such regularity for the initial condition requires modifying the cost functional by including a regularization term.

The practical scenario of pointwise-in-space observations and lower regularity in the initial condition has not been sufficiently addressed in the existing literature. To fill this gap, the specific infinite-dimensional mathematical problem we aim to solve in

the first part of this thesis is the following:

$$\min_{u\in U_{ad}} J(y,u) = \frac{1}{2}\int_0^T \sum_k [y(x_k,t) - z_o(x_k,t)]^2 \, dt + \frac{1}{2}\|u-u_b\|^2_{B^{-1}} \tag{1.1}$$

subject to the semilinear constraint

$$\begin{aligned} \frac{\partial y}{\partial t} + Ay + g(y) = &\quad 0 \quad \text{in } Q, \\ y = &\quad 0 \quad \text{on } \Sigma, \\ y(x,0) = &\quad u \quad \text{in } \Omega, \end{aligned} \tag{1.2}$$

where $\Omega \subset \mathbb{R}^d$, with $d = 2, 3$, is a bounded domain, with boundary Γ, $Q := \Omega \times (0,T)$ represents the space-time cylinder, for a given $T > 0$, and $\Sigma := \Gamma \times (0,T)$. The operator A presents in (1.2) is a linear elliptic second-order differential operator. The terms $u_b \in L^2(\Omega)$ and $B^{-1} \in \mathcal{L}(L^2(\Omega), L^2(\Omega))$, in the cost functional (1.1), are the background information and the inverse of the background error covariance operator, respectively.

In problem (1.1) - (1.2), we consider the observation operator (H) and its error covariance operator (R) equal to the identity. Likewise, the dynamical system we are considering is the parabolic semilinear PDE rather than the equations describing the atmosphere. Even so, this formulation retains some of the major challenges when formulated in function spaces. In fact, given that the observations are retrieved from fixed devices or observation stations, we must be able to evaluate the solution variable pointwise in space. The latter constitutes one of the main analytic challenges since we have to meet both: the pointwise-in-space observations of the state variable and an L^2-energy of the background covariance error B to mimic the structure of problem (2.26). The second analytical challenge is related to the initial condition regularity. In fact, we will consider an initial condition solely in an integrable Lebesgue space $L^\beta(\Omega)$, for some values of β to be determined.

Variational data assimilation problems may be studied as optimal control problems where the control variable is the initial condition or some unknown parameter. Previous contributions dealing with variational data assimilation problems in the infinite-dimensional case (see, e.g., [79, 113]) worked with strong regularity assumptions on the states, which is reflected in the cost function by imposing artificially stronger norms on the background error terms, i.e., the L^2- energy for the background was not considered. An alternative path is proving the well-posedness of the state equation, without changing the L^2-energy framework, which involves exploiting the regularity properties of the underlying PDE model. For some control problems commonly addressed, imposing continuity requirements on the state introduces additional assumptions, such as requiring continuity of the initial state or further constraints on the controls, as

exemplified in [106] for semilinear parabolic problems. Similarly, contributions like [19, 25, 68, 69, 95], among others, deal with quasilinear optimal control problems, where the regularity needed to prove the problem's well-posedness is relatively high. In fact, in some of these problems, continuity of the state variable is required not only in space but also in the time variable. In this regard, some of these works proved the well-posedness of their respective problems by using the *maximal parabolic regularity* of the operator appearing on the problem constraint. Additionally to those mentioned above, the analysis of optimal control problems of semilinear and quasilinear equations using maximal parabolic regularity has been addressed by some authors; we mention some of their contributions [45, 46, 66, 68, 69, 93–96].

After establishing the well-posedness of the state equation, the next step in solving the optimal control problem is to study the existence of optimal controls, which can be done using standard techniques; see, e.g., [118]. Afterward, we are allowed to derive the optimality system of the problem, which lets us characterize the optimal solution. This can be done through the Lagrangian approach. We recall that to prove the existence of the Lagrange multiplier, the problem must satisfy a constraint qualification condition. In our case, due to our problem structure, we will use the Zowe and Kurcyusz approach; see, e.g., [125], where after proving a regularity condition, they obtain the existence of Lagrange multipliers. Once this is achieved, we can proceed to characterize the optimal control through the optimality system. It is worth noting that incorporating pointwise observations in the cost functional results in an adjoint equation whose right-hand side belongs to the regular Borel measures space, which, in turn, leads to a reduction in the regularity of the adjoint state. If the problem constraint is governed by a linear PDE, the first-order necessary conditions are also sufficient, and the problem is fully solved. On the other hand, if our problem constraint is non-linear, first-order optimality conditions are insufficient due to the non-convexity of the problem. As a result, to fully characterize the optimal controls, second-order sufficient optimality conditions should be obtained. This field of study is extensive, as reviewed in [28] and the references therein.

The **main contribution of the first part of this thesis** is addressing the infinite-dimensional $4D$-VAR problem under low regularity assumptions. We explore variational data assimilation problems where the initial condition is considered in spaces of low regularity, specifically, we consider Lebesgue spaces, without modifying the standard $4D$-VAR cost functional, preserving its natural L^2-norm Bayesian framework. Our approach is based on previous works that have used *maximal parabolic regularity* in optimal control problems to meet all the restrictions imposed by our problem. The latter permits the study of the well-posedness of the problem state equation, especially given the challenges of dealing with pointwise-in-space observations in the cost functional.

In the second part of this thesis, we aim to study the applicability of the variational data assimilation methods to real-life problems. Given the global context unleashed by the COVID-19 pandemic, we investigate the parameter estimation of the SARS-CoV-2 propagation model in the presence of uncertainty by using variational data assimilation methods. We extend our analysis to observe how data assimilation ensemble forecasting methods can provide a more accurate picture of the COVID-19 pandemic in Ecuador.

To capture the dynamics of virus propagation, we choose a compartmental model of susceptible, exposed, infected, and removed (SEIR) populations that describes the transitions of the population between these compartments through a system of ordinary differential equations (ODEs). We refer to the seminal work of Kermack and McKendrick, [78], which introduced the basic compartmental model to describe disease transmission using ODEs. These systems must include parameters that describe the virus's dynamics, such as the transmission rate. These parameters can change depending on the region and the population's behavior. Additionally, to catch the particularities of the SARS-CoV-2, such as the presence of asymptomatic infectious, the infected population is divided into two separate compartments: documented and undocumented. The undocumented infected population refers to the individuals who do not report symptomatology. These kinds of models have been studied, for instance, in [17, 38, 86, 103]. The specific SEIR model we consider was proposed in [86] and has the following form:

$$\frac{dS}{dt} = -\frac{\beta S I^r}{N} - \frac{\mu\beta S I^u}{N}, \qquad S(t_0) = S_0, \tag{1.3a}$$

$$\frac{dE}{dt} = \frac{\beta S I^r}{N} + \frac{\mu\beta S I^u}{N} - \frac{E}{\zeta}, \qquad E(t_0) = E_0, \tag{1.3b}$$

$$\frac{dI^r}{dt} = \alpha\frac{E}{\zeta} - \frac{I^r}{\delta}, \qquad I^r(t_0) = I_0^r, \tag{1.3c}$$

$$\frac{dI^u}{dt} = (1-\alpha)\frac{E}{\zeta} - \frac{I^u}{\delta}, \qquad I^u(t_0) = I_0^u, \tag{1.3d}$$

$$\frac{dR}{dt} = \frac{I^r + I^u}{\delta}, \qquad R(t_0) = R_0, \tag{1.3e}$$

where S, E, I^r, I^u, and R represent the susceptible, exposed, documented infected, undocumented infected, and removed population, respectively. The parameter β represents the transmission rate due to documented infected patients, μ is a multiplicative factor reducing the transmission rate of undocumented patients, α represents a fraction of documented infected people that develop severe symptoms, and ζ and δ represent the average latency period and the average duration of the infection, respectively. In addition, the terms $S_0, E_0, I_0^r, I_0^u, R_0$ are the initial conditions of the model's variables.

On the other hand, any parameter estimation process requires real observations.

However, in the Ecuadorian case, the lack of widespread testing and non-coordinated strategies in collecting and reporting COVID-19-positive cases increased the data uncertainty. Regarding previous studies on the evolution of the pandemic in Ecuador, we mention the work of Fernández et al., [58], in which the authors employ a probabilistic model, relying exclusively on official data from the pandemic's first two months for their analysis. Additionally, there are some other contributions that are more descriptive than methodological related to the COVID-19 pandemic in Ecuador, among them, we mention [32, 36], where the authors considered excess mortality during the COVID-19 outbreak to study the impacts of the pandemic in the country.

Since the uncertainty was exceptionally high, any adjustment and parameter estimation process had to consider it as a constitutive component of the analysis. The latter turns variational data assimilation into an ideal model to work with since it integrates observed data into a model describing a phenomenon of interest, accounting for the uncertainty. The mathematical formulation of the parameter estimation problem we aim to solve is the following one:

$$\begin{aligned} \min_{\mathbf{u}_0,\, \rho \in \mathcal{U}_{ad}} \quad & \sum_{i,j} (I^r(t_i) - I_i^{obs}) \mathbf{C}_{ij}^{-1} (I^r(t_j) - I_j^{obs}) + (\rho - \rho^b)^T \mathbf{B}^{-1} (\rho - \rho^b) \\ & + (\mathbf{u}_0 - \mathbf{u}_0^b)^T \mathbf{Q}_0^{-1} (\mathbf{u}_0 - \mathbf{u}_0^b) \\ \text{s.t.} \quad & \text{SEIR model (1.3)}, \end{aligned} \tag{1.4}$$

where $\rho = (\beta, \mu, \alpha, \zeta, \delta)$ is the vector of parameters, and $\mathcal{U}_{ad}$ is its admissible set formed by its initial prior range. The background information of the parameters, ρ^b, is determined by the values given in the extensive COVID-19 literature (see, e.g., [86] and reference therein). $\mathbf{u}_0$ is the vector of initial conditions, while $\mathbf{u}_0^b$ represents its background information. The measured or observed data, I^{obs}, is given by the official entities, while the error covariance matrices $\mathbf{C}$, $\mathbf{B}$, and $\mathbf{Q}_0$ have to be built according to the data or previous information.

The solution of problem (1.4) will be optimal initial conditions and parameters that, once replaced in the virus propagation model, give us an accurate estimation of the model variables. Additionally, due to the high levels of uncertainty, relying on just one source of information could lead to biased results. Assuming that more than one data source is available, a combination of the model outputs obtained with each one after solving problem (1.4) should provide a more comprehensive and reliable understanding of the pandemic's dynamics. The combination of model outputs should be carried out so that the more reliable model output receives a more significant weight. The latter can be seen as a multimodel ensemble forecasting; see, e.g., [80, 111].

We mention some previous contributions where data assimilation methods were used to solve the parameter estimation problem in the context of the COVID-19 pan-

demic; see, e.g., [16, 37, 50, 53, 100]. We remark on the contributions [100] and [16] since they are close to our work. On them, the authors use a variational data assimilation scheme to estimate the model's parameters; however, they do not estimate the problem's initial conditions. Likewise, we mention [37], where the authors introduce a Bayesian sequential data assimilation and forecasting method for non-autonomous dynamical systems. In this work, the authors use observed incidences of COVID-19 cases and deaths. Additionally, the variables to be inferred were the model parameters and initial conditions, which are the inputs and outputs of our problem, too. However, a reliable stream of epidemiological data is required to obtain a reliable forecast with the proposed methodology; therefore, it does not apply to our problem due to the high levels of uncertainty in the Ecuadorian data.

The **main contribution of the thesis's second part** is to develop a rigorous methodological framework to estimate the evolution of the COVID-19 pandemic in Ecuador accurately by:

- Using adequate techniques for estimating the initial conditions and parameters appearing in the SEIR model through a variational data assimilation approach that considers the uncertainty in the data.
- Combining the obtained results considering different data sources as a weighted average where larger weights are assigned to more reliable output models.
- Conducting a comparative analysis of the evolution of the pandemic in Guayas and Pichincha since these two provinces, besides being the most populated, exhibit different geographical features.

We remark that parts of this thesis have been taken from the following published and submitted articles:

[T1] Paula Castro, and Juan Carlos De los Reyes, and Ira Neitzel;
ANALYSIS OF FOUR-DIMENSIONAL VARIATIONAL DATA ASSIMILATION PROBLEMS IN LOW REGULARITY SPACES;
https://arxiv.org/abs/2303.00847

[T2] Paula Castro, and Juan Carlos De los Reyes;
AUTOPSY OF SARS-COV-2 SPREAD DYNAMICS IN ECUADOR USING DATA ASSIMILATION TECHNIQUES: A TALE OF TWO PROVINCES;
Submitted to: *Mathematical Biosciences and Engineering*

[T3] Paula Castro, and Juan Carlos De los Reyes, and Sergio González-Andrade, and Pedro Merino;
ESTIMACIÓN DE PARÁMETROS PARA UN MODELO DEL SARS-COV-2

EN ECUADOR EN PRESENCIA DE INCERTIDUMBRE;
Revista Politécnica 47 (2021); https://doi.org/10.33333/rp.vol47n1.01

1.1 Outline of the Thesis

This thesis is structured as follows.

Chapter 2 - Preliminaries

Chapter 2 provides an introduction to key concepts essential for understanding the subsequent analysis. In Section 2.1, we introduce the basic principles and mathematical formulations of variational data assimilation, setting the stage for later applications. Following this, Section 2.2 provides a brief overview of semigroup theory, with a particular focus on C_0 and analytic semigroups. Section 2.3 introduces the concept of maximal parabolic regularity, a critical property of certain operators that ensures well-posedness in various evolution equations. The discussion in this section is particularly relevant as it forms the basis for later results in the thesis. This section includes embedding results related to interpolation spaces, which play a significant role in analyzing the regularity of solutions considering initial conditions in not-so-regular spaces. Finally, Section 2.4 presents an introduction to epidemiological models, focusing on compartmental models such as the SIR model. This section provides context for the mathematical models discussed later, highlighting how these models are used to simulate the spread of infectious diseases.

Chapter 3 - Linear Variational Data Assimilation Problems in Low Regularity Spaces

The results of this chapter were taken from [T1]. Here, we address the regularity study of the linear fourth-dimensional variational data assimilation problems in low regularity spaces, setting the stage for the more complex nonlinear cases explored in subsequent chapters. In Section 3.1, we define the functional analytical setting for the problem, carefully establishing the spaces and operators that will be used in the analysis. In this section, we prove the well-posedness of the linear constraint by using the maximal parabolic regularity of the second-order differential operator appearing in the state constraint. The discussion here is crucial as it ensures that the linear model equation is well-posed even under minimal regularity assumptions. The existence of a solution for the data assimilation problem is also stated in this section. Finally, in Section 3.2, we show the first-order optimality conditions that, in the linear and convex case, are also sufficient. The chapter concludes with some final remarks.

Chapter 4 - Semilinear Variational Data Assimilation Problems in Low Regularity Spaces

This chapter is based on the results of [T1]. Here, we study the semilinear variational data assimilation problems in low regularity spaces. The chapter begins with Section 4.1, which investigates the Lipschitz continuity and differentiability properties of the Nemytskii operator associated with the nonlinear term. Moving forward, we set a well-posedness result. Our goal is to achieve the same regularity result we obtained for the linear constraint in the previous chapter. To accomplish this, we use known existence results and then enhance the required regularity using the maximal parabolic regularity of the operator jointly with a bootstrapping argument. In Section 4.2, we state the differentiability of the control-to-state mapping, which will be used in Section 4.3 to derive the optimality conditions. In this section, we also prove the well-posedness of the adjoint equation, which, given the nonlinearity, is of non-autonomous type. The latter makes the analysis of the adjoint equation more involved than in the linear case, where some previous results for adjoint operators can be used. The chapter concludes with the derivation of the first-order optimality conditions and some useful results, which constitute a solid foundation for future research on second-order optimality conditions.

Chapter 5 - Variational data assimilation for parameter estimation of a COVID-19 spread model

Chapter 5 is based on the ideas in [T2, T3]. It turns to the practical application of variational data assimilation. In Section 5.1, we set the model designed to capture the dynamics of SARS-CoV-2 transmission. Section 5.2 outlines the variational data assimilation method used to estimate the model's parameters and initial conditions. In this section, we develop the Lagrangian method employed to address the optimization problem. Besides, we verify the sufficient second-order optimality condition. Section 5.2 also covers the essential steps of data preprocessing and the construction of error covariance matrices. Section 5.3 expands on the methodology by introducing a multimodel ensemble forecasting strategy, explaining how different models are combined and appropriately weighted to enhance forecast reliability. Finally, Section 5.4 presents the outcomes of solving the variational data assimilation problem within the parameter estimation context. We show the results obtained with the robust methodology for Pichincha and Guayas, which gives a reliable picture of the pandemic state and its evolution. We conclude this chapter by discussing the results and limitations of the proposed methodology.

Chapter 6 - Conclusions

In this chapter, we summarized the main results of the thesis and pointed out some future research.

Section 1.2 provides a general overview of the notation, functional spaces, and symbols used throughout the manuscript. Additional notation specific to each chapter could be introduced as needed within the corresponding sections.

1.2 General Notation

Throughout this manuscript, the term domain and the symbol Ω refer to a nonempty open subset of $\mathbb{R}^d$. Specific features of Ω, such as boundedness or geometric properties, will be stated explicitly when required. $\Gamma = \partial\Omega$ represents its boundary. Additionally, let $T > 0$ be a fixed real number and $I := (0, T)$. We will denote the space-time cylinder as $Q := \Omega \times I$, and $\Sigma := \Gamma \times I$.

Let p be a positive real number, we denote by $L^p(\Omega)$ the class of all measurable functions u defined on Ω for which

$$\int_\Omega |u(x)|^p dx < \infty.$$

In $L^p(\Omega)$, there are identified functions that are equal almost everywhere (differ only on a set of measure zero) in Ω. Therefore, the elements of $L^p(\Omega)$ are equivalence classes of measurable functions satisfying the above integral. The functional $\|\cdot\|_{L^p(\Omega)}$ defined by

$$\|u\|_{L^p(\Omega)} = \begin{cases} \left(\int_\Omega |u(x)|^p dx\right)^{1/p} & \text{if } p \in [1, \infty), \\ \operatorname{ess\,sup}_{x\in\Omega} |u(x)| & \text{if } p = \infty; \end{cases}$$

is a norm on $L^p(\Omega)$ provided $1 \leq p \leq \infty$. The cases where $0 < p < 1$ do not define a norm. In particular, $L^2(\Omega)$ is a Hilbert space when endowed with the inner product

$$(u, v)_{L^2(\Omega)} = \int_\Omega uv \; dx$$

There will be cases where we will omit Ω or dx where they can be inferred from context.

Let X and Y be Banach spaces. Further properties will be assigned to them in the manuscript wherever required. We will additionally consider the following notations:

$\overline{B}$ is the closure of the set B.

X^* will denote the dual space of X.

$\hookrightarrow$ will be used to denote continuous embeddings.

$\overset{d}{\hookrightarrow}$ will be used to denote dense embeddings.

$\operatorname{supp}(f)$ is the support of the functional f, where $f\colon \Omega \to \mathbb{R}$. It is defined as $\operatorname{supp}(f) = \overline{\{x \in \Omega : f(x) \neq 0\}}$.

$\mathcal{L}(Y, X)$ denotes the normed space of all linear and continuous mappings from Y into X, endowed with the operator norm

$$\|F\|_{\mathcal{L}(Y,X)} = \sup_{\|u\|_Y=1} \|Fu\|_X$$

where $F\colon Y \to X$ is a linear and continuous operator. If $X = Y$, then we write $\mathcal{L}(Y, X) =: \mathcal{L}(Y)$.

$C_0^\infty(\Omega)$ is the set of infinitely continuously differentiable functions with compact support in Ω. It is also denoted as $\mathcal{D}(\Omega)$.

$W^{k,p}(\Omega)$ is the Sobolev space of measurable functions in $L^p(\Omega)$ whose weak derivatives up to order k are also in $L^p(\Omega)$. For the particular case $p = 2$, we write $H^k(\Omega) := W^{k,2}(\Omega)$.

$L^p(I; X)$ is the Bochner space of measurable functions $u\colon I \to X$ endowed with the norm

$$\|u\|_{L^p(I;X)} = \begin{cases} \left(\int_0^T \|u(t)\|_X^p dt\right)^{1/p} & \text{if } p \in [1, \infty), \\ \operatorname{ess\,sup}_{t\in I} \|u(t)\|_X & \text{if } p = \infty. \end{cases}$$

$W^{1,p}(I; X)$ consists of all functions $u \in L^p(I; X)$ such that their weak time derivative also belongs to $L^p(I; X)$.

$W_2^{1,0}(Q)$ consists of all functions in $L^2(Q)$ having weak first-order partial derivatives with respect to $x_1, \ldots, x_d$ in $L^2(Q)$. It is endowed with the norm

$$\|u\|_{W_2^{1,0}(Q)} = \left(\|u\|_{L^2(Q)}^2 + \sum_{i=1}^d \left\|\frac{\partial u}{\partial x_i}\right\|_{L^2(Q)}^2\right)^{1/2}.$$

This space is often referred to in the literature as $H^{1,0}(Q)$, and it coincides- modulo modification on a set of zero measure-with the Bochner space $L^2(I; H^1(\Omega))$.

$W_2^{1,1}(Q)$ consists of all functions in $L^2(Q)$ having weak first-order partial derivatives with respect to $x_1, \ldots, x_d$ and weak time derivative in $L^2(Q)$. Its norm is given by

$$\|u\|_{W_2^{1,1}(Q)} = \left(\|u\|^2_{L^2(Q)} + \sum_{i=1}^{d} \left\| \frac{\partial u}{\partial x_i} \right\|^2_{L^2(Q)} + \left\| \frac{\partial u}{\partial t} \right\|^2_{L^2(Q)} \right)^{1/2}.$$

This space can be seen as the intersection $L^2(I; H^1(\Omega)) \cap H^1(I; L^2(\Omega))$.

$H^{2,1}(Q)$ is the Sobolev space of functions in $L^2(Q)$ such that their weak spatial partial derivatives up to order 2 and its weak time derivative belong to $L^2(Q)$.

$W(0,T)$ is the space of all functions $u \in L^2(I; V)$ having a weak time derivative in $L^2(I; V^*)$, where V denotes a Banach space. Its norm is given by

$$\|u\|_{W(0,T)} = \left(\int_0^T \left(\|u(t)\|^2_V + \left\| \frac{\partial u(t)}{\partial t} \right\|^2_{V^*} \right) dt \right)^{1/2}.$$

It is usual to take $V = H_0^1(\Omega)$. In those cases, $W(0,T)$ can be seen as the intersection $L^2(I; H_0^1(\Omega)) \cap H^1(I; H^{-1}(\Omega))$.

$C(\bar{I}; X)$ is the space of all continuous functions u mapping from $\bar{I}$ to X. It is endowed with the maximum norm

$$\|u\|_{C(\bar{I};X)} = \max_{t \in \bar{I}} \|u(t)\|_X.$$

$\mathbb{W}^p(Y, X)$ denotes the maximal parabolic regularity solution space. Let X and Y be real reflexive Banach spaces such that $Y \overset{d}{\hookrightarrow} X$ and $1 < p < \infty$, this space is defined as

$$\mathbb{W}^p(Y, X) := W^{1,p}(I; X) \cap L^p(I; Y).$$

$(X, Y)_{\theta,r}$ denotes the real interpolation space, where $\theta \in (0,1)$ and $r \in [1, \infty]$, see Definition 2.10.

$[X, Y]_\theta$ denotes the complex interpolation space, where $\theta \in (0,1)$, see Definition 2.12.

RNP A Banach space X has the Radon-Nikodym Property (RNP) if every linear and continuous operator $T\colon L^1[0,1] \to X$ there exists a bounded measurable function $g\colon [0,1] \to X$ such that

$$T(f) = \int_0^1 f(s)g(s)\,ds \quad \text{for every } f \in L^1[0,1],$$

where the integral is the Bochner integral [70, Definition 1]. For different characterizations and more results regarding spaces possessing the RNP, we refer to [42].

Chapter 2

Preliminaries

2.1 Variational Data Assimilation

In general terms, data assimilation (DA) can be described as a method for combining observations with model outputs to estimate in an optimal way the state of a system at a given time in the future, where both sources can be either incomplete or inaccurate. Data assimilation is crucial in numerical weather prediction, but its applicability is widespread in other fields, such as oceanography, geoscience, environmental sciences, and biology, among others; see, e.g., [11, 13, 23]. For instance, a formal definition of data assimilation can be found in [11, Chapter 1.5], where it is stated that DA is the approximation of the true state of some physical system at a given time by combining time-distributed observations with a dynamic model in an optimal way.

There are two main approaches to solving a data assimilation problem: statistical and variational. Moreover, combining them is usual to overcome their drawbacks and exploit their advantages; these latter are called hybrid methods [11, 75, 119]. Before describing these approaches, let us introduce some common components and notation of any data assimilation process.

Key Components of Data Assimilation

The dynamical and observational models are the two critical components of any data assimilation approach. The first refers to the evolution system describing the physical process we aim to study, e.g., the equations of the atmosphere, a system describing a virus propagation, among others. Since such systems evolve in time, they can be

written as a system of differential equations of the type:

$$\begin{aligned} \frac{d\mathbf{x}}{dt} &= \mathcal{M}(\mathbf{x}) + \eta, \\ \mathbf{x}(t_0) &= \mathbf{x}_0, \end{aligned}$$

where $\mathbf{x}$ is the state variable, $\mathbf{x}_0$ is the unknown (or inaccurately known) initial condition, $\mathcal{M}$ is the differential operator describing the dynamical process, which is usually nonlinear, possibly chaotic, and η is the model error, which is assumed to be a random variable. If we set $\eta = 0$, then we are assuming that the model describes the phenomena exactly. On the other hand, taking $\eta \neq 0$ indicates that the model is not perfect. In such cases, η represents the error made by the model prediction of the unknown true state.

The second key component is given by the observational model. We can describe a measurement at a given time as:

$$\mathbf{y} = \mathcal{H}(\mathbf{x}, t) + \epsilon,$$

where $t \in [0, T]$ for a given $T > 0$, $\mathbf{y}$ represents the observations, $\mathcal{H}$ is the observation operator, generally non-linear, transforming model variables into the observational space. These transformations can be based on physical laws for indirect measurements [75]. Similarly to the model error, ϵ represents the observational error, which is a random variable, that counts, for instance, for the instrumental errors in the observing devices.

Since $\mathcal{M}$ is a continuous, non-linear, differential operator, it is usual to introduce a discrete version of it, $\mathbf{M}$. The discretization process can be achieved with numerical methods such as the implicit Euler method. Then, for a given time instant t_i, with $i = 0, 1, \ldots, n$, the approximation of the model dynamics can be represented as

$$\mathbf{x}(t_{i+1}) = \mathbf{x}_{i+1} = \mathbf{M}_{i+1}(\mathbf{x}_i) + \eta_i.$$

Similarly, we denote by $\mathbf{H}$ the discrete version of the observational model $\mathcal{H}$ where

$$\mathbf{y}(t_i) = \mathbf{y}_i = \mathbf{H}(\mathbf{x}_i) + \epsilon_i.$$

Data assimilation relies strongly on these two components. An example of this appears in earth science, where the amount of available observations is usually insufficient to fully describe the system. Therefore, it is the dynamical model the one that has to fill the gaps (spatial and temporal) in the observational network; see, e.g., [23].

Notation for Data Assimilation

We introduce some standard notation for data assimilation problems; for further details, we refer to [11, Chapter 1]. It is usual to use superscripts to describe the nature of the variables involved in the process. We list the most used ones:

- b stands for the *background* information or initial guess,
- f represents a *forecast* variable,
- o represents *observations*,
- t is the unknown *true* state,
- a stands for the *analysis*.

Every data assimilation approach looks to approximate the unknown true state $\mathbf{x}^t$ of a model at a given time based on the observations, dynamical model, and background information; this approximation process is called *analysis*.

Bayesian inference

Since the two key pieces of information of the data assimilation process, the model dynamics and the observations, have a random nature, they can be described in terms of probability density functions (pdf). If we know the *prior* probability density function of $\mathbf{x}$, $p(\mathbf{x})$, and the conditional probability density function (cpdf) of the observations $\mathbf{y}$ given the solution model $\mathbf{x}$, $p(\mathbf{y}|\mathbf{x})$. Then, we can infer the *posterior* distribution of the unknown solution model $\mathbf{x}$ given the data $\mathbf{y}$, $p(\mathbf{x}|\mathbf{y})$, by using Bayes' formula

$$p(\mathbf{x}|\mathbf{y}) = \frac{p(\mathbf{y}|\mathbf{x})p(\mathbf{x})}{p(\mathbf{y})}. \tag{2.1}$$

In this way, the initial estimate of the system *prior* state is updated using incoming observations to obtain a more accurate and informed estimate of the *posterior* state. This recursive update process allows the assimilation of observations, which leads to a continuous improvement in forecast accuracy.

Classical example

Let us consider the following classical example of determining the best estimate of the true value of a scalar quantity, e.g., the true temperature, T_t, given two independent

pieces of information, T_1 and T_2,

$$T_1 = T_t + \varepsilon_1$$
$$T_2 = T_t + \varepsilon_2,$$

where each ε_i, with $i = 1, 2$, represents the observation error. We assumed that these errors satisfy the following statistical information

$$E(\varepsilon_i) = 0 \qquad E(\varepsilon_i^2) = \sigma_i^2 \qquad E(\varepsilon_1 \varepsilon_2) = 0, \tag{2.2}$$

where $E(\cdot)$ represents the expectation. A possible estimate of T_t is obtained as a linear combination of the two observations, i.e.,

$$T_a = \alpha_1 T_1 + \alpha_2 T_2. \tag{2.3}$$

T_a receives the name of *analysis*. This estimate should be unbiased, that is, $E(T_t) = E(T_a)$. Consequently, $\alpha_1 + \alpha_2 = 1$. We will say that T_a is the best estimate of the true temperature T_t if the coefficients of the linear combination are chosen to minimize the mean square error of T_a given by

$$\sigma_a^2 = E[(T_a - T_t)^2] = \alpha_1^2 \sigma_1^2 + (1 - \alpha_1)^2 \sigma_2^2.$$

Differentiating the latter with respect to α_1 and setting the result equal to zero, we obtain that the coefficients that minimize the variance, σ_a^2, are:

$$\alpha_1 = \frac{\sigma_2^2}{\sigma_1^2 + \sigma_2^2} \qquad \alpha_2 = \frac{\sigma_1^2}{\sigma_1^2 + \sigma_2^2},$$

which yields in an optimal analysis of the form

$$T_a = \frac{\sigma_2^2}{\sigma_1^2 + \sigma_2^2} T_1 + \frac{\sigma_1^2}{\sigma_1^2 + \sigma_2^2} T_2.$$

On the other hand, the same estimate of the true temperature, T_t, can be obtained by minimizing a certain function defined as the sum of the square differences between estimate T and the given observations T_1 and T_2, weighted by the corresponding error precision (defined as the inverse of each variance):

$$J(T) = \frac{1}{2} \left[\frac{(T - T_1)^2}{\sigma_1^2} + \frac{(T - T_2)^2}{\sigma_2^2} \right]. \tag{2.4}$$

The cost function (2.4) can be formulated using a Bayesian derivation. In fact, assuming that the observation T_1 represents the background or prior information of

the truth and that its corresponding probability density function is Gaussian, i.e.,

$$p_{\sigma_1}(T) = \frac{1}{\sqrt{2\pi}\sigma_1} \exp\left\{-\frac{(T-T_1)^2}{2\sigma_1^2}\right\}.$$

Likewise, we assume that the probability distribution of the observation T_2 given the true value of the temperature is also Gaussian,

$$p_{\sigma_2}(T_2|T) = \frac{1}{\sqrt{2\pi}\sigma_2} \exp\left\{-\frac{(T-T_2)^2}{2\sigma_2^2}\right\}.$$

Then, the Bayes formula (2.1) let us obtain the posterior probability of the truth given the observation T_2,

$$p_{\sigma_2}(T|T_2) = \frac{p_{\sigma_2}(T_2|T)p_{\sigma_1}(T)}{p_{\sigma_2}(T_2)}. \tag{2.5}$$

The best estimate of the truth is the one maximizing the posterior probability (2.5). Since $p_{\sigma_2}(T_2)$ is independent of T, and considering that the logarithmic function is monotone increasing, this maximization problem can be written as

$$\max_{T} \quad \ln(p_{\sigma_2}(T_2|T)) + \ln(p_{\sigma_1}(T)).$$

After replacing the probability density functions we get

$$\max_{T} \quad -\frac{1}{2}\left(\frac{(T-T_2)^2}{\sigma_2^2} + \frac{(T-T_1)^2}{\sigma_1^2}\right) + \text{cte},$$

which is equivalent to minimizing the cost function $J(T)$ given in (2.4).

To solve this optimization problem, we need to differentiate the function $J(T)$ with respect to T and set the result equal to zero. Performing the latter we obtain:

$$T = \frac{\sigma_2^2}{\sigma_1^2+\sigma_1^2}T_1 + \frac{\sigma_1^2}{\sigma_1^2+\sigma_1^2}T_2,$$

that is, T equals the optimal estimate T_a.

Observe that in the first method, the analysis T_a is obtained by finding the optimal weights of the linear combination (2.3), which correspond to the ones minimizing the analysis error variance. This method belongs to the statistical data assimilation approach. On the other hand, in the second method, the best estimate of the true temperature is found by minimizing the cost function (2.4) where the minimization variable is the temperature itself and not the weights. In what follows, we describe both the statistical and the variational approaches to solving a data assimilation problem.

2.1.1 Statistical approach

The most used techniques of statistical data assimilation are Kalman Filters (KF), extended Kalman Filters (EKF), and ensemble Kalman Filters (EnKF). Kalman Filters are used when the dynamical system and the observational model are linear and when the error in the observations follows a Gaussian distribution. Its extended version, the extended Kalman filters, handles non-linearities in the system and the observational models by working with their tangent linear versions. However, EKF works for moderated deviations from linearity (and Gaussianity); see, e.g., [11, Section 3.6]. In contrast, the ensemble Kalman Filters (EnKF) has been designed to deal with more general non-linearities and non-Guassianities, where the probability density function is described by an ensemble of N model states which are used to approximate the uncertainty in the system.

Kalman Filters

Let us consider the dynamical and the observational models in their discrete versions:

$$\begin{aligned} \mathbf{x}_{k+1} &= \mathbf{M}_{k+1}(\mathbf{x}_k) + \eta_k, \\ \mathbf{y}_k &= \mathbf{H}_k(\mathbf{x}_k) + \epsilon_k, \end{aligned}$$

where η_k and ϵ_k represent the model and the observation errors, respectively. Note that $\mathbf{M}_{k+1}$ and $\mathbf{H}_k$ are assumed to be **linear models**. Likewise, η_k and ϵ_k are assumed to be independent variables with Gaussian probability distributions, i.e.,

$$\begin{aligned} \eta_k &\sim \mathcal{N}(0, \mathbf{Q}_k), \\ \epsilon_k &\sim \mathcal{N}(0, \mathbf{R}_k), \end{aligned}$$

where $\mathbf{Q}_k$ represents the covariance matrix of the model error η_k, while $\mathbf{R}_k$ is covariance matrix of the observation error ϵ_k.

The difference between the forecasted and the unknown true states, $\mathbf{x}_k^f$ and $\mathbf{x}_k^t$, give us the forecast error, and with it, we obtain the forecast error covariance matrix:

$$\mathbf{e}_k^f = \mathbf{x}_k^f - \mathbf{x}_k^t, \quad \mathbf{P}_k^f = \mathrm{cov}(\mathbf{e}_k^f) = E[(\mathbf{e}_k^f)(\mathbf{e}_k^f)^T]. \tag{2.6}$$

The main idea of the Kalman filters is to estimate, at a given time t_k, the unknown true state of the system, $\mathbf{x}_k^t$, as a linear combination of an a priori estimate, $\mathbf{x}_k^f$, and a weighted difference between the observations, $\mathbf{y}_k$, and the predicted observation, $\mathbf{H}_k(\mathbf{x}_k^f)$, that is,

$$\mathbf{x}_k^a = \mathbf{x}_k^f + \mathbf{K}_k(\mathbf{y}_k - \mathbf{H}_k\mathbf{x}_k^f). \tag{2.7}$$

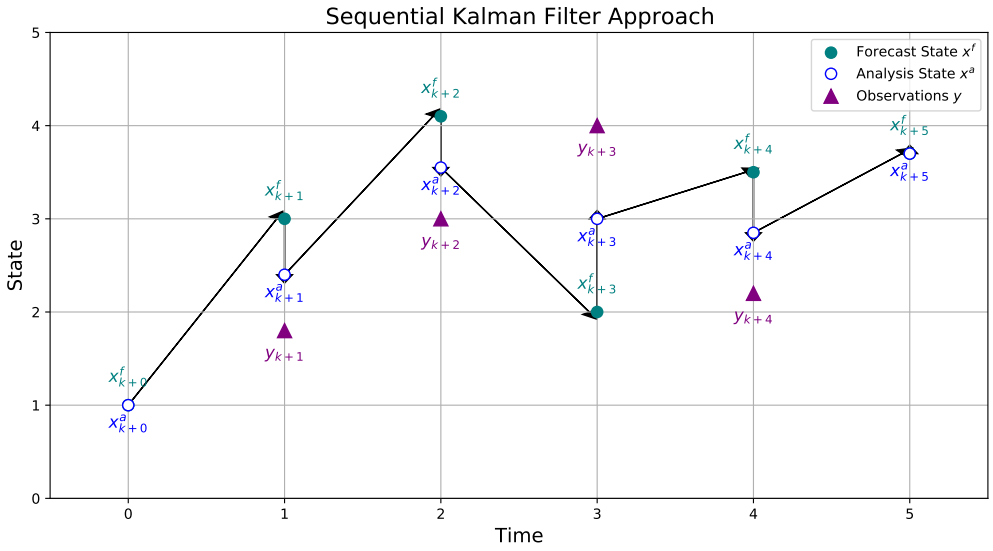

Figure 2.1: Illustration of the sequential Kalman Filter approach.

This linear combination is called analysis state, and it is denoted as $\mathbf{x}_k^a$. Along the iterations, the construction of an analysis state described a sequential process; we depict it in Figure 2.1.

Matrix $\mathbf{K}_k$ in equation (2.7) is the *Kalman gain* matrix. While the difference $(\mathbf{y}_k - \mathbf{H}_k\mathbf{x}_k^f)$ is called *innovation*. To build the gain matrix, let us consider the analysis error covariance matrix given by:

$$\mathbf{P}_k^a = \text{cov}(\mathbf{e}_k^a) = E[(\mathbf{e}_k^a)(\mathbf{e}_k^a)^T], \tag{2.8}$$

where $\mathbf{e}_k^a = \mathbf{x}_k^a - \mathbf{x}_k^t$. Observe that using the form of $\mathbf{y}_k = \mathbf{H}_k(\mathbf{x}_k) + \epsilon_k$ and the linearity of $\mathbf{H}_k$, it follows that

$$\begin{aligned}\mathbf{e}_k^a &= \mathbf{x}_k^a - \mathbf{x}_k^t = \mathbf{x}_k^f + \mathbf{K}_k(\mathbf{y}_k - \mathbf{H}_k\mathbf{x}_k^f) - \mathbf{x}_k^t \\ &= \mathbf{x}_k^f - \mathbf{x}_k^t + \mathbf{K}_k(\mathbf{H}_k\mathbf{x}_k^t + \epsilon_k - \mathbf{H}_k\mathbf{x}_k^f) = \mathbf{e}_k^f + \mathbf{K}_k(-\mathbf{H}_k\mathbf{e}_k^f + \epsilon_k).\end{aligned}$$

Replacing the latter in (2.8), noticing that $\mathbf{R}_k = E[\epsilon_k\epsilon_k^T]$, and realizing that the prior estimation error, $\mathbf{e}_k^f$, is uncorrelated to the observational error, it yields

$$\begin{aligned}\mathbf{P}_k^a &= E[(\mathbf{e}_k^f)(\mathbf{e}_k^f)^T - (\mathbf{K}_k\mathbf{H}_k\mathbf{e}_k^f)(\mathbf{K}_k\mathbf{H}_k\mathbf{e}_k^f)^T + (\mathbf{K}_k\epsilon_k)(\mathbf{K}_k\epsilon_k)^T] \\ &= (\mathbf{I} - \mathbf{K}_k\mathbf{H}_k)\mathbf{P}_k^f(\mathbf{I} - \mathbf{K}_k\mathbf{H}_k)^T + \mathbf{K}_k\mathbf{R}_k\mathbf{K}_k^T.\end{aligned} \tag{2.9}$$

Observe that the recursive formula (2.9) is valid for any $\mathbf{K}_k$, not necessarily the optimal one. The optimal Kalman gain is set as the one minimizing the matrix entries along the diagonal of $\mathbf{P}_k^a$ (see [11, Section 3.4.3]). To do that, we need to derive the

trace of $\mathbf{P}_k^a$ with respect to $\mathbf{K}_k$ and set the result equal to zero, i.e.,

$$\frac{d}{d\mathbf{K}_k}\text{Tr}\mathbf{P}_k^a = -2(\mathbf{H}_k\mathbf{P}_k^f)^T + 2\mathbf{K}_k(\mathbf{H}_k\mathbf{P}_k^f\mathbf{H}_k^T + \mathbf{R}_k) = 0,$$

from where we obtain:

$$\mathbf{K}_k = \mathbf{P}_k^f\mathbf{H}_k^T(\mathbf{H}_k\mathbf{P}_k^f\mathbf{H}_k^T + \mathbf{R}_k)^{-1}. \tag{2.10}$$

Additionally, replacing $\mathbf{K}_k$ in equation (2.9), we obtain an alternative closed formula for the analysis error covariance matrix,

$$\begin{aligned}\mathbf{P}_k^a &= \mathbf{P}_k^f - \mathbf{K}_k(\mathbf{H}_k\mathbf{P}_k^f\mathbf{H}_k^T + \mathbf{R}_k)\mathbf{K}_k^T \\ &= (\mathbf{I} - \mathbf{K}_k\mathbf{H}_k)\mathbf{P}_k^f.\end{aligned} \tag{2.11}$$

In summary, the sequential Kalman filter approaches the solution of the data assimilation problem by performing two main steps: prediction (forecast) and correction (analysis). Both of them are defined recursively through equations (2.7), (2.10), and (2.11) through the following loop:

Initialization:
Initial estimates for $\mathbf{x}_k^a$ and $\mathbf{P}_k^a$.

Prediction:

1. Update the forecast state, $\mathbf{x}_{k+1}^f = \mathbf{M}_{k+1}\mathbf{x}_k^a$,
2. Update the error forecast covariance matrix, $\mathbf{P}_{k+1}^f = \mathbf{M}_{k+1}\mathbf{P}_k^a\mathbf{M}_{k+1}^T + \mathbf{Q}_{k+1}$.

Correction:

1. Compute the Kalman gain $\mathbf{K}_{k+1}$ by using (2.10),

$$\mathbf{K}_{k+1} = \mathbf{P}_{k+1}^f\mathbf{H}_{k+1}^T(\mathbf{H}_{k+1}\mathbf{P}_{k+1}^f\mathbf{H}_{k+1}^T + \mathbf{R}_{k+1})^{-1}$$

2. Update the analysis estimate $\mathbf{x}_{k+1}^a$ using (2.7),

$$\mathbf{x}_{k+1}^a = \mathbf{x}_{k+1}^f + \mathbf{K}_{k+1}(\mathbf{y}_{k+1} - \mathbf{H}_{k+1}\mathbf{x}_{k+1}^f).$$

3. Update the analysis error covariance matrix $\mathbf{P}_{k+1}^a$ using (2.11)

$$\mathbf{P}_{k+1}^a = (\mathbf{I} - \mathbf{K}_{k+1}\mathbf{H}_{k+1})\mathbf{P}_{k+1}^f.$$

As a counterpart, even though there exist closed formulas for computing the KF loop, if the problem is large-scale, then the computation of the covariance matrices can be expensive. Moreover, the described approach has a significant drawback. It was designed for working with the discrete linear version of the dynamic and observational model. If these models are not linear, then a linearized version of them has to be considered, which constitutes a new flavor of the Kalman approach, the so-called extended Kalman filter (EKF); see, e.g., [11, 55].

Ensemble Kalman filters

An *ensemble* in Data Assimilation is a collection or set of multiple simulations or realizations of a specific model. For instance, Ensemble Kalman filters (EnKF) are reduced-order filters that seek to reproduce the KF analysis but with an ensemble of limited size. In general, the EnKF involves truncating the model variables' first and second statistical moments (mean and covariance). Therefore, it solves not the original problem but an approximation. Accordingly to [13] and the reference therein, EnKF and its variants have been successfully applied operationally for atmospheric, climate, and oceanic models, which are highly dimensional dynamical models. The advantage of the EnKF approach is that, with a relatively small number of members of the ensemble, it can recreate the variability of the system by running an ensemble of realizations of the model dynamic.

The proposed method solves one of the drawbacks of the Kalman filter approach, i.e., being highly computationally expensive. The main idea is to emulate the uncertainty of the system with the variability generated by the ensemble members, which are propagated by the model without considering any linearization; see, e.g., [11]. There is a deterministic version of the ensemble Kalman filter approach, also called *ensemble square-root Kalman filter* (EnSRKF); however, we focus on the study of the stochastic EnKF, specifically on the study of its analysis and forecast steps [11, 13].

Analysis and forecast steps:
The EnKF method seeks to mimic the loop generated with the Kalman filter approach to get updates for the analysis state, considering a limited size of ensemble members and without needing to compute the full covariance matrix but using an approximation. The idea of reproducing the KF analysis state was proposed in [54], where the author set the following formula:

$$\mathbf{x}_i^a = \mathbf{x}_i^f + \mathbf{K}(\mathbf{y} - \mathcal{H}\mathbf{x}_i^f), \qquad i \in \{1, \dots, N\}, \tag{2.12}$$

where N represents the number of ensemble members. Additionally, note that matrix $\mathbf{K}$

should be identified with the Kalman gain matrix given by $\mathbf{K} = \mathbf{P}^f\mathbf{H}^T(\mathbf{H}\mathbf{P}^f\mathbf{H}^T+\mathbf{R})^{-1}$. To prove the latter, let us define ensembles of the model realizations for the forecast and the analysis as follows:

$$\mathbf{E}^f = [\mathbf{x}_1^f, \mathbf{x}_2^f, \ldots, \mathbf{x}_N^f]$$
$$\mathbf{E}^a = [\mathbf{x}_1^a, \mathbf{x}_2^a, \ldots, \mathbf{x}_N^a].$$

We know that the error covariance matrices $\mathbf{P}^f$ and $\mathbf{P}^a$ of the forecast and the analysis, respectively, are defined in terms of an unknown true state (see equations (2.6) and (2.8)). However, since we do not know the true state, we find an approximation of these covariance matrices using the ensemble members. In fact, given the ensemble means

$$\bar{\mathbf{x}}^f = \frac{1}{N}\sum_{i=1}^{N}\mathbf{x}_i^f \quad \text{and} \quad \bar{\mathbf{x}}^a = \frac{1}{N}\sum_{i=1}^{N}\mathbf{x}_i^a,$$

we define the ensemble perturbations matrices as follows:

$$\mathbf{X}^f = \frac{1}{\sqrt{N-1}}[\mathbf{x}_1^f - \bar{\mathbf{x}}^f, \mathbf{x}_2^f - \bar{\mathbf{x}}^f, \ldots, \mathbf{x}_N^f - \bar{\mathbf{x}}^f] \tag{2.13}$$
$$\mathbf{X}^a = \frac{1}{\sqrt{N-1}}[\mathbf{x}_1^a - \bar{\mathbf{x}}^a, \mathbf{x}_2^a - \bar{\mathbf{x}}^a, \ldots, \mathbf{x}_N^a - \bar{\mathbf{x}}^a], \tag{2.14}$$

where the columns of $\mathbf{X}^f$ and $\mathbf{X}^a$ are normalized anomalies, i.e., normalized deviations of the ensemble members from the mean of the forecast and the analysis, respectively. Observe that using (2.12) each column of $\mathbf{X}^a$ takes the form

$$\mathbf{X}_i^a = (\mathbf{I} - \mathbf{K}\mathbf{H})\mathbf{X}_i^f. \tag{2.15}$$

Moreover, with the aid of (2.13) and (2.14), we can write the ensemble-based error covariance matrices for the forecast and the analysis in the following way:

$$(\mathbf{P}^e)^f = (\mathbf{X}^f)(\mathbf{X}^f)^T \tag{2.16}$$
$$(\mathbf{P}^e)^a = (\mathbf{X}^a)(\mathbf{X}^a)^T, \tag{2.17}$$

where the super index e denotes that the matrices were built using ensembles. Note that equations (2.16) and (2.17) represent the variation of the ensemble members around the mean, representing the error in the ensemble mean for the forecast and the analysis. They are natural approximations for the error covariance matrices $\mathbf{P}^f$ and $\mathbf{P}^a$, respectively.

Nevertheless, in the ensemble-based construction, matrix $(\mathbf{P}^e)^a$ underestimates the

errors of the observations. In fact, replacing (2.15) in (2.17), we get

$$(\mathbf{P}^e)^a = (\mathbf{I} - \mathbf{KH})\mathbf{P}^f(\mathbf{I} - \mathbf{KH})^T,$$

that is, the term $\mathbf{KRK}^T$ is missing if we compare it with (2.9). This lacking term is related to the observation error covariance matrix $\mathbf{R}$. To get an ensemble analysis error covariance matrix $(\mathbf{P}^e)^a$ consistent with the one in the Kalman filter approach, we perturb the observation vector by adding a random noise $\epsilon_i \sim \mathcal{N}(0, \mathbf{R})$ with $i \in \{1, \ldots, N\}$, obtaining N ensemble members of the kind $\mathbf{y}_i = \mathbf{y} + \epsilon_i$. Let us define $\bar{\mathbf{y}}$ and $\bar{\epsilon}$ as the mean of the samples $\mathbf{y}_i$ and ϵ_i, respectively. Then, the ensemble matrix perturbation of the innovation is defined as follows:

$$\begin{aligned}\mathbf{Y}^f &= \frac{1}{\sqrt{N-1}}[\mathbf{y}_1 - \bar{\mathbf{y}}, \mathbf{y}_2 - \bar{\mathbf{y}}, \ldots, \mathbf{y}_N - \bar{\mathbf{y}}] \\ &= \frac{1}{\sqrt{N-1}}[\mathbf{H}\mathbf{x}_1^f - \epsilon_1 - (\mathbf{H}\bar{\mathbf{x}}^f - \bar{\epsilon}), \ldots, \mathbf{H}\mathbf{x}_N^f - \epsilon_N - (\mathbf{H}\bar{\mathbf{x}}^f - \bar{\epsilon})].\end{aligned}$$

And, the posterior perturbations are modified according to the following equation

$$\mathbf{X}^a = \mathbf{X}^f - \mathbf{KY}^f = (\mathbf{I} - \mathbf{KH})\mathbf{X}^f + \mathbf{KE},$$

where $\mathbf{E} = \frac{1}{\sqrt{N-1}}[\epsilon_1 - \bar{\epsilon}, \ldots, \epsilon_N - \bar{\epsilon}]$. Using this form of $\mathbf{X}^a$, the corresponding analysis error covariance matrix, $\mathbf{P}^a = (\mathbf{X}^a)(\mathbf{X}^a)^T$, and its expectation, we can formulate the gain matrix only in terms of the anomaly matrices,

$$\mathbf{K} = \mathbf{X}^f(\mathbf{Y}^f)^T(\mathbf{Y}^f(\mathbf{Y}^f)^T)^{-1}. \tag{2.18}$$

For the forecast step, the updated ensemble obtained at the analysis state is propagated by the dynamical model, that is,

$$\mathbf{x}_{i,k+1}^f = \mathcal{M}_{k+1}(\mathbf{x}_{i,k}^a), \tag{2.19}$$

for each ensemble member $i \in \{1, \ldots, N\}$ and for an instant of time k. Note that we do not consider a linearized version of the dynamical model. Finally, observe that with equations (2.12), (2.18), and (2.19), it is possible to recreate the Kalman filter loop, but this time using the ensemble error covariance matrices which reduce the computational cost.

2.1.2 Variational approach

According to [18], the term variational assimilation designates a class of assimilation algorithms on which the variable (or variables) to be estimated is explicitly determined as the minimizer of a specific cost function representing the mismatch between model predictions and available observations. With this formulation, variational methods can effectively assimilate data, updating the model state at each time step as new observations become available.

In particular, the *four-dimensional variational* (4D-VAR) data assimilation problem minimizes the misfit between a sequence of model states and observations available over a given assimilation window. Its cost function consists of two main terms: the first penalizes the difference between model predictions and observations. In contrast, the second one is a weighted difference between the solution state and the background knowledge. The weighting terms in both cases are the inverse of the error covariance matrices of the observations and the background information, respectively. In the variational assimilation, the problem is formulated as an optimal control problem. Mathematically, the formulation of the 4D-VAR reads as follows:

$$\begin{aligned} \min_{\mathbf{x}_0} \quad & J(\mathbf{x}, \mathbf{x}_0) = \frac{1}{2} \int_0^T (\mathbf{y}(t) - \mathcal{H}(\mathbf{x}, t))^T \mathbf{R}_t^{-1} (\mathbf{y}(t) - \mathcal{H}(\mathbf{x}, t)) \, d\mu \\ & + \frac{1}{2} (\mathbf{x}_0 - \mathbf{x}_0^b)^T \mathbf{B}^{-1} (\mathbf{x}_0 - \mathbf{x}_0^b), \\ \text{s.t.} \quad & \frac{d\mathbf{x}}{dt} = \mathcal{M}(\mathbf{x}), \\ & \mathbf{x}(0) = \mathbf{x}_0. \end{aligned} \tag{2.20}$$

The control variable is the dynamical system's initial condition, $\mathbf{x}_0$. In (2.20), $\mathbf{x}_0^b$ represents the background or prior information of this initial condition. Likewise, μ corresponds to the Lebesgue measure if the observations are continuous or the counting measure if the observations are acquired pointwise in time. $\mathbf{y}$ represents the observations and $\mathcal{H}$ is the observation operator. $\mathbf{R}_t$ and $\mathbf{B}$ are the observation and the background error covariance operators, respectively. $\mathbf{R}_t$ describes the deviation of observed events from the expected ones, while $\mathbf{B}$ accounts for the difference between the previous estimate and the true ones. The error covariance operators give important information about how much weight one gives to the background or the observations. For instance, if the background errors are more significant than the observation errors, the analysis state will be closer to the observations. We depict the variational data assimilation process in Figure 2.2.

In real-life applications like Numerical Weather Prediction (NWP), the solution to the data assimilation problem (2.20) yields the analysis state $\mathbf{x}^a$. This $\mathbf{x}^a$ represents

the best estimate of the problem's initial condition after incorporating observations. The term $\mathbf{x}_0^b$ is the model's best estimate for this initial condition before the latest observations are assimilated. $\mathbf{x}_0^b$ can be obtained from the immediately preceding assimilation cycle. In that previous cycle, an assimilation process combined a background state with available observations to produce an analysis state, $\mathbf{x}_{prev}^a$. The NWP model (the dynamical system in (2.20)) is then run forward in time, starting from $\mathbf{x}_{prev}^a$. The resulting forecast, valid at the beginning of the current assimilation window, becomes the background initial condition $\mathbf{x}_0^b$ for the current data assimilation problem.

On the other hand, building the background error covariance matrix is significantly more challenging, primarily because the true error statistics are generally unknown. As a result, the matrix $\mathbf{B}$ must be either modeled or estimated. In the context of NWP, a common approach involves estimating $\mathbf{B}$ by comparing forecasts of different lengths that are valid at the same time (e.g., differences between 48h and 24h forecasts). The statistics derived from these differences are then used to model $\mathbf{B}$. Another approach to estimating the error covariance matrix $\mathbf{B}$ involves the use of ensemble-based methods. The main idea is to emulate the uncertainty of the system by analyzing the variability of N model forecasts, starting from slightly perturbed initial conditions (representing the analysis uncertainty from the previous cycle). We refer the reader to Section 5.2.6, where this technique is employed to build the background error covariance matrix $\mathbf{Q}_0$ which accounts for the uncertainty of the system produced by the initial condition.

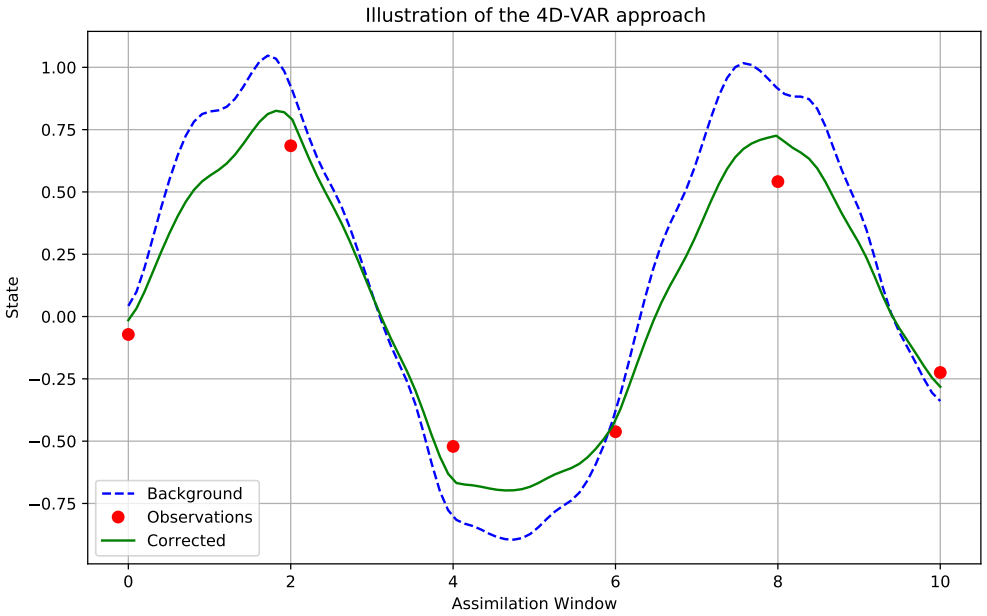

Figure 2.2: Illustration of the four-dimensional variational data assimilation process

The solution to the $4D$-VAR problem is an optimal initial condition, denoted as

$\mathbf{x}_0^a$, which is the one minimizing (2.20), that is,

$$\mathbf{x}_0^a = \arg\min \mathcal{J}(\mathbf{x}_0),$$

where $\mathcal{J}$ is the reduced cost function of $J(\mathbf{x}, \mathbf{x}_0)$. Consequently, solving the $4D$-VAR problem requires solving the equation $\nabla\mathcal{J}(\mathbf{x}_0) = 0$, which will require solving the associated adjoint equation.

To fix ideas, let us consider Example 2.1, retrieved from [11, Section 2.3.4], which will be solved with the aid of the Lagrangian formalism. The purpose of the example below is to give a first glance at how to obtain the adjoint equation and, with it, the gradient of the variational problem. That is, in Example 2.1, we will assume without proof that all the quantities are regular enough, the well-posedness of the state equation, and the existence of the Lagrange multipliers.

Example 2.1 (Initial condition control)**.** *Let us consider the following minimization problem:*

$$\min_{\mathbf{u}} \quad J(\mathbf{x}, \mathbf{u}) = \frac{1}{2}\int_0^T \|\mathbf{H}\mathbf{x} - \mathbf{y}\|^2_{L^2(\Omega)} dt \tag{2.21a}$$

$$\text{s.t.} \quad \frac{d\mathbf{x}}{dt} = \mathbf{M}(\mathbf{x}), \quad \text{in } \Omega \times [0, T], \tag{2.21b}$$

$$\mathbf{x}(0) = \mathbf{u},$$

where $\mathbf{x}$ *is the model state,* $\mathbf{y}$ *represents the observations, and* $\mathbf{u}$ *is the initial condition that we want to estimate. The observation operator and the model dynamics are described by* $\mathbf{H}$ *and* $\mathbf{M}$*, respectively. Observe that in this simplified example, the observation error covariance operator* $\mathbf{R}$ *is equal to the identity operator. Likewise, there is no background misfit term. To solve* (2.21) *with the aid of the Lagrangian formalism, let* $\mathbf{p}$ *and* $\mathbf{q}$ *be the Lagrange multipliers associated with the dynamical model and the initial condition constraints. The Lagrangian of the problem has the form:*

$$\mathcal{L}(\mathbf{x}, \mathbf{u}, \mathbf{p}, \mathbf{q}) = \frac{1}{2}\int_0^T \langle \mathbf{H}\mathbf{x} - \mathbf{y}, \mathbf{H}\mathbf{x} - \mathbf{y}\rangle_{L^2} + \langle \mathbf{p}, \frac{d\mathbf{x}}{dt} - \mathbf{M}(\mathbf{x})\rangle_{L^2} dt + \langle \mathbf{q}, \mathbf{x}(0) - \mathbf{u}\rangle_{L^2} \tag{2.22}$$

The adjoint system is obtained by differentiating (2.22) *with respect to the state variable* $\mathbf{x}$ *in an arbitrary direction* $\mathbf{v}$ *and setting the result equal to zero that is,*

$$\begin{aligned}\nabla_{\mathbf{x}}\mathcal{L}(\mathbf{x},\mathbf{u},\mathbf{p},\mathbf{q})\mathbf{v} &= \int_0^T \langle \mathbf{H}\mathbf{x}-\mathbf{y}, \mathbf{H}\mathbf{v}\rangle_{L^2} + \langle \mathbf{p}, \frac{d\mathbf{v}}{dt} - \frac{\partial \mathbf{M}}{\partial \mathbf{x}}\mathbf{v}\rangle_{L^2} dt + \langle \mathbf{q}, \mathbf{v}(0)\rangle_{L^2} \\ &= \int_0^T \left(\langle \mathbf{H}^*(\mathbf{H}\mathbf{x}-\mathbf{y}), \mathbf{v}\rangle_{L^2} - \langle \frac{d\mathbf{p}}{dt} + \left[\frac{\partial \mathbf{M}}{\partial \mathbf{x}}\right]^* \mathbf{p}, \mathbf{v}\rangle_{L^2} \right) dt \\ &+ \langle \mathbf{p}(T), \mathbf{v}(T)\rangle_{L^2} - \langle \mathbf{v}(0), \mathbf{p}(0)-\mathbf{q}\rangle_{L^2} = 0.\end{aligned}$$

Since the direction $\mathbf{v}$ *was taken arbitrarily, the latter yields the following adjoint equation:*

$$\begin{aligned} -\frac{d\mathbf{p}}{dt} - \left[\frac{\partial \mathbf{M}}{\partial \mathbf{x}}\right]^* \mathbf{p} &= \mathbf{H}^*(\mathbf{y}-\mathbf{H}\mathbf{x}), \qquad \text{in } \Omega \times [0,T] \\ \mathbf{p}(T) &= 0, \end{aligned} \tag{2.23}$$

where additionally, $\mathbf{q} = \mathbf{p}(0)$*. Likewise, to obtain the gradient of the problem, we have to differentiate the Lagrangian* (2.22) *with respect to the initial condition* $\mathbf{u}$ *in an arbitrary direction* $\mathbf{h}$ *and set the result equal to zero. By doing the latter, we obtain:*

$$\nabla_{\mathbf{u}}\mathcal{L}(\mathbf{x},\mathbf{u},\mathbf{p},\mathbf{q})\mathbf{h} = \langle -\mathbf{q}, \mathbf{h}\rangle_{L^2} = \langle -\mathbf{p}(0), \mathbf{h}\rangle_{L^2} = 0, \quad \forall \mathbf{h} \in L^2(\Omega)$$

Consequently,

$$\nabla_{\mathbf{u}}\mathcal{L}(\mathbf{x},\mathbf{u},\mathbf{p},\mathbf{q}) = -\mathbf{p}(0). \tag{2.24}$$

Equations (2.21b)*,* (2.23)*, and* (2.24) *together define the optimality system for the minimization problem described by* (2.21a)-(2.21b)*. Any solution to this minimization problem must satisfy this optimality condition. Therefore, to find the minimum using a gradient descent method, we iteratively solve this optimality system until a specified stopping criterion is met.*

Likewise, depending on the problem, estimating the initial condition and some unknown parameter, θ, could be necessary. In these cases, the variational problem can be extended in the following way:

$$\begin{aligned} \min_{\mathbf{x}_0,\theta} \quad & \frac{1}{2}\int_0^T (\mathbf{y}(t)-\mathcal{H}(\mathbf{x},t))^T \mathbf{R}_t^{-1}(\mathbf{y}(t)-\mathcal{H}(\mathbf{x},t))\, d\mu \\ & + \frac{1}{2}(\theta-\theta^b)^T\boldsymbol{\Theta}^{-1}(\theta-\theta^b) + \frac{1}{2}(\mathbf{x}_0-\mathbf{x}_0^b)^T\mathbf{B}^{-1}(\mathbf{x}_0-\mathbf{x}_0^b), \\ \text{s.t.} \quad & \frac{d\mathbf{x}}{dt} = \mathcal{M}(\mathbf{x},\mathbf{x}_0,\theta), \end{aligned} \tag{2.25}$$

where $\boldsymbol{\Theta}$ and θ^b represent the error covariance operator and the background information

of the model parameters, respectively.

$4D$-VAR problem in the finite-dimensional setting

If the observations are acquired pointwise over a time window $[t_0, t_n]$, i.e., considering a finite number of observations, and considering the discrete version of the observation and the model operators, $\mathbf{H}$ and $\mathbf{M}$, respectively, we obtain the finite formulation of the $4D$-VAR, originally proposed by Le Dimet and Talagrand in [85] where a finite number of observations were considered:

$$\begin{aligned}\min_{\mathbf{x},\mathbf{x}_0}\ & J(\mathbf{x},\mathbf{x}_0) = \frac{1}{2}\sum_{i=0}^{n}\left[\mathbf{H}(\mathbf{x}(t_i)) - \mathbf{y}(t_i)\right]^T \mathbf{R}_i^{-1}\left[\mathbf{H}(\mathbf{x}(t_i)) - \mathbf{y}(t_i)\right] \\ & + \frac{1}{2}(\mathbf{x}_0 - \mathbf{x}_0^b)^T\mathbf{B}^{-1}(\mathbf{x}_0 - \mathbf{x}_0^b) \\ \text{subject to:}\ & \\ & \mathbf{x}(t_i) = \mathbf{M}_i(\mathbf{x}(t_0)), \quad i = 1,\ldots,n \\ & \mathbf{x}(t_0) = \mathbf{x}_0.\end{aligned} \tag{2.26}$$

To solve the minimization problem (2.26) by variational means, we must compute the gradient and the adjoint state [11, 85], which can be done through a Lagrangian approach. The Lagrangian of the problem is given by:

$$\mathcal{L}(\mathbf{x},\mathbf{x}_0,\lambda) = J(\mathbf{x},\mathbf{x}_0) + \sum_{i=0}^{n}\lambda_i^T(\mathbf{x}(t_i) - \mathbf{M}_i(\mathbf{x}_0)),$$

where λ_i, $i = 0,\ldots,n$ is the Lagrange multiplier associated to each problem constraint. Observe that we have set $\mathbf{M}_0 = \mathbf{I}$, where $\mathbf{I}$ represents the identity operator. The adjoint state is obtained by differentiating the Lagrangian with respect to the state variable $\mathbf{x}$, in a given time t_i, and setting the result equal to zero, i.e.,

$$\nabla_{\mathbf{x}(t_i)}\mathcal{L}(\mathbf{x},\mathbf{x}_0,\lambda) = \mathbf{H}^T\mathbf{R}_i^{-1}(\mathbf{H}\mathbf{x}(t_i) - \mathbf{y}(t_i)) + \lambda_i = 0, \quad i = 0,\ldots,n, \tag{2.27}$$

from where it holds that $\lambda_i = -\mathbf{H}^T\mathbf{R}_i^{-1}(\mathbf{H}\mathbf{x}(t_i) - \mathbf{y}(t_i))$ for all $i = 0,\ldots,n$. Likewise, differentiating the Lagrangian with respect to the control variable $\mathbf{x}_0$ and setting the result equal to zero, we obtain:

$$\nabla_{\mathbf{x}_0}\mathcal{L}(\mathbf{x},\mathbf{x}_0,\lambda) = \mathbf{B}^{-1}(\mathbf{x}_0 - \mathbf{x}_0^b) - \sum_{i=0}^{n}\left(\nabla_{\mathbf{x}_0}\mathbf{M}_i(\mathbf{x}_0)\right)^T\lambda_i = 0. \tag{2.28}$$

On the other hand, using the form of λ_i and defining

$$\mathbf{p}_i = -\left(\nabla_{\mathbf{x}_0}\mathbf{M}_i(\mathbf{x}_0)\right)^T\mathbf{H}^T\mathbf{R}_i^{-1}(\mathbf{H}\mathbf{x}(t_i) - \mathbf{y}(t_i)), \quad i = 0,\ldots,n,$$

we can rewrite the gradient equation in (2.28) as

$$\nabla_{\mathbf{x}_0}\mathcal{L}(\mathbf{x}, \mathbf{x}_0, \lambda) = \mathbf{B}^{-1}(\mathbf{x}_0 - \mathbf{x}_0^b) - \sum_{i=0}^{n} \mathbf{p}_i = 0,$$

which represents the optimality condition of problem (2.26). The solutions of the minimization problem (2.26) must satisfy this optimality condition.

Strong and weak $4D$-VAR problem

Formulation (2.26) represents the finite-dimensional *strong constraint four-dimensional variational* data assimilation problem. The term *strong constraint* indicates that the model is assumed to exactly represent the state of the system, meaning that model error is considered zero. The same applies to the infinite-dimensional formulations (2.20) and (5.4). Throughout this thesis, we will work exclusively with this class of $4D$-VAR problems, and if the context is clear, we will drop the strong constraint part and just refer to that problem as $4D$-VAR. Nevertheless, we would like to mention the modifications required when accounting for model errors, which, for simplicity, we describe only in the finite-dimensional case.

In the presence of model uncertainty, the minimization problem is known as *weak constraint four-dimensional variational* data assimilation problem. According to [52, Chapter 5], there are two approaches to handling weak constraint $4D$-VAR. The first approach, known as the *forcing formulation*, assumes that the evolution model also depends on random errors η_k, i.e.,

$$\begin{aligned} \mathbf{x}(t_i) &= \mathbf{M}_i(\mathbf{x}(t_{i-1}), \eta_i), \quad i = 1, \dots, n \\ \mathbf{x}(t_0) &= \mathbf{x}_0. \end{aligned}$$

Then, we can form a vector containing both the initial condition and time-dependent model errors $\eta_1, \dots, \eta_n$,

$$\mathbf{z} = (\mathbf{x}_0, \eta_1, \dots, \eta_n)^T.$$

The weak constraint cost function is given as in the cost function of (2.26) but considering the vector $\mathbf{z}$ and a corresponding error covariance matrix, that is,

$$J(\mathbf{z}) = \frac{1}{2}\sum_{i=0}^{n} \left[\mathbf{H}(\mathbf{z}(t_i)) - \mathbf{y}(t_i)\right]^T \mathbf{R}_i^{-1} \left[\mathbf{H}(\mathbf{z}(t_i)) - \mathbf{y}(t_i)\right] + \frac{1}{2}(\mathbf{z} - \mathbf{z}^b)^T \mathbf{C}^{-1}(\mathbf{z} - \mathbf{z}^b),$$

where $\mathbf{C}$ includes the error covariance of the initial condition and model errors

$$\mathbf{C} = \begin{pmatrix} \mathbf{C}_{\mathbf{x}_0,\mathbf{x}_0} & 0 & \dots & 0 \\ 0 & \mathbf{C}_{\eta_1,\eta_1} & \dots & \mathbf{C}_{\eta_1,\eta_n} \\ \vdots & \vdots & \ddots & \vdots \\ 0 & \mathbf{C}_{\eta_n,\eta_1} & \dots & \mathbf{C}_{\eta_n,\eta_n} \end{pmatrix}.$$

Observe that zero correlation between the initial condition and the model errors is assumed.

The second approach for incorporating model errors is known as the *state-space formulation*. This approach defines the evolution model with additive random errors,

$$\begin{aligned} \mathbf{x}(t_i) &= \mathbf{M}_i(\mathbf{x}(t_{i-1})) + \eta_i, \quad i = 1, \dots, n \\ \mathbf{x}(t_0) &= \mathbf{x}_0, \end{aligned}$$

and modifying the cost function by adding a new term, to account for these errors

$$\begin{aligned} J(\mathbf{x}, \mathbf{x}_0) = \frac{1}{2} \sum_{i=0}^{n} \left[\mathbf{H}(\mathbf{x}(t_i)) - \mathbf{y}(t_i)\right]^T \mathbf{R}_i^{-1} \left[\mathbf{H}(\mathbf{x}(t_i)) - \mathbf{y}(t_i)\right] + \frac{1}{2}(\mathbf{x}_0 - \mathbf{x}_0^b)^T \mathbf{B}^{-1}(\mathbf{x}_0 - \mathbf{x}_0^b) \\ + \frac{1}{2} \sum_{i=1,j}^{n} [\mathbf{x}(t_i) - \mathbf{M}_i(\mathbf{x}(t_i - 1))]^T \mathbf{C}_\eta^{-1}(i,j)[\mathbf{x}(t_j) - \mathbf{M}_j(\mathbf{x}(t_j - 1))], \end{aligned}$$

where

$$\mathbf{C}_\eta = \begin{pmatrix} \mathbf{C}_{\eta_1,\eta_1} & \dots & \mathbf{C}_{\eta_1,\eta_n} \\ \vdots & \ddots & \vdots \\ \mathbf{C}_{\eta_n,\eta_1} & \dots & \mathbf{C}_{\eta_n,\eta_n} \end{pmatrix}.$$

Observe that the double sum in the last term accounts for model-error correlations in time. In the cases of non-correlated errors in time, the model error term will not contain the cross-correlation blocks.

The finite-dimensional stationary case

If observations are available on a given time t_k or over a short time window when the dynamical model can be considered stationary, then the minimization problem (2.26) has the following form:

$$\min_{\mathbf{x}} \quad J(\mathbf{x}) = \frac{1}{2}(\mathbf{H}(\mathbf{x}) - \mathbf{y})^T \mathbf{R}^{-1}(\mathbf{H}(\mathbf{x}) - \mathbf{y}) + \frac{1}{2}(\mathbf{x} - \mathbf{x}^b)^T \mathbf{B}^{-1}(\mathbf{x} - \mathbf{x}^b) \tag{2.29}$$

Problem (2.29) represents the mathematical formulation of the three-dimensional variational ($3D$-VAR) data assimilation approach, which is a robust balance between the

background information and the observed data. Since the problem is unconstrained, the analysis state will be the one satisfying $\nabla J(\mathbf{x}^a) = 0$, i.e.,

$$\nabla J(\mathbf{x}^a) = \mathbf{B}^{-1}(\mathbf{x}^a - \mathbf{x}^b) - \mathbf{H}^T\mathbf{R}^{-1}(\mathbf{y} - \mathbf{H}\mathbf{x}^a) = 0.$$

Solving the equation, it follows that:

$$\begin{aligned}\mathbf{B}^{-1}(\mathbf{x}^a - \mathbf{x}^b) &= \mathbf{H}^T\mathbf{R}^{-1}(\mathbf{y} - \mathbf{H}\mathbf{x}^a)\\ (\mathbf{B}^{-1} + \mathbf{H}^T\mathbf{R}^{-1}\mathbf{H})\mathbf{x}^a &= \mathbf{H}^T\mathbf{R}^{-1}\mathbf{y} + \mathbf{B}^{-1}\mathbf{x}^b,\end{aligned}$$

by adding and subtracting the term $\mathbf{H}^T\mathbf{R}^{-1}\mathbf{H}\mathbf{x}^b$ in the latter, it yields

$$\begin{aligned}\mathbf{x}^a &= \mathbf{x}^b + \underbrace{(\mathbf{B}^{-1} + \mathbf{H}^T\mathbf{R}^{-1}\mathbf{H})^{-1}\mathbf{H}^T\mathbf{R}^{-1}}_{\mathbf{K}}(\mathbf{y} - \mathbf{H}\mathbf{x}^b),\\ &= \mathbf{x}^b + \mathbf{K}(\mathbf{y} - \mathbf{H}\mathbf{x}^b)\end{aligned}$$

$\mathbf{K}$ is called *gain matrix*. Therefore, we can represent the state analysis as a weighted average between the background information and the observations. Accordingly to [11, Section 2.4.3], using the Sherman-Morrison-Woodbury formula, matrix $\mathbf{K}$ can be written in an equivalent way as

$$\mathbf{K} = \mathbf{B}\mathbf{H}^T(\mathbf{R} + \mathbf{H}\mathbf{B}\mathbf{H}^T)^{-1}. \tag{2.30}$$

Observe that (2.30) has the same form of the Kalman gain matrix (2.10) obtained with the statistical data assimilation approach.

Relation between the $3D$-VAR and the statistical DA approach

In the statistical approach, the weighting matrix is known as *Kalman gain* and has the same form as the one computed using the $3D$-VAR approach. Therefore, under some assumptions, the two methods are equivalent and provide the same solutions [11]. In fact, if the observations and the background or prior information are normally distributed, with error covariances matrices $\mathbf{R}$ and $\mathbf{B}$, respectively. Then, the conditional probability density function $p(\mathbf{y}|\mathbf{x})$ takes the form:

$$p(\mathbf{y}|\mathbf{x}) = \frac{1}{(2\pi)^{n/2}|\mathbf{R}|^{1/2}} \exp\left\{-\frac{1}{2}(\mathbf{y} - \mathbf{H}(\mathbf{x}))^T\mathbf{R}^{-1}(\mathbf{y} - \mathbf{H}(\mathbf{x}))\right\}, \tag{2.31}$$

where n is the number of available observations, and $\mathbf{H}$ is the observation operator considered in a determined instant. Likewise, the *prior* probability density function is

given by

$$p(\mathbf{x}) = \frac{1}{(2\pi)^{m/2}|\mathbf{B}|^{1/2}} \exp\left(-\frac{1}{2}(\mathbf{x}-\mathbf{x}^b)^T\mathbf{B}^{-1}(\mathbf{x}-\mathbf{x}^b)\right), \tag{2.32}$$

where m and $\mathbf{x}^b$ are the number of parameters to estimate and the background knowledge about the phenomena, respectively.

In the Bayesian formulation, the objective is to find the best estimator, i.e., the one which maximizes the *posterior* probability density function given by the Bayes formula (2.1). Since $p(\mathbf{y})$ is independent from $\mathbf{x}$, this maximization problem can be written as:

$$\max_{\mathbf{x}} \quad p(\mathbf{y}|\mathbf{x})p(\mathbf{x}). \tag{2.33}$$

The state maximizing the posterior distribution receives the name of Maximum-A-Posteriori (MAP) estimate.

On the other hand, considering that the logarithmic function is monotone increasing and continuous, the maximization problem (2.33) is equivalent to the following one:

$$\max_{\mathbf{x}} \quad \ln(p(\mathbf{y}|\mathbf{x})) + \ln(p(\mathbf{x})). \tag{2.34}$$

Replacing the probability density functions (2.31) and (2.32) in the problem above, we get a minimization problem equivalent to the $3D$-VAR formulation, which, as we proved above, attains a minimum at $\mathbf{x}^a = \mathbf{x}^b + \mathbf{K}(\mathbf{y} - \mathbf{H}\mathbf{x}^b)$, where $\mathbf{K}$ given as in (2.30). Observe that the above extends to the multidimensional case presented in the classical example for one dimension (see the introduction of Section 2.1).

Advantages and drawbacks of the $4D$-VAR method

Among others, the main advantages of the $4D$-VAR formulation are the following ones:

- It considers non-linear dynamics. This is crucial since most real-life problems are modeled by non-linear, maybe chaotic, dynamical systems.
- Moreover, $4D$-VAR lets us incorporate observations in a given time window.
- Considering the dynamics and the observations distributed in time, we can obtain a better reconstruction of the problem's initial condition.
- We can use efficient numerical methods to solve the optimization problem.
- The $4D$-VAR can be formulated as an inverse problem of the form:

$$\min_u \mathcal{J}(u) = \phi(T(u), f) + \lambda S(u),$$

where T is a forward operator modeling the relationship between the minimization variable u and the observed data f. The term $\phi(T(u), f)$ represents a fidelity term that forces u to follow a dynamical model. Likewise, $S(u)$ is a regularization term that includes background information on the minimizer u, and $\lambda > 0$ is a parameter that balances the weight between the prior information and the fidelity term. This formulation allows considering different fidelity terms, including stochastic terms, as well as different types of regularizers.

Conversely, a major drawback of the $4D$-VAR method is that in practical applications, the observation and the background error covariance matrices are large dimensional; therefore, computing the adjoint state is computationally expensive.

2.2 Semigroup theory

In this subsection, we introduce preliminary notions of semigroup theory. We are particularly interested in defining and studying the properties of C_0 and analytic semigroups, as these structures are generated by operators satisfying maximal parabolic regularity. We begin by reviewing some standard definitions and properties. We remark that all results, definitions, and examples presented in this section are standard and have been taken from the literature (see, e.g., [102, Chapter 1] and [51]). We refer to these references for a more detailed discussion of semigroup theory and for the proofs of the results presented in this section.

In what follows, we will consider X a Banach space.

2.2.1 Definition and elementary properties

Definition 2.1. *A family $\{T(t)\}_{t\geq 0}$ of linear and bounded operators mapping X into X is called a* ***semigroup of linear and bounded operators*** *if:*

1. $T(0) = I$ *(I denotes the identity operator on X)*
2. $T(t+s) = T(t)T(s)$ *for all $t, s \geq 0$ (semigroup property).*

A semigroup of bounded and linear operators is **uniformly continuous** if

$$\lim_{t\to 0^+} \|T(t) - I\|_{\mathcal{L}(X)} = 0$$

Definition 2.2. *A linear operator $A\colon D(A) \subset X \to X$ defined by*

$$D(A) = \left\{ x \in X : \lim_{t\to 0^+} \frac{T(t)x - x}{t} \ \textit{exists} \right\}$$

and

$$Ax = \lim_{t \to 0^+} \frac{T(t)x - x}{t}, \qquad \text{for } x \in D(A)$$

is the ***infinitesimal generator*** *of the semigroup* $\{T(t)\}_{t \geq 0}$. $D(A)$ *denotes the domain of* A.

Theorem 2.1 (Differential properties of semigroups)**.** *Assuming that* $x \in D(A)$. *Then,*

(*i*) $T(t)x \in D(A)$ *for each* $t \geq 0$.

(*ii*) $AT(t)x = T(t)Ax$ *for each* $t > 0$.

(*iii*) *The mapping* $t \mapsto T(t)x$ *is differentiable for each* $t > 0$ *and* $\frac{d}{dt}T(t)x = AT(t)x$ *with* $t > 0$.

Definition 2.3. *Let* A *be a closed linear operator on* X *with domain* $D(A)$.

(*i*) *Let* $\lambda \in \mathbb{R}$, *the* ***resolvent set*** *of* A, $\rho(A)$, *is defined as:*

$$\rho(A) := \{\lambda \in \mathbb{R} : \lambda I - A : D(A) \longrightarrow X \text{ is one-to-one}\}.$$

(*ii*) *Let* $\lambda \in \rho(A)$, *the* ***resolvent operator*** *is defined as*

$$R_\lambda : X \longrightarrow X, \quad u \mapsto R_\lambda u := (\lambda I - A)^{-1} u.$$

Where $R_\lambda : X \longrightarrow D(A) \subset X$ *is a bounded linear operator, and,* $AR_\lambda u = R_\lambda Au$ *if* $u \in D(A)$.

We recall that if A is linear, not necessarily bounded, then the resolvent set $\rho(A)$ is defined as the set of $\lambda \in \mathbb{C}$ for which the operator $\lambda I - A$ is invertible.

Definition 2.4. *A semigroup* $\{T(t)\}_{t \geq 0}$ *of bounded linear operators on* X *is a* ***strongly continuous*** *semigroup if*

$$\lim_{t \to 0^+} T(t)x = T(0)x = x, \qquad \text{for every } x \in X.$$

This class of semigroups will be called C_0*-semigroup.*

Theorem 2.2. *Let* $\{T(t)\}_{t \geq 0}$ *be a* C_0*-semigroup on* X. *Then, there exist constants* $\omega \geq 0$ *and* $M > 1$ *such that*

$$\|T(t)\|_{\mathcal{L}(X)} \leq Me^{\omega t}, \qquad \forall t \geq 0. \tag{2.35}$$

The latter implies the continuity of the mapping $[0, +\infty[\ni t \mapsto T(t)x \in X$.

Proposition 2.1. *Let $\{T(t)\}_{t\geq 0}$ be a C_0-semigroup on X, and A its infinitesimal generator. Then, $D(A)$ is dense on X, and A is a closed linear operator.*

Example 2.2. *Let $A\colon D(A) \longrightarrow X$ the infinitesimal generator of the C_0-semigroup $\{T(t)\}_{t\geq 0}$. It holds that $\forall x \in D(A)$, $u(t) = T(t)x \in C^1([0,\infty); X) \cap C([0,\infty); D(A))$ is the solution of the following Cauchy problem:*

$$\begin{cases} u'(t) = Au(t), & t \geq 0 \\ u(0) = x \end{cases} \tag{2.36}$$

In fact, since A generates $\{T(t)\}_{t\geq 0}$, we know that $t \mapsto T(t)x$ is differentiable for each $x \in D(A)$ and $\frac{d}{dt}T(t)x = AT(t)x$ (see Theorem 2.1). Then,

$$u'(t) = \frac{d}{dt}T(t)x = AT(t)x = Au(t).$$

Additionally, $u(0) = T(0)x = Ix = x$, that is, $u(\cdot) = T(\cdot)x$ solves problem (2.36). On the other hand, since $T(\cdot)x$ is differentiable for $t > 0$ and for each $x \in D(A)$, it is continuous. Then, $u \in C([0,+\infty); D(A))$. Moreover, $u'(\cdot) = AT(\cdot)x$ is continuous for all $x \in X$ (see the final remark on Theorem 2.2). Then $u \in C^1([0,+\infty); X)$.

Definition 2.5. *Let $\{T(t)\}_{t\geq 0}$ be a C_0-semigroup. If $\omega = 0$ in (2.35), then $T(t)$ will be uniformly bounded, i.e., $\|T(t)\|_{\mathcal{L}(X)} \leq M$, $\forall t \geq 0$. If additionally, $M = 1$, i.e., $\|T(t)\|_{\mathcal{L}(X)} \leq 1$, $\forall t \geq 0$, then $\{T(t)\}_{t\geq 0}$ will form a C_0-**semigroup of contractions**.*

Theorem 2.3 (Hille-Yosida)**.** *A linear operator A is the infinitesimal generator of a C_0-semigroup of contractions $\{T(t)\}_{t\geq 0}$ if and only if*

- *A is closed and $\overline{D(A)} = X$.*
- *$(0,+\infty) \subset \rho(A)$ and $\|R_\lambda\|_{\mathcal{L}(X)} \leq \frac{1}{\lambda}$ for every $\lambda > 0$.*

Remark 2.1. *Let $\{T(t)\}_{t\geq 0}$ be a C_0-semigroup satisfying $\|T(t)\|_{\mathcal{L}(X)} \leq e^{\omega t}$ for some $\omega \geq 0$. A linear operator A will be the infinitesimal generator of $T(t)$ if and only if*

- *A is closed and $\overline{D(A)} = X$.*
- *$(\omega,+\infty) \subset \rho(A)$ and $\|R_\lambda\|_{\mathcal{L}(X)} \leq \frac{1}{\lambda-\omega}$ for every $\lambda > \omega$.*

Let us now consider a nonhomogeneous linear initial value problem

$$\begin{cases} u'(t) = Au(t) + f(t), & t > 0 \\ u(0) = x, \end{cases} \tag{2.37}$$

where $x \in X$, and $f \in C(\mathbb{R}, X)$ are given. If $x \in D(A)$, we will say that u is a classical solution of the nonhomogeneous problem if u belongs to $C^1([0,+\infty); X) \cap C([0,+\infty); D(A))$ and satisfies (2.37) in a pointwise sense. Moreover, if $A\colon D(A) \to X$ is the infinitesimal generator of a C_0-semigroup $\{T(t)\}_{t\geq 0}$, then any classical solution of problem (2.37) can be represented as

$$u(t) = T(t)x + \int_0^t T(t-s)f(s)ds. \tag{2.38}$$

In fact, for fixed $t > 0$ and $s \in [0,t]$, let us defined the function $h(s) = T(t-s)u(s)$, then

$$\begin{aligned} \frac{dh}{ds} &= -AT(t-s)u(s) + T(t-s)\frac{du}{ds}(s) \\ &= -AT(t-s)u(s) + T(t-s)(Au(s) + f(s)) \\ &= T(t-s)f(s). \end{aligned}$$

Consequently, applying the fundamental theorem of calculus, it holds that

$$h(t) - h(0) = \int_0^t T(t-s)f(s)ds,$$

and, since $h(t) = T(0)u(t) = u(t)$ and $h(0) = T(t)u(0) = T(t)x$, the expression above is equivalent to (2.38). According to [108, Theorem 12.14], if the semigroup $\{T(t)\}_{t\geq 0}$ is uniformly continuous, a classical solution of the nonhomogeneous problem (2.37), can be represented by (2.38). However, if A only generates a C_0-semigroup, then (2.38) may define a function that is not differentiable at any $t > 0$ even if f is a continuous function. The following example shows the aforementioned.

Example 2.3. *Let $\{T(t)\}_{t\geq 0}$ be a C_0-semigroup on X with generator $A\colon D(A) \longrightarrow X$. Let us assume that there exists a $x_0 \in X$ such that $T(t)x_0 \notin D(A)$ for any $t > 0$. Taking $f(t) = T(t)x_0$ and $x = 0$, the nonhomogeneous equation (2.37) takes the form:*

$$\begin{cases} u'(t) = Au(t) + T(t)x_0, & t > 0 \\ u(0) = 0, \end{cases}$$

and, consequently

$$u(t) = \int_0^t T(t-s)T(s)x_0 \, ds = tT(t)x_0,$$

which is continuous on t. However, it is not differentiable at any $t > 0$. In fact, for

all $\lambda > 0$*, it yields*

$$\frac{u(t+\lambda)-u(t)}{\lambda} = T(\lambda)T(t)x_0 + t\ \frac{T(\lambda)T(t)x_0 - T(t)x_0}{\lambda}.$$

Since $\{T(t)\}_{t\geq 0}$ *is a* C_0*-semigroup the limit of the first term in the sum above, as* $\lambda \to 0^+$*, exists and is equal to* $T(t)x_0$*. However, the limit as* $\lambda \to 0^+$ *of the second term exists if and only if* $T(t)x_0 \in D(A)$*, which is not the case. Therefore,* u *is not differentiable.*

The cases where $T(t)x_0$ belongs to $D(A)$ for all $t > 0$ and any $x_0 \in X$ correspond to a specific subset of C_0-semigroups, called analytic semigroups, which will be studied next.

2.2.2 Analytic semigroups

In general, analytic semigroups can be seen as a subset of C_0-semigroups that provide better regularity for solutions to partial differential equations (PDEs). The general idea is to extend the concept of strongly continuous semigroups by introducing additional regularity through analyticity. The definitions and main results of this subsection were taken from [90] to where we refer for further details. In this subsection, we will consider X a complex Banach space.

Definition 2.6. *Let* $A\colon D(A) \subset X \longrightarrow X$ *be a linear operator, with not necessarily dense domain.* A *is said to be* ***sectorial*** *if there are constants* $\omega \in \mathbb{R}$*,* $\theta \in]\frac{\pi}{2}, \pi[$*,* $M > 0$ *such that*

$$\begin{cases} (i) \quad \rho(A) \supset S_{\theta,\omega} = \{\lambda \in \mathbb{C} : \lambda \neq \omega, |\arg(\lambda - \omega)| < \theta\}, \\ (ii) \quad \|R_\lambda\|_{\mathcal{L}(X)} \leq \frac{M}{|\lambda-\omega|}, \forall \lambda \in S_{\theta,\omega}. \end{cases} \tag{2.39}$$

For every $t > 0$, we define a linear bounded operator in X of the form

$$e^{tA} = \frac{1}{2\pi i}\int_{\omega+\gamma_{r,\eta}} e^{t\lambda} R_\lambda\ d\lambda, \quad t > 0 \tag{2.40}$$

where $r > 0$, $\eta \in]\frac{\pi}{2}, \theta[$, and $\gamma_{r,\eta}$ is the curve $\{\lambda \in \mathbb{C} : |\arg(\lambda)| = \eta, |\lambda| \geq r\} \cup \{\lambda \in \mathbb{C} : |\arg(\lambda)| \leq \eta, |\lambda| = r\}$, oriented counterclockwise. Additionally, we set

$$e^{0A}x = x, \quad \forall x \in X. \tag{2.41}$$

According to [90], given that the mapping $\lambda \mapsto e^{t\lambda}R_\lambda$ is holomorphic[1] in $S_{\theta,\omega}$, the

[1] A function $f\colon \Omega \subset \mathbb{C} \to \mathbb{C}$ is **holomorphic** on Ω if it is complex differentiable at each point of Ω; see, e.g., [104]

definition of e^{tA} in (2.40) is independent of r and η. Moreover, note that the mapping $t \mapsto e^{tA}$ verifies the semigroup property $e^{tA}e^{sA} = e^{(t+s)A}$, for all $t, s \geq 0$. These two properties motivate the following definition.

Definition 2.7. *Let $A\colon D(A) \subset X \to X$ be a sectorial operator. The family $\{e^{tA} : t \geq 0\}$ defined by (2.40) and (2.41) is the **analytic semigroup** generated by A on X.*

The following proposition gives us the conditions that this analytic semigroup has to follow to be strongly continuous; for its proof, see [90, Proposition 2.1.4].

Proposition 2.2. *Let $A\colon D(A) \to X$ be a sectorial operator and $\{e^{tA}\}_{t\geq 0}$ be the analytic semigroup generated by A. Then, $\{e^{tA}\}_{t\geq 0}$ is strongly continuous if and only if the domain $D(A)$ is dense in X.*

The following proposition states one of the main properties of the analytic semigroup $\{e^{tA}\}_{t\geq 0}$ generated by the sectorial operator A. For its proof, we refer to [90, Proposition 2.1.1]

Proposition 2.3. *Let $A\colon D(A) \to X$ be a sectorial operator and $\{e^{tA}\}_{t\geq 0}$ the analytic semigroup generated by A. Then, the function $t \mapsto e^{tA}$ belongs to $C^\infty((0,+\infty); \mathcal{L}(X))$ and*

$$\frac{d^k}{dt^k} e^{tA} = A^k e^{tA}, \quad t > 0.$$

Moreover, it has an analytic extension in the sector

$$S_\theta = \left\{ \lambda \in \mathbb{C} : \lambda \neq 0, |\arg(\lambda)| < \theta - \frac{\pi}{2} \right\}.$$

Definition 2.8 (Analytic mapping, [104])**.** *A function $f\colon \Omega \subset \mathbb{C} \to \mathbb{C}$ is said to be **analytic** if for each $z_0 \in \mathbb{C}$ there exists an open ball $B(z_0, \rho) \subset \Omega$, in which f can be written as $f(z) = \sum_{n=0}^{\infty} a_n (z - z_0)^n$ for $z \in B(z_0, \rho)$, with uniquely determined coefficients $\{a_n\}_{n\geq 0}$.*

In the complex plane, a complex differentiable function, i.e., a holomorphic function, is an analytic function, too; see [104, Chapter 4, Theorem 8]. Consequently, it is possible to use the terms analytic and holomorphic interchangeably. The latter does not hold for analytic functions defined in real Banach spaces.

In general, a semigroup $\{T(t)\}_{t>0}$ is said to be analytic if the mapping

$$]0, +\infty[\ni t \mapsto T(t) \in \mathcal{L}(X)$$

is analytic, i.e., if the mapping verifies Definition 2.8. The following Lemma lets us identify the generator of a given analytic semigroup. Its proof can be found in [90, Prop. 2.1.9]

Lemma 2.1. *Let $\{T(t) : t > 0\}$ be a family of linear bounded operators such that the mapping $]0, +\infty[\ni t \mapsto T(t) \in \mathcal{L}(X)$ is differentiable, and,*

1. *$T(t)T(s) = T(t+s)$, for every $t, s > 0$.*
2. *There are $\omega \in \mathbb{R}$, and positive constants M_0, M_1 such that $\|T(t)\|_{\mathcal{L}(X)} \leq M_0 e^{\omega t}$, $\|tT'(t)\|_{\mathcal{L}(X)} \leq M_1 e^{\omega t}$, for $t > 0$.*
3. *There exists $t > 0$ such that $T(t)$ is a bijection, or $\forall x \in X$, $\lim_{t \to 0} T(t)x = x$.*

Then $]0, +\infty[\ni t \mapsto T(t) \in \mathcal{L}(X)$ is an analytic mapping, and there exists a unique sectorial operator $A \colon D(A) \subset X \to X$ such that $T(t) = e^{tA}$, for every $t \geq 0$.

Remark 2.2. *Given a sectorial operator $A \colon D(A) \subset X \to X$, we can define a mapping $T(t)$, for each $t > 0$, by using a variant of equation (2.40) obtained by considering a different curve $\gamma_{r,\eta,\omega}$[2], that is,*

$$T(t) = \int_{\gamma_{r,\eta,\omega}} e^{t\lambda} R_\lambda \, d\lambda. \tag{2.42}$$

This integral is known as the Dunford integral. Similar to e^{tA}, the operator $T(t)$, defined by (2.42) for $t > 0$ and such that $T(0) = I$ is an analytic semigroup generated by the sectorial operator A.

The definition of sectorial functions and analytic semigroups was done in the complex plane; however, in the applications to PDEs, we dealt with operators A defined on real Banach spaces X. Therefore, to be able to use the results of analytic semigroups in real Banach spaces, we need to complexify the space X and the operator A. In fact, let X be a real Banach space, and let $A \colon D(A) \subset X \to X$ be a linear operator, the complexification $X_{\mathbb{C}}$ of X is the set $X_{\mathbb{C}} = \{x + iy : x, y \in X\}$, while the complexification of the operator A is the operator $A_{\mathbb{C}} \colon D(A_{\mathbb{C}}) \subset X_{\mathbb{C}} \to X_{\mathbb{C}}$, where $D(A_{\mathbb{C}}) = \{x + iy : x, y \in D(A)\}$ and $A_{\mathbb{C}}(x + iy) = Ax + iAy$, for every $x + iy \in D(A_{\mathbb{C}})$.

If we identify X with the set $\{x + i0 : x \in X\}$, then the restriction of operator $A_{\mathbb{C}}$ to X is the operator A. Moreover, assuming that $A_{\mathbb{C}}$ is sectorial in $X_{\mathbb{C}}$, and denoting $\{T_{\mathbb{C}}(t)\}_{t \geq 0}$ its associated analytic semigroup, then $T_{\mathbb{C}}(t)(X) \subset X$; see, e.g., [90, Corollary 2.1.3]. Moreover, setting $T(t) = T_{\mathbb{C}}(t)\big|_X$ for $t \geq 0$, then $\{T(t)\}_{t \geq 0}$ defines a semigroup of bounded operators in the real Banach space X, which satisfies the properties that we have established so far.

To conclude this subsection, we would like to comment on the relation between second-order differential operators and analytic semigroups. We refer to [90, Chapter 3] for a detailed analysis of the following remark.

[2]The curve $\gamma_{r,\eta,\omega}$ is defined as the union of three different curves, for a detail description of them, we refer to [87, Section 3.2]

Remark 2.3. *Let $\Omega \subset \mathbb{R}^n$ be an open set with sufficiently smooth boundary $\partial\Omega$, and $\mathcal{A}$ be a second-order differential operator. If the coefficients of $\mathcal{A}$ are smooth enough (alternatively, if the coefficients are measurable and bounded), then $\mathcal{A}$ will be a sectorial operator, so that it generates an analytic semigroup.*

2.3 Maximal parabolic regularity results

Next, we give a formal introduction to maximal parabolic regularity theory, which helps analyze nonlinear partial differential equations (PDEs). This introductory subsection is based on [40, Section 1 & 2], where the main idea of maximal parabolic regularity is to solve nonlinear PDEs by a linearization approach. In order to do that, let us consider an abstract nonlinear equation of the form:

$$\begin{aligned} \frac{\partial y}{\partial t} - F(y)y &= G(y) \\ y(0) &= y_0, \end{aligned} \tag{2.43}$$

where $F(y)$ is a linear operator depending on y and $G(y)$ is a nonlinear function depending on y. For a linearization of equation (2.43), we fix a function y and look for the solution of the following Cauchy problem:

$$\begin{aligned} \frac{\partial v}{\partial t} - F(y)v &= G(y) \\ v(0) &= y_0, \end{aligned} \tag{2.44}$$

which is linear with respect to v, and consequently, it can be treated using methods from linear operators and semigroup theory. The idea of the maximal parabolic regularity approach is to solve the linearized equation (2.44) in appropriate function spaces so that the solution exhibits optimal regularity. In general, (2.44) is a time-dependent (non-autonomous) problem since y and therefore $F(y)$ depend on time. Moreover, setting $A(t) = F(y(t))$ and $\ell(t) = G(y(t))$, we can write (2.44) as:

$$\begin{aligned} \frac{\partial v}{\partial t} - A(t)v &= \ell(t), \qquad t > 0 \\ v(0) &= y_0. \end{aligned} \tag{2.45}$$

We will expect that the solution of (2.45) has optimal regularity if the corresponding solution operator has good mapping properties. Let us denote S_y as the solution operator of the linear equation (2.45), defined in appropriate function spaces $\mathbb{E}$ and $\mathbb{F}$. S_y maps the right-hand side $\ell \in \mathbb{F}$ and the initial condition y_0 to the solution $v \in \mathbb{E}$,

that is,

$$S_y : \mathbb{F} \times \gamma_t\mathbb{E} \to \mathbb{E}, \quad (\ell, y_0) \mapsto S_y(\ell, y_0) = v,$$

where $\gamma_t\mathbb{E}$ denotes the trace space. In the cases of maximal parabolic regularity, we expect two properties to hold: the uniqueness of solution of equation (2.45) and the continuity of its corresponding solution operator S_y. Then, we can say that the nonlinear Cauchy problem (2.43) will be uniquely solvable if and only if the fixed point equation

$$y = S_y(G(y), y_0), \tag{2.46}$$

has a unique solution $y \in \mathbb{E}$.

The notion of maximal parabolic regularity depends on the functional spaces where the equation is defined. Let us consider the Banach spaces X and Y, a real number $T > 0$, and $I = (0, T)$. A typical function space for the right-hand side is $L^r(I; X) := \mathbb{F}$, where $1 < r < \infty$. Likewise, the trace space is defined by $\gamma_t\mathbb{E} := \{\gamma_t y : y \in \mathbb{E}\}$ where $\gamma_t y := y|_{t=0}$.

In order to fix ideas, let us consider first the notion of maximal parabolic regularity in the autonomous case, i.e., for an operator A independent of t. Let $A\colon Y \subset X \longrightarrow X$ be a closed, linear, and densely defined operator, where the latter means that $Y \overset{d}{\hookrightarrow} X$. Let us consider the initial value problem

$$\frac{\partial y(t)}{\partial t} + Ay(t) = \ell(t), \quad y(0) = y_0, \tag{2.47}$$

where $\ell \in \mathbb{F} = L^r(I; X)$ and $y_0 \in \gamma_t\mathbb{E}$, for some space $\mathbb{E}$ to be defined. In an optimal regularity scenario, we will expect that $\frac{\partial y}{\partial t} \in L^r(I; X)$ and $Ay \in L^r(I; X)$, moreover, an even stronger assumptions would include $y \in L^r(I; X)$. Consequently, the *optimal* solution space will be given by

$$\mathbb{E} := W^{1,r}(I; X) \cap L^r(I; Y).$$

Observe that $W^{1,r}(I; X) \hookrightarrow C(I; X)$, see e.g., [110, Lemma 7.1]; then, $\gamma_t y = y(0)$ is well defined. A key result on $\gamma_t\mathbb{E}$ identifies this trace space with a real interpolation space (defined below). Before setting this result rigorously (see Lemma 2.2 below), we will provide precise definitions of real and complex interpolation spaces.

Real and complex interpolation spaces

We now introduce key definitions, properties, and known results concerning interpolation spaces, drawn from the literature (see, e.g., [89, 117]). For a more detailed treatment of interpolation theory, we refer to these sources.

Let X and Y be two real or complex Banach spaces. The couple (X, Y) is said to be an *interpolation couple* if both X and Y are continuously embedded in some larger Hausdorff topological vector space[3], $\mathcal{X}$. In this case, $X \cap Y$ is a linear subspace of $\mathcal{X}$, and it is a Banach space equipped with the norm

$$\|z\|_{X\cap Y} = \max\{\|z\|_X, \|z\|_Y\}.$$

Likewise, the sum $X + Y = \{x + y \mid x \in X, y \in Y\}$ is a linear subspace of $\mathcal{X}$. It is also a Banach space, equipped with the norm

$$\|z\|_{X+Y} = \inf_{x\in X, y\in Y, z=x+y} \{\|x\|_X + \|y\|_Y\}.$$

In general terms, real and complex interpolation spaces are *intermediate* spaces constructed from an interpolation couple (X, Y) using an interpolation method (or interpolation functor),$\mathcal{F}$, which is a procedure, when applied to any interpolation couple (X, Y), produces an intermediate Banach space $Z = \mathcal{F}(X, Y)$ that satisfies the continuous embedding:

$$X \cap Y \hookrightarrow Z \hookrightarrow X + Y.$$

The most known useful families of interpolation spaces are the real interpolation spaces and the complex interpolation spaces. Next, we will describe their corresponding interpolation methods.

Definition 2.9 (K-method)**.** *Let (X, Y) be an interpolation couple. For every $z \in X + Y$, and $t > 0$, set*

$$K(t, z; X, Y) = \inf_{x\in X, y\in Y, z=x+y} (\|x\|_X + t\|y\|_Y).$$

If the context is clear, we can write $K(t, z)$ instead of $K(t, z; X, Y)$. Observe that $K(t, z; X, Y)$ is an equivalent norm in the space $X + Y$, [117, Section 1.3.1].

Definition 2.10 (Real interpolation space, [117])**.** *Let (X, Y) be an interpolation couple, and $0 < \theta < 1$. If $1 \le r < \infty$, the **real interpolation space** is defined as*

$$(X, Y)_{\theta,r} = \left\{ z \in X + Y : \|z\|_{(X,Y)_{\theta,r}} = \left(\int_0^\infty \left[t^{-\theta} K(t, z; X, Y) \right]^r \frac{dt}{t} \right)^{1/r} < \infty \right\}$$

and if $r = \infty$, then

$$(X, Y)_{\theta,\infty} = \left\{ z \in X + Y : \|z\|_{(X,Y)_{\theta,\infty}} = \sup_{t>0} \left\{ t^{-\theta} K(t, z; X, Y) \right\} < \infty \right\}$$

[3] A space where every pair of distinct points can be separated by disjoint open sets [1, Section 1.4], ensuring that elements from X and Y can be unambiguously identified.

Alternative methods for defining real interpolation spaces, beyond the K-method, include the L-method, mean-methods, and the J-method; see [117, Sections 1.4-1.6]. These approaches yield real interpolation spaces $(X, Y)_{\theta,q}$ with equivalent norms. For a detailed discussion of these methods and their equivalence, we refer the reader to the cited reference [117].

The definition of complex interpolation spaces is generally more involved than that of their real counterparts. For a detailed treatment, we refer the reader to, e.g., [89, Section 2.1] or [1, Section 7.51]. To define the complex method, let us consider the open strip S and the closed strip $\bar{S}$ in the complex plane:

$$S = \{s \in \mathbb{C} \mid 0 < \mathrm{Re}(s) < 1\}, \qquad \bar{S} = \{s \in \mathbb{C} \mid 0 \leq \mathrm{Re}(s) \leq 1\}.$$

Definition 2.11 (Function Space for Complex Interpolation)**.** *Let (X, Y) be an interpolation couple over the complex field $\mathbb{C}$. Define $\mathcal{F} = \mathcal{F}(X, Y)$ as the space of functions $F \colon \bar{S} \to X + Y$ satisfying:*

(i) F is continuous on $\bar{S}$, bounded (i.e., $\sup_{s\in\bar{S}} \|F(s)\|_{X+Y} < \infty$), and analytic (holomorphic) in the open strip S.

(ii) For a.e. $\tau \in \mathbb{R}$, the mapping $\tau \mapsto F(i\tau) \in X$ is continuous, and

$$\|F(i\tau)\|_X \to 0 \qquad \text{as } |\tau| \to \infty.$$

(iii) For a.e. $\tau \in \mathbb{R}$, the mapping $\tau \mapsto F(1 + i\tau) \in Y$ is continuous, and

$$\|F(1 + i\tau)\|_Y \to 0 \qquad \text{as } |\tau| \to \infty.$$

The space $\mathcal{F}(X, Y)$ is a Banach space when equipped with the norm

$$\|F\|_{\mathcal{F}} = \max\left(\sup_{\tau\in\mathbb{R}} \|F(i\tau)\|_X, \sup_{\tau\in\mathbb{R}} \|F(1 + i\tau)\|_Y\right).$$

Definition 2.12 (Complex interpolation space, [1])**.** *Let (X, Y) be an interpolation couple, for every $\theta \in (0, 1)$, the **complex interpolation space** is defined as*

$$[X, Y]_\theta = \{z \in X + Y : z = F(\theta) \text{ for some } F \in \mathcal{F}\}.$$

$[X, Y]_\theta$ is a Banach space endowed with the norm

$$\|z\|_{[X,Y]_\theta} = \inf_{z=F(\theta), F\in\mathcal{F}} \|F\|_{\mathcal{F}}.$$

In what follows, we conserve the notation $(X, Y)_{\theta,r}$ for the real and $[X, Y]_\theta$ for the

complex interpolation spaces between X and Y with $0 < \theta < 1$ and $1 \leq r \leq \infty$. Moreover, with these spaces on hand, we can now formalize the result linking the trace space $\gamma_t\mathbb{E}$, used for motivating maximal parabolic regularity, with the real interpolation space $(X, Y)_{\theta,r}$, for a specific value of $\theta \in (0, 1)$. For its proof, we refer to [40] or [89].

Lemma 2.2. *Let $A\colon Y \subset X \longrightarrow X$ be a closed and densely defined operator, and let $\mathbb{E} := W^{1,r}(J; X) \cap L^r(I; Y)$, then the trace space $\gamma_t\mathbb{E}$ coincides with the real interpolation space with parameters $1 - \frac{1}{r}$ and r, that is,*

$$\gamma_t\mathbb{E} = (X, Y)_{1-\frac{1}{r},r}.$$

with $1 \leq r < \infty$.

Given that the definition of maximal parabolic regularity includes initial conditions in the trace space and, due to the last lemma, in real interpolation spaces, it will be useful to collect some embedding results in these spaces for further reference.

Proposition 2.4. *Let X and Y be Banach spaces where $Y \overset{d}{\hookrightarrow} X$. For $0 < \theta < 1$, the following is satisfied*

$$Y \overset{d}{\hookrightarrow} (X, Y)_{\theta,1} \overset{d}{\hookrightarrow} (X, Y)_{\theta,q} \overset{d}{\hookrightarrow} (X, Y)_{\theta,p} \hookrightarrow (X, Y)_{\theta,\infty} \overset{d}{\hookrightarrow} (X, Y)_{\vartheta,1} \overset{d}{\hookrightarrow} X \tag{2.48}$$

for $1 < q < p < \infty$ and $0 < \vartheta < \theta < 1$. Moreover,

$$(X, Y)_{\theta,1} \overset{d}{\hookrightarrow} [X, Y]_\theta \hookrightarrow (X, Y)_{\theta,\infty}. \tag{2.49}$$

For its proof, we refer to [5, section I.2.5] and [15, section 4.4.7].

In subsequent chapters, we will make use of embedding results involving real and complex interpolation spaces. Some necessary results were previously established in Proposition 2.4. Additional embeddings will be drawn from the literature, specifically [117] (see, e.g., Sections 2.4.2 and 2.8.1). It is important to note that the results in [117] are primarily stated for function spaces defined over $\mathbb{R}^d$, namely Besov spaces, $B^s_{p,q}(\mathbb{R}^d)$, Bessel potential spaces $H^s_p(\mathbb{R}^d)$, and Triebel-Lizorkin spaces $F^s_{p,q}(\mathbb{R}^d)$. For precise definitions of these spaces, we refer to [117, Section 2.3.1].

However, our application requires embedding results for Sobolev spaces $W^{s,p}(\Omega)$ defined on a domain $\Omega \subset \mathbb{R}^d$. We address the connection between these settings and the applicability of the results to bounded and Lipschitz domains in the following remark.

Remark 2.4.

1. *For $1 < p < \infty$ and $-\infty < s < \infty$, $H^s_p(\mathbb{R}^d) = F^s_{p,2}(\mathbb{R}^d)$.*

2. *For* $1 < p < \infty$ *and* $s \in \mathbb{N}$, $W^{s,p}(\mathbb{R}^d) = H^s_p(\mathbb{R}^d)$.

3. *According to Theorem 2 in [117, Section 4.3.1], if* $\Omega \subset \mathbb{R}^d$ *is a bounded domain of cone-type, then the embedding results hold after replacing* $\mathbb{R}^d$ *by* Ω.

4. *A bounded domain* Ω *with Lipschitz boundary is said to satisfy a strong Lipschitz condition; see [1, Section 4.9]. Such a domain also satisfies the cone condition [1, Section 4.11].*

So far, we can say that maximal parabolic regularity is a powerful tool to prove the well-posedness of evolutive PDEs. It is established by analyzing the parabolic operator and its associated semigroup, which describes how the solutions evolve. There is a significant amount of literature on maximal parabolic regularity, with general principles discussed in, for example, [5, Chapter III], [6, 7, 45, 46], among others. More specifically, in the field of optimal control, various authors have employed the maximal parabolic regularity property to prove the well-posedness of semilinear and quasilinear state equations, with notable contributions from Rehberg, Meinlschmidt, Bonifacius, Neitzel, Meyer, Susu, and Herzog, among others. For further reading, we refer to [19, 66, 93–96].

In this manuscript, we aim to take advantage of maximal parabolic regularity to prove the well-posedness of a parabolic PDE when the initial condition belongs to a Lebesgue space $L^\beta(\Omega)$, and, at the same time, some continuity restrictions on the solution variable have to be fulfilled. In what follows, we set definitions and properties related to maximal parabolic regularity in general Banach spaces that will be applied to our specific setting in Chapters 3 and 4. Let us agree on the following general assumptions:

Assumption 2.1.

1. *Let* $T > 0$ *be a real number representing the final time of a fixed time interval* $I := (0, T)$.

2. X *and* Y *are real reflexive Banach spaces such that* Y *is continuously and densely embedded in* X, *that is,* $Y \overset{d}{\hookrightarrow} X$.

Assumption 2.1 implies some extra results, for instance, since X and Y are reflexive spaces, for $r \in]1, \infty[$, it holds $(L^r(I; X))^* = L^{r'}(I; X^*)$ and $(L^r(I; Y))^* = L^{r'}(I; Y^*)$, where r' stands for the conjugate exponent, see e.g., [96, Remark 2.4]).

Next, we formalize the definition of maximal parabolic regularity when the operator does not depend on time. We consider the definition given in, e.g., [5, 19].

Definition 2.13 (Autonomous Maximal Parabolic Regularity)**.** *The operator $A\colon Y \to X$ satisfies maximal parabolic $L^r(I;X)$-regularity, with $1 < r < \infty$, if for every $\ell \in L^r(I;X)$ and $y_0 \in (X,Y)_{1-\frac{1}{r},r}$, the equation*

$$\frac{\partial y}{\partial t} + Ay = \ell, \quad y(0) = y_0, \tag{2.50}$$

admits a unique solution $y \in W^{1,r}(I;X) \cap L^r(I;Y)$. Additionally, the solution y satisfies the following estimate:

$$\|y\|_{W^{1,r}(I;X)\cap L^r(I;Y)} \leq c\left(\|\ell\|_{L^r(I;X)} + \|y_0\|_{(X,Y)_{1-\frac{1}{r},r}}\right), \tag{2.51}$$

for some constant $c > 0$.

If there is no ambiguity, we write

$$\mathbb{W}^r(Y,X) := W^{1,r}(I;X) \cap L^r(I;Y).$$

Moreover, if the context is clear, we drop the $L^r(I;X)$-part of the definition and just refer to *maximal parabolic regularity*. Additionally, given the reflexivity of X and Y, with $1 < r < \infty$, the space $\mathbb{W}^r(Y,X)$ is a reflexive Banach space [60, Theorem I.5.13].

Remark 2.5. *We recall some properties related to the maximal parabolic $L^r(I;X)$-regularity of operator A.*

1. *If A satisfies $L^r(I;X)$-maximal parabolic regularity for some single exponent $r \in (1,\infty)$, then A satisfies $L^p(I;X)$-maximal parabolic regularity for all exponents $p \in (1,\infty)$; see e.g., [49, Theorem 4.2] or [40, Lemma 2.7].*

2. *As a consequence of the maximal parabolic regularity of A, $-A$ generates the strongly continuous analytic semigroup $\{e^{-tA} : t \geq 0\}$ on X (see, e.g., [49, Theorem 2.2] or [7, Remark 3.1]). Moreover, $0 \notin \sigma(A)$, where $\sigma(A)$ denotes the spectrum of A.*

3. *Additionally, from [102, Theorem 1.2.2.2], the semigroup is bounded on X for $t \in I$, that is, there exists $\mathcal{M} > 0$ such that*

$$\|e^{-tA}\|_{\mathcal{L}(X)} \leq \mathcal{M}.$$

4. *The analytic semigroup $\{e^{-tA} : t \geq 0\}$, generated by $-A$, maps from X to $D(A^\alpha)$ for every $t > 0$ and $\alpha \geq 0$, see Theorem 6.13 in [102, Section 2.6].*

5. *The inverse of the operator $(\partial_t + A)$ gives the solution of the maximal parabolic regularity problem. In fact, for $\ell \in L^r(I;X)$, $y = (\partial_t + A)^{-1}\ell \in \mathbb{W}^r(Y,X)$ is the unique solution of problem (2.50); see e.g., [9].*

On the other hand, if the operator is non-autonomous, i.e., it depends on time, we consider the following notion of maximal parabolic regularity in the non-autonomous case from [47].

Definition 2.14 (Non-autonomous Maximal Parabolic Regularity)**.** *Let $I \ni t \mapsto \mathcal{A}(t) \in \mathcal{L}(Y,X)$ be a bounded and strongly measurable map and suppose that the operator $\mathcal{A}(t)$ is closed in X for all $t \in I$. Then $\{\mathcal{A}(t)\}_{t\in I}$ satisfies non-autonomous maximal parabolic $L^r(I;X)$-regularity with $r \in]1,+\infty[$, if for any $\ell \in L^r(I;X)$ and $y_0 \in (X,Y)_{1-\frac{1}{r},r}$ there exists a unique solution $y \in W^{1,r}(I;X) \cap L^r(I;Y)$ satisfying*

$$\frac{\partial y(t)}{\partial t} + \mathcal{A}(t)y(t) = \ell(t), \qquad y(0) = y_0, \tag{2.52}$$

for almost all $t \in I$.

In Definition 2.14, $\mathrm{Dom}(\mathcal{A}(t)) = Y$ for all $t \in I$. Note that if the operator is time-independent, the definition coincides with the definition of maximal parabolic regularity for autonomous (time-independent) operators; see, e.g., [5, Section III.1.5].

Throughout Chapters 3 and 4, different notions of solutions for parabolic PDEs involving operators enjoying maximal parabolic regularity will appear. To define them, let us first consider a map $\mathcal{A}\colon I \longrightarrow \mathcal{L}(Y,X)$ such that

$$\mathcal{A} \in L^1(I;\mathcal{L}(Y,X)) \cap \mathcal{L}(\mathbb{W}^r(Y,X), L^r(I;X)),$$

defining the following equation:

$$\frac{\partial y(t)}{\partial t} + \mathcal{A}(t)y(t) = \ell(t), \qquad y(0) = y_0, \tag{L}$$

for almost all $t \in I$, where $\ell \in L^r(I;X)$ and $y_0 \in (X,Y)_{1-\frac{1}{r},r}$.

According to Amann, in [7], equation (L) will have a strong (respectively weak) solution if the following definition holds.

Definition 2.15 (Weak and strong solutions, [7])**.**

(*i*) *$y \in W^{1,r}(I;X) \cap L^r(I;Y)$ is called a **strong solution** of (L) if y satisfies (L) in the pointwise sense almost everywhere, or equivalently in the distribution sense.*

(*ii*) *$y \in L^r(I;Y)$ is a **weak solution** of (L) if y satisfies:*

$$\int_0^T \langle (-\partial_t + \mathcal{A}^*)\,\varphi, y\rangle_{Y^*,Y} dt = \int_0^T \langle \varphi, \ell\rangle_{X^*,X} dt + \langle \varphi(0), y_0\rangle_{(Y^*,X^*)_{\frac{1}{r},r'},(X,Y)_{\frac{1}{r'},r}}$$

where $\mathcal{A}^*(t) := \mathcal{A}(t)^* \in \mathcal{L}(X^*,Y^*)$ for almost every $t \in I$, and $\varphi \in \mathcal{D}([0,T[;X^*)$, i.e., the X^*-valued smooth functions with compact support in $[0,T[$.

It can be shown that, under certain conditions, the definitions of strong and weak solutions are equivalent. This result is formally stated in the next lemma. Its proof can be found in [7, Proposition 6.1].

Lemma 2.3. *If X is a reflexive Banach space, $\mathcal{A}$ satisfies (non-autonomous) maximal parabolic $L^r(I;X)$-regularity, and $\mathcal{A}^*$ satisfies (non-autonomous) maximal parabolic $L^{r'}(I;Y^*)$-regularity. Then y is a weak solution of equation (L) if and only if y is a strong solution.*

The solutions of an operator in $\mathcal{L}(X^*,Y^*)$ satisfying the maximal parabolic $L^{r'}(I;Y^*)$-regularity belongs to the space $W^{1,r'}(I;Y^*)\cap L^{r'}(I;X^*)$. We will denote:

$$\mathbb{W}^{r'}(X^*,Y^*) := W^{1,r'}(I;Y^*)\cap L^{r'}(I;X^*).$$

Moreover, we can formulate Green's formula under these conditions of A and its adjoint A^*. We formalize this result in the next proposition; its proof can be found in [7, Prop. 5.1].

Proposition 2.5. *If $\mathcal{A}$ satisfies (non-autonomous) maximal parabolic $L^r(I;X)$-regularity, and, let $y\in\mathbb{W}^r(Y,X)$ and $v\in\mathbb{W}^{r'}(X^*,Y^*)$, then the Green's formula,*

$$\int_s^t \langle v,(\partial_t+\mathcal{A})y\rangle_{X^*,X}\,dt + \langle v(s),y(s)\rangle_{(Y^*,X^*)_{\frac{1}{r},r'},(X,Y)_{\frac{1}{r'},r}} = \int_s^t \langle(-\partial_t+\mathcal{A}^*)v,y\rangle_{Y^*,Y}\,dt + \langle v(t),y(t)\rangle_{(Y^*,X^*)_{\frac{1}{r},r'},(X,Y)_{\frac{1}{r'},r}} \tag{2.53}$$

holds for $0\le s<t\le T$.

Remark 2.6. *Note that in the autonomous case, we identify $A\in\mathcal{L}(Y,X)$ with the constant mapping $t\mapsto\mathcal{A}(t)=A$. Therefore, the notion of strong and weak solutions, as well as the results on Lemma 2.3 and Proposition 2.5, remain valid for the time-independent operator.*

In the case of autonomous operators, if $A\colon Y\to X$ satisfies maximal parabolic regularity, its adjoint operator $A^*\colon X^*\to Y^*$ satisfies a corresponding property as well. We state this result in the following lemma and refer to [66, Lemma 36] for its proof.

Lemma 2.4. *Let $A\in\mathcal{L}(Y,X)$ be a closed densely defined operator, satisfying (autonomous) maximal parabolic $L^r(I;X)$-regularity. Then its adjoint operator $A^*\in\mathcal{L}(X^*,Y^*)$ satisfies (autonomous) maximal parabolic $L^{r'}(I;Y^*)$-regularity.*

Consequently, if $A \in \mathcal{L}(Y, X)$ satisfies maximal parabolic regularity, then, from Definition 2.13, it holds that the equation:

$$-\frac{\partial p}{\partial t} + A^* p = \nu, \quad p(T) = 0, \tag{2.54}$$

has a unique solution $p \in W^{1,r'}(I; Y^*) \cap L^{r'}(I; X^*) = \mathbb{W}^{r'}(X^*, Y^*)$ if $\nu \in L^{r'}(I, Y^*)$. Additionally, from (2.51), the following estimate for the adjoint state holds:

$$\|p\|_{\mathbb{W}^{r'}(X^*, Y^*)} \leq c_p \|\nu\|_{L^{r'}(I; Y^*)}, \text{ for some constant } c_p > 0. \tag{2.55}$$

Remark 2.7. *As we will see in Chapter 4, in the semilinear setting, the adjoint operator is non-autonomous. Consequently, we cannot apply the result of Lemma 2.4 to ensure the well-posedness of the adjoint state, as this lemma applies only to time-independent operators.*

Likewise, later in Chapters 3 and 4, we will need embedding properties of the space $\mathbb{W}^r(Y, X)$. We collect them in the following proposition.

Proposition 2.6. *Let X, Y be Banach spaces such that $Y \overset{d}{\hookrightarrow} X$. Given $1 \leq r < \infty$ and r' its conjugate exponent, we have:*

(i) If $0 < \theta - \frac{1}{r'} < \frac{1}{q} \leq 1$, then $\mathbb{W}^r(Y, X) \hookrightarrow L^q(I; (X, Y)_{\theta,1})$

(ii) If $\theta = \frac{1}{r'}$, then $\mathbb{W}^r(Y, X) \hookrightarrow C(I; (X, Y)_{\frac{1}{r'},r})$

(iii) If $0 \leq \gamma < \frac{1}{r'} - \theta$, then $\mathbb{W}^r(Y, X) \hookrightarrow C^\gamma(I; (X, Y)_{\theta,1})$.

Moreover, if $\theta \neq \frac{1}{r'}$ and Y is compactly embedded in X, these embeddings are also compact.

The proof of these results can be found in [6, Theorem 3] and [5, Theorem 4.10.2].

To conclude this section, let us introduce the concept of a mild solution, which will be used later in the study of the nonlinear optimization problem, specifically in proving the well-posedness of a generalized linearized equation. Let us consider the following semilinear equation:

$$\begin{aligned} \frac{\partial y(t)}{\partial t} + Ay(t) + g(y(t)) &= 0 \qquad \text{in } I, \\ y(0) &= y_0. \end{aligned} \tag{2.56}$$

By a **mild solution** of (2.56), we mean a function $y \in C(\bar{I}; Z)$ which satisfies the following integral equation:

$$y(t) = e^{-tA} y_0 + \int_0^t e^{-(t-\tau)A} g(y(\tau)) d\tau, \tag{2.57}$$

where $A : Y \to X$, $A \in \mathcal{L}(Y; X)$, $-A$ is the generator of the strongly continuous analytic semigroup $\{e^{-tA} : t \geq 0\}$, on X, and the nonlinear term maps from $Z \subset X$ to X, see e.g., [102, Chapter 6.1].

2.4 Mathematical modeling of epidemics

The mathematical modeling of infectious diseases is a valuable tool for understanding a virus' spreading, estimating the number of individuals that will be infected, and seeing how different strategies can affect the disease's evolution. Even though the analysis of infectious disease data has centuries, the formal mathematical study of epidemics began in 1927 with the seminal work of Kermack and McKendrick in [78], where the basic compartmental model to describe a disease transmission was introduced. These models offer insights into the potential scale that an epidemic outbreak may cause.

Generally speaking, a model is a simplified description of a system that can help us understand it better. In this sense, mathematical modeling allows us to experiment without testing scenarios in the real world, which is valuable in the case of infectious diseases, where testing preventive strategies before a pandemic outbreak is impractical. There are different methods for modeling an infectious disease, each relying on different assumptions. In this work, we will focus on the study of compartmental models, with the Susceptible-Infectious-Recovered (SIR) model being its cornerstone. Nonetheless, it is important to acknowledge the diversity of models available, including stochastic compartmental models, agent-based models (ABMs), and network models. In what follows, we briefly summarize these approaches.

Deterministic compartmental model: In this model, the population is split into compartments representing the different disease stages, e.g., susceptible, infected, and removed. The basic idea is to describe how individuals go from one state to another using a coupled system of ordinary differential equations (ODEs). These models have in their formulation biological parameters that depend on the virus, e.g., the infectious and the recovery rates, which can be estimated from epidemiological data.

Stochastic compartmental models: These models incorporate stochasticity into the framework. Stochastic modeling is important when simulating epidemics in small populations or when the variability of the virus rates, e.g., transmission and recovery, impact the epidemic evolution [4]. In a stochastic framework, the transition probabilities of one compartment to another can be modeled by continuous-time Markov chains (CTMCs) or with stochastic differential equations (SDEs).

Both compartmental models, stochastic and deterministic, belong to a broader category: equation-based models designed for a homogeneous population, as they assume that all members within one compartment are identical. In their simplest form, these models are not computationally expensive. However, considering any additional population feature, such as age or socioeconomic status, requires adding additional equations to the system, making the model more complicated and challenging to solve and analyze.

Network models: These models represent the population as a network of interconnected nodes (individuals, groups, or compartments) and edges (contacts or interactions between nodes). They are powerful tools for understanding the transmission of infections in human populations due to their interactions. Different connectivity patterns between nodes can be considered to cover more and more realistic scenarios. We refer to [76, Chapter 7.6.2] for more details in this respect.

Agent-based models (ABMs): In contrast to the equation-based models, agent-based models intend to capture individual human behavior by representing every person as an *agent*. Relevant variables, such as mobility patterns, health, and socioeconomic status, are used to characterize every agent. ABM aims to capture the agents' interactions and comprehensively view a pandemic outbreak.

Although agent-based models can improve traditional epidemiological approaches because they provide additional information that is not available when using equation-based models, they require large amounts of data, such as mobility and social network data, which could not account for changes in behavior triggered by a pandemic or epidemic. Moreover, they are computationally expensive, requiring large amounts of memory and time; see, e.g., [59, 71].

2.4.1 Deterministic compartmental models

One of the simplest deterministic compartmental models is the SIR-type model. In this one, the population is divided into three compartments: susceptible (S), denoting the number of individuals who are susceptible to the disease; infected (I), which represents the number of infected individuals who can spread the disease by contact with the susceptible population; and removed (R), representing the population who has recovered from the disease and can not be infected again, or the individuals that have died as a consequence of the infection. One assumption of this model is that the size of the population (N) remains constant; that is, demographic factors such as births and deaths are not considered. Therefore, it holds that $N = S(t) + I(t) + R(t)$.

The SIR model is widely used to study the basic dynamics of spreading infectious disease and estimate critical epidemiological parameters, such as the reproduction num-

ber, representing the average number of secondary infections produced by a single infectious individual. Moreover, it serves as a foundation for more complex compartmental models, such as the SEIR or the SEIRD models, where the additional compartments E and D represent the exposed and dead populations, respectively.

In its simplest form, the SIR model depends on two parameters: the transmission rate (β) and the recovery rate (γ). The average infectious period is given by $\frac{1}{\gamma}$, and for most of the diseases, it can be estimated from epidemiological data [76]. Mathematically, the SIR model is described by the following system of ordinary differential equations:

$$\begin{aligned}\frac{dS}{dt} &= -\frac{\beta}{N}SI \\ \frac{dI}{dt} &= \frac{\beta}{N}SI - \gamma I \\ \frac{dR}{dt} &= \gamma I,\end{aligned}$$

where the initial conditions of the system are $S(0) > 0, I(0) > 0$, and $R(0) \geq 0$. Figure 2.3-(a) depicts the time evolution of the model variables with a population of $N = 1000$, 10 infected and 0 removed individuals at time $t = 0$. For the simulation, we consider the parameters $\beta = 0.25$ and $\gamma = 0.1$. As we can observe, the number of infected individuals grows fast at the beginning of the simulation, reaching a peak before starting to decrease; this is the natural behavior of an infectious disease evolution.

However, in a real-life outbreak, waiting for a large part of the population to become infected to mitigate the epidemic is impractical due to the infection's mortality rates. In most cases, governments impose measures to reduce infection. Studying how the peak of the infections will change considering different control strategies can be modeled by solving the SIR model with different values of the transmission rate parameter, see Figure 2.3-(b).

Basic and effective reproduction numbers

Despite its simplicity, the deterministic version of the SIR model can provide a basic description of epidemiological values, such as the *epidemic threshold* separating the epidemic states where it grows exponentially and where there is no disease transmission, see, e.g., [92]. This critical threshold is established according to the basic reproduction number R_0, which measures the average number of secondary infections generated by a single case, as follows: If $R_0 > 1$, the infection will continue growing, while if $R_0 < 1$, the infection should stop increasing.

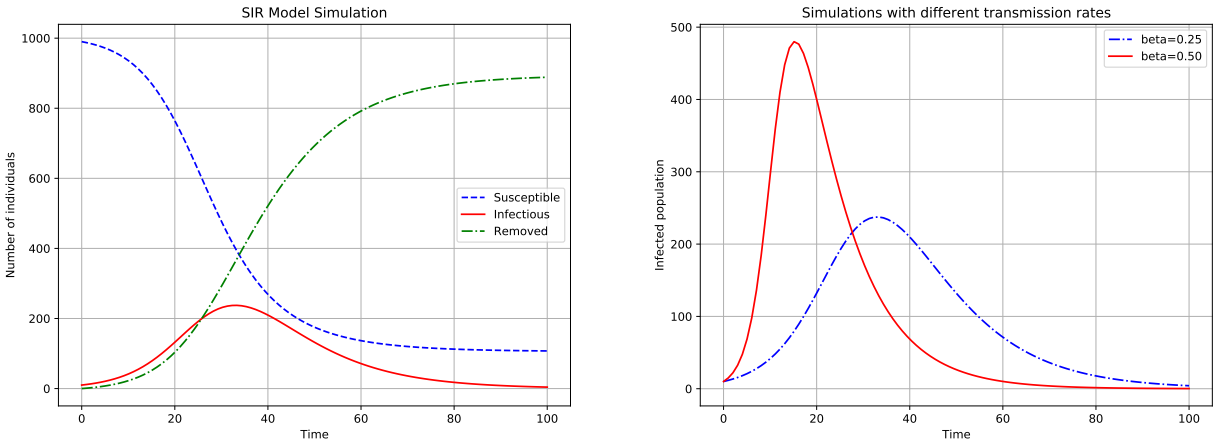

(a) (b)

Figure 2.3: (a) SIR model simulation. (b) Simulations of infected population curves with different transmission rates.

An infection will continue, considering the SIR model, if $\frac{dI}{dt} > 0$; equivalently,

$$\frac{\beta}{N} S(t)I(t) - \gamma I(t) > 0$$
$$\frac{\beta}{\gamma N} S(t)I(t) > I(t).$$

At the beginning of the epidemic, almost everyone is susceptible to infection, i.e., $S(0) \approx N$; consequently,

$$R_0 = \frac{\beta}{\gamma} > 1.$$

This estimate for the basic reproduction number depends on the same assumptions that the considered SIR model, i.e., a homogeneous mixing between susceptible and infectious individuals. On the other hand, since there are individuals transmitting the infection to very few others or not transmitting the infection at all and others who can be considered superspreaders, the assumption of homogeneity is not fulfilled [20]. In view of the latter, different ways to compute the basic reproduction number have emerged in order to obtain a more realistic value, which is also valid when considering more complex compartmental models; see, e.g., [41].

Assuming that the whole population is susceptible to a certain infection can be unrealistic since there can be positive cases that do not infect, e.g., due to previous or natural immunization. Consequently, the average number of secondary cases per infectious case will be lower than the basic reproduction number R_0. To consider the latter, a new quantity is introduced: the effective reproductive number R_e, defined as the average number of secondary cases per infectious case in a population where not all individuals are susceptible. It is estimated as the product of the basic reproductive

number and the fraction of the population that is susceptible at time t, that is,

$$R_e = R_0 \frac{S(t)}{N}.$$

Note that at $t = 0$, $R_e = R_0$, see e.g., [34]. Analogously, if $R_e > 1$, the number of cases will increase; this is the case during the epidemic outbreak. Likewise, if $R_e < 1$, there is a decrease in the number of cases.

When a novel or poorly known infection arrives, we generally do not have detailed information on the precise portion of susceptible, infected, and removed individuals in a population. To obtain an approximation of these quantities and a forecast of the epidemiological variables by solving the SIR model, we must find an estimation for the model parameters. One of the most widely used techniques to estimate an epidemiological model's parameters is the fitting technique, which involves building a function that *best fits* a set of observations. In this context, the best fit is the one that minimizes the distance between an obtained curve and the observations, which corresponds to a least square method; see, e.g., [33]. Nevertheless, this technique does not consider that observations should obey an epidemiological dynamic. Even more, the uncertainty in the data is not taken into account.

To cope with the aforementioned, more sophisticated techniques to solve the parameter estimation problem have been studied. In fact, in [52, 109], among others, it is investigated the use of variational data assimilation to optimally combine an epidemiological model with the observations to obtain accurate forecasts. In the upcoming chapters of this manuscript, we will use the variational data assimilation method to estimate model parameters in a compartmental epidemiological model.

Chapter 3

Linear Variational Data Assimilation Problems in Low Regularity Spaces

In various real-life applications, data assimilation methods are used in the reconstruction of the initial condition of an evolutive system. Depending on the application, this initial condition may not be regular or smooth. Likewise, solving a variational data assimilation problem requires a thorough analysis of the underlying PDE that models the phenomena wanted to be studied. The aforementioned can be challenging when dealing with low regularity in the initial conditions. On the other hand, any data assimilation process requires observable data acquired at specific points within the domain under investigation. What, in the problem's functional setting, means having solutions with continuity in the space variable. The latter makes it possible to consider pointwise evaluations of this solution on the space variable.

As a first approximation to study the $4D$-VAR problem in the infinite-dimensional setting, we consider a linear parabolic equation as constraint, that is,

$$\frac{\partial y}{\partial t} + Ay = 0, \quad y(0) = u, \tag{3.1}$$

with A being a second-order differential operator with sufficiently smooth coefficients. The well-posedness of equation (3.1) has been addressed by many authors. In fact, if the initial condition is taken in $H_0^1(\Omega)$, then equation (3.1) has a unique solution $y \in H^{2,1}(Q)$ (see, e.g., [83]). Moreover, via embedding results in the two- or three-dimensional case, we obtain that $y \in H^{2,1}(Q) \hookrightarrow L^2(0,T;C(\Omega))$, i.e., the continuity in the space for the solution variable is achieved. However, in order to guarantee an initial condition in such a regular space, it is necessary to add a regularization term in the cost functional, which means losing the L^2-norm natural framework of $4D$-VAR problems [29]. Likewise, if now we consider an initial condition belonging to $L^\infty(\Omega)$,

according to [107], the solution y of equation (3.1) belongs to

$$C(\bar{Q}_{\varepsilon,T}) = \{y \in L^2(Q) : y \text{ is continuous on } \bar{\Omega} \times [\varepsilon, T]\}$$

where $\varepsilon > 0$ and $\bar{Q}_{\varepsilon,T} = \bar{\Omega} \times [\varepsilon, T]$; therefore the solution y is continuous in almost the whole space-time cylinder; however, to obtain this regularity of the solution it is necessary to assume boundedness of the initial condition, which can be restrictive depending the nature of the application. Therefore, none of the cited previous contributions let us obtain simultaneously an initial condition belonging solely to a Lebesgue space $L^\beta(\Omega)$ (for given values of β), with a continuous on-space state variable y, and without modifying the $4D-$VAR cost functional.

We remark that, different from settings requiring initial conditions in $L^\infty(\Omega)$ or $H_0^1(\Omega)$, the $L^\beta(\Omega)$ framework offers advantages for handling low-regularity data. It provides a middle ground between dealing with potentially unbounded initial conditions with sharp spatial variations, which are often better characterized by L^β integrability than by pointwise L^∞-bounds, while aiming to retain the standard $L^2(\Omega)$ cost functional. This approach avoids the regularization typically needed for $H_0^1(\Omega)$ initial data. Furthermore, through suitable analytical tools, it allows for establishing the spatial continuity of the state variable y required for incorporating pointwise observations into the cost functional.

The setting described previously finds application, for instance, in data assimilation problems involving highly localized inputs. Examples include modeling abrupt events like a sudden pollutant release (see, e.g., [115]) or initializing numerical forecasts using radar observations of an intense, rapidly developing storm (see, e.g., [116]). In such scenarios, the initial condition (or the analysis increment applied to a background state) typically exhibits sharp peaks, large local magnitudes, and steep gradients over small regions, potentially approximating discontinuities. Observe that while physically bounded, the mathematical treatment of such localized features might have extremely large L^∞-norms. Additionally, this space might fail to capture the essential characteristics of the feature.

For the mathematical study of the theoretical problem we aimed to investigate, we will employ *maximal parabolic regularity* jointly with *real and complex interpolation embedding results*. The latter will let us study the data assimilation problem in its natural L^2-norm framework, with a continuous solution variable in the spatial domain. This approach will allow for a comprehensive treatment of pointwise-in-space observations and low-regular initial conditions. It is worth noting that incorporating pointwise observations in the cost functional results in an adjoint equation whose right-hand side belongs to the regular Borel measures space, as highlighted in [24], which, in turn, leads to a reduction in the regularity of the adjoint state.

The use of maximal parabolic regularity to study a state equation's well-posedness is not a novel concept. In fact, it has been used to address state constraints, semilinear, and quasilinear optimal control problems, as evidenced, in e.g., [19, 25, 48, 66, 68, 69, 93–96], among others. In this line, we start by mentioning the so-called *state constraint problems*, where the solution variable has pointwise upper and lower bounds for every $(x,t) \in Q$. Therefore, continuity of the state variable with respect to time and space is required. In [81], Krumbiegel and Rehberg studied the pointwise constraints on the control and the state of a semilinear parabolic problem by applying the concept of maximal parabolic regularity occurring in the underlying PDE. Likewise, we mention [26], where the maximal parabolic regularity of the heat equation has been used to analyze distributed optimal control problems where the control is in a measure space. Maximal parabolic regularity has been used even for quasilinear PDEs with mixed boundary conditions; see, e.g., [19, 25, 68, 69]; where under the setting of Meinlschmidt and Rehberg, in [95], the amount of regularity required for the state is guaranteed. In fact, continuity of the state variable is required not only in space but also in the time variable, which makes the interval where there exists some β such that A satisfies maximal parabolic regularity narrower than the one considered in this work. Consequently, while some of the analyses and calculations required to prove the well-posedness of our problem are similar to those in the cited contributions, they are not directly applicable to our specific setting. Likewise, it is worth mentioning that these works deal with distributed or boundary controls rather than controlling the initial condition itself, as in our case.

In this chapter, we investigate the linear variational data assimilation problem using the maximal parabolic regularity of the second-order differential operator. Although maximal parabolic regularity has been applied to more complex semilinear and quasilinear parabolic constraints, studying the linear case is crucial. It lays the groundwork for improving the solution's regularity of nonlinear constraints. We deal with this kind of problem in Chapter 4. We begin this chapter by setting the specific functional analytic framework and then examine the linear parabolic constraint with initial conditions in the integrable Lebesgue space $L^\beta(\Omega)$ for selected values of β. Utilizing the framework of maximal parabolic regularity, we establish the well-posedness of the data assimilation problem and justify the continuity of the solution in the spatial domain. Furthermore, we prove the existence of a solution to the minimization problem. The chapter concludes with the derivation of first-order optimality conditions, which, due to linearity, are also sufficient for optimality.

Functional setting

While Section 2.3 discussed maximal parabolic regularity for general Banach spaces X and Y, we now specialize this framework for the theoretical study of the variational data assimilation problem. Let $\Omega \subset \mathbb{R}^d$, with $d = 2$ or $d = 3$, be a bounded domain with boundary Γ. $Q = \Omega \times (0, T)$ denotes the space-time cylinder and $\Sigma = \Gamma \times (0, T)$ its lateral boundary.

In this chapter and the next, we will set $X = W^{-1,\beta}(\Omega)$ and $Y = W_0^{1,\beta}(\Omega)$, for some $\beta \in (1, \infty)$ to be specified later. We recall that $Y = W_0^{1,\beta}(\Omega)$ stands for the closure of $C_0^\infty(\Omega)$ in the $W^{1,\beta}(\Omega)$ norm. Denoting the conjugate exponent by β', it holds that $X = W^{-1,\beta}(\Omega)$ as the dual space of $W_0^{1,\beta'}(\Omega)$. With these choices, the dense and continuous embedding $W_0^{1,\beta}(\Omega) \overset{d}{\hookrightarrow} W^{-1,\beta}(\Omega)$ ensures that Assumption 2.1 holds.

The operator A that we will use throughout this and the next chapter is a linear elliptic second-order differential operator of the form:

$$A \colon W_0^{1,\beta}(\Omega) \longrightarrow W^{-1,\beta}(\Omega), \quad y \mapsto -\operatorname{div} k \nabla y \tag{3.2}$$

such that

$$\langle Ay, v \rangle = \int_\Omega k \nabla y \cdot \nabla v \, dx, \quad y \in W_0^{1,\beta}(\Omega), \quad v \in W_0^{1,\beta'}(\Omega).$$

Likewise, we agree on the following regularity assumptions:

Assumption 3.1.

1. *$\Omega \subset \mathbb{R}^d$, $d = 2, 3$, is a bounded domain with Lipschitz boundary $\Gamma := \partial\Omega$.*
2. *The coefficient function $k \in L^\infty(\Omega; \mathbb{R}^{d \times d})$ is uniformly elliptic and symmetric.*
3. *There exists $\beta \in \left]d, \frac{2d}{d-2}\right[$ such that the operator $A = -\operatorname{div} k\nabla$ forms a topological isomorphism from $W_0^{1,\beta}(\Omega)$ to $W^{-1,\beta}(\Omega)$.*
4. *We assume $r \in \left]\frac{4\beta}{3\beta - d}, 2\right[$ with $r' = \frac{r}{r-1}$ its conjugate exponent.*

From here on, Assumption 3.1 will be tacitly assumed without explicitly mentioning in the following. Note that in particular, Assumption 3.1 guarantees maximal parabolic regularity of A. We formalized this result in the following proposition. For its proof, we refer to [96, Lemma 6.4].

Proposition 3.1. *Let Assumption 3.1 hold. Then the operator $A \colon W_0^{1,\beta}(\Omega) \to W^{-1,\beta}(\Omega)$, defined by $A = -\operatorname{div} k\nabla$, satisfies maximal parabolic $L^r(I; W^{-1,\beta}(\Omega))$-regularity.*

Throughout this and the following chapter, we focus on pure homogeneous Dirichlet boundary conditions, denoted by the index 0 in $W_0^{1,\beta}$; consequently, we assume

$\Gamma_N = \emptyset$. This choice simplifies the analysis, particularly regarding the requirements on the parameter β, compared to settings involving mixed or pure Neumann boundary conditions (see, e.g., [81, Remark 2.8]). Treating cases where $\Gamma_N \neq \emptyset$ is also possible as long the isomorphism property on A also holds, which typically demands stronger assumptions on the domain's regularity. For discussions on various frameworks and conditions ensuring well-posedness under such alternative boundary settings, we refer to [19, 68, 81]. Nevertheless, we will comment on some known results about these more general boundary conditions.

- Let $\Gamma_N \neq \emptyset$ and $\Omega \cup \Gamma_N$ be regular in the sense of Gröger; see [64]. If there is $q_0 > d$ such that $-\nabla\kappa \cdot \nabla + 1 \colon W^{1,q}_{\Gamma_N}(\Omega) \to W^{-1,q}_{\Gamma_N}(\Omega)$ forms a topological isomorphism for all $q \in [q_0', q_0]$; cf. [81, Assumption 2.6]. Then the operator $A = -\nabla\kappa \cdot \nabla$ satisfies maximal parabolic regularity for $q \geq 2$ in the case $d = 2$ or $q \in [3, 6]$ in the case $d = 3$, cf. [81, Proposition 2.10].

- In dimension two, when considering mixed boundary conditions, if additionally to the Lipschitz condition on the domain, we assume that $\Omega \cup \Gamma_N$ is Gröger regular. Then, Assumption 3.1–2 is enough to imply the isomorphism property of the operator, $-\nabla \cdot \kappa\nabla + 1 \colon W^{1,q}_{\Gamma_N}(\Omega) \to W^{-1,q}_{\Gamma_N}(\Omega)$, for all $q \in [2, q_0]$, cf. [81, Proposition A.1]. Moreover, this range can be extended to cover more values of q, cf. [81, Corollary. A.2].

- The three-dimensional case is more involved. For instance, in [81, Proposition A.21], the authors state that if $\Omega \subset \mathbb{R}^3$ is strongly Lipschitz and $\kappa : \Omega \to \mathbb{R}^{3\times 3}$ is uniformly continuous in Ω_0 and $\Omega \backslash \bar{\Omega}_0$ with $\Omega_0 \subset \Omega$ a C^1– subdomain, then A forms a topological isomorphism for some $q > 3$.

- On the other hand, if Ω is convex and its boundary is of Lipschitz class, there exists a $\hat{q}$ with $\hat{q} > 4$ if $d = 2$ and $\hat{q} > 3$ if $d = 3$ such that $\Delta : W^{1,q}_0(\Omega) \to W^{-1,q}(\Omega)$ is an isomorphism for each $\hat{q}' < q < \hat{q}$, where $\frac{1}{\hat{q}'} + \frac{1}{\hat{q}} = 1$; see [26, Section 2.2].

Next, we provide a boundedness result of the analytic semigroup generated by $-A$.

Proposition 3.2. *Let Assumption 3.1 hold. Then, the operator $-A$ generates a strongly continuous analytic semigroup $\{e^{-tA}\}_{t\geq 0}$ on $W^{-1,\beta}(\Omega)$, which satisfies the following estimate*

$$\|e^{-tA}z\|_{L^\beta(\Omega)} \leq C\|z\|_{W^{-1,\beta}(\Omega)}, \qquad \text{for some } C > 0. \tag{3.3}$$

Proof. Since A satisfies maximal parabolic regularity due to Proposition 3.1, the result on Remark 2.5-2 guaratees that $-A$ generates the strongly continuous analytic semi-

group $\{e^{-tA}\}_{t\geq 0}$ on $W^{-1,\beta}(\Omega)$. Moreover, if we take $\alpha = \frac{1}{2}$ in Remark 2.5-4, then the analytic semigroup maps from $W^{-1,\beta}(\Omega)$ to $D(A^{1/2})$.

Observe that from [91, Corollary 11.5.3], $D(A^{1/2}) = (W^{-1,\beta}(\Omega), D(A))_{\frac{1}{2},1}$. Moreover, Proposition 2.4 guaratees $(W^{-1,\beta}(\Omega), D(A))_{\frac{1}{2},1} \hookrightarrow [W^{-1,\beta}(\Omega), D(A)]_{\frac{1}{2}}$, while from [14, Theorem 1.3] we know that $[W^{-1,\beta}(\Omega), W_0^{1,\beta}(\Omega)]_{\frac{1}{2}} = L^\beta(\Omega)$. Writing all together, it holds that

$$D(A^{1/2}) = (W^{-1,\beta}(\Omega), W_0^{1,\beta}(\Omega))_{\frac{1}{2},1} \hookrightarrow [W^{-1,\beta}(\Omega), W_0^{1,\beta}(\Omega)]_{\frac{1}{2}} = L^\beta(\Omega).$$

Consequently, there exists a positive constant c such that:

$$\|e^{-tA}z\|_{L^\beta(\Omega)} \leq c\|e^{-tA}z\|_{D(A^{1/2})} \leq c\|e^{-tA}\|_{\mathcal{L}(W^{-1,\beta}(\Omega),D(A^{1/2}))}\|z\|_{W^{-1,\beta}(\Omega)} \leq c\mathcal{M}\|z\|_{W^{-1,\beta}(\Omega)},$$

where $\|e^{-tA}\|_{\mathcal{L}(W^{-1\beta}(\Omega),D(A^{1/2}))} \leq \mathcal{M}$, the result follows taking $C := c\mathcal{M} > 0$. Observe that the latter lets us conclude that $e^{-tA} \in \mathcal{L}(W^{-1,\beta}(\Omega), L^\beta(\Omega))$ for every $t \in I$. □

The result of this proposition will be used in Chapter 4 to prove the existence of mild solutions for the semilinear equation and the non-homogeneous linearized equations.

Linear Variational Data Assimilation Problem

As a first approximation to study the infinite-dimensional $4D$-VAR formulation, we set the observation error covariance operators, R_i, and the observation operator, H, equal to the identity to simplify our analysis. Likewise, we consider the system model, M, as a linear parabolic PDE. Thus, the linear variational data assimilation problem we will study reads as follows:

$$\min_{u\in U_{ad}} J(y,u) = \frac{1}{2}\int_0^T \sum_k [y(x_k,t) - z_o(x_k,t)]^2 \, dt + \frac{1}{2}\|u - u_b\|^2_{B^{-1}} \tag{P}$$

subject to the linear system:

$$\begin{aligned} \frac{\partial y}{\partial t} + Ay &= \ell \quad \text{in } Q, \\ y &= 0 \quad \text{on } \Sigma, \\ y(x,0) &= u \quad \text{in } \Omega. \end{aligned} \tag{3.4}$$

For the data appearing in the cost functional (P), we make the following assumptions.

Assumption 3.2.

1. *For a given constant $b > 0$, the admissible set for the initial condition u is defined as*

$$U_{ad} = \left\{ u \in L^\beta(\Omega) : \int_\Omega |u(x)|^\beta dx \leq b \right\}. \tag{3.5}$$

2. *The number of observation points $N \in \mathbb{N}$ and the spatial observations points $x_1, \ldots, x_N \in \Omega$ are fixed. Additionally, z_o is assumed to be sufficiently regular, and $z_o(x_k, \cdot)$ represents an observation obtained at the spatial point x_k.*

3. *The terms $u_b \in L^2(\Omega)$ and $B^{-1} \in \mathcal{L}(L^2(\Omega), L^2(\Omega))$ are the background information and the inverse of the background error covariance operator, respectively. We assume that B^{-1} is a self-adjoint and positive definite operator, which defines a continuous and coercive bilinear form*

$$(u, v)_{B^{-1}} := \int_\Omega v(x)(B^{-1}u)(x)\ dx.$$

Furthermore, observe that $\|u - u_b\|^2_{B^{-1}} := \int_\Omega (u - u_b)B^{-1}(u - u_b)\ dx$.

Note that U_{ad} is a non-empty, closed, convex, and bounded subset of $L^\beta(\Omega)$. Imposing that kind of box constraint for the control variable is necessary to prove the existence of a solution for the data assimilation problem. It is, however, less restrictive than assuming boundedness of the initial condition, i.e., $u \in L^\infty(\Omega)$. Alternatively, to prove the existence of a solution for the data assimilation problem an L^β cost term could be added to the cost functional, which, however, will modify the typical L^2-energy in the cost functional.

Observe that the cost functional (P), involving pointwise evaluations $y(x_k, t)$, requires the spatial continuity of the state variable y. Before rigorously establishing this continuity property, let us illustrate the relevance of this setup with applications where observations are pointwise in space but effectively continuous in time. Consider, for instance, weather stations on land and buoys at sea, located at fixed points x_k. These stations record variables like temperature, pressure, wind speed, humidity, and sea surface temperature at very high frequencies (e.g., every minute or second). Although technically discrete, this sampling frequency is often much higher than the characteristic timescales of the atmospheric or oceanic features being modeled. Therefore, the data $z_o(x_k, t)$ can often be treated as continuous in time within the assimilation window $(0, T)$.

On the other hand, for applications where observations are available also at discrete time instances, the state variable y should be sufficiently regular, in both space and time, i.e., $y \in C(\bar{Q})$. One approach for dealing with this kind of problem in practice

includes a modification of the observation term in the cost functional (P), by including a temporal mollification, as done in [29].

3.1 Well-posedness of the linear equation

In this work, we consider an initial condition belonging to the space $L^\beta(\Omega)$ and exploit the regularity properties of the underlying PDE to fulfill the requirements of the problem, such that, continuity of the state variable in the spatial domain. This property is essential due to pointwise evaluations in space in the cost functional. In this line, it is important to mention the recent contribution [48], where the authors prove the $L^p(I; C^\alpha(\Omega))$ regularity of a linear diffusion equation with mix boundary conditions, where the initial condition only has $L^q(\Omega)$ regularity and where the right-hand side belongs to $L^r(I; L^q(\Omega))$, with $2 \leq r < \infty$. Observe that this result aligns with our problem constraint; however, using the maximal parabolic regularity of the second-order differential operator A, jointly with real and complex interpolation results, we will be able to obtain integrability in time and continuity in space of the state variable, even for less regular data on the right-hand side; see Theorem 3.1 below.

We prove the well-posedness of the state equation by using the maximal parabolic regularity of A. This approach has been used to guarantee the existence of solutions of quasilinear or state-constraint state equations; see, e.g., [19, 26, 68, 69, 81]. In some of these works, more than continuity in space is required. For instance, in [81], the authors studied an optimal control problem of a semilinear parabolic equation with pointwise state constraints; therefore, continuity in time and space is required. By using maximal parabolic regularity techniques and for adequate values of the exponents involved, it is proved that the state variable belongs to $C^\gamma(Q)$, with some $\gamma > 0$. Likewise, existence and regularity theory of quasilinear parabolic PDEs can be more involved, given that the amount of regularity required for the state is relatively high. Such regularity is guaranteed within the setting of [95]; see, e.g., [19, 68]. However, the latter will also require a more regular initial condition than the one we want to consider. Therefore, these previous results are not directly applicable, even though some of the calculations we will present are similar.

Observe that under our assumptions on β, there exists $r \in \left]\frac{4\beta}{3\beta-d}, 2\right[$ which is also greater than 1. This, jointly with embedding results, guarantees the well-posedness of the data assimilation problem constraint, as we will see in the following theorem.

Before starting the analysis, let us agree on the following notation that will be used in what follows:

$$\mathbb{W}_0^r := \mathbb{W}^r(W_0^{1,\beta}(\Omega), W^{-1,\beta}(\Omega)) \qquad \mathbb{W}_0^{r'} := \mathbb{W}^{r'}(W_0^{1,\beta'}(\Omega), W^{-1,\beta'}(\Omega)).$$

We recall that

$$\mathbb{W}^r(W_0^{1,\beta}(\Omega), W^{-1,\beta}(\Omega)) = W^{1,r}(I; W^{-1,\beta}(\Omega)) \cap L^r(I; W_0^{1,\beta}(\Omega))$$
$$\mathbb{W}^{r'}(W_0^{1,\beta'}(\Omega), W^{-1,\beta'}(\Omega)) = W^{1,r'}(I; W^{-1,\beta'}(\Omega)) \cap L^{r'}(I; W_0^{1,\beta'}(\Omega)).$$

Theorem 3.1. *Let Assumptions 3.1 and 3.2 hold. Then, Problem (3.4) is well-posed in the following sense: For each $\ell \in L^r(I; W^{-1,\beta}(\Omega))$ and $u \in L^\beta(\Omega)$, there exists a unique $y \in \mathbb{W}_0^r \hookrightarrow L^{r'}(I; C(\bar{\Omega}))$ solving equation (3.4). Additionally, this solution satisfies the following estimates:*

$$\|y\|_{\mathbb{W}_0^r} \leq c_1(\|\ell\|_{L^r(I;W^{-1,\beta}(\Omega))} + \|u\|_{L^\beta(\Omega)}), \tag{3.6a}$$
$$\|y\|_{L^{r'}(I;C(\bar{\Omega}))} \leq c_2(\|\ell\|_{L^r(I;W^{-1,\beta}(\Omega))} + \|u\|_{L^\beta(\Omega)}), \tag{3.6b}$$

for some constants $c_1, c_2 > 0$ independents of y, u, and ℓ.

Proof. First, note that taking β and r as assumed, it follows that $r' > 2$. Now, we start by proving the existence of a unique solution $y \in \mathbb{W}_0^r$ of Problem (3.4) for every $u \in L^\beta(\Omega)$ and $\ell \in L^r(I; W^{-1,\beta}(\Omega))$. In order to do that, due to Proposition 3.1, it suffices to show that $L^\beta(\Omega) \hookrightarrow (W^{-1,\beta}(\Omega), W_0^{1,\beta}(\Omega))_{1-\frac{1}{r},r}$. In fact, in [14, Theorem 1.3], it is guaranteed that

$$L^\beta(\Omega) = [W^{-1,\beta}(\Omega), W_0^{1,\beta}(\Omega)]_{\frac{1}{2}}. \tag{3.7}$$

Using (3.7) jointly with Proposition 2.4 yields

$$L^\beta(\Omega) = [W^{-1,\beta}(\Omega), W_0^{1,\beta}(\Omega)]_{\frac{1}{2}} \hookrightarrow (W^{-1,\beta}(\Omega), W_0^{1,\beta}(\Omega))_{\frac{1}{2},\infty}$$
$$\overset{d}{\hookrightarrow} (W^{-1,\beta}(\Omega), W_0^{1,\beta}(\Omega))_{\frac{1}{r'},1} \overset{d}{\hookrightarrow} (W^{-1,\beta}(\Omega), W_0^{1,\beta}(\Omega))_{1-\frac{1}{r},r},$$

where $\frac{1}{r'} = 1 - \frac{1}{r} < \frac{1}{2}$. Now, we have to show that y also belongs to $L^{r'}(I; C(\bar{\Omega}))$. From Proposition 2.6, it follows that

$$\mathbb{W}^r(W_0^{1,\beta}(\Omega), W^{-1,\beta}(\Omega)) \hookrightarrow L^{r'}\left(I; (W^{-1,\beta}(\Omega), W_0^{1,\beta}(\Omega))_{\theta,1}\right) \tag{3.8}$$

for all θ with $0 < \theta - \frac{1}{r'} < \frac{1}{r'} \leq 1$. Moreover, if $\gamma := 2\theta - 1 - \frac{d}{\beta}$ is positive, Proposition 2.4 and [117, Theorem 2.8.1] (jointly with Remark 2.4) guarantee

$$(W^{-1,\beta}(\Omega), W_0^{1,\beta}(\Omega))_{\theta,1} \overset{d}{\hookrightarrow} [W^{-1,\beta}(\Omega), W_0^{1,\beta}(\Omega)]_\theta \hookrightarrow C^\gamma(\bar{\Omega}) \hookrightarrow C(\bar{\Omega}). \tag{3.9}$$

Hence, we need to show that there is $\theta > 0$ such that

$$\frac{1}{r'} < \theta < 2 - \frac{2}{r} \leq 1 + \frac{1}{r'} \quad \text{and} \quad \theta > \frac{1}{2} + \frac{d}{2\beta}. \tag{3.10}$$

Note first that $\frac{2}{r'} = 2 - \frac{2}{r} \leq 1 + \frac{1}{r'}$ is satisfied since $r' > 2$. Moreover, since $\frac{1}{r'} < \frac{1}{2}$ and $\frac{1}{2} < \frac{1}{2} + \frac{d}{2\beta}$, to show that there exists θ such that (3.10) holds, it suffices to prove that

$$\frac{1}{2} + \frac{d}{2\beta} < 2 - \frac{2}{r}.$$

The last inequality is equivalent to

$$r > \frac{4\beta}{3\beta - d} = \frac{4}{3 - \frac{d}{\beta}}$$

which are exactly the values of r that we consider (see Assumption 3.1), thus from (3.8) and (3.9) the result holds. Finally, estimate (3.6a) is obtained from (2.51) and using the proved embedding $L^\beta(\Omega) \hookrightarrow (W^{-1,\beta}(\Omega), W_0^{1,\beta}(\Omega))_{1-\frac{1}{r},r}$. Likewise, estimate (3.6b) follows directly from (3.6a) and embedding $\mathbb{W}_0^r \hookrightarrow L^{r'}(I; C(\bar{\Omega}))$. □

Remark 3.1. *Our regularity assumptions allow us to work with initial conditions in $L^\beta(\Omega)$, where $d < \beta < \frac{2d}{d-2}$, and right-hand sides in $L^r(I; W^{-1,\beta}(\Omega))$, with $\frac{4\beta}{3\beta-d} < r < 2$. In comparison, the framework of [48] guarantees $L^p(I; C^\alpha(\Omega)$-regularity for initial conditions in $L^q(\Omega)$, and right-hand sides in $L^r(I; L^q(\Omega))$, with $r \geq 2$, $q > \frac{d}{2}$, and $p = \min(r, \tilde{p})$ with $\tilde{p} < \frac{2q}{d}$. Therefore, it allows for less regular initial conditions at the expense of requiring higher regularity of the right-hand sides and less time-regularity.*

3.1.1 Existence of a solution for the Data Assimilation problem

As a result of the well-posedness of the linear constraint, we can introduce the solution operator

$$S \colon L^\beta(\Omega) \to \mathbb{W}_0^r, \qquad u \mapsto Su = y,$$

where $y = Su$ represents the solution of the state equation (3.4).We recall that $y \in \mathbb{W}_0^r$ implies $y \in L^{r'}(I; C(\bar{\Omega}))$ by embeddings.

Moreover, from estimate (3.6a) and the fact that $\ell \in L^r(I; W^{-1,\beta}(\Omega))$ is given data, it holds that the linear operator S is also continuous. This is an important property, as it allows us to rewrite the optimization problem in its reduced form:

$$\min_{u \in U_{ad}} f(u) = \frac{1}{2} \int_0^T \sum_k [Su(x_k, t) - z_o(x_k, t)]^2 \, dt + \frac{1}{2} \|u - u_b\|_{B^{-1}}^2.$$

We recall that the data appearing in the cost functional satisfies Assumption 3.2. While the indices β and r satisfies Assumption 3.1, i.e., $\beta \in \left]d, \frac{2d}{d-2}\right[$ and $r \in \left]\frac{4\beta}{3\beta-d}, 2\right[$.

Pointwise-in-space observations at locations $x_k \in \Omega$ within the cost functional (P) can be represented using the Dirac measure δ_{x_k}. This measure defines a continuous

linear functional on $C(\bar{\Omega})$ via the evaluation map:

$$C(\bar{\Omega}) \ni \varphi \mapsto \delta_{x_k}\varphi = \langle \delta_{x_k}, \varphi \rangle = \varphi(x_k) \in \mathbb{R}.$$

Here, δ_{x_k} belongs to $\mathcal{M}(\Omega)$, the space of regular Boreal measures on Ω (the dual of $C(\bar{\Omega})$). Alternatively, the evaluation of φ at x_k can be expressed using integral notation as $\varphi(x_k) = \int_\Omega \varphi(x)\, d\delta_{x_k}(x)$. Likewise, for its latter use, we will denote the space of weakly measurable functions by $L^{r'}(I; \mathcal{M}(\Omega))$.

Using the pairing notation, the reduced cost functional takes the form:

$$\min_{u \in U_{ad}} f(u) = \frac{1}{2} \int_0^T \sum_k \langle \delta_{x_k}, Su(\cdot, t) - z_o(\cdot, t) \rangle^2 dt + \frac{1}{2} \|u - u_b\|^2_{B^{-1}}, \tag{3.11}$$

where, thanks to Theorem 3.1, $Su(\cdot, t)$ and $z_o(\cdot, t)$ possess sufficient spatial continuity for the evaluation pairing to be well-defined.

With the existence and regularity result of the state equation at hand, we can discuss the existence of solution of the optimization problem, as well as the characterization of the first-order optimality condition. First of all, we prove an existence result for the optimization problem. Its proof follows standard arguments and can be found, for instance, in [118, Theorem 2.14] in a slightly different functional analytic framework.

Theorem 3.2. *Let Assumptions 3.1 and 3.2 hold. Then, the data assimilation problem (3.11) admits a unique optimal solution $\bar{u} \in L^\beta(\Omega)$.*

Proof. The continuity of the operator S from $L^\beta(\Omega)$ to $\mathbb{W}^r_0$ and the continuity norm imply the continuity of the reduced cost functional. Hence, f is convex and continuous; therefore, f is weakly lower semicontinuous. This allows us to deduce an existence result in a classical way. In fact, since $f \geq 0$, there exists the infimum $j := \inf_{u \in U_{ad}} f(u) \in \mathbb{R}^+$. Let $\{u_n\}_{n \geq 1} \subset U_{ad}$ be a minimizing sequence. Since U_{ad} is weakly sequentially compact [118, Theorem 2.11], there exists a subsequence, denoted the same, and a limit $\bar{u} \in U_{ad}$ such that $u_n \rightharpoonup \bar{u}$ in U_{ad} as $n \to \infty$. From the weakly lower semicontinuity of f, we find $f(\bar{u}) \leq \liminf_{n \to \infty} f(u_n) = j$. Consequently, $\bar{u} \in U_{ad}$ is the solution of the data assimilation problem. Moreover, this solution is unique since the solution operator is linear, and the cost function is strictly convex due to the properties of B^{-1} present in the second term of the cost functional. □

3.2 First-order optimality conditions

In the linear and convex case, the study of the optimization problem requires proving first-order necessary - and due to convexity also sufficient - optimality conditions at

$\bar{u} \in U_{ad} \subset L^{\beta}(\Omega)$. To do that and prove the existence of Lagrange multipliers, we rewrite the reduced cost functional (3.11) in the following way:

$$\min f(u), \quad u \in L^{\beta}(\Omega) \quad \text{and} \quad \psi(u) \in K, \tag{3.12}$$

where

$$\psi \colon L^{\beta}(\Omega) \longrightarrow \mathbb{R}, \quad u \mapsto \psi(u) = b - \int_{\Omega} |u(x)|^{\beta} dx,$$

and $K = \{\kappa \in \mathbb{R} : \kappa \geq 0\}$ a closed and convex set of $\mathbb{R}$. Moreover, note that $L^{\beta}(\Omega) \ni u \mapsto \psi'(u) \in \mathcal{L}(L^{\beta}(\Omega), \mathbb{R})$, and

$$\psi'(u) \colon L^{\beta}(\Omega) \longrightarrow \mathbb{R}, \quad h \mapsto \psi'(u)h = -\int_{\Omega} \beta |u(x)|^{\beta-2} u(x) h(x) \, dx.$$

Problems of the type (3.12) were treated by Zowe and Kurcyusz (see, e.g., [125]), where after proving a regularity condition of the kind:

$$\psi'(\bar{u}) L^{\beta}(\Omega) - \mathcal{K}(\psi(\bar{u})) = \mathbb{R},$$

they obtain the existence of Lagrange multipliers. Note that due to our problem structure, these Lagrange multipliers will belong to $\mathbb{R}$. Before formulating the first-order optimality conditions, let us comment on the problem's adjoint equation.

3.2.1 Study of the adjoint equation

Due to the pointwise evaluations in the cost functional, the adjoint equation will have regular Borel measures on its right-hand side. In particular, we have:

$$\begin{aligned} -p_t + A^* p = & \sum_k \left[Su(x_k, \cdot) - z_o(x_k, \cdot) \right] \delta_{x_k} && \text{in } Q, \\ p = & \ 0 && \text{on } \Sigma, \\ p(x, T) = & \ 0 && \text{in } \Omega. \end{aligned} \tag{3.13}$$

Since A satisfies maximal parabolic $L^r(I; W^{-1,\beta}(\Omega))$-regularity, Lemma 2.4 guarantees that the adjoint operator A^* satisfies maximal parabolic $L^{r'}(I; W^{-1,\beta'}(\Omega))$-regularity. Therefore, to prove that the solution of the adjoint equation (3.13) belongs to $\mathbb{W}_0^{r'}$, it only remains to show that its right-hand side $\sum_k \left[Su(x_k, \cdot) - z_o(x_k, \cdot) \right] \delta_{x_k}$ is an element of $L^{r'}(I; W^{-1,\beta'}(\Omega))$. We will prove this result in the following lemma.

Lemma 3.1. *Let Assumptions 3.1 and 3.2 hold, and let $u \in L^{\beta}(\Omega)$ with associated state $y = Su \in \mathbb{W}_0^r \cap L^{r'}(I; C(\bar{\Omega}))$. Then, $\sum_k \left[Su(x_k, \cdot) - z_o(x_k, \cdot) \right] \delta_{x_k} \in L^{r'}(I; W^{-1,\beta'}(\Omega))$.*

Proof. Since z_o is given fixed data, and the sum in the right-hand side of (3.13) is finite, it is only necessary to show that $y(x_k,\cdot)\delta_{x_k} \in L^{r'}(I;W^{-1,\beta'}(\Omega))$. In fact, since $\beta > d$, it follows that $W_0^{1,\beta}(\Omega) \hookrightarrow C(\bar{\Omega})$ (see e.g. [21, Corollary 9.14]), and, therefore their corresponding dual spaces $(C(\bar{\Omega}))^*$, $(W_0^{1,\beta}(\Omega))^*$ identify with $\mathcal{M}(\Omega)$ and $W^{-1,\beta'}(\Omega)$, respectively, satisfy the embedding $\mathcal{M}(\Omega) \hookrightarrow W^{-1,\beta'}(\Omega)$. Consequently, $L^{r'}(I;\mathcal{M}(\Omega)) \hookrightarrow L^{r'}(I;W^{-1,\beta'}(\Omega))$. Additionally, from the norm definition in the weakly measurable space and using the last embedding, there exists a constant $c_1 > 0$ such that

$$
\begin{aligned}
&\|y(x_k,\cdot)\delta_{x_k}\|_{L^{r'}(I;W^{-1,\beta'}(\Omega))} \leq c_1 \|y(x_k,\cdot)\delta_{x_k}\|_{L^{r'}(I;\mathcal{M}(\Omega))} \\
&= c_1 \left(\int_0^T \left(\sup_{\substack{\|\varphi\|_\infty \leq 1 \\ \varphi \in C_0(\Omega)}} \langle \varphi, y(x_k,t)\delta_{x_k} \rangle \} \right)^{r'} dt \right)^{1/r'} \leq c_1 \left(\int_0^T \left(\sup_{\substack{\|\varphi\|_\infty \leq 1 \\ \varphi \in C_0(\Omega)}} \{ |\varphi(x_k) y(x_k,t)| \} \right)^{r'} dt \right)^{1/r'} \\
&\leq c_1 \left(\int_0^T |y(x_k,t)|^{r'} \left(\sup_{\substack{\|\varphi\|_\infty \leq 1 \\ \varphi \in C_0(\Omega)}} |\varphi(x_k)| \right)^{r'} dt \right)^{1/r'} \\
&\leq c_1 \left(\int_0^T |y(x_k,t)|^{r'} \, dt \right)^{1/r'} \leq c_1 \left(\int_0^T \|y(\cdot,t)\|_{C(\bar{\Omega})}^{r'} dt \right)^{1/r'} = c_1 \|y\|_{L^{r'}(I;C(\bar{\Omega}))}.
\end{aligned}
$$

Note that, due to Theorem 3.1, $\|y\|_{L^{r'}(I;C(\bar{\Omega}))}$ is finite and the assertion holds. □

Observe that we are considering the Dirac measure δ_{x_k} as an element of $W^{-1,\beta'}(\Omega)$, which is allowed since $\mathcal{M}(\Omega) \hookrightarrow W^{-1,\beta'}(\Omega)$ and $\delta_{x_k} \in \mathcal{M}(\Omega)$. Given that $W^{-1,\beta'}(\Omega)$ is a reflexive Banach space, it satisfies the Radon-Nikodym property (RNP); see, e.g., [43, Chapter III, Corollary 13]. Consequently, the weak measurability and the (Bochner) measurability coincide. The latter follows from the Pettis Measurability Theorem; see, e.g., [43, Chapter II, Theorem 2] combined with properties of RNP spaces (see, e.g., the theory developed in [43, Chapters II and III]).

Remark 3.2. *Since $r' > 2$, Proposition 2.4 jointly with [14, Theorem 1.3] yields*

$$
(W^{-1,\beta'}(\Omega), W_0^{1,\beta'}(\Omega))_{1-\frac{1}{r'},r'} \hookrightarrow [W^{-1,\beta'}(\Omega), W_0^{1,\beta'}(\Omega)]_{\frac{1}{2}} = L^{\beta'}(\Omega).
$$

Consequently, from Proposition 2.6-(ii), the following embedding is satisfied

$$
\mathbb{W}^{r'}(W_0^{1,\beta'}(\Omega), W^{-1,\beta'}(\Omega)) \hookrightarrow C(\bar{I}; L^{\beta'}(\Omega)).
$$

Therefore, the continuity of the adjoint state in the time variable holds, and the term $p(T)$ in the adjoint state makes sense.

With the results of the state and the adjoint equations, we will set the optimality conditions of the linear data assimilation problem.

3.2.2 Optimality conditions

Theorem 3.3. *Let Assumptions 3.1 and 3.2 hold. A control $\bar{u} \in U_{ad} \subset L^{\beta}(\Omega)$, solution of (3.12), with $\bar{y} = S\bar{u} \in \mathbb{W}_0^r$ its associated optimal state. Then, there exists a unique scalar Lagrange multiplier $\bar{\lambda} \geq 0$ and a unique adjoint state $\bar{p} \in \mathbb{W}_0^{r'}$ satisfying:*

State equation :

$$\begin{aligned} \bar{y}_t + A\bar{y} &= \ell \quad in\ Q, \\ \bar{y} &= 0 \quad on\ \Sigma, \\ \bar{y}(x,0) &= \bar{u} \quad in\ \Omega. \end{aligned} \tag{3.14a}$$

Adjoint equation :

$$\begin{aligned} -\bar{p}_t + A^*\bar{p} &= \sum_k \left[S\bar{u}(x_k,\cdot) - z_o(x_k,\cdot)\right]\delta_{x_k} \quad in\ Q, \\ \bar{p} &= 0 \quad on\ \Sigma, \\ \bar{p}(x,T) &= 0 \quad in\ \Omega. \end{aligned} \tag{3.14b}$$

Gradient equation :

$$\bar{p}(0) + B^{-1}(\bar{u} - u_b) + \bar{\lambda}\beta|\bar{u}|^{\beta-2}\bar{u} = 0 \ in\ \Omega. \tag{3.14c}$$

Complementarity System :

$$\bar{\lambda} \geq 0, \quad b - \int_\Omega |\bar{u}(x)|^{\beta} dx \geq 0, \quad \bar{\lambda}\left(b - \int_\Omega |\bar{u}(x)|^{\beta} dx\right) = 0. \tag{3.14d}$$

Proof. Note that the differentiability of the solution operator S follows since it is a linear and bounded operator. Consequently, by the chain rule, the reduced cost functional is also differentiable. Now, in order to prove the existence of a Lagrange multiplier $\bar{\lambda} \in \mathbb{R}$, we follow Zowe and Kurcyusz in [125, pp.50]. Therefore, we have to verify the following regularity condition:

$$\psi'(\bar{u})L^{\beta}(\Omega) - \mathcal{K}(\psi(\bar{u})) = \mathbb{R}, \tag{3.15}$$

where $\mathcal{K}(\psi(\bar{u})) = \{\kappa - \vartheta\psi(\bar{u}) : \kappa \in K, \vartheta \geq 0\}$. For our problem setting, the left-hand

side of (3.15) takes the form

$$\psi'(\bar{u})L^{\beta}(\Omega) - \mathcal{K}(\psi(\bar{u})) = \Big\{ \beta \int_{\Omega} |\bar{u}(x)|^{\beta-2}\bar{u}(x)h(x)dx - \kappa + \vartheta b - \vartheta \int_{\Omega} |\bar{u}(x)|^{\beta} dx : \\ h \in L^{\beta}(\Omega), \vartheta \geq 0, \kappa \geq 0 \Big\}.$$

To verify the regularity condition, let us take $z \in \mathbb{R}$. If $z \leq 0$, it will belong to $\psi'(\bar{u})L^{\beta}(\Omega) - \mathcal{K}(\psi(\bar{u}))$ by setting: $\vartheta = 0$, $h = 0 \in L^{\beta}(\Omega)$, and $\kappa = -z \geq 0$. In the same way, if $z \geq 0$, it will belong to $\psi'(\bar{u})L^{\beta}(\Omega) - \mathcal{K}(\psi(\bar{u}))$ if $\vartheta = \frac{z+\kappa}{b} \geq 0$, $\kappa \geq 0$, and $h(x) = \frac{\vartheta}{\beta}\bar{u}(x) \in L^{\beta}(\Omega)$. Consequently, condition (3.15) follows. Therefore, there exists a Lagrange multiplier $\bar{\lambda} \in \mathbb{R}$, such that:

$$\bar{\lambda} \geq 0, \tag{3.16a}$$

$$\bar{\lambda}\left(b - \int_{\Omega} |\bar{u}(x)|^{\beta} dx\right) = 0, \tag{3.16b}$$

$$\langle f'(\bar{u}) - \bar{\lambda}\psi'(\bar{u}), h\rangle_{L^{\beta'},L^{\beta}} = 0, \qquad \forall h \in L^{\beta}(\Omega). \tag{3.16c}$$

Moreover, since $\bar{u} \in L^{\beta}(\Omega)$ is the minimizer of problem (3.12), it satisfies the constraint, i.e., $\psi(\bar{u}) = b - \int_{\Omega} |\bar{u}(x)|^{\beta} dx \geq 0$. This fact jointly with (3.16a)-(3.16b), implies the complementarity system (3.14d). To prove the gradient equation (3.14c) we calculate the derivative of f at $\bar{u} \in U_{ad}$ in some direction $h \in L^{\beta}(\Omega)$. In fact, by the chain rule, we obtain

$$f'(\bar{u})h = \int_0^T \sum_k \delta_{x_k}[S\bar{u}(\cdot,t) - z_o(\cdot,t)]\delta_{x_k} S'(\bar{u})h(\cdot,t)\ dt + \int_{\Omega} (\bar{u}(x) - u_b(x))B^{-1}h\ dx,$$

and since S is linear, it holds that

$$\begin{aligned} f'(\bar{u})h &= \int_0^T \sum_k \delta_{x_k}[S\bar{u}(\cdot,t) - z_o(\cdot,t)]\delta_{x_k} Sh(\cdot,t)\ dt + \int_{\Omega} (\bar{u}(x) - u_b(x))B^{-1}h\ dx \\ &= \int_0^T \sum_k [S\bar{u}(x_k,t) - z_o(x_k,t)]\delta_{x_k} Sh(\cdot,t)\ dt + \int_{\Omega} (\bar{u}(x) - u_b(x))B^{-1}h\ dx. \end{aligned} \tag{3.17}$$

Note that due to Theorem 3.1 Sh belongs to $W^{1,r}(I; W^{-1,\beta}(\Omega)) \cap L^{r}(I; W_0^{1,\beta}(\Omega))$, then $Sh \in L^{r}(I; W_0^{1,\beta}(\Omega))$. Likewise, the term $\sum_k [S\bar{u}(x_k,\cdot) - z_o(x_k,\cdot)]\,\delta_{x_k}$ belongs to $L^{r'}(I; W^{-1,\beta'}(\Omega))$ due to Lemma 3.1, so that the integral (3.17) is well defined. Observe that the first term in the integral above corresponds to the right-hand side of the adjoint equation (3.14b). By replacing it in (3.17), we obtain

$$f'(\bar{u})h = \int_0^T \langle(-\partial_t + A^*)\bar{p}, Sh\rangle_{W^{-1,\beta'},W^{1,\beta}}\, dt + \int_{\Omega} (\bar{u}(x) - u_b(x))\, B^{-1}h\ dx.$$

Hereafter and since A^* satisfies maximal parabolic $L^{r'}(I;W^{-1,\beta'}(\Omega))$-regularity, it holds that the solution to the adjoint equation $\bar{p} \in \mathbb{W}_0^{r'}$ (see Lemma 2.4). Then, applying the Green's identity (2.53), and, taking into account equation (3.14b), the following is satisfied:

$$\begin{aligned} f'(\bar{u})h &= \int_0^T \langle \bar{p}, (\partial_t + A)Sh\rangle_{W^{1,\beta'},W^{-1,\beta}}\, dt + \langle \bar{p}(0), (Sh)(0)\rangle_{(W^{-1,\beta'},W^{1,\beta'})_{\frac{1}{r},r'},(W^{-1,\beta},W^{1,\beta})_{\frac{1}{r'},r}} \\ &\quad - \langle \bar{p}(T), (Sh)(T)\rangle_{(W^{-1,\beta'},W^{1,\beta'})_{\frac{1}{r},r'},(W^{-1,\beta},W^{1,\beta})_{\frac{1}{r'},r}} + \int_\Omega (\bar{u}(x) - u_b(x))\, B^{-1}h\, dx \\ &= \int_\Omega \left(\bar{p}(0) + (\bar{u} - u_b)B^{-1}\right) h\, dx, \end{aligned}$$

for all $h \in L^\beta(\Omega)$, since $(Sh)(0) = h$. Observe that $h \in L^\beta(\Omega) \hookrightarrow (W^{-1,\beta}(\Omega), W_0^{1,\beta}(\Omega))_{\frac{1}{r'},r}$ (see the proof of Theorem 3.1), and $\bar{p}(0) \in (W^{-1,\beta'}, W_0^{1,\beta'}(\Omega))_{\frac{1}{r},r'} \hookrightarrow L^{\beta'}(\Omega)$ (see Remark 3.2). Note that $\bar{p}(0) \in L^{\beta'}(\Omega)$ is well defined since $\mathbb{W}_0^{r'} \hookrightarrow C(\bar{I}; L^{\beta'}(\Omega))$. Inserting this and the form of ψ' into equation (3.16c) yields

$$\int_\Omega \left(\bar{p}(0) + (\bar{u} - u_b)B^{-1}\right) h(x)\, dx + \bar{\lambda}\beta \int_\Omega |\bar{u}(x)|^{\beta-2}\bar{u}(x)h(x)\, dx = 0, \qquad \forall h \in L^\beta(\Omega),$$

which corresponds to the weak formulation of (3.14c). Finally, since there is a unique optimal solution $\bar{u} \in L^\beta(\Omega)$ and the state and adjoint equations are well-posed, it holds that $\bar{p}(0)$ is also unique which help us prove the uniqueness of the Lagrange multiplier. Reasoning in cases, if $\bar{u} \neq 0$, then $\beta|\bar{u}|^{\beta-2}\bar{u} \neq 0$, from the gradient equation (3.14c), we can conclude the uniqueness of the Lagrange multiplier $\bar{\lambda} \in \mathbb{R}$. In fact, assuming that there exists $\lambda_1, \lambda_2 \in \mathbb{R}$ with $\lambda_1 \neq \lambda_2$ such that satisfies (3.14c), i.e.,

$$\begin{aligned} \bar{p}(0) + B^{-1}(\bar{u} - u_b) + \lambda_1\beta|\bar{u}|^{\beta-2}\bar{u} = 0 \text{ a.e } x \in \Omega \\ \bar{p}(0) + B^{-1}(\bar{u} - u_b) + \lambda_2\beta|\bar{u}|^{\beta-2}\bar{u} = 0 \text{ a.e } x \in \Omega. \end{aligned}$$

Subtracting both equations, it holds that $(\lambda_1 - \lambda_2)\beta|\bar{u}|^{\beta-2}\bar{u} = 0$. Given that $\beta|\bar{u}|^{\beta-2}\bar{u} \neq 0$ it must hold that $\lambda_1 = \lambda_2$. Consequently, in this case, the multiplier is unique. On the other hand, if $\bar{u} = 0$, then from (3.14d) and since $b > 0$, it holds that $\bar{\lambda} = 0$, that is, it is also unique in this case. □

Remark 3.3. *Observe that for the linear and convex case, the existence of the Slater point $u \equiv 0$ readily guarantees that the Slater constraint qualification holds. Consequently, there exists a non-negative Lagrange multiplier $\bar{\lambda}$ satisfying the necessary and sufficient optimality conditions.*

However, we opt for using the Zowe-Kurcyusz constraint qualification since it remains valid for the semilinear (and non-convex) problem, where Slater's condition can not be verified. This ensures a unified analytical approach suitable for both problem

types. On the other hand, the detailed verification of the Zowe-Kurcyusz constraint qualification for the linear problem, although potentially appearing over-elaborate here, provides a result that can be directly used when analyzing the more complex semilinear case.

Remarks of the chapter

As final remarks on this chapter, we would like to comment on the following:

- The analysis of the $4D$-VAR problem in functional spaces, without adding a regularization term, requires using maximal parabolic regularity theory.
- The pointwise nature of the observations (in space) leads to an optimality system with regular Borel measures. Proving the well-posedness of the adjoint equation will also require using the maximal parabolic regularity of operator A and its adjoint A^*.
- Due to the linearity and convexity of the problem, the necessary first-order optimality conditions are also sufficient. Therefore, the system above fully characterizes the optimal solution to the linear variational data assimilation problem.
- We do not carry on a numerical implementation of the data assimilation problem subject to a linear parabolic constraint since the numerical applications are not the focus of this chapter. Nevertheless, any numerical implementation, either with descent algorithms or optimization solvers, first needs to compute the problem's optimality conditions that we already characterized.
- The study of the well-posedness of the parabolic linear constraint is interesting itself. However, it becomes a key result when studying the existence and regularity of solutions when the problem's constraint is a nonlinear parabolic equation. We explore this case in the following chapter.

Chapter 4

Semilinear Variational Data Assimilation Problems in Low Regularity Spaces

The study of optimization problems with semilinear equations is more involved than those with linear ones. It requires additional analyses, such as studying the differentiability properties of the solution operator and ensuring the well-posedness of the linearized equation. Additionally, the pointwise observations present in the cost functional make the problem closely related to control problems with pointwise state constraints, further complicating the analysis, as shown in works such as [27, 81, 105].

This chapter aims to extend the results obtained for the linear case to the semilinear $4D$-VAR problem in the infinite-dimensional setting. Before detailing the specific problem setup, we highlight some applications where data assimilation for semilinear parabolic systems becomes crucial. This could happen when aspects of these systems are uncertain and observations are available to improve estimates or predictions. Consider, for instance, a chemical reaction-diffusion system for modeling the concentration $y_i(x,t)$ of a certain chemical. Often, the initial concentrations are poorly characterized. This system is typically described by equations of the form:

$$\frac{\partial y_i}{\partial t} - \nabla \cdot (\kappa_i \nabla y_i) = f_i(y_1, \ldots, y_n),$$

where the reaction terms f_i are typically nonlinear functions of the concentrations. Another relevant application is the contaminant transport modeling. In scenarios like chemical spills, the initial spatial distribution and magnitude of the contaminant, $y(x,0)$, are frequently unknown. The transport process can often be modeled using an

advection-diffusion-reaction equation for the concentration $y(x,t)$:

$$\frac{\partial y}{\partial t} + \mathbf{v} \cdot \nabla y - \nabla \cdot (\kappa \nabla y) = f(y),$$

where $\mathbf{v}$ is the advection velocity, and the term $f(y)$ can represent nonlinear decay processes.

The mathematical problem we aim to study in this chapter must fulfill the same requirements as those of the previous chapter: preserving low regularity in the initial condition and continuity in the space for the state variable, while keeping the L^2-norm in the cost functional. The first step in solving an optimal control problem with a semilinear constraint involves analyzing the well-posedness of the state equation, which has a solution for specific types of non-linearities, such as Lipschitz and bounded ones. However, even though such a solution exists, it may not have the desired regularity. Here, the well-posedness result proved in the linear case becomes crucial, as it allows us to improve the regularity of the solution using a boot-strapping argument.

The presence of non-linearities in the state equation complicates the derivation of the first-order optimality conditions, as well, particularly when studying the well-posedness of the adjoint equation in the corresponding spaces. In fact, for a given semilinear state equation, its adjoint operator is in general non-autonomous. Previous results on maximal parabolic regularity state that if an autonomous operator $A \in \mathcal{L}(Y, X)$ satisfies maximal parabolic regularity, then its adjoint operator $A^* \in \mathcal{L}(X^*, Y^*)$ (which is also autonomous) satisfies this property as well (see Lemma 2.4). However, this result does not directly extend to time-dependent operators. Consequently, we must prove by hand the well-posedness of our adjoint state.

In this chapter, we study the semilinear variational data assimilation problem in depth. In Section 4.1, we explore the properties of the superposition operators and the differentiability of the nonlinear term. The well-posedness of the semilinear state equation is also established here. We aim to obtain the same regularity for the semilinear state equation as for the linear case. In order to do that, we will use some known existence results to then improve its regularity by using the maximal parabolic regularity of the operator and a boot-strapping technique. In Section 4.2, we prove the differentiability of the solution operator S, which will be used in Section 4.3 in the derivation of the optimality conditions. In this section, we state the well-posedness of the adjoint equation. We conclude the chapter with some remarks.

Semilinear Data Assimilation Problem

Now we consider the non-linear variational data assimilation problem formed by the cost functional:

$$\min_{u\in U_{ad}} J(y,u) = \frac{1}{2}\int_0^T \sum_k [y(x_k,t) - z_o(x_k,t)]^2 \, dt + \frac{1}{2}\|u-u_b\|^2_{B^{-1}} \tag{P}$$

subject to the semilinear equation

$$\begin{aligned} \frac{\partial y}{\partial t} + Ay + g(y) &= 0 \quad \text{in } Q \\ y &= 0 \quad \text{on } \Sigma \\ y(x,0) &= u \quad \text{in } \Omega. \end{aligned} \tag{4.1}$$

Similar to the linear case, in the cost functional (P), each $z_o(x_k,\cdot)$ represents an observation obtained at x_k, $u_b \in L^2(\Omega)$ is the background information, and B^{-1} represents inverse of the background error covariance operator. The data terms are assumed to satisfy Assumption 3.2. Likewise, U_{ad}, given as in (3.5), represents the admissible set. For the sake of a simpler exposition and since the distributed term (present in the linear case) $\ell \in L^r(I;W^{-1,\beta}(\Omega))$ is not a control variable, we take $\ell = 0$. However, we pointed out that the results presented here can be extended to non-homogeneous right-hand sides. Considering, for instance, $\ell \in L^2(I;L^2(\Omega)) \hookrightarrow L^r(I;W^{-1,\beta}(\Omega))$, this regularity is sufficient to start our discussion of solutions of the semilinear equation in classical function spaces, following, e.g., [83, 118].

Our work focuses on analyzing the semilinear data assimilation problem, considering the initial condition in $u \in L^\beta(\Omega)$ and obtaining the same regularity of the state as the one in the linear case. In this sense, for the study of the semilinear problem, we will consider the functional analytical framework defined in Chapter 3. Furthermore, to prove well-posedness and differentiability results, we impose a set of assumptions over the non-linear term $g(y)$ (see Assumption 4.1 below) that allows us to apply existence results from [83, 118] as well as differentiability results on associated Nemytskii-operators from, e.g., [63].

Assumption 4.1.

1. *Let $g\colon \mathbb{R} \to \mathbb{R}$ be a measurable function. Moreover, g is twice differentiable and satisfies the boundedness condition of order 2; that is, there exists $\mathcal{K} > 0$ such that*

$$|g^{(k)}(\cdot)| \leq \mathcal{K}, \qquad \textit{for all } \ 0 \leq k \leq 2.$$

2. *Additionally, g' is globally Lipschitz continuous, i.e., there exists $L > 0$ such that*

$$|g'(y_1) - g'(y_2)| \leq L|y_1 - y_2|, \qquad \forall y_1, y_2 \in \mathbb{R}.$$

3. *g is monotone increasing, i.e., $g(y_1) \leq g(y_2)$ for all $y_1 \leq y_2$.*

Note that under these conditions, g is also globally Lipschitz. This follows using the boundedness of g' jointly with the mean value theorem.

A variety of functions satisfy Assumption 4.1. Examples include standard sigmoid-type functions such as $g(y) = a_1 \arctan(y) + a_2$ for constants $a_1 > 0$ and $a_2 \in \mathbb{R}$. Algebraic sigmoid-like functions, for instance $g(y) = \frac{b_1 y}{\sqrt{1+b_2^2 y^2}} + b_3$ with constants $b_1 > 0$, $b_2 \neq 0$, and $b_3 \in \mathbb{R}$, also fulfill the requirements. Furthermore, one can construct suitable examples using piecewise polynomials that smoothly transition between constant values for large positive and negative arguments while maintaining $\mathcal{C}^2$ regularity. Functions defined via integrals can also satisfy the assumption; specifically, the scaled error function $g(y) = \frac{2c_1}{\sqrt{\pi}} \int_0^{c_2 y} e^{-\tau^2} d\tau + c_3$, with constants $c_1 > 0$, $c_2 \neq 0$, and $c_3 \in \mathbb{R}$, meets all conditions of Assumption 4.1.

While the relevance of semilinear data assimilation problems was highlighted in the introduction, as well of some practice applications, we acknowledge that the specific conditions imposed on the nonlinear term g in Assumption 4.1 (such as global boundedness of its derivatives) can be restrictive compared to nonlinearities encountered in some real-life applications. These assumptions were, however, adopted since they are needed for rigorously establishing the well-posedness of the variational data assimilation problem within the theoretical framework of this work.

4.1 Analysis of the semilinear state equation

In this section, we discuss the well-posedness of equation (4.1) under Assumptions 3.1, 3.2, and 4.1. Let us first fix the following exponents

$$s = \frac{d\beta}{d+\beta}, \quad \tilde{s} = \frac{2s}{2-s}, \quad q = \frac{4\beta}{\beta - d}, \quad \tilde{q} = \frac{qr}{q-r} \tag{4.2}$$

where $\frac{1}{s} = \frac{1}{\tilde{s}} + \frac{1}{2}$ and $\frac{1}{r} = \frac{1}{\tilde{q}} + \frac{1}{q}$ and $\tilde{s} > s$, $\tilde{q} > r$. Observe, further that for $d = 2$, $\tilde{s} = \beta > 2$ and for $d = 3$, $\tilde{s} = \frac{6\beta}{6-\beta}$. The quantities in (4.2) satisfy:

$$\beta \geq s, \quad 1 \leq \tilde{q} \leq q, \tag{4.3a-b}$$

$$\beta > 2s > s, \quad \tilde{q} < q, \quad r < \tilde{q} < \frac{q}{2}, \quad q > r'. \tag{4.3c-f}$$

Additionally, let us fix some embeddings that will be used in what follows. In fact, from [21, Corollary 9.14] it holds that

$$L^s(\Omega) \hookrightarrow W^{-1,\beta}(\Omega), \qquad W_0^{1,\beta'}(\Omega) \hookrightarrow L^{s'}(\Omega) \tag{4.4}$$

Likewise from Propositions 2.6 and 2.4 in Section 2.3, and the proof of Theorem 3.1, the following embeddings hold

$$\begin{aligned} &\mathbb{W}_0^r \hookrightarrow L^q(I; L^\beta(\Omega)), \quad \mathbb{W}_0^r \hookrightarrow L^{r'}(I; L^p(\Omega)), \quad \forall p \leq \infty, \\ &\mathbb{W}_0^r \hookrightarrow L^{r'}(I; C(\bar{\Omega})), \quad \mathbb{W}_0^{r'} \hookrightarrow L^{r'}(I; L^\vartheta(\Omega)), \quad \forall \vartheta \leq \beta' \end{aligned} \tag{4.5}$$

We introduce the following Nemytskii operators associated with g, denoted by $\mathbf{g}$ and $\mathbf{G}$, and defined by

$$\begin{aligned} \mathbf{g}\colon L^\beta(\Omega) &\longrightarrow L^s(\Omega), & \mathbf{g}(z)(x) &= g(z(x)), \\ \mathbf{G}\colon L^q(I; L^\beta(\Omega)) &\longrightarrow L^{\tilde{q}}(I; L^s(\Omega)), & \mathbf{G}(w)(t) &= \mathbf{g}(w(t)). \end{aligned}$$

We can define Nemytskii operators generated by the first and second derivatives g' and g''. We denote these ones by $\mathbf{g}', \mathbf{g}''$ and $\mathbf{G}', \mathbf{G}''$, respectively. We will prove in Proposition 4.2 below that they correspond indeed to the derivatives of $\mathbf{g}$ and $\mathbf{G}$.

Next, we state some properties verified by the superposition operators, such as Lipschitz continuity and differentiability.

Proposition 4.1. *Let Assumptions 3.1, 3.2, and 4.1 hold, and let inequalities (4.3a-b) satisfy. Then, the Nemytskii operators* $\mathbf{g}$ *and* $\mathbf{G}$ *are globally Lipschitz, i.e., there exist positive constants* $\mathbf{L}_g$ *and* $\mathbf{L}_G$ *such that*

$$\|\mathbf{g}(z_1) - \mathbf{g}(z_2)\|_{L^s(\Omega)} \leq \mathbf{L}_g \|z_1 - z_2\|_{L^\beta(\Omega)}, \quad \forall z_1, z_2 \in L^\beta(\Omega), \tag{4.6a}$$

$$\|\mathbf{G}(w_1) - \mathbf{G}(w_2)\|_{L^{\tilde{q}}(I;L^s(\Omega))} \leq \mathbf{L}_G \|w_1 - w_2\|_{L^q(I;L^\beta(\Omega))}, \quad \forall w_1, w_2 \in L^q(I; L^\beta(\Omega)). \tag{4.6b}$$

Moreover, $\mathbf{g}$ *is Lipschitz from* $L^\beta(\Omega)$ *to* $W^{-1,\beta}(\Omega)$ *and* $\mathbf{G}$ *is Lipschitz from* $\mathbb{W}_0^r$ *to* $L^{\tilde{q}}(I; L^s(\Omega))$.

Proof. Given that g satisfies the uniformly boundedness and Lipschitz continuity, the proof of this result follows the lines of [118, Lemma 4.11], which consider an L^∞–setting, jointly with the final remark on [118, p.198], which let us extend this result to any L^p–space when the nonlinearity is uniformly bounded. In fact, the Lipschitz continuity of g with Lipschitz constant $L > 0$ yields

$$\|\mathbf{g}(z_1) - \mathbf{g}(z_2)\|_{L^s(\Omega)} = \left(\int_\Omega |g(z_1(x)) - g(z_2(x))|^s dx \right)^{\frac{1}{s}} \leq L \left(\int_\Omega |z_1(x) - z_2(x)|^s dx \right)^{\frac{1}{s}}.$$

that is $\|\mathbf{g}(z_1) - \mathbf{g}(z_2)\|_{L^s(\Omega)} \leq L\|z_1 - z_2\|_{L^s(\Omega)}$. However, since $s \leq \beta$, there exists a constant $c > 0$ such that $\|z_1 - z_2\|_{L^s(\Omega)} \leq c\|z_1 - z_2\|_{L^\beta(\Omega)}$. The result for $\mathbf{g}$ holds, taking $\mathbf{L}_g = cL > 0$.

Using the Lipschitz result of $\mathbf{g}$, we can obtain the Lipschitz continuity of $\mathbf{G}$,

$$\|\mathbf{G}(w_1) - \mathbf{G}(w_2)\|_{L^{\tilde{q}}(I;L^s(\Omega))} = \left(\int_0^T \|\mathbf{g}(w_1(t)) - \mathbf{g}(w_2(t))\|^{\tilde{q}}_{L^s(\Omega)} dt \right)^{\frac{1}{\tilde{q}}}$$
$$\leq \mathbf{L}_g \|w_1 - w_2\|_{L^{\tilde{q}}(I;L^\beta(\Omega))} \leq c_1 \mathbf{L}_g \|w_1 - w_2\|_{L^q(I;L^\beta(\Omega))} =: \mathbf{L}_G \|w_1 - w_2\|_{L^q(I;L^\beta(\Omega))},$$

for some $c_1 > 0$, which exists since $L^q(I; L^\beta(\Omega)) \hookrightarrow L^{\tilde{q}}(I; L^\beta(\Omega))$, given that $\tilde{q} \leq q$. To prove the results of $\mathbf{g}$ in $W^{-1,\beta}(\Omega)$ and of $\mathbf{G}$ in $\mathbb{W}_0^r$, we only need to apply embeddings (4.5) in the above. □

Due to the differentiability properties of $g\colon \mathbb{R} \to \mathbb{R}$ settled in Assumptions 4.1, the superposition operator $\mathbf{g}$ is Fréchet differentiable from $L^\beta(\Omega)$ to $L^s(\Omega)$ if $s < \beta$. Additionally, if $2s < \beta$, we can obtain a second-order differentiability result for $\mathbf{g}$, see e.g., [118, Section 4.9]. Likewise, we can prove first- and second-order differentiability of $\mathbf{G}$ if $\tilde{q} < q$ and $\tilde{q} < \frac{q}{2}$, respectively, where q and $\tilde{q}$ represent the indices in the time component of the Bochner spaces; see, e.g., [63]. We formalize these results in the following proposition.

Proposition 4.2. *Let Assumptions 3.1, 3.2, and 4.1 hold, and let inequalities (4.3c-f) satisfy. Then,*

(a) $\mathbf{g}$ *is Fréchet differentiable from* $L^\beta(\Omega)$ *to* $L^s(\Omega)$*, with* $(\mathbf{g}'(z)h)(x) = g'(z(x))h(x)$*, for a.e.* $x \in \Omega$*, and all* $h \in L^\beta(\Omega)$*. Additionally, for* $d = 2$*, if* $\beta > 4$*,* $\mathbf{g}$ *is twice Fréchet differentiable,* $\mathbf{g}''\colon L^\beta(\Omega) \to \mathcal{L}(L^\beta(\Omega), \mathcal{L}(L^\beta(\Omega), L^s(\Omega)))$*, where* $(\mathbf{g}''(z)[h_1, h_2])(x) = g''(z(x))h_1(x)h_2(x)$*, for a.e.* $x \in \Omega$*, and* $h_1, h_2 \in L^\beta(\Omega)$*.*

(b) $\mathbf{G}$ *is Fréchet differentiable,* $\mathbf{G}'\colon L^q(I; L^\beta(\Omega)) \to \mathcal{L}(L^q(I; L^\beta(\Omega)), L^{\tilde{q}}(I; L^s(\Omega)))$*, and its derivative is given by* $(\mathbf{G}'(w)k)(t) = \mathbf{g}'(w(t))k(t)$*,* $t \in I$ *and* $w, k \in L^q(I; L^\beta(\Omega))$*. Additionally, for* $d = 2$*,* $\mathbf{G}$ *is twice Fréchet differentiable,* $\mathbf{G}''$ *goes from* $L^q(I; L^\beta(\Omega))$ *to* $\mathcal{L}(L^q(I; L^\beta(\Omega)), \mathcal{L}(L^q(I; L^\beta(\Omega)), L^{\tilde{q}}(I; L^s(\Omega))))$ *and*

$$(\mathbf{G}''(w)[k_1, k_2])(t) = \mathbf{g}''(w(t))k_1(t)k_2(t), \quad t \in I, \quad w, k_1, k_2 \in L^q(I; L^\beta(\Omega)).$$

Proof. (*a*) The proof of the first-order differentiability of $\mathbf{g}$ follows the approach used in [118, Lemma 4.12], which establishes the differentiability of the Nemytskii operator in $L^\infty(\Omega)$. The uniform boundedness of g' allows this result to be extended to general L^p spaces, as discussed in [118, Section 4.3.3]. In fact, to state the first-order

differentiability result for our specific problem, we have to prove that for $h \in L^\beta(\Omega)$, it yields

$$\|\mathbf{g}(z+h) - \mathbf{g}(z) - \mathbf{g}'(z)h\|_{L^s(\Omega)} = o(\|h\|_{L^\beta(\Omega)}).$$

Since g' is uniformly bounded, $\mathbf{g}'(z(\cdot)) \in L^\infty(\Omega)$. Then, using a Hölder inequality, it can be proved that $\mathbf{g}'(z(\cdot))h \in L^s(\Omega)$. Moreover, a Taylor expansion yields

$$|g(z(x)+h(x)) - g(z(x)) - g'(z(x))h(x)| = |g''(z(x)+\gamma h(x))h(x)^2| \leq \mathcal{K}|h(x)^2|,$$

with $0 \leq \gamma \leq 1$ and $\mathcal{K}$ independent of x. Consequently,

$$\begin{aligned}
&\|\mathbf{g}(z+h) - \mathbf{g}(z) - \mathbf{g}'(z)h\|_{L^s(\Omega)} \leq \mathcal{K}\left(\int_\Omega |h(x)^2|^s dx\right)^{\frac{1}{s}} = \mathcal{K}\|h^2\|_{L^s(\Omega)} \\
&\leq \mathcal{K}\|h\|_{L^{\frac{\beta s}{\beta - s}}(\Omega)}\|h\|_{L^\beta(\Omega)} \leq c\mathcal{K}\|h\|^2_{L^\beta(\Omega)}, \qquad \text{for some } c > 0,
\end{aligned}$$

where the last inequalities follow by using a Hölder inequality with $\frac{1}{s} = \frac{1}{\beta} + \frac{\beta s}{\beta - s}$ and the embedding $L^\beta(\Omega) \hookrightarrow L^{\frac{\beta s}{\beta - s}}(\Omega)$, which holds given that $\beta > \frac{\beta s}{\beta - s}$. Consequently,

$$\frac{\|\mathbf{g}(z+h) - \mathbf{g}(z) - \mathbf{g}'(z)h\|_{L^s(\Omega)}}{\|h\|_{L^\beta(\Omega)}} \to 0 \quad \text{as} \quad \|h\|_{L^\beta(\Omega)} \to 0,$$

that is the first-order Fréchet differentiability of $\mathbf{g}$ holds.

The proof of the second-order differentiability of $\mathbf{g}$ follows the approach used in [118, Theorem 4.22], which establishes the differentiability result in $L^\infty(\Omega)$, and can be extended to L^p spaces, as discussed in [118, Section 4.9]. In fact, to prove the second-order differentiability of $\mathbf{g}$, in the case $d = 2$ and with $\beta > 4$, we have to prove first that the mapping $\mathbf{g}''(z) : h_1 \mapsto \mathbf{g}''(z)h_1$ defines a linear and continuous operator from $L^\beta(\Omega)$ to $\mathcal{L}(L^\beta(\Omega), L^s(\Omega))$. For h_1 and $h_2 \in L^\beta(\Omega)$, the last assertion holds using the uniform boundedness of g'', a Hölder inequality with the same exponents and embedding as before. In fact,

$$\begin{aligned}
&\|\mathbf{g}''(z)\|_{\mathcal{L}(L^\beta(\Omega),\mathcal{L}(L^\beta(\Omega),L^s(\Omega)))} = \sup_{\|h_1\|_{L^\beta(\Omega)}=\|h_2\|_{L^\beta(\Omega)}=1} \|\mathbf{g}''(y(t))h_1h_2\|_{L^s(\Omega)} \\
&\leq \mathcal{K} \sup_{\|h_1\|_{L^\beta(\Omega)}=\|h_2\|_{L^\beta(\Omega)}=1} \|h_1\|_{L^\beta(\Omega)}\|h_2\|_{L^{\frac{\beta s}{\beta - s}}(\Omega)} \leq c\mathcal{K}, \qquad \text{for some } c > 0.
\end{aligned}$$

Now, we have to show that the derivative of $\mathbf{g}'$ is given by $\mathbf{g}''$, that is,

$$\frac{\|\mathbf{g}'(z+h_1) - \mathbf{g}'(z) - \mathbf{g}''(z)h_1\|_{\mathcal{L}(L^\beta(\Omega),L^s(\Omega))}}{\|h_1\|_{L^\beta(\Omega)}} \to 0, \text{ as } \|h_1\|_{L^\beta(\Omega)} \to 0. \tag{4.7}$$

Proceeding as above, it can be proved that $\mathbf{g}''(z)h_1h_2 \in L^s(\Omega)$. Likewise, the

differentiability properties of g' yields

$$g'(z(x)+h_1(x))-g'(z(x))=g''(z(x))h_1(x)+r_{g'}(z(x),h_1(x)),\quad \text{for a.e.} x\in\Omega,$$

where $r_{g'}(z(x),h_1(x))$ denotes the remainder of g' at $z(x)$ in some direction $h_1(x)$. Besides, a Taylor expansion with integral remainder (see, e.g., [8, pp.15]) yields

$$g'(z(x)+h_1(x))-g'(z(x))=\int_0^1 g''(z(x)+\gamma h_1(x))h_1(x)d\gamma.$$

Comparing both representations of $g'(z(x)+h_1(x))$, we find that

$$r_{g'}(z(x),h_1(x))=\int_0^1 [g''(z(x)+\gamma h_1(x))-g''(z(x))]h_1(x)d\gamma,$$

then, from the Lipschitz continuity of g'' with constant $L>0$, it holds that

$$|r_{g'}(z(x),h(x))|\leq\int_0^1 L\gamma|h(x)|^2d\gamma=\frac{L}{2}|h(x)|^2,$$

and, consequently,

$$\begin{aligned}
&\|\mathbf{g}'(z+h_1)-\mathbf{g}'(z)-\mathbf{g}''(z)h_1\|_{\mathcal{L}(L^\beta(\Omega),L^s(\Omega))}\\
&=\sup_{\|h_2\|_{L^\beta(\Omega)}=1}\|(\mathbf{g}'(z+h_1)-\mathbf{g}'(z)-\mathbf{g}''(z)h_1)h_2\|_{L^s(\Omega)}\\
&\leq\sup_{\|h_2\|_{L^\beta(\Omega)}=1}\|(\mathbf{g}'(z+h_1)-\mathbf{g}'(z)-\mathbf{g}''(z)h_1)\|_{L^{\frac{\beta s}{\beta-s}}(\Omega)}\|h_2\|_{L^\beta(\Omega)}\\
&\leq\frac{L}{2}\left(\int_\Omega|h_1(x)^2|^{\frac{\beta s}{\beta-s}}dx\right)^{\frac{\beta-s}{\beta s}}=\frac{L}{2}\|h_1^2\|_{L^{\frac{\beta s}{\beta-s}}(\Omega)}\leq\frac{L}{2}\|h_1\|_{L^\beta(\Omega)}\|h_1\|_{L^{\frac{\beta s}{\beta-2s}}(\Omega)},
\end{aligned}$$

where the last follows by using a Hölder inequality. Moreover, since $\beta>2d$, it holds that $\frac{\beta s}{\beta-2s}<\beta$, and therefore, there exists a positive constant c, such that

$$\|\mathbf{g}'(z+h_1)-\mathbf{g}'(z)-\mathbf{g}''(z)h_1\|_{\mathcal{L}(L^\beta(\Omega),L^s(\Omega))}\leq\frac{Lc}{2}\|h_1\|^2_{L^\beta(\Omega)}.$$

Consequently, (4.7) holds, which proves the result.

(*b*) Given that $\tilde{q}<q$, [63, Theorem 7] yields the first order Fréchet derivative of $\mathbf{G}$. Moreover, since $2\tilde{q}<q$, then by using [63, Theorem 9], the second-order Fréchet derivative of $\mathbf{G}$ holds. We recall that the uniform boundedness of g' and g'' are required to apply Theorems 7 and 9 in [63], respectively. □

Observe that the second-order differentiability of $\mathbf{g}$ holds if $\beta>2d$. The latter excludes the case $d=3$ since it will imply $\beta>6$, which contradicts the assumptions

regarding the exponent β in Assumption 3.1.

Note that due to the strong assumptions on the nonlinearity g and its derivatives stated in Assumption 4.1, we can obtain Lipschitz results for the Nemytskii operators $\mathbf{g}'$ and $\mathbf{G}'$. We state this result in the following proposition.

Proposition 4.3. *Let Assumptions 3.1, 3.2, and 4.1 hold. Then the operators* $\mathbf{g}'$ *and* $\mathbf{G}'$ *are globally Lipschitz, i.e., there exist positive constants* $\mathbf{L}_{g'}$ *and* $\mathbf{L}_{G'}$ *such that*

$$\|\mathbf{g}'(z_1) - \mathbf{g}'(z_2)\|_{\mathcal{L}(L^\beta(\Omega),L^s(\Omega))} \leq \mathbf{L}_{g'}\|z_1 - z_2\|_{L^\beta(\Omega)}, \quad \forall z_1, z_2 \in L^\beta(\Omega). \tag{4.8a}$$

$$\|\mathbf{G}'(w_1) - \mathbf{G}'(w_2)\|_{\mathcal{L}(L^q(I;L^\beta(\Omega)),L^{\tilde{q}}(I;L^s(\Omega)))} \leq \mathbf{L}_{G'}\|w_1 - w_2\|_{L^q(I;L^\beta(\Omega))}, \tag{4.8b}$$

for all $w_1, w_2 \in L^q(I; L^\beta(\Omega))$.

Proof. The proof follows using the Lipschitz continuity of g' with Lipschitz constant $L_{g'} > 0$, jointly with a Hölder inequality, with indices $\frac{1}{s} = \frac{1}{\beta} + \frac{\beta - s}{\beta s}$. In fact,

$$\|\mathbf{g}'(z_1) - \mathbf{g}'(z_2)\|_{\mathcal{L}(L^\beta(\Omega),L^s(\Omega))} = \sup_{\|h\|_{L^\beta}=1} \|(\mathbf{g}'(z_1) - \mathbf{g}'(z_2))h\|_{L^s(\Omega)} \leq \|\mathbf{g}'(z_1) - \mathbf{g}'(z_2)\|_{L^{\frac{\beta s}{\beta - s}}(\Omega)}$$
$$\leq L_{g'}\left(\int_\Omega |z_1(x) - z_2(x)|^{\frac{\beta s}{\beta - s}} dx\right)^{\frac{\beta - s}{\beta s}} \leq c_1 L_{g'} L \|z_1 - z_2\|_{L^\beta(\Omega)}$$

for some $c_1 > 0$ which exists since $\frac{\beta s}{\beta - s} < \beta$ yields the embedding $L^\beta(\Omega) \hookrightarrow L^{\frac{\beta s}{\beta - s}}(\Omega)$. The result for $\mathbf{g}'$ holds taking $\mathbf{L}_{g'} = c_1 L_{g'} > 0$. Using the Lipschitz result of $\mathbf{g}'$, we obtain the Lipschitz continuity of $\mathbf{G}'$. In fact,

$$\|\mathbf{G}'(w_1) - \mathbf{G}'(w_2)\|_{\mathcal{L}(L^q(I;L^\beta(\Omega)),L^{\tilde{q}}(I;L^s(\Omega)))} = \sup_{\|k\|_{L^q(I;L^\beta(\Omega))}=1} \|(\mathbf{G}'(w_1) - \mathbf{G}'(w_2))k\|_{L^{\tilde{q}}(I;L^s(\Omega))}$$
$$\leq \sup_{\|k\|_{L^q(I;L^\beta(\Omega))}=1} \left(\int_0^T \|\mathbf{g}'(w_1(t)) - \mathbf{g}'(w_2(t))\|_{L^{\frac{\beta s}{\beta - s}}(\Omega)}^{\frac{\tilde{q}q}{q - \tilde{q}}} dt\right)^{\frac{q - \tilde{q}}{\tilde{q}q}} \|k\|_{L^q(I;L^\beta(\Omega))}$$
$$\leq \mathbf{L}_{g'}\left(\int_0^T \|w_1(t) - w_2(t)\|_{L^\beta(\Omega)}^{\frac{\tilde{q}q}{q - \tilde{q}}} dt\right)^{\frac{q - \tilde{q}}{\tilde{q}q}} = \mathbf{L}_{g'}\|w_1 - w_2\|_{L^{\frac{\tilde{q}q}{q - \tilde{q}}}(I;L^\beta(\Omega))}$$
$$\leq c_2 \mathbf{L}_{g'}\|w_1 - w_2\|_{L^q(I;L^\beta(\Omega))},$$

for some $c_2 > 0$, which exists since $L^q(I; L^\beta(\Omega)) \hookrightarrow L^{\frac{\tilde{q}q}{q - \tilde{q}}}(I; L^\beta(\Omega))$ given that $2\tilde{q} \leq q$. The result follows taking $\mathbf{L}_{G'} = c_2 \mathbf{L}_{g'} > 0$. □

4.1.1 Well-posedness of the semilinear equation

We will carry on the study of the well-posedness of the semilinear state equation as follows: We first rely on the properties of the operator $\mathbf{g}$, which let us apply existence results on a rather classical setting to obtain a weak solution; see, e.g., [83, 118]. Second, the required improved regularity is obtained via bootstrapping jointly with maximal parabolic regularity results obtained in the linear case. Before setting the existence result of the semilinear equation in the following theorem, let us recall the definition of weak solution of the semilinear equation in the classical setting (see, e.g., [118]). Let Assumption 4.1 hold, $y \in L^2(I; H_0^1(\Omega)) \cap L^\infty(I; L^2(\Omega))$ is said to be a weak solution of the semilinear equation (4.1) if

$$\iint_Q \left(-y\frac{\partial \varphi}{\partial t} + Ay\varphi\right) dxdt = \int_\Omega u\varphi(\cdot, 0)\ dx - \iint_Q g(y)\varphi\ dxdt, \tag{4.9}$$

for every $\varphi \in W_2^{1,1}(Q)$, such that $\varphi(x, T) = 0$. In what follows, we will refer to this notion of solution as weak solutions in the sense of Tröltzsch; see [118, Section 3.3]. So that we can differentiate this and the weak solution notion in the sense of Amann introduced in Definition 2.15.

Given the Assumptions over the nonlinearity, it is clear that equation (4.1) admits a unique weak solution (in the sense of Tröltzsch) that actually is a weak solution in

$$W(0, T) \hookrightarrow C(\bar{I}; L^2(\Omega)),$$

since $u \in L^\beta(\Omega) \hookrightarrow L^2(\Omega)$; see, e.g., [118, Lemma 5.3]. These results were proven in [118] for Neumann boundary conditions; however, they can be adapted for the homogeneous Dirichlet boundary case. Moreover, the solution fulfills

$$\|y\|_{L^2(I;H_0^1(\Omega))} + \|y\|_{C(\bar{I};L^2(\Omega))} + \|y\|_{H^1(I;H^{-1}(\Omega))} \leq c(1 + \|u\|_{L^2(\Omega)}), \tag{4.10}$$

for some positive constant c. Moreover, the solution of the semilinear equation (4.1) satisfies the additionally regularity

$$y \in \mathbb{W}_0^r \cap L^{r'}(I; C(\bar{\Omega})) \cap L^q(I; L^\beta(\Omega)).$$

We formalize this result in the following theorem.

Theorem 4.1. *Let Assumptions 3.1, 3.2, and 4.1 hold. For each $u \in L^\beta(\Omega)$, equation*

(4.1) *has a unique solution* $y \in \mathbb{W}_0^r$. *Additionally, the following estimates hold:*

$$\|y\|_{\mathbb{W}_0^r} \leq C_1(1 + \|u\|_{L^\beta(\Omega)}), \quad \text{for some } C_1 > 0, \tag{4.11}$$

$$\|y\|_{L^{r'}(I;C(\bar{\Omega}))} \leq C_2(1 + \|u\|_{L^\beta(\Omega)}), \quad \text{for some } C_2 > 0, \tag{4.12}$$

$$\|y\|_{L^q(I;L^\beta(\Omega))} \leq C_3(1 + \|u\|_{L^\beta(\Omega)}), \quad \text{for some } C_3 > 0, \tag{4.13}$$

where C_1, C_2, *and* C_3 *are independent of* y *and* u.

Proof. Since $u \in L^2(\Omega)$ due to $\beta > 2$, there exists a unique weak solution, in the sense of Tröltzsch, $y \in L^2(I; H_0^1(\Omega)) \cap L^\infty(I; L^2(\Omega))$ of the semilinear equation (4.1). Observe that for every $\varphi \in W_2^{1,1}(Q)$, this weak solution satisfies,

$$\int_0^T \langle(-\partial_t + A^*)\varphi(t), y(t)\rangle dt = \langle u, \varphi(0)\rangle - \int_0^T \langle \mathbf{g}(y(t)), \varphi(t)\rangle dt \ , \quad \forall \varphi \in W_2^{1,1}(Q). \tag{4.14}$$

To improve the regularity of the solution, we apply a boot-strapping argument to the following auxiliary linear problem

$$\frac{\partial \phi(t)}{\partial t} + A\phi(t) = -\mathbf{g}(y(t)), \quad \phi(x,0) = u. \tag{4.15}$$

To apply the maximal parabolic regularity of A and get a solution to the auxiliary problem (4.15) in the target space, it remains to prove that its right-hand side belongs to $L^r(I; W^{-1,\beta}(\Omega))$. The latter holds given the uniform boundedness of g, from where $\mathbf{G}(y)$ can be identified with an element in $L^2(I; L^2(\Omega)) \hookrightarrow L^r(I; W^{-1,\beta}(\Omega))$, where the embedding holds since $r < 2$ and $\beta > 2$. Therefore, we can apply Theorem 3.1 to guarantee the existence of a unique (strong) solution $\phi \in \mathbb{W}_0^r$ of equation (4.15). Note that Lemma 2.3 guarantees that the unique strong solution is also the weak solution (in the sense of Definition 2.15) of equation (4.15). Therefore, $\phi \in L^r(I; W_0^{1,\beta}(\Omega))$ satisfies

$$\begin{aligned}\int_0^T \langle(-\partial_t + A^*)\,\varphi(t), \phi(t)\rangle_{W^{-1,\beta'},W_0^{1,\beta}} dt = \int_0^T \langle \varphi(t), -\mathbf{g}(y(t))\rangle_{W_0^{1,\beta'},W^{-1,\beta}} dt \\ + \langle \varphi(0), u\rangle_{(W^{-1,\beta'},W_0^{1,\beta'})_{\frac{1}{r},r',(W^{-1,\beta},W_0^{1,\beta})_{\frac{1}{r'},r}}}, \quad \forall \varphi \in \mathcal{D}([0,T[; W_0^{1,\beta'}(\Omega)).\end{aligned} \tag{4.16}$$

Moreover, (4.15) has a unique weak solution, in the sense of Tröltzsch, $\phi \in L^2(I; H_0^1(\Omega)) \cap L^\infty(I; L^2(\Omega))$ satisfying

$$\int_0^T \langle(-\partial_t + A^*)\varphi(t), \phi(t)\rangle dt = \langle u, \varphi(0)\rangle - \int_0^T \langle \mathbf{g}(y(t)), \varphi(t)\rangle dt.$$

Observe that the last equation and (4.14) have the same right-hand side. Therefore, ϕ is a weak solution (in the sense of Tröltzsch) of the equation (4.1), and consequently $y =$

$\phi \in L^2(I; H_0^1(\Omega)) \cap L^\infty(I; L^2(\Omega))$. Observe that to conclude the result, it only remains to prove that $y = \phi \in L^r(I; W_0^{1,\beta}(\Omega))$, which follows since $2 < r$, $y = \phi \in L^r(I; H_0^1(\Omega))$, and $\phi \in L^r(I; W_0^{1,\beta}(\Omega))$. Then, $y \in L^r(I; W_0^{1,\beta}(\Omega))$ is the unique weak solution (in the sense of Definition 2.15), and consequently, $y \in \mathbb{W}_0^r$ solves the semilinear equation.

Estimate (4.11) follows from (2.51) in Theorem 3.1 applied to (4.15). In fact, given that $L^q(I; L^s(\Omega)) \hookrightarrow L^r(I; W^{-1,\beta}(\Omega))$, we obtain:

$$\|y\|_{\mathbb{W}_0^r} \leq c \left(\|\mathbf{G}(y)\|_{L^r(I;W^{-1,\beta}(\Omega))} + \|u\|_{L^\beta(\Omega)} \right) \leq c_1 \|\mathbf{G}(y)\|_{L^q(I;L^s(\Omega))} + c\|u\|_{L^\beta(\Omega)}$$

for positive constants c and c_1. The result holds, given that $\|\mathbf{G}(y)\|_{L^q(I;L^s(\Omega))} \leq \mathcal{K}_1$ for some $\mathcal{K}_1 > 0$ which exist due to the uniformly boundedness of the nonlinearity. Estimates (4.12) and (4.13) follow directly using (4.11) and embeddings in (4.5). □

In Theorem 4.1, we have used established existence results for *weak solutions* of linear and semilinear parabolic equations, as discussed in [118] and [83], among others. An alternative approach involves initially finding a *mild solution* for the semilinear equation. The existence of such mild solutions is explored in works like [56, 57, 102]. Similar to our methodology, the regularity of the solution is then improved through a bootstrapping argument. In this scenario, it is necessary to consider the properties of the strongly continuous semigroup generated by $-A$, which holds given that A satisfies maximal parabolic regularity. We refer to [96], where the authors use this alternative approach (by using mild solutions) to establish the well-posedness of a semilinear parabolic state equation. To make this result clear, we write here its proof for a possibly nonhomogeneous right-hand side.

Lemma 4.1. *Let Assumptions 3.1, 3.2, and 4.1 hold. For all $u \in L^\beta(\Omega)$ and $\ell \in L^r(I; W^{-1,\beta}(\Omega))$, there exists a unique mild solution $y \in C(\bar{I}; L^\beta(\Omega))$ of the semilinear equation:*

$$\frac{\partial y(t)}{\partial t} + Ay(t) + \mathbf{g}(y(t)) = \ell(t), \quad y(x,0) = u. \tag{4.17}$$

Proof. Let us define the Picard iterations as:

$$\begin{cases} y_0(t) & = u \\ y_{k+1}(t) & = e^{-tA} + \displaystyle\int_0^t e^{-(t-\tau)A}(\ell(\tau) - \mathbf{g}(y_k(\tau)))d\tau. \end{cases}$$

Taking $t_0 = 0$ and assuming that $y_k(t)$ is defined in $I_\alpha := [t_0, t_0 + \alpha]$, for some $\alpha > 0$, we will prove that the mapping $\mathcal{J}$,

$$(\mathcal{J}y_{k+1})(t) = e^{-tA}u + \int_0^t e^{-(t-\tau)A}(\ell(\tau) - \mathbf{g}(y_k(\tau)))d\tau,$$

is a contraction in I_α. In fact, the Lipschitz continuity of $\mathbf{g}$ with Lipschitz constant $\mathbf{L}_g$ and Proposition 2.5 yield

$$\begin{aligned}
&\|\mathcal{J}y_{k+1}(t) - \mathcal{J}y_k(t)\|_{L^\beta(\Omega)} \\
&\leq \int_0^t \|e^{-(t-\tau)A}\|_{\mathcal{L}(W^{-1,\beta}(\Omega),L^\beta(\Omega))}\|\mathbf{g}(y_k(\tau)) - \mathbf{g}(y_{k-1}(\tau))\|_{W^{-1,\beta}(\Omega)}d\tau \\
&\leq \mathcal{M}\mathbf{L}_g \int_0^t \|y_k(\tau) - y_{k-1}(\tau)\|_{L^\beta(\Omega)} \leq \mathcal{M}\mathbf{L}_g\alpha\|y_k - y_{k-1}\|_{C(I_\alpha;L^\beta(\Omega))}.
\end{aligned}$$

Taking $\alpha < \frac{1}{\mathcal{M}\mathbf{L}_g}$, the operator $\mathcal{J}$ is a contraction in I_α. Then, $\mathcal{J}$ has a unique fix point $y \in C(I_\alpha; L^\beta(\Omega))$ such that

$$y(t) = e^{-tA}u + \int_0^t e^{-(t-\tau)A}(\ell(\tau) - \mathbf{g}(y(\tau)))d\tau, \quad t_0 \leq t \leq t_0 + \alpha. \tag{4.18}$$

Observe that this solution can be extended for $t \in [\underbrace{t_0 + \alpha}_{t_1}, t_1 + \alpha_1] =: I_{\alpha_1}$, for adequate values of $\alpha_1 > 0$. By repeating this procedure iteratively, a concatenation argument yields a solution $y \in C(\bar{I}; L^\beta(\Omega))$ satisfying (4.18). □

4.1.2 Continuity of the solution operator S

Based on Theorem 4.1, we introduce the solution operator

$$S\colon L^\beta(\Omega) \longrightarrow \mathbb{W}_0^r, \quad u \mapsto S(u) = y,$$

as the solution operator associated with the semilinear parabolic problem (4.1). Note that, from Theorem 4.1, the solution y has improved regularity, including $L^{r'}(I; C(\bar{\Omega}))$ and $L^q(I; L^\beta(\Omega))$, which holds by embedding results. Moreover, although we use the same notation as in the linear case, in this chapter, the operator S specifically refers to the solution operator for the semilinear PDE. This operator satisfies continuity properties, which will be set in the following lemmas.

Lemma 4.2. *Let Assumptions 3.1, 3.2, and 4.1 hold. The solution operator S is Lipschitz continuous, i.e., there exist positive constants $\mathbf{L}_{s_1}$ and $\mathbf{L}_{s_2}$ such that*

$$\|S(u_1) - S(u_2)\|_{L^2(I;H_0^1(\Omega))} + \|S(u_1) - S(u_2)\|_{C(\bar{I};L^2(\Omega))} \leq \mathbf{L}_{s_1}\|u_1 - u_2\|_{L^2(\Omega)}, \tag{4.19a}$$

for all $u_1, u_2 \in L^2(\Omega)$. Additionally,

$$\|S(u_1) - S(u_2)\|_{\mathbb{W}_0^r} \leq \mathbf{L}_{s_2}\|u_1 - u_2\|_{L^\beta(\Omega)}, \qquad \forall u_1, u_2 \in L^\beta(\Omega). \tag{4.19b}$$

Proof. Let us denote $y_i = S(u_i)$, the states associates with $u_i \in L^\beta(\Omega)$, $i = 1, 2$.

Observe that y_1 and y_2 satisfy the regularity properties from Theorem 4.1. We find that the difference $\hat{y} = y_1 - y_2$ satisfies

$$\frac{\partial \hat{y}(t)}{\partial t} + A\hat{y}(t) = \mathbf{g}(y_2(t)) - \mathbf{g}(y_1(t)), \quad \hat{y}(x,0) = u_1 - u_2, \tag{4.20}$$

where for each $t \in I$, the right-hand side of equation (4.20) can be written as:

$$\mathbf{g}(y_2(t)) - \mathbf{g}(y_1(t)) = \left(\int_0^1 \mathbf{g}'(y_1(t) + \tau(y_2(t) - y_1(t)))d\tau \right) (y_2(t) - y_1(t)) := -g_0(t)\hat{y}(t).$$

Due to the boundedness of g', $g_0(t) \in L^\infty(\Omega)$, and consequently, $g_0 \in L^\infty(I; L^\infty(\Omega))$, which implies that $g_0 \in L^\rho(I; L^v(\Omega))$ for any $\rho, v \geq 1$. Moreover, since $u_1 - u_2 \in L^2(\Omega)$, and taking, in particular, $\rho = 2$ and $v = d$, which satisfy

$$\frac{1}{\rho} + \frac{2}{2v} = 1,$$

Theorem 4.1 in [83, Theorem III.4.1] implies that $\hat{y} \in L^2(I; H_0^1(\Omega)) \cap L^\infty(I; L^2(\Omega))$ solves:

$$\frac{\partial \hat{y}}{\partial t} + A\hat{y} + g_0\hat{y} = 0, \quad \hat{y}(0) = u_1 - u_2. \tag{4.21}$$

Moreover, from [83, Theorem III.2.1], there exists a constant $L_1 > 0$, depending on the uniform bound of g_0 proving (4.19a). We can now argue similar to Theorem 4.1. Since $u_1 - u_2 \in L^\beta(\Omega)$ and the right-hand side of (4.20) belongs to $L^r(I; W^{-1,\beta}(\Omega))$, we apply Theorem 3.1 to obtain $\hat{y} \in \mathbb{W}_0^r$. Estimate (2.51) and the Lipschitz continuity of $\mathbf{G}$ in $L^r(I; L^\beta(\Omega))$ along with $L^\beta(\Omega) \hookrightarrow W^{-1,\beta}(\Omega)$ yield

$$\begin{aligned}
\|\hat{y}\|_{\mathbb{W}_0^r} &\leq c \left(\|\mathbf{G}(y_1) - \mathbf{G}(y_2)\|_{L^r(I;W^{-1,\beta}(\Omega))} + \|u_1 - u_2\|_{L^\beta(\Omega)} \right) \\
&\leq c \left(\|y_1 - y_2\|_{L^r(I;L^\beta(\Omega))} + \|u_1 - u_2\|_{L^\beta(\Omega)} \right) \\
&\leq c \left(\|y_1 - y_2\|_{L^2(I;H_0^1(\Omega))} + \|u_1 - u_2\|_{L^\beta(\Omega)} \right) \leq c\|u_1 - u_2\|_{L^\beta(\Omega)},
\end{aligned}$$

for some $c > 0$. Note that we used (4.19a) along with $r < 2$ and $H_0^1(\Omega) \hookrightarrow L^\beta(\Omega)$ and $\beta < 2d \leq 6$. □

Next, we prove the weak continuity of the solution operator S. We state and prove this result in the following Lemma; for its proof in a slightly different analytic framework, we refer to [96].

Lemma 4.3. *Let Assumptions 3.1, 3.2, and 4.1 hold. Then, the solution operator S is weakly continuous from $L^\beta(\Omega)$ to $\mathbb{W}_0^r$.*

Proof. Let $u_n \rightharpoonup u$ in $L^\beta(\Omega)$ and set $y_n = S(u_n)$ and $y = S(u)$. Thanks to estimate

(4.11) and the boundedness of $\{u_n\}_{n\geq 1}$ in $L^\beta(\Omega)$, there exists a constant $C > 0$ such that $\|y_n\|_{\mathbb{W}_0^r} \leq C$, for all $n \in \mathbb{N}$. Consequently, due to the reflexivity of $\mathbb{W}_0^r$, there exists a weakly convergent subsequence, denoted the same, and a limit point $\tilde{y} \in \mathbb{W}_0^r$ such that $y_n \rightharpoonup \tilde{y}$ in $\mathbb{W}_0^r$, as $n \to \infty$. Additionally, since $\{y_n\}_{n\geq 1}$ is bounded in $L^r(I; W^{1,\beta}(\Omega))$ and $\left\{\frac{\partial y_n}{\partial t}\right\}_{n\geq 1}$ is bounded in $L^r(I; W^{-1,\beta}(\Omega)) \hookrightarrow L^1(I; W^{-1,\beta}(\Omega))$, it holds that $\{y_n\}_{n\geq 1}$ is relatively compact in $L^r(I; L^\beta(\Omega))$ [114, Corollary 4]. Consequently, $y_n \to \tilde{y}$ strongly in $L^r(I; L^\beta(\Omega))$. Further, thanks to the Lipschitz continuity of $\mathbf{g}(y(\cdot))$, $\mathbf{g}(y_n(\cdot)) \to \mathbf{g}(\tilde{y}(\cdot))$ strongly in $L^r(I; W^{-1,\beta}(\Omega))$. On the other hand, since $y_n \in \mathbb{W}_0^r$ is the unique solution of the following equation

$$\begin{aligned} \frac{\partial y_n}{\partial t} + Ay_n + g(y_n(t)) &= 0 \\ y_n(0) &= u_n, \end{aligned} \tag{4.22}$$

then, for any $n \in \mathbb{N}$, y_n satisfies the weak formulation:

$$\begin{aligned} \int_0^T \langle (-\partial_t + A^*)\,\varphi, y_n(t)\rangle_{W^{-1,\beta'},W_0^{1,\beta}} dt = \int_0^T \langle \varphi, \mathbf{g}(y_n(t))\rangle_{W_0^{1,\beta'},W^{-1,\beta}} dt \\ + \langle \varphi(0), u_n\rangle_{(W^{-1,\beta'},W_0^{1,\beta'})_{\frac{1}{r},r'},(W^{-1,\beta},W_0^{1,\beta})_{\frac{1}{r'},r}} \quad \forall \varphi \in \mathcal{D}([0,T[; W_0^{1,\beta'}(\Omega)). \end{aligned}$$

Passing to the limit as $n \to \infty$, and using the convergence of $y_n \rightharpoonup \tilde{y}$ in $\mathbb{W}_0^r$, $\mathbf{g}(y_n(\cdot)) \to \mathbf{g}(\tilde{y}(\cdot))$ in $L^r(I; W^{-1,\beta}(\Omega))$, and $u_n \rightharpoonup u$ in $L^\beta(\Omega)$, it holds that

$$\begin{aligned} \int_0^T \langle (-\partial_t + A^*)\,\varphi, \tilde{y}(t)\rangle_{W^{-1,\beta'},W_0^{1,\beta}} dt = \int_0^T \langle \varphi, \mathbf{g}(\tilde{y}(t))\rangle_{W_0^{1,\beta'},W^{-1,\beta}} dt \\ + \langle \varphi(0), u\rangle_{(W^{-1,\beta'},W_0^{1,\beta'})_{\frac{1}{r},r'},(W^{-1,\beta},W_0^{1,\beta})_{\frac{1}{r'},r}} \quad \forall \varphi \in \mathcal{D}([0,T[; W_0^{1,\beta'}(\Omega)). \end{aligned}$$

Therefore, $\tilde{y}$ is the unique weak solution, and consequently, $\tilde{y} \in \mathbb{W}_0^r$ is also the unique strong solution corresponding to the initial condition $u \in L^\beta(\Omega)$, i.e., $\tilde{y} = S(u)$. Moreover, due to the uniqueness of the solution, it follows that $\tilde{y} = y$, and the assertion holds. □

4.2 Differentiability of the solution operator S

The derivation of optimality conditions requires the solution operator to be differentiable. First, we state an existence result for a *non-homogeneous linearized equation*.

Lemma 4.4. *Let Assumptions 3.1, 3.2, and 4.1 hold and let $y \in C(\bar{I}; L^\beta(\Omega))$ be given. Then for all $\xi \in L^r(I; W^{-1,\beta}(\Omega))$, and $h \in L^\beta(\Omega)$, there exists a unique mild solution*

$\eta \in C(\bar{I}; L^\beta(\Omega))$ *of*

$$\frac{\partial \eta(t)}{\partial t} + A\eta(t) + \mathbf{g}'(y(t))\eta(t) = \xi(t), \quad \eta(x,0) = h, \tag{4.23}$$

which satisfies the additional regularity $\eta \in \mathbb{W}_0^r$. *Moreover, there exists a positive constant* c *such that*

$$\|\eta\|_{\mathbb{W}_0^r} \leq c(\|\xi\|_{L^r(I;W^{-1,\beta}(\Omega))} + \|h\|_{L^\beta(\Omega)}).$$

Proof. Let us define the mapping $\mathcal{J}\colon C(\bar{I}; L^\beta(\Omega)) \to C(\bar{I}; L^\beta(\Omega))$ by

$$(\mathcal{J}\eta)(t) = e^{-tA}h + \int_0^t e^{-(t-\tau)A}(\xi(\tau) - \mathbf{g}'(y(\tau))\eta(\tau))d\tau, \qquad 0 \leq t \leq T. \tag{4.24}$$

Proposition 3.2 yields

$$\|(\mathcal{J}\eta_1)(t) - (\mathcal{J}\eta_2)(t)\|_{L^\beta(\Omega)} \leq \mathcal{M} \int_0^t \|\mathbf{g}'(y)(\eta_1 - \eta_2)(\tau)\|_{W^{-1,\beta}(\Omega)}d\tau, \tag{4.25}$$

and the embedding $L^\beta(\Omega) \hookrightarrow W^{-1,\beta}(\Omega)$ and the boundedness of g' allow to estimate

$$\|(\mathcal{J}\eta_1)(t) - (\mathcal{J}\eta_2)(t)\|_{L^\beta(\Omega)} \leq \mathcal{M}\mathcal{K} \int_0^t \|\eta_1(\tau) - \eta_2(\tau)\|_{L^\beta(\Omega)}d\tau \leq \mathcal{M}\mathcal{K}t\|\eta_1 - \eta_2\|_{C(\bar{I},L^\beta(\Omega))}, \tag{4.26}$$

for $0 \leq t \leq T$ and where $\mathcal{M} > 0$ is the bound of $\|e^{-tA}\|_{\mathcal{L}(W^{-1,\beta}(\Omega),L^\beta(\Omega))}$ and $\mathcal{K} > 0$ is the uniform bound of the nonlinear term. Moreover, since

$$\mathcal{J}^2\eta_1(t) - \mathcal{J}^2\eta_2(t) = \int_0^t e^{-(t-\tau)A}\left(\mathbf{g}'(y(\tau))\mathcal{J}\eta_2(\tau) - \mathbf{g}'(y(\tau))\mathcal{J}\eta_1(\tau)\right)d\tau,$$

using (4.26), we get

$$\begin{aligned}\|\mathcal{J}^2\eta_1(t) - \mathcal{J}^2\eta_2(t)\|_{L^\beta(\Omega)} &\leq \mathcal{M}\mathcal{K} \int_0^t \mathcal{M}\mathcal{K}\tau\|\eta_1 - \eta_2\|_{C(\bar{I};L^\beta(\Omega))}d\tau \\ &= \frac{(\mathcal{M}\mathbf{L}_{g'}t)^2}{2}\|\eta_1 - \eta_2\|_{C(\bar{I};L^\beta(\Omega))}.\end{aligned}$$

By an induction argument, we obtain

$$\|(\mathcal{J}^m\eta_1)(t) - (\mathcal{J}^m\eta_2)(t)\|_{L^\beta(\Omega)} \leq \frac{(\mathcal{M}\mathcal{K}t)^m}{m!}\|\eta_1 - \eta_2\|_{C(\bar{I};L^\beta(\Omega))},$$

and, consequently

$$\|\mathcal{J}^m\eta_1 - \mathcal{J}^m\eta_2\|_{C(\bar{I};L^\beta(\Omega))} \leq \frac{(\mathcal{M}\mathcal{K}T)^m}{m!}\|\eta_1 - \eta_2\|_{C(\bar{I};L^\beta(\Omega))}. \tag{4.27}$$

Since $\frac{(\mathcal{MK}T)^m}{m!} \to 0$ as $m \to \infty$, the operator $\mathcal{J}^m$ is a contraction. Consequently, according to [12, Section 5], $\mathcal{J}$ has a unique fix-point $\eta \in C(\bar{I}; L^\beta(\Omega))$ such that $\eta(t) = \mathcal{J}(\eta(t))$, which is the mild solution of (4.23).

We improve the regularity of the solution by a bootstrapping argument. Observe that $\mathbf{G}'(y)\eta \in L^r(I; W^{-1,\beta}(\Omega))$. In fact, using the embeddings:

$$C(\bar{I}; L^\beta(\Omega)) \hookrightarrow L^q(I; L^\beta(\Omega)) \hookrightarrow L^{\tilde{q}}(I, L^s(\Omega)) \hookrightarrow L^r(I; W^{-1,\beta}(\Omega)),$$

where $r < \tilde{q} < q$ and $L^\beta(\Omega) \hookrightarrow L^s(\Omega) \hookrightarrow W^{-1,\beta}(\Omega)$ [122, Proposition. 23.2], we get

$$\begin{aligned}
&\|\mathbf{G}'(y)\eta\|_{L^r(I;W^{-1,\beta}(\Omega))} \leq c_1 \|\mathbf{G}'(y)\eta\|_{L^{\tilde{q}}(I;L^s(\Omega))} \\
&\leq c_1 \|\mathbf{G}'(y)\|_{\mathcal{L}(L^q(I;L^\beta(\Omega)),L^{\tilde{q}}(I;L^s(\Omega)))} \|\eta\|_{L^q(I;L^\beta(\Omega))} \leq c_1 c_2 \mathcal{K} \|\eta\|_{C(\bar{I};L^\beta(\Omega))},
\end{aligned}$$

which is finite since $\eta \in C(\bar{I}; L^\beta(\Omega))$ and where $\mathcal{K} > 0$ is the bound of $\mathbf{G}'(y)$ in $\mathcal{L}(L^q(I; L^\beta(\Omega)), L^{\tilde{q}}(I; L^s(\Omega)))$, which holds given the uniform boundedness of g'. Then, Theorem 3.1 applied to

$$\frac{\partial \eta(t)}{\partial t} + A\eta(t) = -\mathbf{g}(y(t))\eta(t) + \xi(t), \quad \eta(0) = h$$

yields the higher regularity of η, and (2.51) yields the estimate. □

Remark 4.1. *For almost every $t \in I$, let us define the operator $\mathcal{A}(t) := A + \mathbf{g}'(y(t))$, acting from $W_0^{1,\beta}(\Omega)$ to $W^{-1,\beta}(\Omega)$. Note that $\mathcal{A}(t)$ is linear, continuous, and closed since A and $\mathbf{g}'(y(t))$ possess these properties. Moreover, the mapping $t \ni I \mapsto \mathcal{A}(t) \in \mathcal{L}(W_0^{1,\beta}(\Omega), W^{-1,\beta}(\Omega))$ is measurable and bounded. The measurability follows given the fact that $\mathbf{g}'$ is measurable (see, e.g., [118, Section 4.3.2]), while the boundedness holds given that g' is uniformly bounded and $A \in \mathcal{L}(W_0^{1,\beta}(\Omega), W^{-1,\beta}(\Omega))$. Since we have proved that for any $h \in L^\beta(\Omega) \hookrightarrow (W^{-1,\beta}(\Omega), W_0^{1,\beta}(\Omega))_{1-\frac{1}{r},r}$ and $\xi \in L^r(I; W^{-1,\beta}(\Omega))$, the non-homogeneous linearized equation (4.23) has a unique solution $\eta \in \mathbb{W}_0^r$, we have thus established the maximal parabolic regularity of the non-autonomous operator $A + \mathbf{g}'(y(\cdot))$.*

Observe that the result of Lemma 4.4 is proven for all initial conditions in $L^\beta(\Omega)$, whereas the standard definition of maximal parabolic regularity (Definition 2.14) requires the property to hold for all initial condition in $(W^{-1,\beta}(\Omega), W_0^{1,\beta}(\Omega))_{\frac{1}{r'},r}$. Nevertheless, proving the property for the entire $L^\beta(\Omega)$, which includes the case $h = 0$, is sufficient to conclude maximal parabolic regularity, indeed, this formulation is equivalent to Definition 2.14 as established in [7, Proposition 2.1].

Since the control variable is not a distributed term, the corresponding linearized equation will have a regular right-hand side. As a result, the linearized equation exhibits additional regularity properties. We present these results below.

Lemma 4.5. *Let Assumptions 3.1, 3.2, and 4.1 hold, and $y = Su \in \mathbb{W}_0^r$ be the solution of (4.1) for some $u \in L^\beta(\Omega)$. Then for a given $h \in L^\beta(\Omega)$, there is a unique solution $\eta \in L^2(I; H_0^1(\Omega)) \cap L^\infty(I; L^2(\Omega))$ of the linearized equation*

$$\frac{\partial \eta(t)}{\partial t} + A\eta(t) + \mathbf{g}'(y(t))\eta(t) = 0, \quad \eta(x,0) = h, \tag{4.28}$$

that satisfies the additional regularity $\eta \in \mathbb{W}_0^r \cap L^{r'}(I; C(\bar{\Omega})) \cap L^q(I; L^\beta(\Omega))$.

Additionally, for $d = 2$, there exists a unique solution $\omega \in L^2(I; H_0^1(\Omega)) \cap L^\infty(I; L^2(\Omega))$ of the second order linearized equation

$$\frac{\partial \omega(t)}{\partial t} + A\omega(t) + \mathbf{g}'(y(t))\omega(t) = -\mathbf{g}''(y(t))\eta(t)^2, \quad \omega(x,0) = 0, \tag{4.29}$$

which satisfies the additional regularity $\omega \in \mathbb{W}_0^r \cap L^{r'}(I; C(\bar{\Omega})) \cap L^q(I; L^\beta(\Omega))$.

Moreover, these solutions satisfy the following estimates:

$$\|\eta\|_{L^2(I;H_0^1(\Omega))} + \|\eta\|_{C(\bar{I};L^2(\Omega))} \le K_1 \|h\|_{L^2(\Omega)}, \quad \text{for some } K_1 > 0, \tag{4.30}$$

$$\|\omega\|_{L^2(I;H_0^1(\Omega))} + \|\omega\|_{C(\bar{I};L^2(\Omega))} \le K_2 \|h\|_{L^2(\Omega)}^2, \quad \text{for some } K_2 > 0, \tag{4.31}$$

$$\|\eta\|_{\mathbb{W}_0^r} \le K_3 \|h\|_{L^\beta(\Omega)}, \quad \text{for some } K_3 > 0, \tag{4.32}$$

$$\|\omega\|_{\mathbb{W}_0^r} \le K_4 \|h\|_{L^2(\Omega)}^2, \quad \text{for some } K_4 > 0. \tag{4.33}$$

Proof. The uniform boundedness of g' and [83, Theorems III.4.1 & III.2.1] yield the existence of a classical solution $\eta \in L^2(I; H_0^1(\Omega)) \cap L^\infty(I; L^2(\Omega))$ of (4.28) which satisfies estimate (4.30). The improved regularity $\eta \in \mathbb{W}_0^r$ and estimate (4.32) follow directly by applying Lemma 4.4 with $\xi(t) = 0$, since $y \in C(\bar{I}; L^\beta(\Omega))$ due to Lemma 4.1.

To prove the existence and regularity of the second-order linearized equation, we need to guarantee that $\mathbf{G}''(y)\eta^2 \in L^1(I; L^2(\Omega))$ (to use the results in [83]). The boundedness of g'', a Hölder inequality, and estimate (4.30) yield

$$\|\mathbf{G}''(y)\eta^2\|_{L^1(I;L^2(\Omega))} \le c\|\eta\|_{L^2(I;L^4(\Omega))}^2 \le c\|\eta\|_{L^2(I;H_0^1(\Omega))}^2 \le c\|h\|_{L^2(\Omega)}^2, \tag{4.34}$$

which is finite since $h \in L^\beta(\Omega)$ and $\beta > 2$. Consequently, [83, Theorem III.4.1 & Remark III.1.1] guarantee existence of a unique weak solution $\omega \in L^2(I; H_0^1(\Omega)) \cap L^\infty(I; L^2(\Omega))$ satisfying estimate (4.31). To obtain the improved regularity by taking $\xi(t) = \mathbf{g}''(y(t))\eta^2(t)$ in Lemma 4.4, we need to prove that $\mathbf{G}''(y)\eta^2 \in L^r(I; W^{-1,\beta}(\Omega))$. In fact, the boundedness of g'', the embedding results (4.4) and (4.5), and the Hölder inequality yield

$$\|\mathbf{G}''(y)\eta^2\|_{L^r(I;W^{-1,\beta}(\Omega))} \le c\|\mathbf{G}''(y)\eta^2\|_{L^r(I;L^s(\Omega))} \le c\|\eta\|_{L^q(I;L^\beta(\Omega))}\|\eta\|_{L^{\tilde{q}}(I;L^2(\Omega))}.$$

This implies, jointly with (4.30) and (4.32), and given that $\beta > 2$

$$\|\mathbf{G}''(y)\eta^2\|_{L^r(I;W^{-1,\beta}(\Omega))} \leq c\|\eta\|_{\mathbb{W}_0^r}\|h\|_{L^2(\Omega)} \leq c\|h\|^2_{L^\beta(\Omega)}.$$

From this, we obtain existence and uniquiness of $\omega \in \mathbb{W}_0^r$, which verifies the estimate $\|\omega\|_{\mathbb{W}_0^r} \leq c\|h\|^2_{L^\beta(\Omega)}$. To obtain estimate (4.33), observe that

$$\|\mathbf{G}''(y)\eta^2\|_{L^r(I;W^{-1,\beta}(\Omega))} \leq c\|\eta^2\|_{L^r(I;L^s(\Omega))} \leq c\|\eta\|_{L^\infty(I;L^2(\Omega))}\|\eta\|_{L^2(I;L^{\tilde{s}}(\Omega))} \leq c\|h\|^2_{L^2(\Omega)}$$

by Hölder's inequality, and using $r < 2$. Since $d = 2$, the embedding $H_0^1(\Omega) \hookrightarrow L^{\tilde{s}}(\Omega)$ for $d = 2$. Using the latter jointly with estimate in Lemma 4.4 conclude the proof. □

Remark 4.2. *It has been proved in [81, Theorem 2.15], under stronger assumptions, that the linear, non-autonomous, initial boundary value problem*

$$\begin{aligned} w_t - \nabla \cdot k\nabla w + c_0 w &= \ell \quad \text{in } Q, \\ \nu \cdot k\nabla w &= 0 \quad \text{on } \Gamma_N \times I, \\ w &= 0 \quad \text{on } \Gamma_D \times I, \\ w(x,0) &= 0 \quad \text{in } \Omega. \end{aligned} \tag{4.35}$$

admits a unique solution in the maximal parabolic regularity space $L^r(I; W^{1,q}_{\Gamma_N}(\Omega)) \cap W^{1,r}(I; W^{-1,q}_{\Gamma_N}(\Omega))$, for given values of r and q. Where $c_0 \in L^\infty(Q)$, Γ_N and Γ_D denote the Neumann and Dirichlet boundary parts, respectively, and ν defines the outward unit normal at the boundary part Γ_N. The proof of this result relies on using a perturbation argument, cf., [9, Prop. 1.3].

Theorem 4.2. *Let Assumptions 3.1, 3.2, and 4.1 hold. Then, the solution operator S is Fréchet-differentiable from $L^\beta(\Omega)$ to $\mathbb{W}_0^r$. Additionally, for $d = 2$, S is twice Fréchet-differentiable from $L^\beta(\Omega)$ to $\mathbb{W}_0^r$, where $y = S(u)$, $h \in L^\beta(\Omega)$, $\eta = S'(u)h$ and $\omega = S''(u)h^2$ correspond to the unique solutions of the linearized equation (4.28) and the second-order linearized equation (4.29), respectively.*

Proof. Given our collected regularity results for state and linearized state equations, the proof now follows by classical arguments provided in, e.g., [118]. In fact, let us consider the increment $y_h = S(u + h)$, with $h \in L^\beta(\Omega)$, $y = S(u)$, and $y_\rho = y_h - y - \eta$ the solution of equation

$$\frac{\partial y_\rho(t)}{\partial t} + Ay_\rho(t) + \mathbf{g}(y_h(t)) - \mathbf{g}(y(t)) - \mathbf{g}'(y(t))\eta(t) = 0, \qquad y_\rho(x,0) = 0. \tag{4.36}$$

Note that, from the differentiability properties of $\mathbf{g}$, it holds that

$$\mathbf{g}(y_h(t)) - \mathbf{g}(y(t)) - \mathbf{g}'(y(t))\eta(t) = \mathbf{g}'(y(t))y_\rho(t) + r_g(t),$$

where $r_g \in L^{\tilde{q}}(I; L^s(\Omega))$ is a remainder term that fulfills

$$\|r_g(y, y_h - y)\|_{L^{\tilde{q}}(I;L^s(\Omega))} = o(\|y_h - y\|_{L^q(I;L^\beta(\Omega))}).$$

From the latter, we can write equation(4.36) in the following form:

$$\frac{\partial y_\rho(t)}{\partial t} + Ay_\rho(t) + \mathbf{g}'(y(t))y_\rho(t) = -r_g(t), \qquad y_\rho(x, 0) = 0. \tag{4.37}$$

Given that $r < \tilde{q}$, then $L^{\tilde{q}}(I; L^s(\Omega)) \hookrightarrow L^r(I; W^{-1,\beta}(\Omega))$. Consequently, r_g belongs to $L^r(I; W^{-1,\beta}(\Omega))$, and, proceeding as in the proof of the first-order linearized equation, we can prove that $y_\rho \in \mathbb{W}_0^r$ is the unique solution of (4.37) satisfying the following estimate

$$\|y_\rho\|_{\mathbb{W}_0^r} \leq c\|r_g\|_{L^r(I;W^{-1,\beta}(\Omega))} \leq c\|r_g\|_{L^r(I;L^s(\Omega))} = o(\|y_h - y\|_{L^q(I;L^\beta(\Omega))}) \tag{4.38}$$

Then, we observe that

$$\frac{\|y_\rho\|_{\mathbb{W}_0^r}}{\|h\|_{L^\beta(\Omega)}} \leq \frac{\|y_\rho\|_{\mathbb{W}_0^r}}{\|y_h - y\|_{L^q(I;L^\beta(\Omega))}} \frac{\|y_h - y\|_{L^q(I;L^\beta(\Omega))}}{\|h\|_{L^\beta(\Omega)}} \leq c\frac{\|y_\rho\|_{\mathbb{W}_0^r}}{\|y_h - y\|_{L^q(I;L^\beta(\Omega))}}$$

by the Lipschitz continuity of S from Lemma 4.2, see estimate (4.19b). Due to the same Lemma, we obtain $\|y_h - y\|_{L^q(I;L^\beta(\Omega))} \to 0$ for $\|h\|_{L^\beta(\Omega)} \to 0$, hence (4.38) yields the remainder term property for first order Fréchet differentiability. Therefore,

$$\|y_h - y - \eta\|_{\mathbb{W}_0^r} = o(\|h\|_{L^\beta(\Omega)}), \tag{4.39}$$

and the first-order differentiability result holds.

Now, we will prove the second-order differentiability of S in the 2-dimensional case. Let us consider $y_\omega := y_h - y - \eta - \omega$ and observe that it solves

$$\begin{aligned} \tfrac{\partial y_\omega(t)}{\partial t} + Ay_\omega(t) = \; & -(\mathbf{g}(y_h(t)) - \mathbf{g}(y(t)) - \mathbf{g}'(y(t))\eta(t) - \mathbf{g}'(y(t))\omega(t) - \tfrac{1}{2}\mathbf{g}''(y(t))\eta(t)^2), \\ y_\omega(x, 0) = \; & 0. \end{aligned} \tag{4.40}$$

Observe that from the differentiability properties of $\mathbf{g}$, for each $t \in I$, the right-hand side of equation (4.40) takes the form

$$-r_g^2(t) - \mathbf{g}'(y(t))y_\omega(t) - \frac{1}{2}\mathbf{g}''(y(t))[(y_h(t) - y(t))^2 - \eta^2(t)],$$

with $r_g^2 \in L^{\tilde{q}}(I; L^s(\Omega))$ the second order remainder term, which satisfies

$$\|r_g^2(y, y_h - y)\|_{L^{\tilde{q}}(I;L^s(\Omega))} = o(\|y_h - y\|^2_{L^q(I;L^\beta(\Omega))}). \tag{4.41}$$

Proceeding as in the proof of the second-order linearized equation, we can prove that $y_\omega \in \mathbb{W}_0^r$ satisfies the estimate

$$\|y_\omega\|_{\mathbb{W}_0^r} \leq c\left(\|r_g^2\|_{L^r(I;W^{-1,\beta}(\Omega))} + \left\|\mathbf{G}''(y)[(y_h-y)^2-\eta^2]\right\|_{L^r(I;W^{-1,\beta}(\Omega))}\right). \tag{4.42}$$

Therefore, to prove the results, we only need to show that each term on the right-hand side of the inequality above is of order $o(\|h\|^2_{L^\beta(\Omega)})$. In fact, given that $\|r_g^2\|_{L^r(I;W^{-1,\beta}(\Omega))} \leq c_1\|r_g^2\|_{L^{\tilde{q}}(I;L^s(\Omega))}$, due to (4.41) the discussion of the first term is completed by the Lipschitz result for S from Lemma 4.2. It remains to prove that

$$\|\mathbf{G}''(y)\left[(y_h-y)^2-\eta^2\right]\|_{L^r(I;W^{-1,\beta}(\Omega))} = o(\|h\|^2_{L^\beta(\Omega)}).$$

In fact, the embedding $L^s(\Omega) \hookrightarrow W^{-1,\beta}(\Omega)$, the boundedness of the nonlinearity, and the generalized Hölder inequality yield

$$\begin{aligned}\|\mathbf{G}''(y)\left[(y_h-y)^2-\eta^2\right]\|_{L^r(I;W^{-1,\beta}(\Omega))} &\leq c_3\|\mathbf{G}''(y)\left[(y_h-y-\eta)(y_h-y+\eta)\right]\|_{L^r(I;L^s(\Omega))}\\ &\leq c_2\|y_h-y-\eta\|_{L^q(I;L^\beta(\Omega))}\|y_h-y+\eta\|_{L^{\frac{qr}{q-r}}(I;L^2(\Omega))} \qquad \text{for some } c_2>0,\end{aligned}$$

with $q = \frac{4\beta}{\beta-d}$ as fixed in (4.2) at the beginning of this section. Due to the embedding results (4.5), this takes the form:

$$\|\mathbf{G}''(y)\left[(y_h-y)^2-\eta^2\right]\|_{L^r(I;W^{-1,\beta}(\Omega))} \leq \|y_h-y-\eta\|_{\mathbb{W}_0^r}\|y_h-y+\eta\|_{L^{\frac{qr}{q-r}}(I;L^2(\Omega))}.$$

Besides applying the triangular inequality in the last term above, jointly with estimates (4.19a) and (4.30), we eventually obtain

$$\|y_h-y+\eta\|_{L^{\frac{qr}{q-r}}(I;L^2(\Omega))} \leq c_4\|h\|^2_{L^\beta(\Omega)},$$

for some $c_4>0$. Consequently, using the first-order differentiability result (4.39)

$$\frac{\|\mathbf{G}''(y)\left[(y_h-y)^2-\eta^2\right]\|_{L^r(I;W^{-1,\beta})}}{\|h\|^2_{L^\beta(\Omega)}} \leq c_4\frac{o(\|h\|_{L^\beta(\Omega)})}{\|h\|_{L^\beta(\Omega)}}\frac{\|h\|^2_{L^\beta(\Omega)}}{\|h\|_{L^\beta(\Omega)}},$$

which goes to zero as $\|h\|_{L^\beta(\Omega)} \to 0$. □

The following lemma states a Lipschitz continuity result for the solution to the first-order linearized equation η.

Lemma 4.6. *Let Assumptions 3.1, 3.2, and 4.1 hold, and let $y = S(u)$, $\tilde{y} = S(\tilde{u})$ and $\eta = S'(u)h$, $\tilde{\eta} = S'(\tilde{u})h$ denote the states and linearized states for $u, \tilde{u} \in U_{ad}$ and $h \in L^\beta(\Omega)$. Then, there exist positive constants $\mathbf{C}_1$ and $\mathbf{C}_2$ such that*

$$\|\eta-\tilde{\eta}\|_{L^2(I;H_0^1(\Omega))} + \|\eta-\tilde{\eta}\|_{C(\bar{I};L^2(\Omega))} \leq \mathbf{C}_1\|u-\tilde{u}\|_{L^2(\Omega)}\|h\|_{L^2(\Omega)} \tag{4.43a}$$

$$\|\eta - \tilde{\eta}\|_{\mathbb{W}_0^r} \leq \mathbf{C}_2 \|u - \tilde{u}\|_{L^\beta(\Omega)} \|h\|_{L^2(\Omega)}. \tag{4.43b}$$

Moreover, if $d = 2$, there exists a positive constant $\mathbf{C}_3$ such that

$$\|\eta - \tilde{\eta}\|_{\mathbb{W}_0^r} \leq \mathbf{C}_3 \|u - \tilde{u}\|_{L^2(\Omega)} \|h\|_{L^2(\Omega)}. \tag{4.44}$$

Proof. Observe that $\hat{\eta} := \eta - \tilde{\eta}$ fulfills:

$$\frac{\partial \hat{\eta}(t)}{\partial t} + A\hat{\eta}(t) + \mathbf{g}'(y(t))\hat{\eta}(t) = \left[\mathbf{g}'(y(t)) - \mathbf{g}'(\tilde{y}(t))\right]\tilde{\eta}(t), \quad \hat{\eta}(x,0) = 0. \tag{4.45}$$

Observe that the right-hand side of (4.45) belongs to $L^1(I; L^2(\Omega))$. In fact, a Hölder inequality, the Lipschitz continuity (4.19a), and (4.30) yield

$$\begin{aligned} &\|[\mathbf{G}'(y) - \mathbf{G}'(\tilde{y})]\tilde{\eta}\|_{L^1(I;L^2(\Omega))} \leq c\|\mathbf{G}'(y) - \mathbf{G}'(\tilde{y})\|_{L^2(I;L^4(\Omega))}\|\tilde{\eta}\|_{L^2(I;L^4(\Omega))} \\ &\leq c\|y - \tilde{y}\|_{L^2(I;L^4(\Omega))}\|\tilde{\eta}\|_{L^2(I;L^4(\Omega))} \leq c\|y - \tilde{y}\|_{L^2(I;H_0^1(\Omega))}\|\tilde{\eta}\|_{L^2(I;H_0^1(\Omega))} \\ &\leq c\|u - \tilde{u}\|_{L^2(\Omega)}\|h\|_{L^2(\Omega)} < \infty \end{aligned} \tag{4.46}$$

which holds using the embedding $H_0^1(\Omega) \hookrightarrow L^4(\Omega)$. Then, [83, Theorem III.4.1 & Theorem III.2.1] imply that $\hat{\eta} \in L^2(I; H_0^1(\Omega)) \cap L^\infty(I; L^2(\Omega))$ solves (4.45) and estimate (4.43a) holds. Now, proceeding as in the proof of Lemma 4.5 for homogeneous initial conditions, we obtain by applying a Hölder inequality,

$$\begin{aligned} \|\hat{\eta}\|_{\mathbb{W}_0^r} &\leq c\|(\mathbf{G}'(y) - \mathbf{G}'(\tilde{y}))\tilde{\eta}\|_{L^r(I;L^s(\Omega))} \leq c\|\mathbf{G}'(y) - \mathbf{G}'(\tilde{y})\|_{L^q(I;L^\beta(\Omega))}\|\tilde{\eta}\|_{L^{\tilde{q}}(I;L^2(\Omega))} \\ &\leq c\|y - \tilde{y}\|_{L^q(I;L^\beta(\Omega))}\|h\|_{L^2(\Omega)}, \end{aligned}$$

or in the case $d = 2$ where $H_0^1(\Omega) \hookrightarrow L^{\tilde{s}}(\Omega)$

$$\begin{aligned} \|\hat{\eta}\|_{\mathbb{W}_0^r} &\leq c\|(\mathbf{G}'(y) - \mathbf{G}'(\tilde{y}))\tilde{\eta}\|_{L^r(I;L^s(\Omega))} \leq c\|\mathbf{G}'(y) - \mathbf{G}'(\tilde{y})\|_{L^2(I;L^{\tilde{s}}(\Omega))}\|\tilde{\eta}\|_{L^\infty(I;L^2(\Omega))} \\ &\leq c\mathbf{L}_{G'}\|y - \tilde{y}\|_{L^2(I;H_0^1(\Omega))}\|h\|_{L^2(\Omega)}. \end{aligned}$$

The Lipschitz continuity (4.19a) stated in Lemma 4.2 yields the assertion. □

4.3 Study of the minimization problem

In this section, we will study the variational optimization problem. We will start the discussion by showing the existence of a solution for the semilinear data assimilation problem. Then, we will derive the first-order optimality conditions.

4.3.1 Existence of solution for the semilinear DA problem

By using the solution operator S, we can rewrite the cost functional, and thus the minimization problem, in the following way:

$$\min_{u\in U_{ad}} J(Su,u) = \frac{1}{2}\int_0^T \sum_k [Su(x_k,t) - z_o(x_k,t)]^2 dt + \frac{1}{2}\|u-u_b\|^2_{B^{-1}}, \tag{P}$$

recalling that $U_{ad} = \left\{u \in L^\beta(\Omega) : \int_\Omega |u(x)|^\beta dx \leq b\right\}$, for a given constant $b > 0$.

Theorem 4.3. *Let Assumptions 3.1, 3.2, and 4.1 hold. Then, the data assimilation problem (P) has at least one optimal solution $\bar{u} \in U_{ad} \subset L^\beta(\Omega)$ with $\bar{y} = S\bar{u} \in \mathbb{W}_0^r$ being its associated optimal state.*

Proof. Since the functional $J(Su,u)$ is nonnegative, it is bounded from below. Then, the infimum $j = \inf_{u\in U_{ad}} J(Su,u) \in \mathbb{R}$ exists. Let $\{(y_n,u_n)\}_{n\geq 1}$ be a minimizing sequence, that is, let $u_n \in U_{ad}$ and $y_n = S(u_n)$, for $n \in \mathbb{N}$, be such that $J(y_n,u_n) \to j$ as $n \to \infty$. Since U_{ad} is weakly sequentially compact [118, Theorem 2.11], there exists a subsequence, denoted the same, and a limit $\bar{u} \in U_{ad}$ such that $u_n \rightharpoonup \bar{u}$ in U_{ad} as $n \to \infty$. By Lemma 4.3, the sequence of associated states also converges weakly in $\mathbb{W}_0^r$, i.e., $y_n \rightharpoonup \bar{y}$ in $\mathbb{W}_0^r$ as $n \to \infty$. To show the optimality of $\bar{u} \in U_{ad}$, notice that the second term of the cost functional (P) is weakly lower semicontinuous, and, consequently,

$$\begin{aligned} j &= \lim_{n\to\infty} J(y_n,u_n) = \lim_{n\to\infty} \frac{1}{2}\int_0^T \sum_k [y_n(x_k,t) - z_o(x_k,t)]^2 dt + \liminf_{n\to\infty} \frac{1}{2}\|u_n - u_b\|^2_{B^{-1}} \\ &\geq \frac{1}{2}\int_0^T \sum_k [\bar{y}(x_k,t) - z_o(x_k,t)]^2 dt + \frac{1}{2}\|\bar{u} - u_b\|^2_{B^{-1}} = J(\bar{y},\bar{u}). \end{aligned}$$

By definition of the infimum, it must hold that $J(\bar{y},\bar{u}) = j$, which proves the optimality. □

4.3.2 First order optimality conditions

Let us start by studying the adjoint equation in the semilinear setting. We consider the following adjoint problem:

$$\begin{aligned} -\frac{\partial p}{\partial t} + A^* p + [\mathbf{g}'(y)]^* p &= \chi \quad \text{in } Q \\ p &= 0 \quad \text{on } \Sigma \\ p(x,T) &= 0 \quad \text{in } \Omega, \end{aligned} \tag{4.47}$$

where $\chi \in L^{r'}(I; W^{-1,\beta'}(\Omega))$. Observe that in the semilinear setting, the adjoint operator is non-autonomous. Therefore, we are not able to use the result of Lemma 2.4 to guarantee the well-posedness of the adjoint state since it holds for operators that do not depend on time.

In fact, for the non-autonomous case, the well-posedness of (4.47) in adequate spaces has to be proved "by hand"; we formalize this result in the following lemma. We recall that its proof follows some of the techniques discussed in [67, Sec. 6.2 - 6.3]. Moreover, for use in the lemma's proof, we will denote the dual of a given space Z by Z^*.

Lemma 4.7. *Let Assumptions 3.1, 3.2, and 4.1 hold, and let $\chi \in L^{r'}(I; W^{-1,\beta'}(\Omega))$. Then, the adjoint equation (4.47) has a unique solution $p \in W^{1,r'}(I; W^{-1,\beta'}(\Omega)) \cap L^{r'}(I; W_0^{1,\beta'}(\Omega))$. Moreover, there exists a constant $c_p > 0$ such that*

$$\|p\|_{\mathbb{W}_0^{r'}} \leq c_p \|\chi\|_{L^{r'}(I; W^{-1,\beta'}(\Omega))}.$$

Proof. Since the non-homogeneous linearized equation (4.23) admits a unique solution in $\mathbb{W}^r(W_0^{1,\beta}(\Omega), W^{-1,\beta}(\Omega))$, from [7, Proposition 2.1], the linear operator,

$$\partial_t + A + \mathbf{g}'(y) \colon \mathbb{W}^r(W_0^{1,\beta}(\Omega), W^{-1,\beta}(\Omega)) \longrightarrow L^r(I; W^{-1,\beta}(\Omega))$$

is bounded and continuously invertible. Therefore, its adjoint operator,

$$(\partial_t + A + \mathbf{g}'(y))^* \colon L^{r'}(I; W_0^{1,\beta'}(\Omega)) \longrightarrow (\mathbb{W}^r(W_0^{1,\beta}(\Omega), W^{-1,\beta}(\Omega)))^*$$

is also continuously invertible. Consequently, for all $\chi \in (\mathbb{W}^r(W_0^{1,\beta}(\Omega), W^{-1,\beta}(\Omega)))^*$, the equation

$$(\partial_t + A + \mathbf{g}'(y(\cdot)))^* p = \chi \tag{4.48}$$

admits a unique solution $p \in L^{r'}(I; W_0^{1,\beta'}(\Omega))$.

On the other hand, since $W^{1,r}(I; W^{-1,\beta}(\Omega)) \cap L^r(I; W_0^{1,\beta}(\Omega)) \hookrightarrow L^r(I; W_0^{1,\beta}(\Omega))$, then $L^{r'}(I; W^{-1,\beta'}(\Omega)) \hookrightarrow (\mathbb{W}^r(W_0^{1,\beta}(\Omega), W^{-1,\beta}(\Omega)))^*$. Now, assuming that χ is more regular, i.e., $\chi \in L^{r'}(I; W^{-1,\beta'}(\Omega))$, we aim to prove the time differentiability of the solution p. To do the latter, testing (4.48) with $\zeta \in C_0^\infty(I; W_0^{1,\beta}(\Omega))$ satisfying $\zeta(t) =$

$\varphi(t)\nu$ with $\varphi \in C_0^\infty(0,T)$ and $\nu \in W_0^{1,\beta}(\Omega)$, we obtain

$$\int_0^T \langle \chi, \zeta \rangle_{W^{-1,\beta'}(\Omega), W_0^{1,\beta}(\Omega)} dt = \int_0^T \varphi \langle \chi, \nu \rangle_{W^{-1,\beta'}(\Omega), W_0^{1,\beta}(\Omega)} dt$$
$$= \int_0^T \varphi \langle (\partial_t + A + \mathbf{g}'(y))^* p, \nu \rangle_{W^{-1,\beta'}(\Omega), W_0^{1,\beta}(\Omega)} = \int_0^T \langle p, (\partial_t + A + \mathbf{g}'(y))\varphi\nu \rangle_{W_0^{1,\beta'}(\Omega), W^{-1,\beta}(\Omega)}$$
$$= \int_0^T \varphi' \langle p, \nu \rangle_{W_0^{1,\beta'}(\Omega), W^{-1,\beta}(\Omega)} dt + \int_0^T \varphi \langle A^* p + [\mathbf{g}'(y)]^* p, \nu \rangle_{W^{-1,\beta'}(\Omega), W_0^{1,\beta}(\Omega)} dt,$$

and, consequently,

$$\int_0^T \varphi' \langle p, \nu \rangle_{W_0^{1,\beta'}(\Omega), W^{-1,\beta}(\Omega)} dt = \int_0^T \varphi \langle \chi - A^* p - [\mathbf{g}'(y)]^* p, \nu \rangle_{W^{-1,\beta'}(\Omega), W_0^{1,\beta}(\Omega)} dt$$
$$= \left\langle \int_0^T \varphi(\chi - A^* p - [\mathbf{g}'(y)]^* p) dt, \nu \right\rangle_{W^{-1,\beta'}(\Omega), W_0^{1,\beta}(\Omega)}$$

where the last equality holds since ν does not depends on t. Moreover, since $W_0^{1,\beta}(\Omega) \hookrightarrow W^{-1,\beta}(\Omega)$, it holds that $W_0^{1,\beta'}(\Omega) \hookrightarrow W^{-1,\beta'}(\Omega)$. Therefore, identifying $p \in W_0^{1,\beta'}(\Omega)$ with an element of $W^{-1,\beta'}(\Omega)$, we can rewrite the equality above as:

$$\left\langle \int_0^T \varphi' p \, dt, \nu \right\rangle_{W^{-1,\beta'}(\Omega), W_0^{1,\beta}(\Omega)} = \left\langle \int_0^T \varphi(\chi - A^* p - [\mathbf{g}'(y)]^* p) dt, \nu \right\rangle_{W^{-1,\beta'}(\Omega), W_0^{1,\beta}(\Omega)}$$

Additionally, since $\nu \in W_0^{1,\beta}(\Omega)$ was taken arbitrarily, it holds that

$$\int_0^T \varphi' p \, dt = \int_0^T \varphi(\chi - A^* p - [\mathbf{g}'(y)]^* p) dt, \quad \text{in } W^{-1,\beta'}(\Omega), \ \forall \varphi \in C_0^\infty(0,T).$$

Therefore, the distributional time derivative of p is given by $\chi - A^* p - [\mathbf{g}'(y)]^* p \in L^{r'}(I; W^{-1,\beta'}(\Omega))$, that is,

$$-\frac{\partial p}{\partial t} = \chi - A^* p - [\mathbf{g}'(y)]^* p \qquad \text{in } W^{-1,\beta'}(\Omega), \text{ a.e. } t \in I, \tag{4.49}$$

which shows that $p \in W^{1,r'}(I; W^{-1,\beta'}(\Omega))$. Therefore,

$$p \in L^{r'}(I; W_0^{1,\beta}(\Omega)) \cap W^{1,r'}(I; W^{-1,\beta'}(\Omega)) =: \mathbb{W}^{r'}(W_0^{1,\beta'}(\Omega), W^{-1,\beta'}(\Omega)).$$

It remains to prove that $p(T) = 0$. In fact, by using Green's formula (see [7, Prop 5.1]), taking $z \in \mathbb{W}^r(W_0^{1,\beta}(\Omega), W^{-1,\beta}(\Omega))$ and $p \in \mathbb{W}^{r'}(W_0^{1,\beta'}(\Omega), W^{-1,\beta'}(\Omega))$, it holds that

$$\int_0^T \langle \chi, z \rangle_{W^{-1,\beta'}(\Omega), W_0^{1,\beta}(\Omega)} dt = \int_0^T \langle p, (\partial_t + A + \mathbf{g}'(y))z \rangle_{W_0^{1,\beta}(\Omega), W^{-1,\beta}(\Omega)} dt$$

$$\int_0^T \langle (\partial_t + A + \mathbf{g}'(y))^* p, z \rangle_{W^{-1,\beta'}(\Omega), W_0^{1,\beta}(\Omega)} dt + \langle p(T), z(T) \rangle_{(W^{-1,\beta'}, W_0^{1,\beta'})_{\frac{1}{r}, r'}, (W^{-1,\beta}, W_0^{1,\beta})_{\frac{1}{r'}, r}}$$

From equation (4.49), it follows that

$$0 = \langle p(T), z(T) \rangle_{(W^{-1,\beta'}, W_0^{1,\beta'})_{\frac{1}{r}, r'}, (W^{-1,\beta}, W_0^{1,\beta})_{\frac{1}{r'}, r}}, \quad \forall z \in \mathbb{W}^r(W_0^{1,\beta}(\Omega), W^{-1,\beta}(\Omega)).$$

Consequently, $p(T) = 0$, and, therefore such $p \in \mathbb{W}^{r'}(W_0^{1,\beta'}(\Omega), W^{-1,\beta'}(\Omega))$ is the unique solution of the adjoint equation (4.47).Therefore, it follows that $A^* + [\mathbf{g}'(y(\cdot))]^*$ satisfies the maximal parabolic $L^{r'}(I; W^{-1,\beta'}(\Omega))$-regularity, and the estimate holds. □

In order to derive the first-order optimality conditions, we proceed as in the linear case by rewriting the admissible set using the functional

$$\psi \colon L^\beta(\Omega) \to \mathbb{R}, \quad u \mapsto \psi(u) = b - \int_\Omega |u(x)|^\beta dx,$$

and, consequently, problem (P) can be expressed, analogous to (3.12), as:

$$\min f(u) = J(Su, u), \quad u \in L^\beta(\Omega) \quad \text{and} \quad \psi(u) \in K, \tag{4.50}$$

with $K = \{\kappa \in \mathbb{R} : \kappa \geq 0\}$ being a closed and convex set of $\mathbb{R}$.

Theorem 4.4. *Let Assumptions 3.1, 3.2, and 4.1 hold, and let $\bar{u} \in L^\beta(\Omega)$ be a local solution of (4.50), with $\bar{y} \in \mathbb{W}_0^r$ its associated optimal state. Then, there exists a unique scalar Lagrange multiplier $\bar{\lambda} \geq 0$ and a unique adjoint state $\bar{p} \in \mathbb{W}_0^{r'}$ satisfying:*

State equation :

$$\begin{aligned} \frac{\partial \bar{y}}{\partial t} + A\bar{y} + \mathbf{g}(\bar{y}(\cdot)) &= 0 \quad \text{in } Q, \\ \bar{y} &= 0 \quad \text{on } \Sigma, \\ \bar{y}(x, 0) &= \bar{u} \quad \text{in } \Omega. \end{aligned} \tag{4.51a}$$

Adjoint equation :

$$\begin{aligned} -\frac{\partial \bar{p}}{\partial t} + A^*\bar{p} + [\mathbf{g}'(\bar{y}(\cdot))]^*\bar{p} = & \sum_k [S\bar{u}(x_k,\cdot) - z_o(x_k,\cdot)]\,\delta_{x_k} && \text{in } Q \\ \bar{p} = & \ 0 && \text{on } \Sigma \\ \bar{p}(x,T) = & \ 0 && \text{in } \Omega. \end{aligned} \tag{4.51b}$$

Gradient equation :

$$\bar{p}(0) + B^{-1}(\bar{u} - u_b) + \bar{\lambda}\beta|\bar{u}|^{\beta-2}\bar{u} = 0 \ \text{ in } \Omega. \tag{4.51c}$$

Complementarity System :

$$\bar{\lambda} \geq 0, \quad b - \int_\Omega |\bar{u}(x)|^\beta dx \geq 0, \quad \bar{\lambda}\left(b - \int_\Omega |\bar{u}(x)|^\beta dx\right) = 0. \tag{4.51d}$$

Proof. Proceeding as in the linear case and using the regularity result of Zowe and Kurcyusz [125], we obtain the existence of a Lagrange multiplier $\bar{\lambda} \geq 0$ that satisfies the complementarity system (4.51d) as well as the equation:

$$\langle f'(\bar{u}) - \bar{\lambda}\psi'(\bar{u}), h\rangle_{L^{\beta'},L^\beta} = 0, \qquad \forall h \in L^\beta(\Omega). \tag{4.52}$$

Further, since S is differentiable, by applying the chain rule to the reduced cost functional, we get, for any direction $h \in L^\beta(\Omega)$,

$$f'(\bar{u})h = \int_0^T \sum_k [S\bar{u}(x_k,t) - z_o(x_k,t)]\delta_{x_k} S'(\bar{u})h(\cdot,t)\ dxdt + \int_\Omega (\bar{u}(x) - u_b(x))B^{-1}h\ dx.$$

Using the adjoint equation (4.51b) and relying on $\eta = S'(\bar{u})h \in \mathbb{W}_0^r \subset L^r(I; W^{1,\beta}(\Omega))$ being the solution of the linearized equation (4.28), it follows that

$$f'(\bar{u})h = \int_0^T \langle(-\partial_t + A^* + [\mathbf{g}'(\bar{y}(t))]^*)\bar{p}, \eta\rangle_{W^{-1,\beta'},W^{1,\beta}}\, dt + \int_\Omega (\bar{u}(x) - u_b(x))\, B^{-1}h\ dx.$$

Applying Green's identity to the latter and considering the linearized equation (4.28), it holds

$$\begin{aligned} f'(\bar{u})h = & \int_0^T \langle\bar{p}, (\partial_t + A + [\mathbf{g}'(\bar{y}(t))])\eta\rangle_{W^{1,\beta'},W^{-1,\beta}}\, dt + \langle\bar{p}(0), \eta(0)\rangle_{(W^{-1,\beta'},W^{1,\beta'})_{\frac{1}{r},r'},(W^{-1,\beta},W^{1,\beta})_{\frac{1}{r'},r}} \\ & - \langle\bar{p}(T), \eta(T)\rangle_{(W^{-1,\beta'},W^{1,\beta'})_{\frac{1}{r},r'},(W^{-1,\beta},W^{1,\beta})_{\frac{1}{r'},r}} + \int_\Omega (\bar{u}(x) - u_b(x))\, B^{-1}h\ dx \\ = & \int_\Omega \left(\bar{p}(0) + (\bar{u} - u_b)B^{-1}\right) h\ dx, \qquad \forall h \in L^\beta(\Omega). \end{aligned}$$

Replacing the above result into equation (4.52), we finally get

$$\int_\Omega \left(\bar{p}(0) + (\bar{u} - u_b)B^{-1}\right) h(x)\, dx + \bar{\lambda}\beta \int_\Omega |\bar{u}(x)|^{\beta-2}\bar{u}(x)h(x)\, dx = 0, \forall h \in L^\beta(\Omega),$$

which corresponds to the weak formulation of (4.51c). Moreover, $\bar{u} \in L^\beta(\Omega)$ is unique, and the state and adjoint equations are well-posed, it holds that $\bar{p}(0)$ is also unique. Additionally, likewise, to the linear case, we can verify the uniqueness of the Lagrange multiplier $\bar{\lambda} \in \mathbb{R}$ for each fixed control. □

Similar to the state, the adjoint variable satisfies useful estimates.

Lemma 4.8. *Let Assumptions 3.1, 3.2, and 4.1 hold. Setting $d = 2$, with $u, \tilde{u} \in U_{ad}$ and p, $\tilde{p}$ be adjoint states associated with $y = S(u)$ and $\tilde{y} = S(\tilde{u})$, respectively. Then the following estimates hold:*

$$\|p\|_{\mathbb{W}_0^{r'}} \leq C_1, \text{ for some } C_1 > 0, \tag{4.53a}$$

$$\|p - \tilde{p}\|_{\mathbb{W}_0^{r'}} \leq C_2\|u - \tilde{u}\|_{L^\beta(\Omega)}, \text{ for some } C_2 > 0. \tag{4.53b}$$

Proof. To prove estimate (4.53a), we first apply the result of Lemma 4.7, from where there exists a positive constant c_1 such that

$$\|p\|_{\mathbb{W}_0^{r'}} \leq c_1 \left(\sum_k \|y(x_k, \cdot)\delta_{x_k}\|_{L^{r'}(I;W^{-1,\beta'}(\Omega))} + 1 \right).$$

Lemma 3.1 states that there exists $c_2 > 0$, $\|y(x_k, \cdot)\delta_{x_k}\|_{L^{r'}(I;W^{-1,\beta'}(\Omega))} \leq c_2\|y\|_{L^{r'}(I;C(\bar{\Omega}))}$. Therefore, using both results joining with the embedding, $\mathbb{W}_0^r \hookrightarrow L^{r'}(I; C(\bar{\Omega}))$, yields

$$\|p\|_{\mathbb{W}_0^{r'}} \leq c_1c_2 \left(\sum_k \|y\|_{\mathbb{W}_0^r} + 1 \right) \leq c_3 \left(\|u\|_{L^\beta(\Omega)} + 1 \right), \quad \text{for some } c_3 > 0,$$

where the last inequality follows using estimate (4.11). Finally, since $u \in U_{ad} \subset L^\beta(\Omega)$, taking $C_1 := c_3(b + 1)$, the first assertion holds.

For proving estimate (4.53b), observe that the difference $\hat{p} = p - \tilde{p} \in \mathbb{W}_0^{r'}$ satisfies

$$\begin{aligned} -\partial_t\hat{p} + A^*\hat{p} + [\mathbf{g}'(y(\cdot))]^*\hat{p} = & \sum_k [y(x_k, \cdot) - \tilde{y}(x_k, \cdot)]\, \delta_{x_k} - (\mathbf{g}'(\tilde{y}(\cdot)) - \mathbf{g}'(y(\cdot)))\, \tilde{p}, \\ \hat{p}(x, T) = & \ 0. \end{aligned}$$

Its right-hand side belongs to $L^{r'}(I; W^{-1,\beta'}(\Omega))$. In fact, proceeding as in the proof of Lemma 3.1 and using the embeddings $L^{\beta'}(\Omega) \hookrightarrow W^{-1,\beta'}(\Omega)$ and $\mathbb{W}_0^r \hookrightarrow L^{r'}(I; C(\bar{\Omega}))$,

there exist positive constants c_1 and c_2 such that

$$\begin{aligned} I &= \| \sum_k \left[y(x_k, \cdot) - \tilde{y}(x_k, \cdot) \right] \delta_{x_k} - \left(\mathbf{G}'(\tilde{y}) - \mathbf{G}'(y) \right) \tilde{p} \|_{L^{r'}(I; W^{-1,\beta'}(\Omega))} \\ &\leq c_1 \| y - \tilde{y} \|_{L^{r'}(I; C(\bar{\Omega}))} + c_2 \| \left(\mathbf{G}'(\tilde{y}) - \mathbf{G}'(y) \right) \tilde{p} \|_{L^{r'}(I; L^{\beta'}(\Omega))} \end{aligned}$$

From the Lipschitz result (4.19b), and using a Hölder's inequality with $\frac{1}{\beta'} = \frac{1}{2} + \frac{\beta-2}{2\beta}$ jointly with the Lipschitz continuity of $\mathbf{G}'$ (with constant $\mathbf{L}_{G'} > 0$), it holds

$$\begin{aligned} I &\leq c_1 \mathbf{L}_{s_2} \| u - \tilde{u} \|_{L^\beta(\Omega)} + c_2 \mathbf{L}_{G'} \| \tilde{y} - y \|_{L^{r'}(I; L^2(\Omega))} \| \tilde{p} \|_{L^{r'}(I; L^{\frac{2\beta}{\beta-2}}(\Omega))} \\ &\leq c_1 \mathbf{L}_{s_2} \| u - \tilde{u} \|_{L^\beta(\Omega)} + c_2 \mathbf{L}_{G'} \mathbf{L}_{s_1} \| \tilde{u} - u \|_{L^\beta(\Omega)} \| \tilde{p} \|_{\mathbb{W}_0^{r'}} \end{aligned}$$

where the last inequality holds from (4.19a) and embeddings $L^\beta(\Omega) \hookrightarrow L^2(\Omega)$ and $W^{1,\beta'}(\Omega) \hookrightarrow L^{\frac{2\beta}{\beta-2}}(\Omega)$ [21, Corollary 9.14]. The result holds by using (4.53a). □

Even though the second-order optimality conditions are out of the scope of this thesis, we would like to take a look at the second derivative of the cost functional, which, for $d = 2$, exists due to the chain rule and the results for Theorem 4.2. Therefore, let us consider the two-dimensional case in this section. For each $u \in L^\beta(\Omega)$ and each direction $h \in L^\beta(\Omega)$ we obtain by straight forward calculations

$$f''(u)h^2 = \int_0^T \left(\sum_k (\delta_{x_k} \eta)^2 + [S\bar{u}(x_k, t) - z_o(x_k, t)] \delta_{x_k} \omega \right) dt + \int_\Omega h(x) B^{-1} h(x) \, dx,$$

where $y = S(u)$, $\eta = S'(u)h$, and $\omega = S''(u)h^2$. Using the adjoint equation (4.51b), $f''(u)h^2$ takes the form

$$f''(u)h^2 = \int_0^T \sum_k (\delta_{x_k} \eta)^2 dt + \int_0^T \langle (\partial_t + A + \mathbf{g}'(y(t)))^* p, \omega \rangle_{W^{-1,\beta'}, W_0^{1,\beta}} dt + \|h\|_{B^{-1}}^2.$$

Note that $\omega \in \mathbb{W}_0^r \hookrightarrow L^r(I; L^s(\Omega))$, and using (4.29), it follows that $(\partial_t + A + \mathbf{g}'(y(\cdot))\omega = -\mathbf{g}''(y(\cdot))\eta^2 \in L^r(I; L^s(\Omega))$. Moreover, since $p \in L^{r'}(I; W_0^{1,\beta'}(\Omega)) \hookrightarrow L^{r'}(I; L^{s'}(\Omega))$, and g'' is bounded, we find that $p\mathbf{g}''(y(\cdot)) \in L^{r'}(I; L^{s'}(\Omega))$. Consequently, integrating by parts; see, e.g., [110, Lemma7.3], yields

$$f''(u)h^2 = \int_0^T \sum_k (\delta_{x_k} \eta)^2 dt - \iint_Q p\mathbf{g}''(y(\cdot))\eta^2 dx dt + \|h\|_{B^{-1}}^2, \tag{4.54}$$

taking into account that $p(T) = \omega(0) = 0$.

Remarks of the chapter

As final remarks on this chapter, we would like to comment on what follows:

- In this and the previous chapter, we have studied the infinite-dimension $4D$-VAR problems subject to linear and semilinear parabolic PDE constraints with an initial condition in spaces of low regularity and considering pointwise evaluation in the space and an L^2-energy for the background error term, that is, without modifying the $4D$-VAR cost functional. The key element to achieving the aforementioned is maximal parabolic regularity in optimal control problems.

- Proving the well-posedness of the semilinear state equation strongly relies on the results established for the linear case. In fact, to extend results from linear to semilinear $4D$-VAR problems in infinite dimensions, it is necessary to first ensure the existence of a solution and then improve this regularity through a bootstrapping argument.

- Lemma 4.4 states the well-posedness of the non-homogeneous linearized equation in a mild sense. Then, the regularity is improved, obtaining a solution in $\mathbb{W}_0^r$. Consequently, we have proved that the non-autonomous operator, $\mathcal{A}(t) = A + \mathbf{g}'(y(t))$, satisfies maximal parabolic regularity. A similar result for non-autonomous operators can be achieved using a perturbation argument [9, Proposition 1.3]. However, to use this result, it is necessary to impose even stronger assumptions on the nonlinear term. In fact, it means that the uniform bound $\mathcal{K} > 0$, such that $g(\cdot) \leq \mathcal{K}$ (see Assumption 4.1), would additionally satisfy a size restriction of the kind $\mathcal{K} \leq \frac{1}{2M}$, for some unknown constant M, linking the operator A with the nonlinear term.

- In the semilinear setting, the adjoint operator is non-autonomous. Since there is no result, as in the linear case, establishing that the adjoint of an operator satisfying maximal parabolic regularity satisfies this property as well (see, e.g., [66, Lemma 31]). We must show the adjoint equation solution's existence by analyzing the equation itself. The latter was done using the regularity results obtained for the first-order linearized equation using the ideas given in [67].

- The analysis of the semilinear $4D$-VAR problem presented in this thesis concludes with the first-order necessary optimality conditions; establishing sufficient second-order optimality conditions (SSC) is beyond its scope. We refer to our related work [31] for the rigorous derivation of these SSC. While some estimates proven in this thesis, particularly those for the Lipschitz continuity of the linearized and adjoint equations, form a foundational part of the analysis in [31], they are by themselves insufficient to establish the crucial Lipschitz continuity

of f''. To overcome this, in [31] we developed an improved regularity framework and sharper estimates, which provided the necessary tools to establish the required Lipschitz continuity for f'' within our problem setting, thereby enabling the complete derivation of the SSC as presented therein.

Chapter 5

Variational data assimilation for parameter estimation of a COVID-19 spread model

In this chapter, we study an application of variational data assimilation in the mathematical modeling of infectious diseases. Given the global context due to the COVID-19 pandemic, we focus on studying the parameter estimation of the SARS-CoV-2 propagation model, which must consider the virus' behavior. We chose a compartmental model of susceptible, exposed, infected, and removed population that describe the transitions between these compartments through ordinary differential equations (ODEs). The system must include parameters to capture the virus behavior in different regions. The latter makes data assimilation methods ideal candidates to deal with the problem since they integrate observed data into the mathematical model, allowing accurate parameter estimation in the presence of uncertainty.

In Ecuador, the first confirmed case of SARS-CoV-2 was reported on February 29th, 2020, and two months later, our country became one of the worst hit in the region by the COVID-19 pandemic [82]. Nevertheless, this situation was not reflected in the data provided by the Public Health Ministry (MSP), which recorded positive COVID-19 cases. The lack of widespread testing and non-coordinated strategies to collect and report infections increased the uncertainty in the observed data that did not reflect the actual number of positive cases. Consequently, relying on a single source of information could introduce biases in the results (see, e.g., [88]). To mitigate this problem, it becomes necessary to incorporate multiple data sources. In our study, in addition to the official COVID-19 statistics, we also consider the official death records from the Ecuadorian Civil Registry from where we estimate the excess mortality attributed to the pandemic.

The main objective of this chapter is to develop a robust methodology to estimate

the evolution of the COVID-19 pandemic in Ecuador accurately. The latter requires adequate techniques to estimate the model parameters, which will be done using variational data assimilation methods, where the data uncertainty is considered in the covariance matrices present in the cost functional. Moreover, we look for estimating the initial condition of the model variables in addition to the parameters. Additionally, to capture the non-deterministic nature of the model variables and parameters, we consider them as random variables with a given probability distribution, as done by Li et al. in [86] in its supplementary material. To better capture the pandemic state, we combine the results obtained with data from different sources, the Public Health Ministry and the Civil Registry, considering the reliability of each source based on the number of PCR tests applied to the population. Additionally, we conducted a comparative study of the COVID-19 pandemic in Guayas and Pichincha to see how the pandemic affected each province.

This chapter is organized as follows: In the first section, we introduce the mathematical model for the virus' propagation. Section 5.2 gives a general scheme of the variational data assimilation formulation for parameter and initial condition estimation. In this section, we develop the Lagrangian approach we used to solve the minimization problem and the sufficient second-order optimality conditions. Additionally, we described the data preparation and the process to obtain the error covariance matrices. Section 5.3 briefly discusses the multimodel ensemble forecasting approach and the weights we will use for each output model. Section 5.4 presents the results of solving the variational data assimilation problem in the parameter estimation setting. Likewise, we present the results obtained with the robust methodology for Pichincha and Guayas, which gives a more reliable picture of the pandemic state and its evolution. We conclude this chapter by discussing the results and some limitations of the developed method.

5.1 SEIR Compartmental Model

To mathematically capture the behavior of the SARS-CoV-2, we use a propagation model of SEIR type (Susceptible-Exposed-Infectious-Removed), in which the infected population is divided into two compartments: documented and undocumented cases, alternatively called reported and unreported cases, respectively. We mention the following contributions [17, 38, 86, 103] where this model has been used.

The compartment of documented infected individuals consists of those who have been officially diagnosed by the public health system based on the severity of their symptoms, while the undocumented cases compartment refers to positive cases that exhibit mild or no symptoms (asymptomatic cases) that can expose a more significant

portion of the population to the virus due to its capacity of going unrecognized. The model consists of a system of coupled differential equations that describe the evolution of the model variables for a given period, considering the initial conditions for each variable. The variables in the model include S (susceptible), E (exposed), I^r (documented infected), I^u (undocumented infected), R (removed), and N (total population) of a given city or region. Additionally, the model relies on several coefficients, which play a crucial role in the dynamics of the system:

- β: Transmission rate due to documented or symptomatically infected patients.
- μ: Multiplicative factor reducing the transmission rate of undocumented patients (patients with no symptoms).
- α: Fraction of documented infected people that develop severe symptoms.
- ζ: The average latency period of the virus. It is measured in days.
- δ: The average duration of the infection. It is measured in days.

$$\frac{dS}{dt} = -\frac{\beta S I^r}{N} - \frac{\mu\beta S I^u}{N}, \qquad S(t_0) = S_0, \tag{5.1a}$$
$$\frac{dE}{dt} = \frac{\beta S I^r}{N} + \frac{\mu\beta S I^u}{N} - \frac{E}{\zeta}, \qquad E(t_0) = E_0, \tag{5.1b}$$
$$\frac{dI^r}{dt} = \alpha\frac{E}{\zeta} - \frac{I^r}{\delta}, \qquad I^r(t_0) = I_0^r, \tag{5.1c}$$
$$\frac{dI^u}{dt} = (1-\alpha)\frac{E}{\zeta} - \frac{I^u}{\delta}, \qquad I^u(t_0) = I_0^u, \tag{5.1d}$$
$$\frac{dR}{dt} = \frac{I^r + I^u}{\delta}, \qquad R(t_0) = R_0. \tag{5.1e}$$

According to Li et. al in [86], the model parameters have the following prior ranges: $0.8 \leq \beta \leq 1.5$, $0.2 \leq \mu \leq 1$, $0.02 \leq \alpha \leq 1$, a mean latency period ζ between 2 and 5 days, and an average duration of the infection, δ, in infected patients from 2 to 5 days. These intervals were computed at a 95% confidence level using a Latin hypercube sampling (LHS) with $n = 300$ simulations. This information will be helpful later while building one of the error covariance matrices.

We recall that the SEIR model (5.1) assumes no mobility between cities or provinces. As a result, we will examine how the virus behaves and spreads within individual provinces that are isolated from one another. In our particular case, this assumption is logical since one of the government's measures during the COVID-19 crisis was restricting travel between provinces. For a complete model where mobility between cities plays a crucial role, we refer to [86].

On the other hand, since the spread of the virus depends on random encounters between infected and non-infected individuals, the model would have to account for the stochasticity. According to [86], in its supplementary material, the core model (5.1) can be integrated stochastically using a random sample from a Poisson distribution on each term on the right-hand side of the coupled system:

$$U_1 = \text{Poiss}\left(\frac{\beta S I^r}{N}\right), \quad U_2 = \text{Poiss}\left(\frac{\mu\beta S I^u}{N}\right), \quad U_3 = \text{Poiss}\left(\frac{E}{\zeta}\right),$$
$$U_4 = \text{Poiss}\left(\alpha\frac{E}{\zeta}\right), \quad U_5 = \text{Poiss}\left(\frac{I^r}{\delta}\right), \quad U_6 = \text{Poiss}\left((1-\alpha)\frac{E}{\zeta}\right),$$
$$U_7 = \text{Poiss}\left(\frac{I^u}{\delta}\right).$$

Then, the non-deterministic virus spread model takes the form:

$$\frac{dS}{dt} = -U_1 - U_2, \qquad S(t_0) = S_0 \tag{5.2a}$$
$$\frac{dE}{dt} = U_1 + U_2 - U_3, \qquad E(t_0) = E_0 \tag{5.2b}$$
$$\frac{dI^r}{dt} = U_4 - U_5, \qquad I^r(t_0) = I_0^r \tag{5.2c}$$
$$\frac{dI^u}{dt} = U_6 - U_7, \qquad I^u(t_0) = I_0^u \tag{5.2d}$$
$$\frac{dR}{dt} = \frac{I^r + I^u}{\delta}, \qquad R(t_0) = R_0. \tag{5.2e}$$

The model parameters must be computed, considering the population's behavior in the studied region, reflected in observable data, such as the number of positive COVID-19 cases. To do that, we use the time-evolving Bayesian variational data assimilation approach that accounts for the epidemiological dynamics. Additionally, this approach allows us to consider the uncertainty associated with the observed data, which is exceptionally high in the Ecuadorian case. We will develop this approach in the following section.

5.2 Variational data assimilation problem

5.2.1 Problem statement

Given the significant level of uncertainty in the Ecuadorian context, it is essential to incorporate it into the problem formulation [30]. In particular, we employ a *variational data assimilation* method, which considers the dynamical model and observations obtained at different instants. We recall the mathematical formulation of the variational

data assimilation scheme to solve the parameter estimation problem:

$$\begin{aligned} \min_{\rho} \quad & \frac{1}{2}\int_0^T (y(t)-\mathcal{H}(\mathbf{u},t))^T\mathbf{C}_t^{-1}(y(t)-\mathcal{H}(\mathbf{u},t))\ d\mu + \frac{1}{2}(\rho-\rho^b)^T\mathbf{B}^{-1}(\rho-\rho^b), \\ \text{s.t.} \quad & \frac{d\mathbf{u}}{dt} = \mathcal{M}(\mathbf{u},\rho,t),, \\ & \mathbf{u}(0)=\mathbf{u}_0, \end{aligned} \tag{5.3}$$

where ρ represents the parameters of the propagation model $\mathcal{M}$ that we aim to estimate. Matrices $\mathbf{B}$ and $\mathbf{C}_t$ represent the error covariance matrices of the background information and the observations, respectively. Matrix $\mathbf{C}_t$ describes the deviation between observed and expected events. Meanwhile, matrix $\mathbf{B}$ measures the error in the background information. If additionally to the parameters, we want to obtain an accurate estimation of the initial condition, we must include an additional term in the cost functional, resulting in the following formulation:

$$\begin{aligned} \min_{\mathbf{u}_0,\rho} \quad & \frac{1}{2}\int_0^T (y(t)-\mathcal{H}(\mathbf{u},t))^T\mathbf{C}_t^{-1}(y(t)-\mathcal{H}(\mathbf{u},t))\ d\mu \\ & + \frac{1}{2}(\rho-\rho^b)^T\mathbf{B}^{-1}(\rho-\rho^b) + \frac{1}{2}(\mathbf{u}_0-\mathbf{u}_0^b)^T\mathbf{Q}_0^{-1}(\mathbf{u}_0-\mathbf{u}_0^b), \\ \text{s.t.} \quad & \frac{d\mathbf{u}}{dt} = \mathcal{M}(\mathbf{u},\mathbf{u}_0,\rho,t), \end{aligned} \tag{5.4}$$

where $\mathbf{u}_0$ represents the model's initial condition, and $\mathbf{B}$ and $\mathbf{Q}_0$ are the error covariance matrices of the background information of the model parameters and the initial condition, respectively.

In the SARS-CoV-2 setting, if there is no mobility between regions, the constraint of the minimization problems (5.3) and (5.4) is the propagation model (5.1). In the first case, the solutions of the data assimilation variational problem are optimal parameters $\rho = (\beta, \mu, \alpha, \zeta, \delta)$, while in the second, in addition to them, we obtain optimal initial conditions $\mathbf{u}_0 = (E_0, I_0^r, I_0^u, R_0)$. The mathematical formulation we used to solve the parameter estimation problem jointly with an estimation of the initial conditions of

the virus propagation model reads as follows:

$$\min_{\mathbf{u}_0,\,\rho\,\in\,\mathcal{U}_{ad}} \quad \sum_{i,j}(I^r(t_i)-I_i^{obs})\mathbf{C}_{ij}^{-1}(I^r(t_j)-I_j^{obs}))+(\rho-\rho^b)^T\mathbf{B}^{-1}(\rho-\rho^b) \tag{5.5a}$$

$$+(\mathbf{u}_0-\mathbf{u}_0^b)^T\mathbf{Q}_0^{-1}(\mathbf{u}_0-\mathbf{u}_0^b)=J(\bar{\mathbf{u}},\bar{\rho},\bar{\mathbf{u}}_0)$$

$$\text{s.t.} \quad \frac{dS}{dt}=-\frac{\beta SI^r}{N}-\frac{\mu\beta SI^u}{N}, \qquad S(t_0)=S_0, \tag{5.5b}$$

$$\frac{dE}{dt}=\frac{\beta SI^r}{N}+\frac{\mu\beta SI^u}{N}-\frac{E}{\zeta}, \qquad E(t_0)=E_0, \tag{5.5c}$$

$$\frac{dI^r}{dt}=\alpha\frac{E}{\zeta}-\frac{I^r}{\delta}, \qquad I^r(t_0)=I_0^r, \tag{5.5d}$$

$$\frac{dI^u}{dt}=(1-\alpha)\frac{E}{\zeta}-\frac{I^u}{\delta}, \qquad I^u(t_0)=I_0^u, \tag{5.5e}$$

$$\frac{dR}{dt}=\frac{I^r+I^u}{\delta}, \qquad R(t_0)=R_0, \tag{5.5f}$$

where $\rho=(\beta,\mu,\alpha,\zeta,\delta)^T$ is the vector of parameters, and $\mathcal{U}_{ad}$ represents the admissible set formed by the intervals of each parameter. The variable I_i^{obs}, $i=1,\ldots,n$, represents the active COVID-19 cases obtained from two different data sources, the first one the official records provided by the Ecuadorian Public Health Ministry, and the second one computed from the mortality excess retrieved from the Civil Registry. With these optimal inputs, we can compute the SARS-CoV-2 propagation model outputs, $\mathbf{u}=(S,E,I^r,I^u,R)$, for a given time window. Moreover, to account for the stochasticity, once the optimal parameters and initial conditions have been computed, we will calculate the solution vector $\mathbf{u}$ using the stochastic SEIR model (5.2).

5.2.2 First-order optimality condition

Since the constraint of the minimization problem (5.5) is a system of differential equations, it has to be solved as an optimal control problem. In this framework, the state variable $\mathbf{u}=(S,E,I^r,I^u,R)$ is an element of the absolutely continuous functions $AC([t_0,t_n],\mathbb{R}^5)$. This choice is justified by the measurability of the right-hand side of equations (5.1a)-(5.1e) with respect to time for a fixed $\mathbf{u}$, its differentiability with respect to $\mathbf{u}$ for any t, and the boundedness of this derivative in compact sets; see, e.g., [3, Section 2.5.1].

We compute the first-order optimality system using the Lagrangian approach. The

Lagrangian of the problem has the form:

$$\begin{aligned}\mathcal{L} = J(\mathbf{u}, \mathbf{u}_0, \rho) + \int_{t_0}^{t_n} \Bigg(& \lambda_S \left[-\frac{dS}{dt} - \frac{\beta S I^r + \mu \beta S I^u}{N} \right] + \lambda_I \left[-\frac{dI^r}{dt} + \alpha \frac{E}{\zeta} - \frac{I^r}{\delta} \right] \\ & + \lambda_E \left[-\frac{dE}{dt} + \frac{\beta S I^r + \mu \beta S I^u}{N} - \frac{E}{\zeta} \right] + \lambda_U \left[-\frac{dI^u}{dt} + (1-\alpha)\frac{E}{\zeta} - \frac{I^u}{\delta} \right] \\ & + \lambda_R \left[-\frac{dR}{dt} + \frac{I^r + I^u}{\delta} \right] \Bigg) \, dt + \theta_S (N - S(t_0) - E_0 - I_0^r - I_0^u - R_0) \\ & + \theta_E (E_0 - E(t_0)) + \theta_I (I_0^r - I^r(t_0)) + \theta_U (I_0^u - I^u(t_0)) + \theta_R (R_0 - R(t_0)),\end{aligned} \tag{L}$$

where $\boldsymbol{\lambda} = (\lambda_S, \lambda_E, \lambda_I, \lambda_U, \lambda_R) \in AC([t_0, t_n], \mathbb{R}^5)$ is the Lagrange multiplier associated with the problem's constraint, and $\boldsymbol{\theta} = (\theta_S, \theta_E, \theta_I, \theta_U, \theta_R) \in \mathbb{R}^5$ is the multiplier associated with the initial condition of the problem.

The existence of the Lagrange multipliers is guaranteed if a regularity condition is satisfied. To state this condition, let us introduce the following sets and functions. Let U be an open set in $\mathbb{R} \times \mathbb{R}^5 \times \mathbb{R}^5$ and let the function $\varphi(t, \mathbf{u}(t), \rho) \colon U \longrightarrow \mathbb{R}^5$ denote abbreviately the right-hand side of the differential system equations (5.1a)-(5.1e). Additionally, let us write the problem's initial condition as

$$\begin{bmatrix} -1 & -1 & -1 & -1 \\ 1 & 0 & 0 & 0 \\ 0 & 1 & 0 & 0 \\ 0 & 0 & 1 & 0 \\ 0 & 0 & 0 & 1 \end{bmatrix} \mathbf{u}_0 + \begin{bmatrix} N \\ 0 \\ 0 \\ 0 \\ 0 \end{bmatrix} =: \mathbf{M}\mathbf{u}_0 + m.$$

Besides, let us consider the mapping $e \colon \mathcal{U} \longrightarrow L^1([t_0, t_n], \mathbb{R}^5) \times \mathbb{R}^5$ determined by

$$\mathcal{U} \ni (\mathbf{u}, \rho, \mathbf{u}_0) \mapsto e(\mathbf{u}, \rho, \mathbf{u}_0) = \left(\frac{d\mathbf{u}}{dt} - \varphi(\cdot, \mathbf{u}, \rho) \ , \quad \mathbf{u}(t_0) - \mathbf{M}\mathbf{u}_0 - m \right),$$

where

$$\mathcal{U} = \{(\mathbf{u}(\cdot), \rho, \mathbf{u}_0) : (t, \mathbf{u}(t), \rho) \in U, t_0 \leq t \leq t_n, \mathbf{u}_0 \in \mathbb{R}^4_+\} \subset AC([t_0, t_n], \mathbb{R}^5) \times \mathbb{R}^5 \times \mathbb{R}^4.$$

The mapping e defines a superposition operator, which is differentiable in $\mathcal{U}$; see Proposition 3 in [3, Section 2.4.1]. Likewise, $e'(\mathbf{u}, \rho, \mathbf{u}_0)$ defines the linear and continuous

mapping:

$$e'(\mathbf{u},\rho,\mathbf{u}_0)\colon AC([t_0,t_n],\mathbb{R}^5)\times\mathbb{R}^5\times\mathbb{R}^4 \longrightarrow L^1([t_0,t_n],\mathbb{R}^5)\times\mathbb{R}^5$$
$$\mathbf{h}=(h,h_\rho,h_0)\mapsto e'(\mathbf{u},\rho,\mathbf{u}_0)\mathbf{h}=\begin{bmatrix}\frac{d(\cdot)}{dt}-\varphi_{\mathbf{u}} & -\varphi_\rho & \mathbf{0}\\ \delta_{t_0}(\cdot) & \mathbf{0} & -\mathbf{M}\end{bmatrix}\mathbf{h}$$

where the subindex on φ stands for the partial derivative of this function with respect to its corresponding variables. We will be using this notation for other functions in what follows. Likewise, $\delta_{t_0}(\cdot)$ denotes the evaluation operator, that is, $\delta_{t_0}(v)=v(t_0)$ for some function v. Consequently,

$$e'(\mathbf{u},\rho,\mathbf{u}_0)\mathbf{h}(t)=\left(\frac{dh(t)}{dt}-\varphi_{\mathbf{u}}(t)h(t)-\varphi_\rho(t)h_\rho,\quad h(t_0)-\mathbf{M}h_0\right). \tag{5.6}$$

Note that, for each t, the partial derivatives of φ with respect to $\mathbf{u}$ and ρ are given by

$$\varphi_{\mathbf{u}}(t)=\begin{bmatrix}\frac{-\beta I^r-\mu\beta I^u}{N} & 0 & -\frac{\beta S}{N} & -\frac{\mu\beta S}{N} & 0\\ \frac{\beta I^r+\mu\beta I^u}{N} & -\frac{1}{\zeta} & \frac{\beta S}{N} & \frac{\mu\beta S}{N} & 0\\ 0 & \frac{\alpha}{\zeta} & -\frac{1}{\delta} & 0 & 0\\ 0 & \frac{1-\alpha}{\zeta} & 0 & -\frac{1}{\delta} & 0\\ 0 & 0 & \frac{1}{\delta} & \frac{1}{\delta} & 0\end{bmatrix},$$

$$\varphi_\rho(t)=\begin{bmatrix}\frac{-SI^r-\mu SI^u}{N} & -\frac{\beta SI^u}{N} & 0 & 0 & 0\\ \frac{SI^r+\mu SI^u}{N} & \frac{\beta SI^u}{N} & 0 & \frac{E}{\zeta^2} & 0\\ 0 & 0 & \frac{E}{\zeta} & -\frac{\alpha E}{\zeta^2} & \frac{I^r}{\delta^2}\\ 0 & 0 & -\frac{E}{\zeta} & -\frac{(1-\alpha)E}{\zeta^2} & \frac{I^u}{\delta^2}\\ 0 & 0 & 0 & 0 & -\frac{I^r+I^u}{\delta^2}\end{bmatrix}.$$

The existence of Lagrange multipliers is guaranteed if

$$Im\left[e'(\mathbf{u},\rho,\mathbf{u}_0)\right]=\{(y(\cdot),\theta)\in L^1([t_0,t_n],\mathbb{R}^5)\times\mathbb{R}^5 : \exists(h(\cdot),h_\rho,h_0)\in AC([t_0,t_n],\mathbb{R}^5)\times\mathbb{R}^5\times\mathbb{R}^4$$
$$\text{such that } e'(\mathbf{u},\rho,\mathbf{u}_0)[h(\cdot),h_\rho,h_0]=(y(\cdot),\theta)\}$$

is a closed subspace of $L^1([t_0,t_n],\mathbb{R}^5)\times\mathbb{R}^5$; see [3, Section 3.2]. Note that for each $(y(\cdot),\theta)\in L^1([t_0,t_n],\mathbb{R}^5)\times\mathbb{R}^5$, the equation $e'(\mathbf{u},\rho,\mathbf{u}_0)[h,h_\rho,h_0](t)=(y(t),\theta)$ is equivalent to the linear differential equation, with continuous coefficients,

$$\begin{cases}\frac{dh(t)}{dt}-\varphi_{\mathbf{u}}(t)h(t)-\varphi_\rho(t)h_\rho & =y(t),\\ h(t_0)-\mathbf{M}h_0 & =\theta,\end{cases} \tag{5.7}$$

which according to [3, Section 2.5.4] possesses a solution $h(\cdot) \in AC([t_0, t_n], \mathbb{R}^5)$. Consequently, the mapping $e'(\mathbf{u}, \rho, \mathbf{u}_0)$ is surjective, that is, its image coincides with $L^1([t_0, t_n], \mathbb{R}^5) \times \mathbb{R}^5$, from where we can conclude its closedness.

On the other hand, observe that for fixed $h_\rho \in \mathbb{R}^5$ and $h_0 \in \mathbb{R}^4$, and for each $(y(\cdot), \theta) \in L^1([t_0, t_n], \mathbb{R}^5) \times \mathbb{R}^5$, the linear differential equation:

$$\begin{cases} \frac{dh(t)}{dt} - \varphi_{\mathbf{u}}(t)h(t) & = y(t) + \varphi_\rho(t)h_\rho, \\ h(t_0) & = \theta + \mathbf{M}h_0, \end{cases}$$

has a unique solution, i.e., the operator $e_{\mathbf{u}}(\mathbf{u}, \rho, \mathbf{u}_0)$ is bijective. As a result, the bijectivity of $e_{\mathbf{u}}(\mathbf{u}, \rho, \mathbf{u}_0)$ ensures the existence of Lagrange multipliers.

The adjoint system is obtained by differentiating equation (L) with respect to the state variable $\mathbf{u} = (S, E, I^r, I^u, R)$ in an arbitrary direction $\boldsymbol{\nu} = (\sigma, \xi, w, v, r)$ and set the result equal to zero (see, e.g., [3, 39]). That is,

$$\begin{aligned}
\nabla_S \mathcal{L}[\sigma] &= \int_{t_0}^{t_n} \left[\frac{d\lambda_S}{dt} + \left(\frac{\beta I^r}{N} + \frac{\mu\beta I^u}{N} \right) (\lambda_E - \lambda_S) \right] \sigma \, dt - \lambda_S(t_n)\sigma(t_n) \\
&\quad + \sigma(t_0)(\lambda_S(t_0) + \theta_S) = 0 \\
\nabla_E \mathcal{L}[\xi] &= \int_{t_0}^{t_n} \left[\frac{d\lambda_E}{dt} + \alpha\frac{\lambda_I}{\zeta} + (1-\alpha)\frac{\lambda_U}{\zeta} - \frac{\lambda_E}{\zeta} \right] \xi \, dt - \lambda_E(t_n)\xi(t_n) \\
&\quad + \xi(t_0)(\lambda_E(t_0) + \theta_E) = 0 \\
\nabla_{I^r} \mathcal{L}[w] &= \int_{t_0}^{t_n} \left[\frac{d\lambda_I}{dt} + \frac{\partial J}{\partial I^r} - \frac{\beta S\lambda_S}{N} + \frac{\beta S\lambda_E}{N} - \frac{\lambda_I}{\delta} + \frac{\lambda_R}{\delta} \right] w \, dt \\
&\quad + w(t_n)(C_{nn}^{-1}(I^r(t_n) - I_n^{obs}) - \lambda_I(t_n)) + w(t_0)(\lambda_I(t_0) + \theta_I) = 0 \\
\nabla_{I^u} \mathcal{L}[v] &= \int_{t_0}^{t_n} \left[\frac{d\lambda_U}{dt} - \frac{\mu\beta S\lambda_S}{N} + \frac{\mu\beta S\lambda_E}{N} - \frac{\lambda_U}{\delta} + \frac{\lambda_R}{\delta} \right] v \, dt - v(t_n)\lambda_U(t_n) \\
&\quad + v(t_0)(\lambda_U(t_0) + \theta_U) = 0 \\
\nabla_R \mathcal{L}[r] &= \int_{t_0}^{t_n} \frac{d\lambda_R}{dt} r \, dt - r(t_n)\lambda_R(t_n) + r(t_0)(\lambda_R(t_0) + \theta_R) = 0.
\end{aligned}$$

Finally, since the direction $\boldsymbol{\nu}$ was taken arbitrarily, the latter yields the following adjoint

system:

$$-\frac{d\lambda_S}{dt} = \left(\frac{\beta I^r}{N} + \frac{\mu\beta I^u}{N}\right)(\lambda_E - \lambda_S), \qquad \lambda_S(t_n) = 0 \tag{5.8a}$$

$$-\frac{d\lambda_E}{dt} = -\frac{1}{\zeta}\lambda_E + \frac{\alpha}{\zeta}\lambda_I + \frac{(1-\alpha)}{\zeta}\lambda_U, \qquad \lambda_E(t_n) = 0 \tag{5.8b}$$

$$-\frac{d\lambda_I}{dt} = \frac{\partial J}{\partial I^r} - \frac{\beta S}{N}(\lambda_S - \lambda_E) - \frac{\lambda_I}{\delta} + \frac{\lambda_R}{\delta}, \qquad \lambda_I(t_n) = C_{nn}^{-1}(I^r(t_n) - I_n^{obs}) \tag{5.8c}$$

$$-\frac{d\lambda_U}{dt} = -\frac{\mu\beta S}{N}(\lambda_S - \lambda_E) - \frac{\lambda_U}{\delta} + \frac{\lambda_R}{\delta}, \qquad \lambda_U(t_n) = 0 \tag{5.8d}$$

$$-\frac{d\lambda_R}{dt} = 0, \qquad \lambda_R(t_n) = 0. \tag{5.8e}$$

Additionally, the multiplier $\boldsymbol{\theta}$ takes the value of the adjoint at the initial time $\boldsymbol{\lambda}(t_0)$, that is:

$$\theta_S = \lambda_S(t_0), \quad \theta_E = \lambda_E(t_0), \quad \theta_I = \lambda_I(t_0), \quad \theta_U = \lambda_u(t_0), \quad \theta_R = \lambda_R(t_0).$$

To get the gradient of the problem, we have to derive the Lagrangian (L) with respect to the parameters and with respect to the initial conditions. Computing first the derivative with respect to $\rho = (\beta, \mu, \alpha, \zeta, \delta)^T$, we obtain:

$$\nabla_\beta J = \mathbf{B}_\beta^{-1}(\beta - \beta^b) - \int_0^T \frac{S}{N}(I^r + \mu I^u)(\lambda_S - \lambda_E)\, dt, \tag{5.9a}$$

$$\nabla_\mu J = \mathbf{B}_\mu^{-1}(\mu - \mu^b) - \int_0^T \beta\frac{S}{N} I^u (\lambda_S - \lambda_E)\, dt, \tag{5.9b}$$

$$\nabla_\alpha J = \mathbf{B}_\alpha^{-1}(\alpha - \alpha^b) + \int_0^T \frac{E}{\zeta}(\lambda_I - \lambda_u) dt, \tag{5.9c}$$

$$\nabla_\zeta J = \mathbf{B}_\zeta^{-1}(\zeta - \zeta^b) + \int_0^T \frac{E}{\zeta^2}(\lambda_E - \alpha\lambda_I - (1-\alpha)\lambda_U) dt, \tag{5.9d}$$

$$\nabla_\delta J = \mathbf{B}_\delta^{-1}(\delta - \delta^b) + \int_0^T \frac{1}{\delta^2}(I^r\lambda_I + I^u\lambda_u - \lambda_R(I^r + I^u))\, dt. \tag{5.9e}$$

Likewise, computing the derivative of the Lagrangian with respect to the initial conditions, $\mathbf{u}_0 = (E_0, I_0^r, I_0^u, R_0)$, we get the following system:

$$\nabla_{E_0} J = \left(\mathbf{Q}_0^{-1}(\mathbf{u}_0 - \mathbf{u}_0^b)\right)_1 - \lambda_S(t_0) + \lambda_E(t_0), \tag{5.10a}$$

$$\nabla_{I_0^r} J = \left(\mathbf{Q}_0^{-1}(\mathbf{u}_0 - \mathbf{u}_0^b)\right)_2 - \lambda_S(t_0) + \lambda_I(t_0), \tag{5.10b}$$

$$\nabla_{I_0^u} J = \left(\mathbf{Q}_0^{-1}(\mathbf{u}_0 - \mathbf{u}_0^b)\right)_3 - \lambda_S(t_0) + \lambda_U(t_0), \tag{5.10c}$$

$$\nabla_{R_0} J = \left(\mathbf{Q}_0^{-1}(\mathbf{u}_0 - \mathbf{u}_0^b)\right)_4 - \lambda_S(t_0) + \lambda_R(t_0), \tag{5.10d}$$

where$\left(\mathbf{Q}_0^{-1}(\mathbf{u}_0 - \mathbf{u}_0^b)\right)_i$ represent the i-component of the vector $\left(\mathbf{Q}_0^{-1}(\mathbf{u}_0 - \mathbf{u}_0^b)\right)_{1\times 4}^T$.

Since the control variable corresponding to the model parameters belongs to the admissible set $\mathcal{U}_{ad}$, the optimality condition of the problem is defined with the following variational inequality:

$$\nabla J(\bar{\mathbf{u}}_0, \bar{\rho})^T[(\mathbf{u}_0, \rho) - (\bar{\mathbf{u}}_0, \bar{\rho})] \geq 0, \qquad \forall \rho \in \mathcal{U}_{ad}, \forall \mathbf{u}_0 \in \mathbb{R}^4_+, \tag{5.11}$$

where the partial derivatives forming the gradient $\dfrac{\partial J}{\partial \rho}$ and $\dfrac{\partial J}{\partial \mathbf{u}_0}$ are given in (5.9) and (5.10), respectively. Note that since the box constraint for ρ and $\mathbf{u}_0$ are convex sets: $\mathcal{U}_{ad} = \{\rho \in \mathbb{R}^5 : \rho_\ell \leq \rho \leq \rho_u\}$ where for each $i \in \{1, \ldots, 5\}$, ρ_i^ℓ and ρ_i^u represent the lower and upper bounds for each parameter, and, for each $j \in \{1, \ldots, 4\}$, the lower bound of $\mathbf{u}_0^j$ is taken as 0. Then, the variational inequality (5.11) can be replaced for a pointwise projection (see e.g., [39, Section 5.2]), as follows:

$$\begin{aligned} &\bar{\rho}_i - P\left(\bar{\rho}_i - \gamma \nabla_{\rho_i} J\right) = 0, && \text{for } i \in \{1, \ldots, 5\} \\ &\bar{\mathbf{u}}_0^j - P\left(\bar{\mathbf{u}}_0^j - \gamma \nabla_{\mathbf{u}_0^j} J\right) = 0, && \text{for } j \in \{1, \ldots, 4\}, \end{aligned}$$

for every $\gamma > 0$. Where the projection operators are given by:

$$P(\rho)_i = \begin{cases} \rho_i^\ell, & \rho_i \leq \rho_i^\ell, \\ \rho_i, & \rho_i^\ell < \rho_i < \rho_i^u, \\ \rho_i^u, & \rho_i^u \leq \rho_i \end{cases} \qquad P(\mathbf{u}_0)_j = \begin{cases} 0, & \mathbf{u}_0^j \leq 0, \\ \mathbf{u}_0^j, & 0 < \mathbf{u}_0^j < +\infty. \end{cases}$$

Remark 5.1. *We acknowledge that Pontryagin's Maximum Principle provides a standard approach for deriving the optimality conditions; see, e.g., [35, Theorem 22.2] which can be applied in our problem setting to directly obtain the optimality conditions. However, in this section, we decided to work with the Lagrangian method. This choice is motivated by our objective not only to obtain the adjoint and gradient equations but also to explicitly establish the regularity conditions that ensure the existence of the Lagrange multipliers within our problem's framework, as detailed in the discussion preceding the adjoint system derivation.*

5.2.3 Sufficient second-order optimality condition

To analyze the second-order optimality condition, we use the Hamiltonian associated to the problem:

$$\begin{aligned} H \colon \mathbb{R}^5 \times \mathbb{R}^4 \times \mathbb{R}^5 \times \mathbb{R}^5 &\longrightarrow \mathbb{R} \\ (\rho, \mathbf{u}_0, \mathbf{u}(t), \boldsymbol{\lambda}(t)) &\mapsto H(\rho, \mathbf{u}_0, \mathbf{u}(t), \boldsymbol{\lambda}(t)), \end{aligned}$$

where, for a.e. $t \in (t_0, t_n)$,

$$H(\rho, \mathbf{u}_0, \mathbf{u}(t), \boldsymbol{\lambda}(t)) = J(\mathbf{u}, \rho, \mathbf{u}_0) + \lambda_S(t)\left(-\frac{\beta S(t) I^r(t) + \mu\beta S(t) I^u(t)}{N}\right) + \lambda_I(t)\left(\alpha\frac{E(t)}{\zeta} - \frac{I^r(t)}{\delta}\right) + \lambda_E(t)\left(\frac{\beta S(t) I^r(t) + \mu\beta S(t) I^u(t)}{N} - \frac{E(t)}{\zeta}\right) + \lambda_U(t)\left((1-\alpha)\frac{E(t)}{\zeta} - \frac{I^u(t)}{\delta}\right) + \lambda_R(t)\left(\frac{I^r(t) + I^u(t)}{\delta}\right).$$

Observe that by integrating by parts, we can rewrite the Lagrangian, using the Hamiltonian, as follows

$$\mathcal{L} = \int_0^T \left(H(\rho, \mathbf{u}_0, \mathbf{u}(t), \boldsymbol{\lambda}(t)) + \frac{d\boldsymbol{\lambda}(t)}{dt}\mathbf{u}(t)\right) dt - \boldsymbol{\lambda}(T)\mathbf{u}(T) + \boldsymbol{\lambda}(0)\mathbf{u}(0) + \boldsymbol{\theta}(u_0 - \mathbf{u}(0)).$$

Consequently, the second-order derivative of the Lagrangian in a direction $[h, h_\rho, h_0]$ can be expressed by using the second-order derivative of the Hamiltonian, that is,

$$\nabla^2_{\mathbf{u},\rho,\mathbf{u}_0}\mathcal{L}[(h, h_\rho, h_0), (h, h_\rho, h_0)] = \int_{t_0}^{t_n} \nabla^2_{\mathbf{u}} H[h, h]dt + \int_{t_0}^{t_n} \nabla^2_{\rho} H[h_\rho, h_\rho]dt + \int_{t_0}^{t_n} \nabla^2_{\mathbf{u}_0} H[h_0, h_0]dt + 2\int_{t_0}^{t_n} \nabla^2_{(\mathbf{u},\rho)} H[h, h_\rho]dt, \quad (5.12)$$

since $\nabla^2_{(\mathbf{u},\mathbf{u}_0)}H = \nabla^2_{(\rho,\mathbf{u}_0)}H = \mathbf{0}_{5\times 4}$. Moreover $\nabla^2_{\mathbf{u}_0}H = \mathbf{Q}_0^{-1}$, and $\nabla^2_{\mathbf{u}}H$ and $\nabla^2_{(\mathbf{u},\rho)}H$ have the form:

$$\nabla^2_{\mathbf{u}}H = \begin{bmatrix} 0 & 0 & \frac{\beta}{N}(\lambda_E(t) - \lambda_S(t)) & \frac{\mu\beta}{N}(\lambda_E(t) - \lambda_S(t)) & 0 \\ 0 & 0 & 0 & 0 & 0 \\ \frac{\beta}{N}(\lambda_E(t) - \lambda_S(t)) & 0 & \frac{\partial^2 J}{\partial I_r^2} & 0 & 0 \\ \frac{\mu\beta}{N}(\lambda_E(t) - \lambda_S(t)) & 0 & 0 & 0 & 0 \\ 0 & 0 & 0 & 0 & 0 \end{bmatrix},$$

$$\nabla^2_{(\mathbf{u},\rho)}H = \begin{bmatrix} \nabla^2_{(S,\beta)}H & \nabla^2_{(S,\mu)}H & 0 & 0 & 0 \\ 0 & 0 & \nabla^2_{(E,\alpha)}H & \nabla^2_{(E,\zeta)}H & 0 \\ \nabla^2_{(I^r,\beta)}H & 0 & 0 & 0 & \nabla^2_{(I^r,\delta)}H \\ \nabla^2_{(I^u,\beta)}H & \nabla^2_{(I^u,\mu)}H & 0 & 0 & \nabla^2_{(I^u,\delta)}H \\ 0 & 0 & 0 & 0 & 0 \end{bmatrix},$$

with

$$\nabla^2_{(S,\beta)}H = \left[\frac{I^r}{N}(\lambda_E(t)-\lambda_S(t)) + \frac{\mu I^u(t)}{N}(\lambda_E(t)-\lambda_S(t))\right],$$

$$\nabla^2_{(E,\zeta)}H = \frac{1}{\zeta^2}[\lambda_E(t)-\alpha\lambda_I(t)-(1-\alpha)\lambda_U(t)], \quad \nabla^2_{(E,\alpha)}H = \frac{1}{\zeta}(\lambda_I(t)-\lambda_U(t)),$$
$$\nabla^2_{(I^r,\beta)}H = \frac{S}{N}(\lambda_E(t)-\lambda_S(t)), \qquad \nabla^2_{(I^r,\delta)}H = \frac{1}{\delta^2}(\lambda_I(t)-\lambda_R(t)),$$
$$\nabla^2_{(I^u,\beta)}H = \frac{\mu S}{N}(\lambda_E(t)-\lambda_S(t)), \qquad \nabla^2_{(I^u,\mu)}H = \frac{\beta S}{N}(\lambda_E(t)-\lambda_S(t)),$$
$$\nabla^2_{(I^u,\delta)}H = \frac{1}{\delta^2}(\lambda_U(t)-\lambda_R(t)) \qquad \nabla^2_{(S,\mu)}H = \frac{\beta I^u(t)}{N}(\lambda_E(t)-\lambda_S(t)).$$

Likewise, $\nabla^2_\rho H(\rho, \mathbf{u}_0, \mathbf{u}(t), \boldsymbol{\lambda}(t))$ has the form:

$$\begin{pmatrix} \mathbf{B}_\beta^{-1} & \nabla^2_{(\beta,\mu)}H & 0 & 0 & 0 \\ \nabla^2_{(\beta,\mu)}H & \mathbf{B}_\mu^{-1} & 0 & 0 & 0 \\ 0 & 0 & \mathbf{B}_\alpha^{-1} & \nabla^2_{(\zeta,\alpha)}H & 0 \\ 0 & 0 & \nabla^2_{(\zeta,\alpha)}H & \nabla^2_\zeta H & 0 \\ 0 & 0 & 0 & 0 & \nabla^2_\delta H \end{pmatrix}$$

with

$$\nabla^2_{(\beta,\mu)}H = \frac{S(t)I(t)^u}{N}(\lambda_E(t)-\lambda_S(t))$$
$$\nabla^2_{(\zeta,\alpha)}H = \frac{E(t)}{\zeta^2}(\lambda_U(t)-\lambda_I(t))$$

$$\nabla^2_\zeta H = \mathbf{B}_\zeta^{-1} - \frac{2E(t)}{\zeta^3}[\lambda_E(t)-\alpha\lambda_I(t)-(1-\alpha)\lambda_U(t)],$$
$$\nabla^2_\delta H = \mathbf{B}_D^{-1} - \frac{2I^r(t)}{\delta^3}[\lambda_I(t)-\lambda_R(t)] - \frac{2I^u(t)}{\delta^3}[\lambda_U(t)-\lambda_R(t)].$$

Before evaluating the quantities in (5.12) and since most of the matrices above include the term $\boldsymbol{\lambda}(t)$, let us find a bound for the adjoint variable. In fact, writing $V(t) = \varphi_u(t)^T$ and transforming the time variable $t \to t_n - t + t_0$, we can write the adjoint system (5.8) forward in time as follows:

$$\frac{d\boldsymbol{\lambda}(t)}{dt} - V(t)\boldsymbol{\lambda}(t) = \mathbf{b}, \qquad \boldsymbol{\lambda}(t_0) = \boldsymbol{\lambda}_0, \tag{5.13}$$

where $\mathbf{b} = (0, 0, \frac{\partial J}{\partial I^r}, 0, 0)^T$, with $\frac{\partial J}{\partial I^r} = \sum_i (I^r(t_i) - I_i^{obs})\mathbf{C}_{ii}^{-1}$.

Moreover, $\boldsymbol{\lambda}_0 = (0, 0, \mathbf{C}_{nn}^{-1}(I^r(t_n) - I_n^{obs}), 0, 0)^T$. Equivalently, using the integral

representation of the system (5.13), we obtain

$$\boldsymbol{\lambda}(t) = \boldsymbol{\lambda}_0 + \int_{t_0}^{t_n} V(\tau)\boldsymbol{\lambda}(\tau)d\tau + \int_{t_0}^{t_n} \mathbf{b}\ d\tau.$$

Computing the norm of the above expression and using Gronwall's inequality yields

$$\begin{aligned}\|\boldsymbol{\lambda}(t)\| &\leq (\|\boldsymbol{\lambda}_0\| + \|\mathbf{b}\|(t_n - t_0)) \exp\left(\int_{t_0}^{t} \|V(\tau)\|d\tau\right) \\ &\leq \kappa\left(\left|\mathbf{C}_{nn}^{-1}(I^r(t_n) - I_n^{obs})\right| + (t_n - t_0)\sum_i \left|\mathbf{C}_{ii}^{-1}(I^r(t_i) - I_i^{obs})\right|\right), \end{aligned} \tag{5.14}$$

for some $\kappa > 0$, which exists since $V(t)$ is bounded in compact sets. Observe that if the value of the observation is near to the solution variable I^r in a given time, weighted by the observation error covariance term; then, the adjoint variable $\boldsymbol{\lambda}(t)$ will be bounded by a sufficiently small value, for a.e. $t \in (t_0, t_n)$.

The assumption of closeness between observations and solutions is fundamental to obtaining second-order conditions. In fact, for sufficiently small values of the adjoint variable $\boldsymbol{\lambda}(t) = (\lambda_S(t), \lambda_E(t), \lambda_I(t), \lambda_U(t), \lambda_R(t))$ for a.e. $t \in (t_0, t_n)$, the matrix $\nabla^2_\rho H$ is positive definite since the terms of the diagonal matrix $\mathbf{B}^{-1}$ are strictly positive. Therefore, there exists $\delta_1 > 0$ such that $\nabla^2_\rho H[h_\rho, h_\rho] \geq \delta_1\|h_\rho\|^2$, for every $h_\rho \in \mathbb{R}^5$. Consequently,

$$\int_{t_0}^{t_n} \nabla^2_\rho H[h_\rho, h_\rho]dt \geq \int_{t_0}^{t_n} \delta_1\|h_\rho\|^2 dt = (t_n - t_0)\delta_1\|h_\rho\|^2. \tag{5.15}$$

Likewise, since $\mathbf{Q}_0^{-1}$ is positive definite, there exists $\delta_2 > 0$ such that $\nabla^2_{\mathbf{u}_0} H[h_0, h_0] \geq \delta_2\|h_0\|^2$ for every $h_0 \in \mathbb{R}^4$, and,

$$\int_{t_0}^{t_n} \nabla^2_{\mathbf{u}_0} H[h_0, h_0]dt \geq (t_n - t_0)\delta_2\|h_0\|^2. \tag{5.16}$$

Observe that (5.16) and (5.15) hold for every $(h_\rho, h_0) \in \mathbb{R}^5 \times \mathbb{R}^4$. Likewise, considering $h(\cdot) = (h_1(\cdot), h_2(\cdot), h_3(\cdot), h_4(\cdot), h_5(\cdot)) \in AC([t_0, t_n], \mathbb{R}^5)$, for sufficiently small values of $\boldsymbol{\lambda}(t)$ for a.e. $t \in (t_0, t_n)$, given that the terms of the diagonal matrix $\mathbf{C}^{-1}$ are strictly positive, it holds that $\nabla^2_{\mathbf{u}} H[h, h] = \sum_i h_3(t_i)^2\mathbf{C}_{ii}^{-1} \geq 0$, and consequently,

$$\int_{t_0}^{t_n} \nabla^2_{\mathbf{u}} H[h, h]dt \geq 0. \tag{5.17}$$

Moreover, analyzing the matrix $\nabla^2_{(\mathbf{u},\rho)}H$, it holds that

$$\left|\nabla^2_{(\mathbf{u},\rho)}H[h,h_\rho]\right| \leq c\|\boldsymbol{\lambda}(t)\|\|h(t)\|\|h_\rho\|, \qquad \text{for some } c>0. \tag{5.18}$$

Observe that for $\mathbf{h}=(h,h_\rho,h_0)\in AC([t_0,t_n],\mathbb{R}^5)\times\mathbb{R}^5\times\mathbb{R}^4$ satisfying $e'(\mathbf{u},\rho,\mathbf{u}_0)\mathbf{h}=(0,0)$, that is,

$$\frac{dh(t)}{dt}-\varphi_{\mathbf{u}}(t)h(t)-\varphi_\rho(t)h_\rho=0, \qquad h(t_0)-\mathbf{M}h_0=0,$$

we can compute a bound in terms on $\|h_\rho\|$ and $\|h_0\|$. In fact, from the integral representation of (5.2.3), which has the form

$$h(t)=\mathbf{M}h_0+\int_{t_0}^{t_n}\varphi_{\mathbf{u}}(\tau)h(\tau)d\tau+\int_{t_0}^{t_n}\varphi_\rho(\tau)h_\rho\ d\tau,$$

Gronwall's inequality yields

$$\begin{aligned}\|h(t)\| &\leq \left(\|\mathbf{M}\|\|h_0\|+\|h_\rho\|\int_{t_0}^{t}\|\varphi_\rho(\tau)\|d\tau\right)\exp\left(\int_{t_0}^{t}\|\varphi_{\mathbf{u}}(\tau)\|d\tau\right)\\ &\leq \kappa_1\left(\|\mathbf{M}\|\|h_0\|+\kappa_2(t_n-t_0)\|h_\rho\|\right)\leq\kappa(\|h_0\|+\|h_\rho\|),\end{aligned}$$

for some $\kappa_1,\kappa_2>0$, which exists since $\varphi_{\mathbf{u}}(t)$ and $\varphi_\rho(t)$ are bounded in compact sets, and where $\kappa=\max\{\kappa_1\|\mathbf{M}\|,\kappa_1\kappa_2(t_n-t_0)\}$. Therefore,

$$\left|\nabla^2_{(\mathbf{u},\rho)}H[h,h_\rho]\right|\leq c\kappa\|\boldsymbol{\lambda}(t)\|\|h_\rho\|(\|h_0\|+\|h_\rho\|).$$

Observe that if $\|h_\rho\|\leq\|h_0\|$, it holds that $\left|\nabla^2_{(\mathbf{u},\rho)}H[h,h_\rho]\right|\leq 2c\kappa\|\boldsymbol{\lambda}(t)\|\|h_0\|^2$. Analogously, if $\|h_0\|\leq\|h_\rho\|$ then $\left|\nabla^2_{(\mathbf{u},\rho)}H[h,h_\rho]\right|\leq 2c\kappa\|\boldsymbol{\lambda}(t)\|\|h_\rho\|^2$. Let us consider the first case, i.e., $\|h_\rho\|\leq\|h_0\|$, then the above inequality yields

$$-2c\kappa(t_n-t_0)\|\boldsymbol{\lambda}(t)\|\|h_0\|^2\leq\int_{t_0}^{t_n}\nabla^2_{(\mathbf{u},\rho)}H[h,h_\rho]dt\leq 2c\kappa(t_n-t_0)\|\boldsymbol{\lambda}(t)\|\|h_0\|^2. \tag{5.19}$$

Therefore, using (5.15), (5.16), and (5.19) in (5.12), it follows that,

$$\begin{aligned}\nabla^2_{\mathbf{u},\rho,\mathbf{u}_0}\mathcal{L}[(h,h_\rho,h_0),(h,h_\rho,h_0)] &\geq (t_n-t_0)\left(\delta_1\|h_\rho\|^2+(\delta_2-2c\kappa\|\boldsymbol{\lambda}(t)\|)\|h_0\|^2\right)\\ &\geq\delta\|(h_\rho,h_0)\|^2,\end{aligned}$$

where $\delta:=(t_n-t_0)\min\{\delta_1,\delta_2-2c\kappa\|\boldsymbol{\lambda}(t)\|\}$ which is positive given that, accordingly to (5.14), $\|\boldsymbol{\lambda}(t)\|$ is bounded and sufficiently small for a.e. $t\in(t_0,t_n)$, given that the observations I^{obs} and the solution variable I^r are close enough. Consequently,

the sufficient second-order optimality condition holds for every $\mathbf{h} = (h, h_\rho, h_0) \in AC([t_0, t_n], \mathbb{R}^5) \times \mathbb{R}^5 \times \mathbb{R}^4$ satisfying $e'(\mathbf{u}, \rho, \mathbf{u}_0)\mathbf{h} = (0, 0)$ if $\|\mathbf{C}_{ii}^{-1}(I^r - I^{obs})\|$ is sufficiently small.

5.2.4 Numerical algorithms

In this section, we describe the algorithms we use to solve the data assimilation problems that appear in this chapter. For our analysis, we have chosen a *discretize-then-optimize* approach since it offers advantages while finding the numerical solution to the minimization problem by employing iterative methods. In particular, we will use the projected BFGS algorithm.

Euler methods to solve the state and adjoint equations

In our case, the numerical solution of the state and adjoint equations needed for computing the cost functional gradient was solved using an explicit Euler scheme implemented in Python. In fact, for our specific SEIR problem given by equations (5.1a)-(5.1e), given a $0 \leq t_0 < T$, setting $S[t_0] = S_0$, $E[t_0] = E_0$, $I^r[t_0] = I_0^r$, $I^u[t_0] = I_0^u$, and $R[t_0] = R_0$, and $h = 1$, the explicit Euler iteration scheme has the form:

```
for i in range(t_n - 1):
        S[i+1] = S[i] - (beta*S[i]*Ir[i])/N - (mu*beta*S[i]*Iu[i])/N
        E[i+1] = E[i] + (beta*S[i]*Ir[i])/N + (mu*beta*S[i]*Iu[i])/N - (1/Z)*E[i]
        Ir[i+1] = Ir[i] + (alpha/Z)*E[i] - (1/D)*Ir[i]
        Iu[i+1] = Iu[i] + ((1-alpha)/Z)*E[i] - (1/D)*Iu[i]
        R[i+1] = R[i] + (1/D)*Ir[i] + (1/D)*Iu[i]
```

where $S[i] = S(t_i)$, $E[i] = E(t_i)$, $Ir[i] = I^r(t_i)$, $Iu[i] = I^u(t_i)$, and $R[i] = R(t_i)$, with $t_i = t_0 + i$ and $i = 1, \ldots, T$.

Likewise, for solving the adjoint system (5.8), considering the final conditions $\lambda_S[t_n] = \lambda_E[t_n] = \lambda_U[t_n] = \lambda_R[t_n] = 0$, and $\lambda_I[t_n] = \mathbf{C}_{nn}^{-1}(I^r(t_n) - I_n^{obs})$, the explicit Euler scheme backward in time, is given as follows:

```
for i in range(t_n - 1, 0, -1):
  lambda_S[i-1] = lambda_S[i] + (beta/N)*(Ir[i]+mu*Iu[i])*(lambda_E[i]-lambda_S[i])
  lambda_E[i-1] = lambda_E[i] - lambda_E[i]/Z
                + (alfa/Z)*lambda_I[i]  + (1-alfa)/Z * lambda_U[i]
  lambda_I[i-1] = lambda_I[i] + der[i] - (beta/N)*S[i]*(lambda_S[i]-lambda_E[i])
                - (lambda_I[i]/D) + (lambda_R[i]/D)
  lambda_U[i-1] = lambda_U[i] - (mu*beta/N)*S[i]*(lambda_S[i]-lambda_E[i])
                - (lambda_U[i]/D) + (lambda_R[i]/D)
  lambda_R[i-1] = lambda_R[i]
```

where `der` corresponds $\frac{\partial J}{\partial I^r}$.

Remark 5.2. *Employing an explicit Euler scheme for the time discretization of both the state and adjoint equations means that the resulting gradient is an approximation, rather than the exact gradient of the fully discretized cost functional. However, the inexact gradient obtained via the explicit Euler adjoint serves as a computationally inexpensive approximation. The practical viability of this approach is shown by the convergence performance of the optimization method, as shown in Table 5.1.*

Besides, the solution to the problem can be found using this Hessian matrix by employing projected Newton's methods. However, the latter will require solving ODEs' systems on each iteration, which could be computationally expensive. Instead, we will solve the minimization problem using Quasi-Newton projected methods. Specifically, we use the projected BFGS algorithm with an estimation of $\epsilon-$active sets. We detail this method in the upcoming section.

Projected Quasi-Newton methods

Projected methods are used to solve minimization problems with box constraints, $\min_{w\in U_{ad}} f(w)$, with $U_{ad} = \{w : a_i \leq w_i \leq b_i\}$. Generally, these methods use the descent directions of the unconstrained problem and project the next iteration on the admissible set, that is,

$$w_{k+1} = P_{U_{ad}}(w_k + \alpha_k d_k), \tag{5.20}$$

where P represents the projection operator, d_k is a descend direction, and α_k is a projected line search parameter; see, e.g., [39, Section 5.3]. For the projected Quasi-Newton methods, it is necessary to use the information of the reduced Hessian (or its approximations) based on the estimation of $\epsilon-$active sets:

$$A^\epsilon(w) = \{i : a_i \leq w_i \leq a_i + \epsilon \text{ or } b_i \geq w_i \geq b_i - \epsilon\},$$

with $0 \leq \epsilon \leq \min_i\{b_i - a_i\}/2$. Its complement forms the $\epsilon-$inactive set, $I^\epsilon(w)$. The reduced Hessian, or an approximation, is defined as follows:

$$\tilde{R}(w_k, \epsilon_k, H_k) \quad = R_{A^{\epsilon_k}(w_k)} + R_{I^{\epsilon_k}(w_k)} H_k R_{I^{\epsilon_k}(w_k)} \quad = \begin{cases} \delta_{ij}, \text{if } i \in A^{\epsilon_k}(w_k) \text{ or } j \in A^{\epsilon_k}(w_k) \\ (H_k)_{ij}, \text{ otherwise,} \end{cases}$$

where $(R_S(w))_i = w_i$ if $i \in S$, and $(R_S(w))_i = 0$ if this is not the case, for any index set S. The model iterations will be given as follows:

$$w_{k+1} = P_{U_{ad}}(w_k - \alpha_k \tilde{R}(w_k, \epsilon_k, H_k)^{-1} \nabla f(w_k)).$$

BFGS projected method

If the approximation of the Hessian matrix is given by the BFGS method (Broyden-Fletcher-Goldfarb-Shanno), its reduced matrix will be:

$$H_{k+1} = R_{I_{k+1}} H_k R_{I_{k+1}} - R_{I_{k+1}} \frac{H_k s_k s_k^T H_k}{s_k^T H_k s_k} R_{I_{k+1}} + \frac{y_k^{\#} (y_k^{\#})^T}{s_k^T y_k^{\#}},$$

where $I_{k+1} = I^{\epsilon_{k+1}}(w_{k+1})$, $s_k = w_{k+1} - w_k$, and $y_k^{\#} = R_{I_{k+1}} (\nabla f(w_{k+1}) - \nabla f(w_k))$. In some problems, it is helpful to get updates for the generalized inverse of H_k, i.e., B_{k+1}. According to [77, Section 5.5.3], this update has the form:

$$B_{k+1} = \left(I - \frac{s_k^{\#} (y_k^{\#})^T}{(y_k^{\#})^T s_k^{\#}} \right) R_{I_{k+1}} B_k R_{I_{k+1}} \left(I - \frac{y_k^{\#} (s_k^{\#})^T}{(y_k^{\#})^T s_k^{\#}} \right) + \frac{s_k^{\#} (s_k^{\#})^T}{(y_k^{\#})^T s_k^{\#}} , \tag{5.21}$$

where $s_k^{\#} = R_{I_{k+1}}(w_{k+1} - w_k)$. Both matrices, H_k and B_k, let us compute the descent direction of the method, in particular using the update of the generalized inverse; it yields

$$d_k = -B_k \nabla f(w_k) - R_{A^{\epsilon_k}(w_k)} \nabla f(w_k).$$

The method iterations will be updated accordingly to (5.20).

The numerical solution of the minimization problem (5.5) will be found using the BFGS projected method. In our implementation, we used the reduced matrix update given by (5.21). To see the form of this matrix for our specific problem, let us set the following values: in the iteration k, $w_k = (\rho_k, \mathbf{u}_0^k)$. Let $U_{ad} = \{w = (\rho, \mathbf{u}_0) : \rho \in \mathcal{U}_{ad}, \text{ and } 0 \leq \mathbf{u}_0 \leq U\}$ represent the admisible set, where $U > 0$ is an artificially high bound for the initial conditions, and $\mathcal{U}_{ad} = \{\rho : \rho_\ell \leq \rho \leq \rho_u\}$ where ρ_ℓ and ρ_u denotes the lower and upper bound for the model parameters, respectively. Note that $w = (\rho, \mathbf{u}_0) \in \mathbb{R}^9$, then, for a given value of ϵ, the ϵ-active set has the form

$$A^{\epsilon}(w) = \{i : (\rho_\ell)_i \leq w_i \leq (\rho_\ell)_i + \epsilon \text{ or } (\rho_u)_i - \epsilon \leq w_i \leq (\rho_u)_i \text{ if } i \in \{1, \ldots, 5\}, \text{ or}$$
$$0 \leq w_i \leq \epsilon \text{ or } U - \epsilon \leq w_i \leq U \text{ if } i \in \{6, \ldots, 9\}\}.$$

We will denote $I_{k+1} = I^{\epsilon}(w_{k+1}) = (A^{\epsilon}(w_{k+1}))'$, $s_k^{\#} = R_{I_{k+1}}((\rho_{k+1}, \mathbf{u}_0^{k+1}) - (\rho_k, \mathbf{u}_0^k))$, and

$$y_k^{\#} = R_{I_{k+1}} \left(\left[\frac{\partial J(\rho_{k+1}, \mathbf{u}_0^{k+1})}{\partial \rho}, \frac{\partial J(\rho_{k+1}, \mathbf{u}_0^{k+1})}{\partial \mathbf{u}_0} \right]^T - \left[\frac{\partial J(\rho_k, \mathbf{u}_0^k)}{\partial \rho}, \frac{\partial J(\rho_k, \mathbf{u}_0^k)}{\partial \mathbf{u}_0} \right]^T \right),$$

where $\dfrac{\partial J}{\partial \rho}$ and $\dfrac{\partial J}{\partial \mathbf{u}_0}$ are given in (5.9) and (5.10). Replacing these terms in (5.21), we obtain an update of the generalized inverse B_k, and consequently, a descend direction

of the form

$$d_k = -B_k \left[\frac{\partial J(\rho_k, \mathbf{u}_0^k)}{\partial \rho}, \frac{\partial J(\rho_k, \mathbf{u}_0^k)}{\partial \mathbf{u}_0} \right]^T - R_{A^{\epsilon_k}(w_k)} \left[\frac{\partial J(\rho_k, \mathbf{u}_0^k)}{\partial \rho}, \frac{\partial J(\rho_k, \mathbf{u}_0^k)}{\partial \mathbf{u}_0} \right]^T \tag{5.22}$$

that jointly with the method iteration, let us computed $w_{k+1} = (\rho_{k+1}, \mathbf{u}_0^{k+1})$. We will provide a detailed analysis of the numerical performance of the projected BFGS algorithm for our specific problem in Section 5.4.

5.2.5 Data preparation

The specific variational problem that we will solve limits the observable variable to the reported infected cases since it is not feasible to directly observe other variables, such as the susceptible population, exposed individuals, or undocumented infected population. Although it will be possible to observe the removed population with information on positive cases and COVID-19 deaths, we do not consider them as an observable variable since the significant underreporting of COVID-19-related deaths could lead to biased results.

We analyze data from March 2020, when the pandemic hit the country, to August 2021, when the vaccination process started for most of the Ecuadorian population. We used two data sources: the official count of COVID-19-positive cases and the mortality data. We describe them below.

COVID-19 positive cases: This data is obtained from the official records of confirmed COVID-19 cases reported by the Ecuadorian Public Health Ministry (MSP). It considers individuals who have tested positive with a PCR test based on their symptomatology.

COVID-19 deaths: We employ mortality data associated with the pandemic to estimate the number of symptomatic COVID-19 cases. This mortality data is obtained from the Ecuadorian Civil Registry [44]. While this data is considered more reliable than the one provided by the Public Health Ministry, there is a delay of up to 4 weeks on its consolidation. Consequently, any real-time analysis with this data is not feasible. Below, we describe the processes first to estimate the mortality excess and, second, the observed documented infected population from the Civil Registry data.

Mortality excess estimation via SARIMA forecast model

To compute an approximation of the COVID-19-related deaths, we calculate the difference between the total deaths during the pandemic and the expected number under

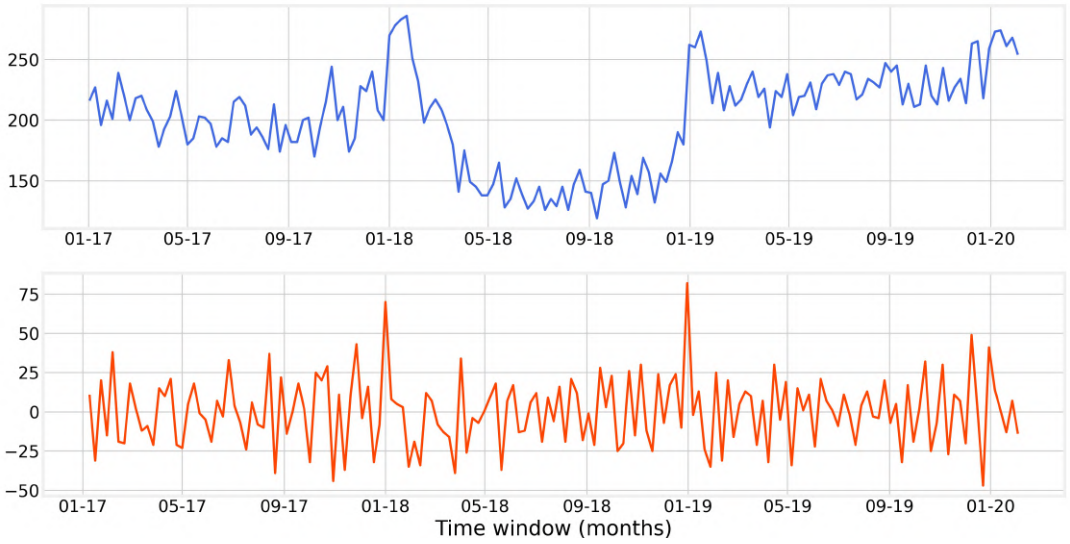

Figure 5.1: The first row presents the series of registered deaths in Pichincha from 2 January 2017 to 3 February 2020. The second row presents the series after performing one difference.

normal circumstances. We estimate the expected deaths from 4 February 2020 to 2 September 2021 using a Seasonal Autoregressive Integrated Moving Average (SARIMA) forecast model. Historical data of daily deaths from 2 January 2017 to 3 February 2020 was used. The accuracy of the prediction model was verified using the last 182 days of this period.

$SARIMA(p, d, q)(P, D, Q, s)$ model requires an adequate setting of its parameters to give reliable predictions. The parameter d is the easiest to determine; it indicates the number of times a time series must be differenced to obtain a stationary one. In figure 5.1, we observe the original series and the series after one difference. The first one is non-stationary, while the second is stationary. Therefore, we set $d = 1$.

The coefficients p and q are related to the autoregressive (AR) and the moving average processes (MA). The first determines how many past values or lagged observations in the time series affect the present, while the second indicates the number of past error terms that affect the present. Preliminary values of p and q can be obtained by observing the partial autocorrelation function (PACF) and autocorrelation function (ACF) plots. The order p of an autoregressive process $AR(p)$ is obtained if there is a significant spike at lag p in the PACF plot and there is no larger one beyond. Likewise, the q order of a moving average process $MA(q)$ comes if such a significant spike is obtained at lag q in the ACF plot, see e.g., [123]. The second row of Figure 5.2 helps us determine $p = q = 1$ as preliminary values. The autocorrelation plot criteria let us estimate the parameters of pure AR and MA processes. Therefore, we must verify if there is a combined $ARIMA(p, 1, q)$ model with $p > 0$ and $q > 0$ simultaneously that

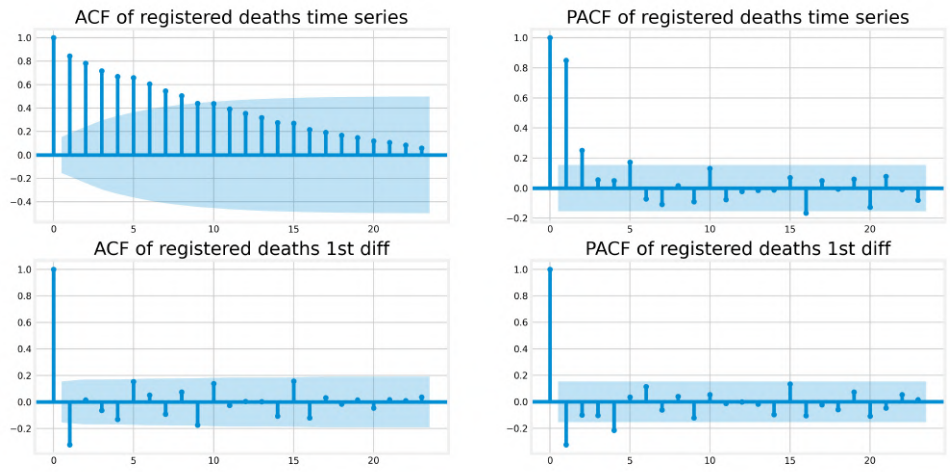

Figure 5.2: The first row presents the ACF and the PACF plot of the series of registered deaths in Pichincha from 2 January 2017 to 3 February 2020. The second row presents the ACF and PACF plots of the series after performing one difference.

performs better. In order to do that, we conduct the *Akaike Information Criterion* (AIC) test, on which the parameter combination with the lower AIC-value will be the best. According to the latter, the best model is $ARIMA(1, 1, 2)$.

We set $(P, D, Q, s) = (1, 1, 0, 52)$ as the model's seasonal parameter. We consider a seasonality of one year, i.e., $s = 52$ weeks. Like d, D represents the number of seasonal differences required to remove seasonality in the time series; we set $D = 1$. This model considers the relationship between the current observation and the observation from the same period in the previous year, i.e., $P = 1$. Moreover, the model's seasonal moving average component is not present, that is, $Q = 0$. After identifying the model, $ARIMA(1, 1, 2)(1, 1, 0, 52)$, we must run a diagnostic test to ensure that its residuals are uncorrelated and normally distributed. We display these results in Figure 5.3.

Observed documented infected population from mortality excess

Since our observable data is the infected population, when using our second data source, we have to retrieve it from mortality excess. Our study was conducted in hindcast, so we already know the mortality rate (mr). Therefore, we can estimate the number of deaths, m, on day X, as the number of cases or infected population, I, on day $(X - T)$, multiplied by the mortality rate, i.e., $m = \text{mr} \times I$, where T represents the time from case confirmation to death. In our case, we consider a lag of 15 days from symptom onset to death as an average of those reported on the MIDAS Online COVID-19 portal [97]. Additionally, since the infected population is divided into reported and unreported cases, we can obtain estimates or approximations of the reported and

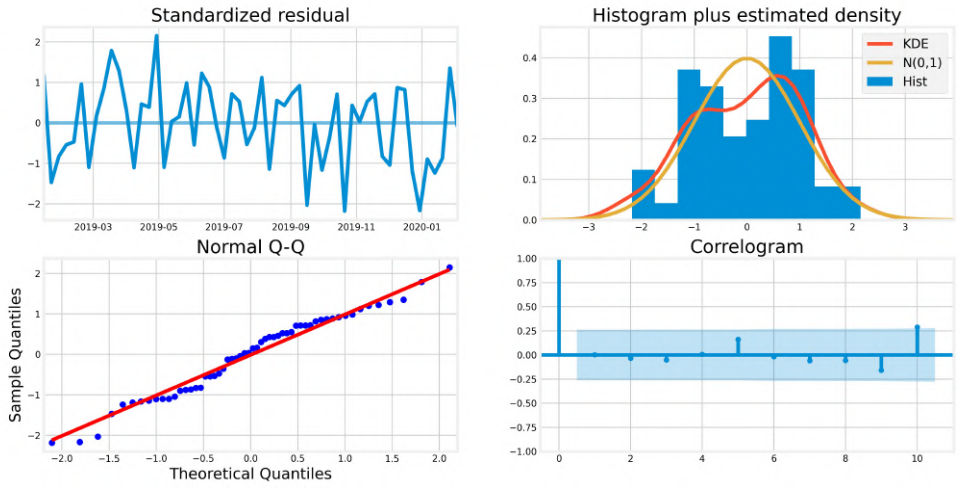

Figure 5.3: Diagnostic graphics. The residual plot (top left) does not display any seasonality. This is confirmed by the correlogram plot (bottom right), which shows that the residuals have a low correlation with lagged versions of themselves. The normal Q–Q plot (bottom left) shows that the ordered distribution of residuals (blue dots) follows the linear trend of the samples taken from a N(0,1) distribution.

unreported mortality rates, which yield the following equation:

$$m = 66.86\%\ I\ \mathrm{mr}_r + 33.14\%\ I\ \mathrm{mr}_u, \tag{5.23}$$

where the subindices r and u denote if the rates correspond to the reported or unreported cases. Equation (5.23) considers that around one-third of the infections are asymptomatic (unreported). We set this value at 33.14%, as the average of the values in the literature, see e.g., [62, 101, 112]. An estimation for the unreported infection mortality rate, mr_u, is given by the mortality rate of the younger population (0 - 19 years old). This follows since asymptomatic patients were younger compared with the symptomatic ones (see, e.g., [101, 120]). In Ecuador, this rate was set at 0.24% [98]. Even though mortality in asymptomatic patients is generally considered negligible, as they exhibit mild or no symptoms, we have chosen to account for a non-negligible mortality rate. This assumption would allow us to consider individuals initially classified as asymptomatic who were actually presymptomatic, meaning they later developed symptoms, including severe complications [121]. Additionally, albeit to a lesser extent, it would consider cases where underlying health conditions may increase the risk of fatal outcomes. On the other hand, the mortality rate of the reported infected population, mr_r, depends on the region. For the studied provinces, the mortality rate due to reported COVID-19 cases from February, 29th 2020 to December, 6th 2021 was 2.17% in Pichincha's case and 6.84% for Guayas; according to the National Epidemiological Surveillance System [98].

5.2.6 Building error covariance matrices

A critical element in the data assimilation approach is the calculation of the error covariance matrices. In the SARS-CoV-2 setting, matrix $\mathbf{C}$ represents the error covariance matrix of the observations; its construction changes depending on the data source. Matrices $\mathbf{B}$ and $\mathbf{Q}_0$ are the error covariance matrices of the background information of the model parameters and the initial condition, respectively. In what follows, we explain how these matrices were built for our specific problem and data.

1. Matrix C - Public Health Ministry data

We consider the number of PCR tests applied to the population and the effectiveness of these tests in detecting the virus. Matrix $\mathbf{C}$ is built as a diagonal matrix where its elements will be given by:

$$\sigma_{ii}^2 = \frac{\kappa}{\eta_i}\sigma_{PCR}^2, \tag{5.24}$$

where κ represents the "ideal" weekly number per million inhabitants of PCR tests, which is set at 4000 considering countries that have accomplished effective testing campaigns; additionally, σ_{PCR} is the standard deviation inherent from the PCR tests, and η_i is the number of PCR tests per million inhabitants per week performed in the region of interest.

2. Matrix C - Civil Registry data

As the estimated number of infected patients is retrieved from the excess in mortality, the observation error is directly related to the inaccuracies of computing the mortality excess. Since the mortality excess represents the discrepancy between reported deaths and forecasted ones, any error in its estimation will come from these sources. As an assumption, we consider that the error in the reported deaths is statistically insignificant; the latter makes sense since the Civil Registry typically takes 3 to 4 weeks to compile and cure the data. Consequently, we will assume that inaccuracies in the excess mortality primarily result from errors in the forecast of expected deaths.

The errors or residuals of the forecasted expected mortality, generated with the seasonal ARIMA forecast model, form a stationary time series with a constant variance; see, e.g., [22, Section 1.4]. In our case, the standard deviations for the residuals of the forecasted expected mortality for Pichincha and Guayas are $\sigma_P = 27.29$ and $\sigma_G = 45.25$, respectively.

3. Matrix B

The background knowledge of the parameters, like their confidence intervals, is taken from the COVID-19 literature. Knowing the prior range for the model parameters and how they were built, it is possible to compute a measure of uncertainty of the background knowledge of the parameters. In fact, according to [65], the lower and upper bounds of the confidence intervals at 95% confidence level are computed as:

$$\bar{\rho} \pm t_{1-\frac{\tilde{\alpha}}{2}} s_\rho, \tag{5.25}$$

where $\rho \in \{\beta, \mu, \alpha, \zeta, \delta\}$ and $\bar{\rho} \in \{\bar{\beta}, \bar{\mu}, \bar{\alpha}, \bar{\zeta}, \bar{\delta}\}$. With $n = 300$ and $t_{1-\frac{\tilde{\alpha}}{2}} = 1.968$, given the lower and upper bounds, we can compute the standard deviation, s_ρ, by using equation (5.25). The square values of these elements will form the diagonal matrix $\mathbf{B}$.

4. Matrix $\mathbf{Q}_0$

Matrix $\mathbf{Q}_0$ accounts for the uncertainty of the system due to the initial conditions by using the variability of a collection of vectors. First, it is necessary to form a set of initial conditions. Since our study was carried out on a weekly basis, we took the first element of that set as the solution variables of the previous week, i.e., $\mathbf{u}_{k-1}$. Then, for each $\ell = 1, \ldots, M$, we form

$$\mathbf{u}_{0_k}^\ell = \mathbf{u}_{k-1} + \varepsilon_\ell, \qquad \varepsilon_\ell \sim N(0, \sigma_\ell^2),$$

with $\sigma_\ell = 0.2\mathbf{u}_{k-1}$. Then, solving the SARS-CoV-2 propagation model, we obtained a collection of M state vectors $\mathbf{u}_k^\ell = (E_k^\ell, Ir_k^\ell, Iu_k^\ell, R_k^\ell)$. The estimation, in the $k-$week, of matrix $\mathbf{Q}_0$ will be retrieved with the information of these ensemble members as follows:

$$\mathbf{Q}_0 = \frac{1}{M-1} \sum_{\ell=1}^{M} (\mathbf{u}_k^\ell - \bar{\mathbf{u}})(\mathbf{u}^\ell - \bar{\mathbf{u}})^T, \tag{5.26}$$

where $\bar{\mathbf{u}} = \dfrac{1}{M} \displaystyle\sum_{\ell=1}^{M} \mathbf{u}_k^\ell$.

5.3 Multimodel ensemble forecasting

Apart from the SARS-CoV-2 propagation model and the variational data assimilation model used to calculate optimal initial conditions and parameters, we will use the multimodel ensemble forecasting approach to develop a robust methodology that better captures the evolution of the COVID-19 pandemic.

The multimodel ensemble approach consists of combining multiple models' outputs

to produce a single forecast. The main idea is to obtain a more accurate forecast by combining the outputs of the different models, which lets us consider the strengths and weaknesses of each single model. Doing this is crucial when individual models have high degrees of uncertainty. The contribution of each model to the final average can be assigned depending on the models' performance [80].

We will use the multimodel ensemble approach to get robust outputs of the SARS-CoV-2 propagation model. In order to do so, we compute the optimal parameters (ρ) and initial conditions ($\mathbf{u}_0$) by solving the variational data assimilation problem (5.5) considering data coming from two data sources, MSP and RC. As a result, we will obtain two sets of optimal solutions: $(\mathbf{u}_0^{MSP}, \rho^{MSP})$ and $(\mathbf{u}_0^{RC}, \rho^{RC})$. Then, using the computed initial conditions and parameters, we solve the stochastic virus spread model (5.2) to see how each model variable evolves in a given time window. To consider more scenarios, we solve the stochastic SEIR model 80 times, where each one considers a perturbed parameter β obtained by adding random Gaussian noise to the optimal one. The solution variables will be taken as the average of these realizations. Since the described process is done with MSP and RC data, we obtain two sets of model outputs, $\mathbf{u}^{MSP}$ and $\mathbf{u}^{RC}$.

The weights assigned to the model's outputs obtained with each data source will depend on the number of PCR tests conducted weekly. In instances of a low PCR-test count, the model outputs derived from Civil Registry data will get a higher weight. Conversely, during the weeks when the number of PCR tests increased, the weight corresponding to the outputs from the model using Health Ministry data will be greater. We will use a PCR testing capacity indicator to determine when the count of PCR is *low*. We will show the details of the weights calculation below.

5.3.1 Model weights and testing capacity indicator

We consider the number of PCR tests per 1000 inhabitants per week as an indicator of whether the control entities are testing enough people to reflect the actual virus spreading. According to [72], at least one test every 1000 inhabitants per week must be taken to carry out an adequate testing campaign.

We use the testing capacity indicator to compute the weight of the output models obtained with MSP data. The latter makes sense since the Public Health Ministry is responsible for testing the population; if the number of PCR tests is insufficient, the weight of the solutions obtained with MPS data will be low. To compute this weight, we use the following sigmoid function

$$w_{MSP} = \frac{1}{1 + \exp(a(x - b))}, \tag{5.27}$$

where x is the number of PCR tests per 1000 inhabitants per week, and a and b are coefficients required by the function. We chose the sigmoid function since it gives us a value between 0 and 1, and, through its parameters, it considers the different behavior of each province. In fact, the same value of this indicator gives different weights depending on the parameters a and b. For instance, in Pichincha's case, we set $a = -1.25$ and $b = 1.5$, while in the case of Guayas, $a = -3.75$ and $b = 1.0$.

The weight corresponding to the solutions computed with the Civil Registry data will be the complement of this value, that is, $w_{RC} = 1 - w_{MSP}$.

5.4 Results

We present the results obtained using the described methodology. It is divided into two main sections. The first one shows the results obtained during the first months of the COVID-19 pandemic in Ecuador, i.e., when the data was being collected. Therefore, the results could have served as an *online* indicator of the pandemic state. The second section considers data unavailable in the pandemic's first stages. The main idea is to use more information and data sources to perform a *hindcast analysis* and figure out the actual evolution of the pandemic in Ecuador.

Previously, we start by analyzing the numerical performance of the selected algorithm for computing the optimal model parameters. Additionally, we describe the formula for the effective reproduction number, which is calculated using these optimal parameters.

Estimation of COVID-19 model parameters

To obtain the optimal parameters (ρ) and initial conditions ($\mathbf{u}_0$) by solving the variational data assimilation problem (5.5), we proceed iteratively using the projected BFGS method described in Section 5.2.4, until a stopping criterion is met. Since the computations are performed weekly, the initial point for the algorithm is set to the parameters obtained in the previous week, ρ_{k-1}, while for the initial conditions, $\mathbf{u}_0$, the observations at the first day of the studied week are considered. The BFGS direction is determined by (5.22), and the parameters and initial conditions are updated following (5.20). The stopping criterion is defined by $e(w_k) = \|w_k - P_{U_{ad}}(w_k - \nabla f(w_k))\| \leq \texttt{tol}$, where $w_k = (\rho_k, \mathbf{u}_0^k)$ and $\texttt{tol} > 0$ is a fixed tolerance value; see, e.g., [39, Chapter 5.3]

If the iterations of the projected BFGS start near a non-degenerate local minimum and a good initial approximation to the reduced Hessian is available, it is expected that the iterations of the method will converge q-superlinearly; see [77, Theorem 5.5.4]. This is verified also in our experiment, see Table 5.1, where we summarize the method perfor-

mance for a subsample of weeks. We recall that the algorithm converges superlinearly if the convergence rate, p is between 1 and 2.

Studied week	**iter**	$f(\bar{w})$	$e(\bar{w})$	**Conv. rate** (p)
13-19 mar 2020	8	3.003	1.71×10^{-11}	1.37
19-25 jun 2020	10	4.908	3.01×10^{-10}	1.10
20-26 nov 2020	8	4.212	2.12×10^{-10}	1.97
9-15 april 2021	9	3.258	9.14×10^{-9}	1.74
28 may - 3 jun 2021	11	14.59	1.99×10^{-8}	2.14

Table 5.1: Performance of the projected BFGS method with RC data for Guayas.

Effective reproduction number (R_t)

A correct estimation of the model parameters is crucial to get a reliable effective reproduction number, R_t, which measures the average of new cases generated by a single COVID-19 patient; it is computed in the following way:

$$R_t = \alpha\beta\delta + (1-\alpha)\mu\beta\delta, \tag{5.28}$$

and it can be interpreted as follows: an R_t value higher than two represents exponential growth of the disease. Moreover, if the reproduction number is between one and two, it means a less accelerated increase in the infection. Finally, when the R_t values are steadily lower than one, we can say that the spread of the virus is under control. Computing this value with a certain regularity, e.g., weekly, let us obtain an evolution of the pandemic state.

5.4.1 Online results

The first set of numerical simulations was developed relied only on data from the Public Health Ministry since the results had to be provided in real-time to the control entities that were monitoring the evolution of the pandemic in Ecuador. The uncertainty associated with these data was carefully considered and incorporated through the covariance matrices of the variational data assimilation model. As a result, the performed numerical simulations yielded estimations of the model parameters and its initial conditions. With these inputs, it is possible to estimate the effective reproduction number and compute short-term forecasts of the infected population.

Contagion probability map

The numerical resolution of the minimization problem (5.5) leads to a parameter estimation that considers the uncertainty of the official data. Using these parameters in equation (5.28), we get an update on the effective reproduction number, which, additionally to reflect the pandemic state, gives an idea of the contagion situation in each studied place.

To simplify the visualization of the COVID-19 contagion information, we present it through a heat map showing each region's contagion risk probability. This probability is computed using a logistic model which considers the effective reproduction number and the active cases,

$$P(\text{Risk}) = \frac{1}{1 + \exp(a_1 + a_2 R_t + a_3 y)} \ ,$$

where a_1, a_2, and a_3 are coefficients required for the logistic function, and y represents the active cases per 100000 inhabitants in the studied area. We divided this contagion risk probability into five categories: low, moderate, high, very high, and extremely high. Figure 5.4 shows the COVID-19 contagion risk probability for Pichincha and Guayas at different times.

5.4.2 Hindcast results: A comparative analysis between Pichincha and Guayas

One of the advantages of conducting a retrospective analysis is the availability of data that was not consolidated at the time of the crisis. For instance, in the Ecuadorian case, the information about deceased people in the context of the COVID-19 pandemic was not cured until months after the outbreak. The number of COVID-19 deaths that the Public Health Ministry reported on April 8, 2020 [99] was 242 in the whole country, which contrasted strongly not only with the values reported posteriorly by the Civil Registry but with the shocking images of abandoned bodies on the streets in Guayaquil by these dates [61, 124].

To evaluate the size of this mismatch, we analyzed the mortality excess using the Civil Registry data for Ecuador's two most populated provinces, Guayas and Pichincha. Figures 5.5 and 5.6 show the obtained results, revealing a significant gap between the forecasted number of deaths (dashed line) and the registered ones (solid line) for Pichincha and Guayas, respectively.

The significative gap, especially in Guayas' case, suggests that the number of people who had gotten the infection and died was much higher than the Public Health Ministry reported. The underestimation of COVID-19 cases and posterior deaths may have been

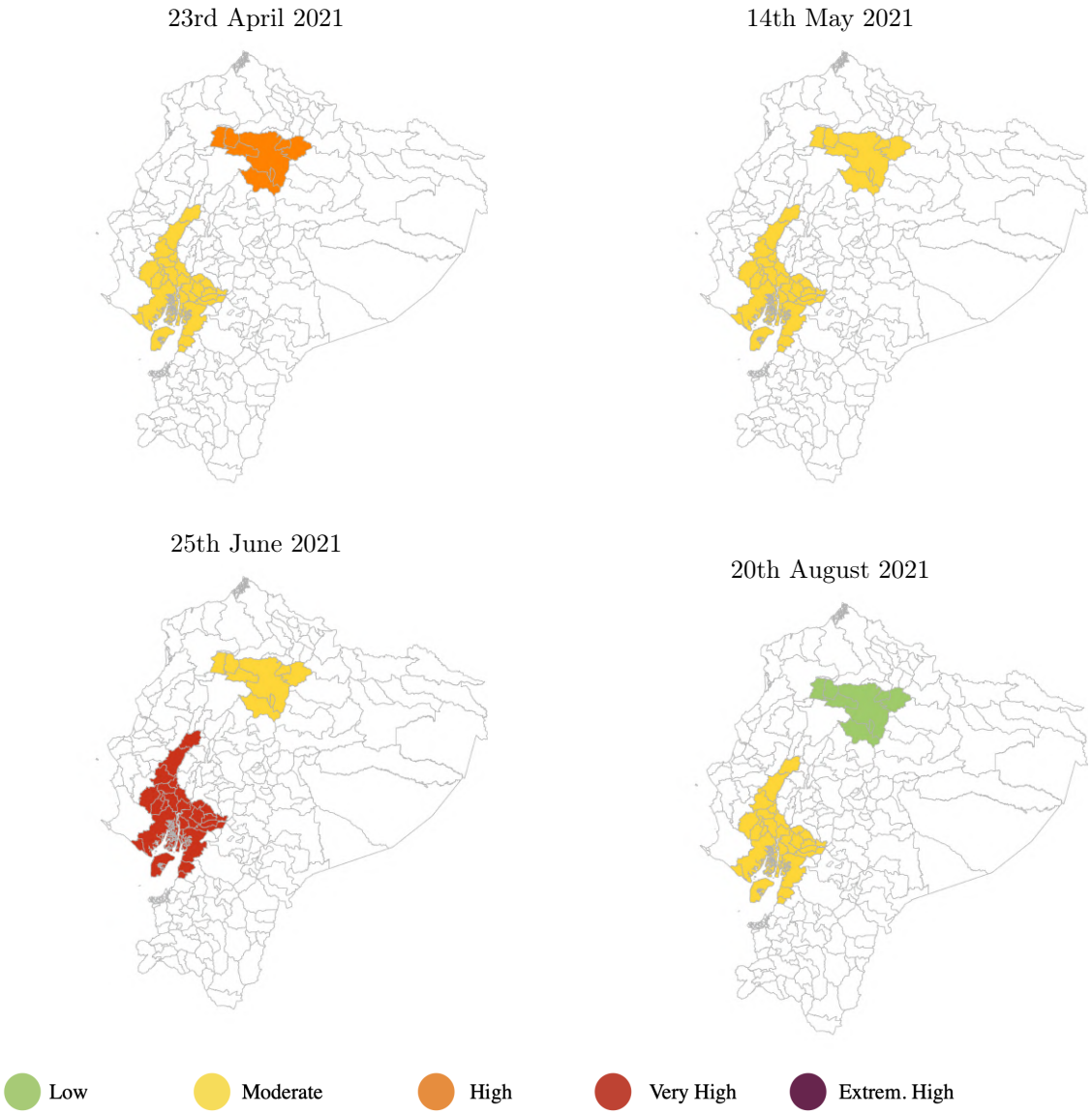

Figure 5.4: Contagion risk probability for Guayas and Pichincha at different times.

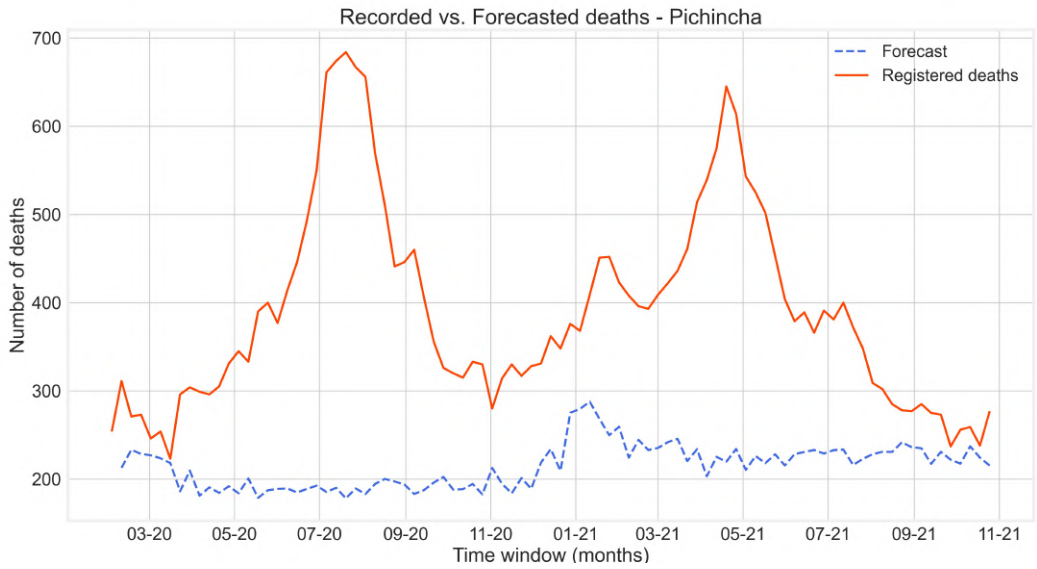

Figure 5.5: Comparison between recorded and forecasted deaths in Pichincha from February 2020 to October 2021. The gap between both represents the mortality excess attributed to the COVID-19 pandemic.

a result of insufficient testing capacity and the misattribution of COVID-19 deaths to other causes. Moreover, the delayed recognition of the virus and the magnitude of the pandemic could have played a crucial role in overwhelming the healthcare system in Ecuador [32, 82].

Even though the discrepancy in the number of deaths obtained with each data source is significant for both provinces, it is larger in Guayas. To explain the differences between Pichincha and Guayas, we will highlight some specific socioeconomic factors that could have influenced the different management of the pandemic. These factors include access to healthcare services, hospital infrastructure, housing conditions, and overcrowding. According to the Statistical Record of Health Resources and Activities in the year 2020, [73], Guayas had 667 healthcare establishments, of which just 58.3% belong to the public system, while Pichincha counted 498 healthcare establishments, 72.3% of them public. Concerning private non-profit facilities, they receive financial support from the central government; however, this does not imply free health services, which means little or no access to private entities by the poorest sector of the population. 14.6% of facilities in Guayas are of this kind, in contrast to the 5.2% of Pichincha.

Apart from the limited healthcare resources, the dynamics of COVID-19 transmission made densely populated areas more vulnerable to virus spread if an infected person was present. According to the National Institute of Statistics (INEC) [74], Guayas had an overcrowding rate of 13.7% in 2019, exceeding the national rate of 9.9%. In contrast,

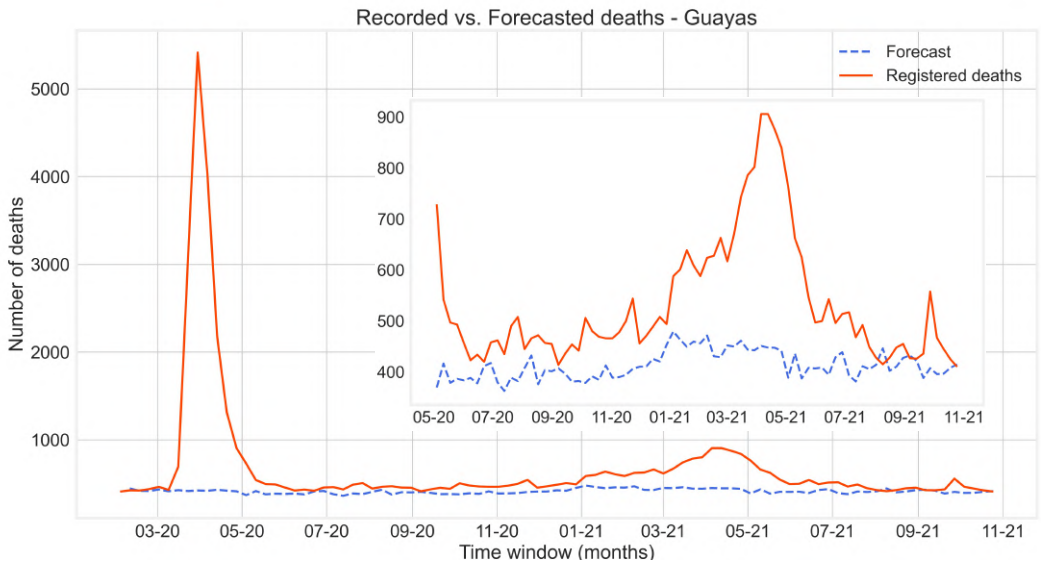

Figure 5.6: Comparison between recorded and forecasted deaths in Guayas from February 2020 to October 2021. A zoomed image of the results from May 2020 to October 2021 is shown inside.

Pichincha's overcrowding rate was much lower at 3.8%. This substantial difference implies that Pichincha's population was relatively less susceptible to the adverse effects of overcrowding, potentially contributing to the lower impact of the pandemic in its initial stages when compared to Guayas, where more people were confined to smaller living spaces, increasing the likelihood of household transmission.

Jointly, limited healthcare resources and unfavorable living conditions may have created a favorable environment for the fast spread of the virus, resulting in the collapse of the healthcare systems, particularly evident in Guayaquil during the pandemic onset. The different socioeconomic conditions between Pichincha and Guayas may have contributed to the discrepancy in the number of COVID-19 cases, highlighting the importance of targeted interventions tailored to the specific context of each region.

In this study, we conducted separate analyses for Guayas and Pichincha, solving the parameter estimation problem using each data source. We compared and combined these results to achieve a more accurate representation of the COVID-19 crisis in these provinces. We examined the evolution of the effective reproduction number as a clear indicator of the pandemic's status and analyzed the dynamics of the documented infected population in each case. The data considered for this analysis extends from March 2020 to August 2021, covering the pandemic's early stages to the beginning of the vaccination process of the Ecuadorian population.

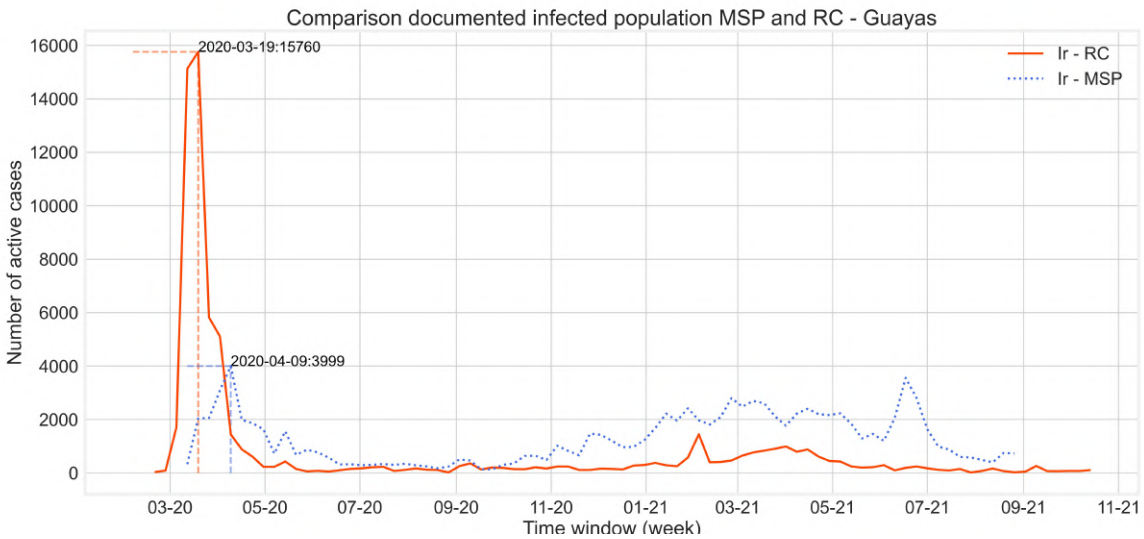

Figure 5.7: Comparison of the evolution of the variable *reported infected population* computed with MSP data (solid line) and RC data (dotted line) - Guayas.

Documented infected population

With the aid of the optimal parameters and initial conditions obtained with the variational data assimilation approach, applied to the stochastic virus propagation model (5.2), we obtain solution vectors describing the SEIR variables' evolution in the given period, e.g., seven days. By doing this computation weekly, it is possible to get the evolution of the model variables. Mainly, we are interested in the evolution of the *documented infected* COVID-19 cases, denoted as I^r, as it can be directly observed. We solve the stochastic SEIR model with perturbed parameters to consider more scenarios. We vary the optimal parameter corresponding to the transmission rate β in the following way:

$$\beta_\ell = \beta + \varepsilon_\beta^\ell, \qquad \varepsilon_\beta^\ell \sim N(0, \sigma_\beta^2), \tag{5.29}$$

where $\sigma_\beta = 0.02\beta$ and for all $\ell = 1, \ldots, 80$. By using them while solving system (5.2), we will obtain 80 sets of solution vectors. The solution that we will report corresponds to the average of these realizations.

We report the results for I^r, in Guayas and Pichincha, computed using the official COVID-19 data from the Public Health Ministry ($I^r - MSP$) and the one obtained with the mortality excess data from the Civil Registry ($I^r - RC$). Figures 5.7 and 5.8 show the evolution of the *documented infected* population for Guayas and Pichincha, respectively, where $I^r - MSP$ is represented in a solid line and $I^r - RC$ in dotted line.

In Guayas' case, the differences between the two series are evident. The maximum number of contagious reached with the mortality excess data is almost four

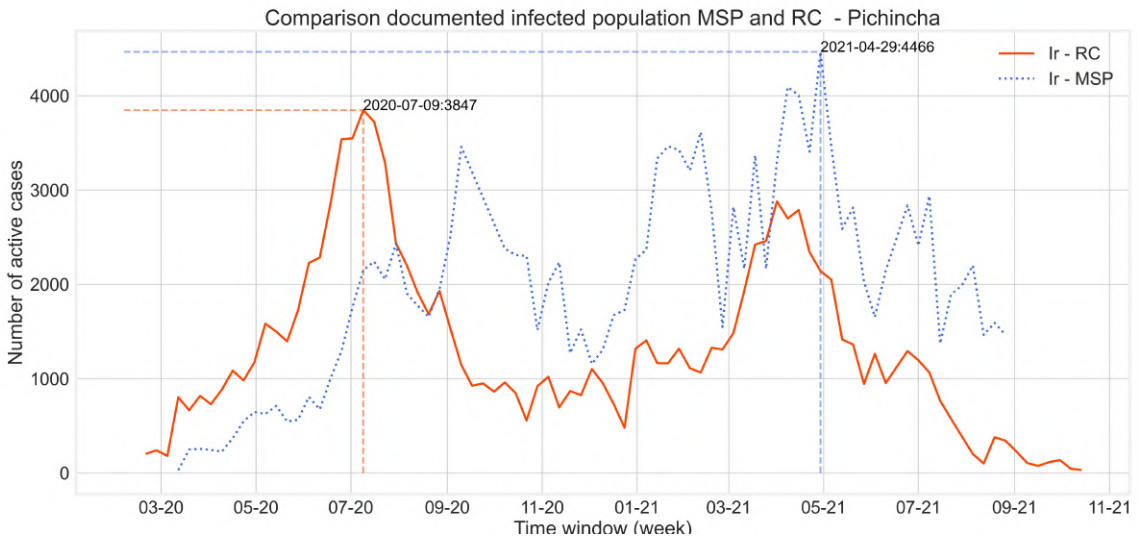

Figure 5.8: Comparison of the evolution of the variable *reported infected population* computed with MSP data (solid line) and RC data (dotted line) - Pichincha.

times greater than the one obtained with the official count of COVID-19 cases, with $I^r(RC)_{max} = 15760$ and $I^r(MSP)_{max} = 3999$. The dates of the observed peaks showed a delay of around two weeks, which can be attributed to the time it took for people to get tested for COVID-19 and receive their test results.

In Pichincha's case, it is important to note that the results of repressed PCR tests were released in mid-September 2020, artificially increasing the number of observed positive COVID-19 cases. Therefore, the results obtained from MSP data for those dates were artificially high. To deal with that, we treat these results as outliers, and to correct them, we used a linear interpolation of the generated I^r-serie. Taking the latter into account, we find that for both data sources, the first critical increment of the infection occurred during the early days of July 2020. In contrast to the results in Guayas, comparing the two series in Pichincha reveals a higher number of infected individuals when considering the data from the Public Health Ministry. However, the peak values show a difference of less than 1.5 times; specifically, $I^r(MSP)_{max}$ is 4466, while $I^r(RC)_{max}$ is 3847.

Robust documented infected population evolution

To accurately depict the pandemic's evolution using the available data sources, we compute the weighted average of the obtained results to get a robust and more reliable one. The weights for each model output will be determined based on the number of PCR tests conducted per week according to (5.27). For instance, in Guayas, the number of PCR tests was notably low, especially during the pandemic onset. For

instance, from March 6 to March 12, 2020, only 813 PCR tests were conducted. In Pichincha, the situation was initially similar, with the number of PCR tests ranging between 215 and 691 per week during the first three weeks of the study (March 6 - 26, 2020). Fortunately, the province's situation improved starting from the 4th week of the study, with a significant increase in the number of PCR tests. The testing capacity indicator evolution for Guayas and Pichincha is depicted in Figure 5.9.

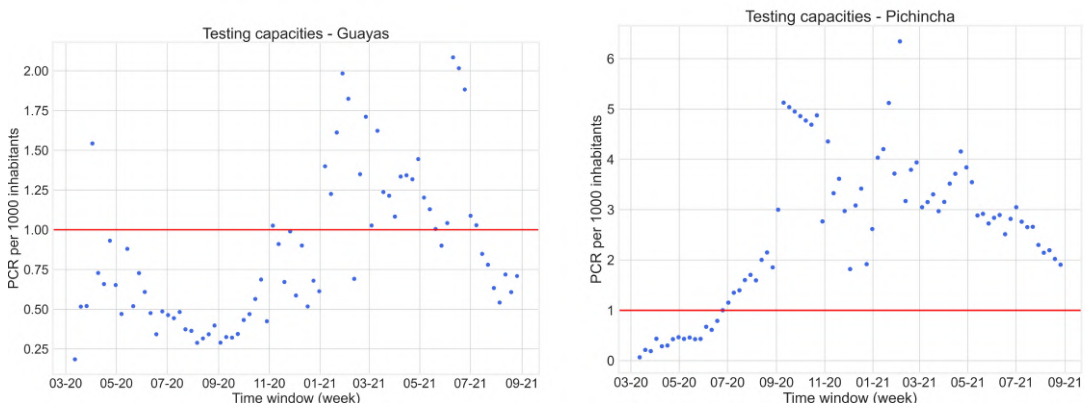

Figure 5.9: PCR Testing capacity indicator for Guayas (left) and Pichincha (right).

For our analysis, we will assign weights to the *documented infected population*, I^r, computed with each data source based on the testing capacity indicator. The result for the weighted average for the variable I^r for Guayas and Pichincha is illustrated in Figures 5.10 and 5.11.

In the case of Guayas, the weights assigned to $I^r - RC$ are more significant than $I^r - MSP$, which aligns with our assumption that the data from the excess of mortality has less uncertainty than the official count of COVID-19-positive cases reported by the Health Ministry. The robust I^r gives greater weight to the Civil Registry data for the first nine months of the pandemic, after which $I^r - MSP$ starts gaining more weight in the robust solution. This suggests that in Guayas, the official count of COVID-19 cases could have been highly underreported not only in the initial stages of the pandemic but throughout the year 2020.

In contrast, a similar analysis for Pichincha indicates that starting in August 2020 and until the end of the study, the weights corresponding to $I^r - MSP$ are more significant than $I^r - RC$. Since the underreported cases were significantly lower in Pichincha than in Guayas, the results obtained from MSP data in this province are reliable during the indicated period. However, this was not the case in the first months of the pandemic, where the use of Civil Registry data was crucial to obtaining a more accurate picture of the situation at that stage.

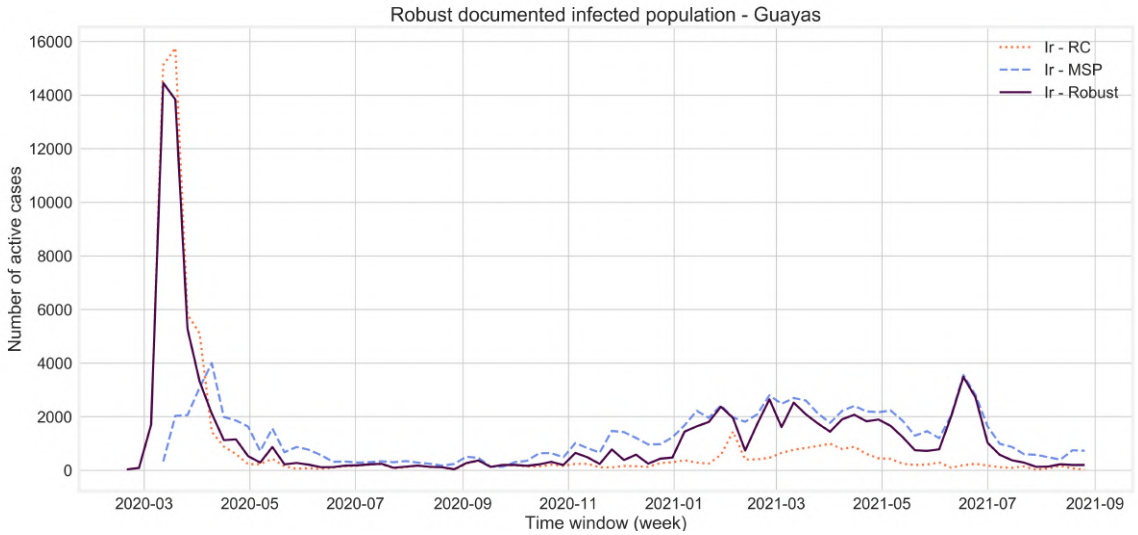

Figure 5.10: Evolution of the robust *documented infected population* I_r - Guayas.

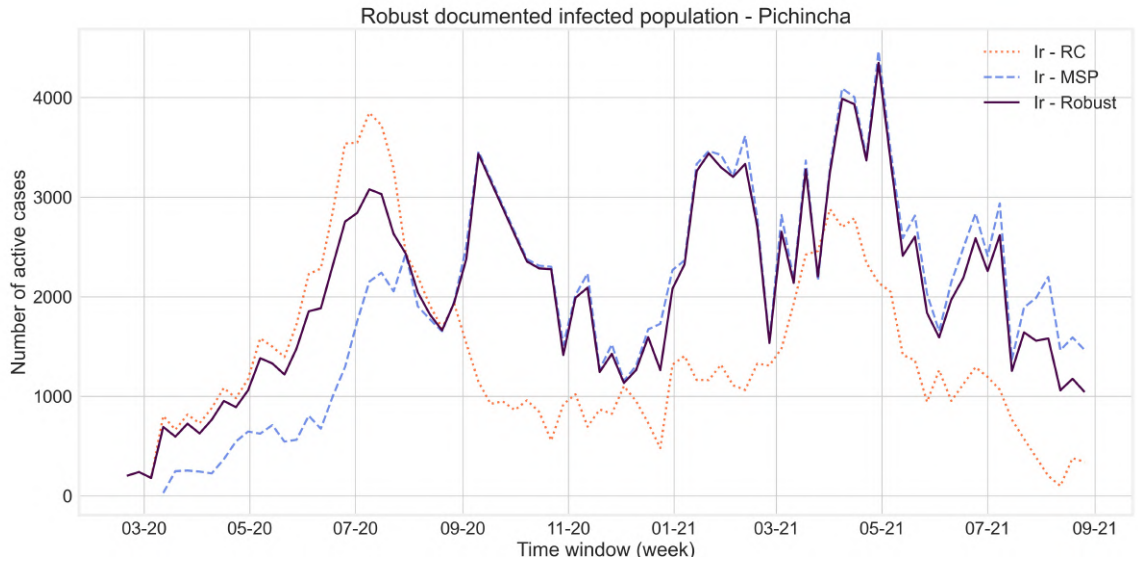

Figure 5.11: Evolution of the robust *documented infected population* I_r - Pichincha.

Validation

A validation process can be described as comparing the model's outputs with real observations. The outputs for the validation have to be computed considering the inputs obtained in a previous learning stage. For us, the validation period will correspond to the last three months of our study, from 3 June 2021 to 26 August 2021.

We find the weekly outputs for the validation iteratively. In the first two weeks of the validation period, we use the last initial conditions and parameters computed in the learning stage to solve the SEIR model and see the evolution of the variables at a given time window, e.g., two weeks. The computation is performed 80 times to consider more scenarios, where each one takes a perturbed transmission rate; see equation (5.29). The solution variable for the validation will be taken as the average of these realizations. For the remaining weeks, it is necessary to update the value of the parameters and initial conditions. To do that, we solve the variational data assimilation problem using the results obtained in the previous weeks as observations. We find the model outputs for a new week using the updated parameters and initial conditions and repeating the process described above.

Since our observable variable is the reported infected population, one kind of validation of the obtained Robust documented infected population, $I_r - Robust$, consists of measuring the deviation of this solution variable with respect to the observation I_{obs}. We will consider that the robust solution performs better than the single solution variables if its error is less than one calculated with $I^r - MSP$ and $I^r - RC$. However, since the official count of COVID-19 cases conducted by the Public Health Ministry was not reliable, we checked our models' outputs against the observed mortality excess caused by the pandemic. Therefore, it is necessary to retrieve the deceased population from the computed infected one. To do that, we use again the formula:

$$m = I^r mr_r + I^u mr_u,$$

where $mr_r = 2.17\%$ in Pichincha and $mr_r = 6.8\%$ in Guayas. Likewise, we take $mr_u = 0.24\%$ for both provinces.

Figures 5.12 and 5.13 show a comparison between the observed mortality excess (solid line) from 3 June 2021 to 26 August 2021, and the estimated COVID-19 deceased population computed with the MSP data (dashed line), RC data (dotted line), and with the robust estimator (dash-dotted line) for Guayas and Pichincha, respectively. In both cases, we observe that the robust estimator fits better the observations.

Moreover, to evaluate the performance of the estimated deceased population with each approach, we compare the relative error between the observed excess of mortality attributed to COVID-19 (m^{obs}) and the estimated deceased population with the

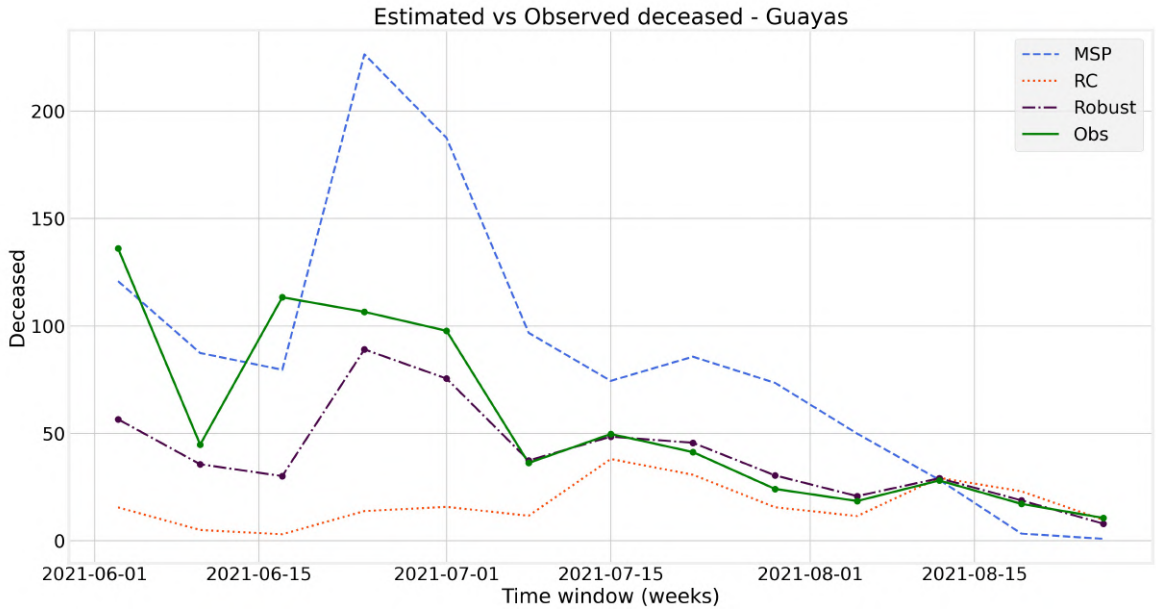

Figure 5.12: Validation - Estimated vs Observed deceased population: Comparison of the deceased population estimated with MSP and RC data, its weighted average, and the real observed mortality excess. Guayas, 3 June 2021 - 26 August 2021.

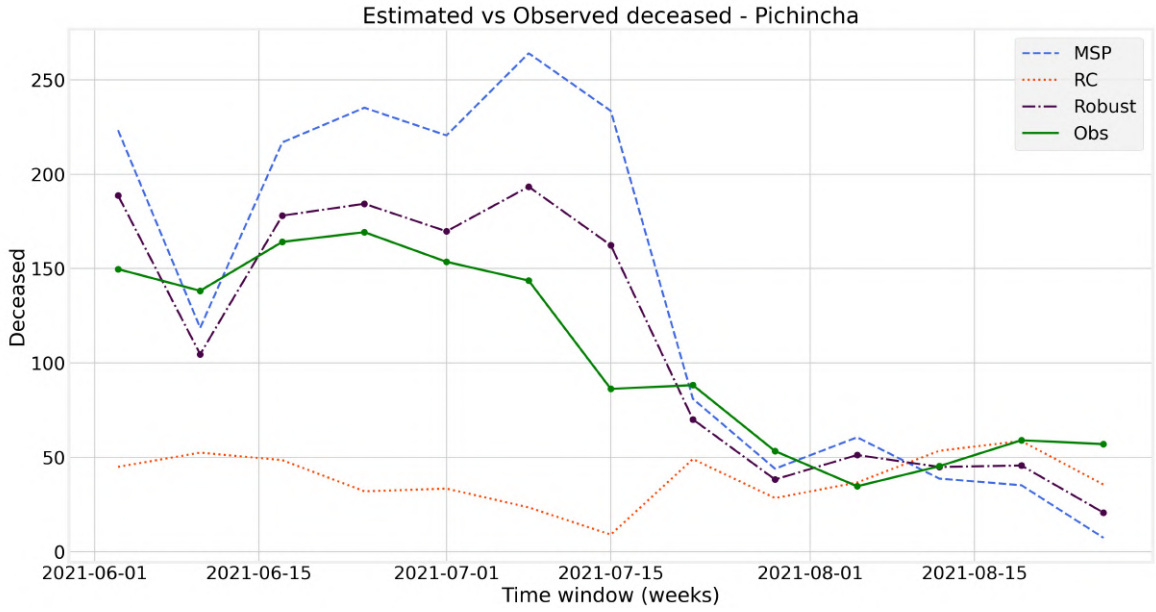

Figure 5.13: Validation - Estimated vs Observed deceased population: Comparison of the deceased population estimated with MSP and RC data, its weighted average, and the real observed mortality excess. Pichincha, 3 June 2021 - 26 August 2021.

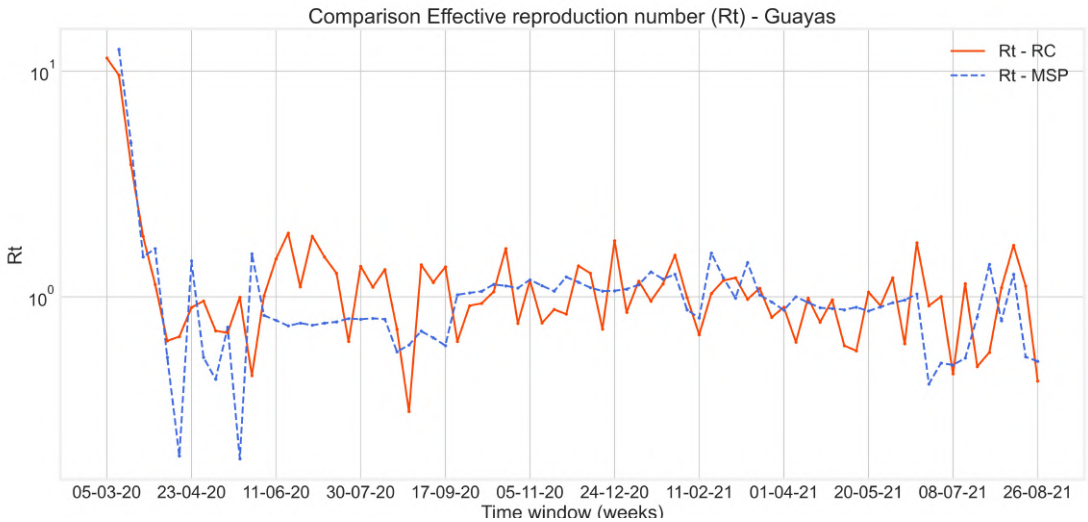

Figure 5.14: Evolution of the effective reproduction number in Guayas calculated with MSP and RC data from 5 March 2020 to 26 August 2021.

$i-$approach (m_i), where $i \in \{\text{MSP}, \text{RC}, \text{Robust}\}$, computed at the validation period $(k = 12$ weeks), i.e.,

$$e_i = \frac{\sum_{k=1}^{12} m_k^i}{\sum_{k=1}^{12} m_k^{obs}}.$$

We summarize the obtained results in Table 5.2. As depicted, the relative errors

	e_{MSP}	e_{RC}	e_{Robust}
Guayas	0.7579	0.8486	0.4789
Pichincha	0.5826	0.7210	0.2868

Table 5.2: Relative errors for the estimated deceased population.

obtained with the weighted average are lower than the ones obtained considering just one data source.

Efffective reproduction number evolution

We use the parameter estimated from both data sources to compute two different R_t series to then compare and combine them. In what follows, $R_t - MSP$ reefers to the effective reproduction number computed with the data obtained from the Public Health Ministry, and $R_t - RC$ the one obtained with the Civil Registry data. Figure 5.14 shows, in semilogarithmic scale, the evolution of the reproduction number for Guayas between 5 March 2020 and 26 August 2021 for $R_t - RC$ in solid line, and between 12 March 2020 and 26 August 2021 for $R_t - MSP$ in dashed line.

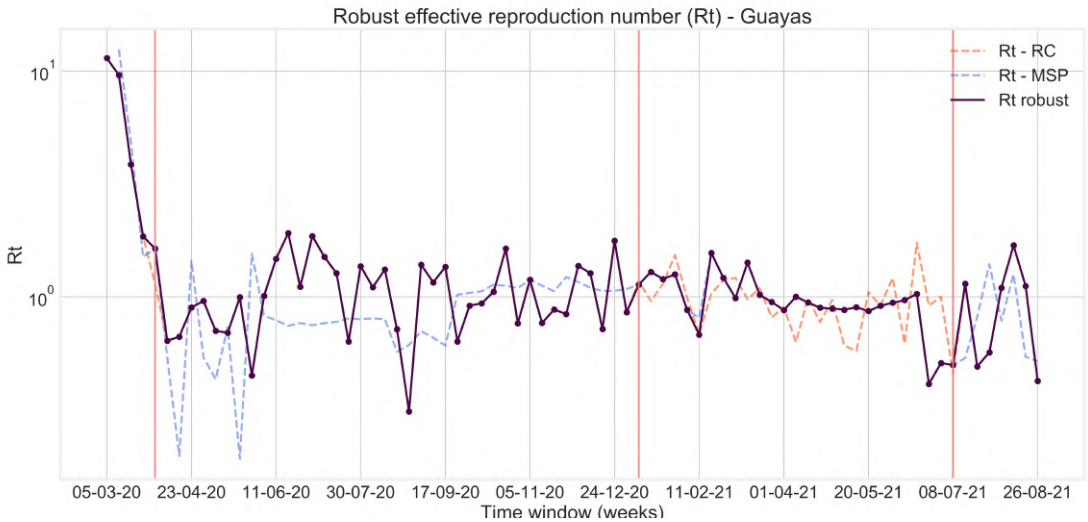

Figure 5.15: Evolution of the Robust R_t for Guayas. The vertical lines indicate when the robust estimator changes from $R_t - MSP$ to $R_t - RC$ and vice versa.

A comparison of the two series reveals that $R_t - MSP$ shows fewer oscillations and remains more stable over time, while $R_t - RC$ exhibits more fluctuations and reaches higher values compared to $R_t - MSP$. In the early months of the pandemic, $R_t - RC$ reached values equal to or higher than two, indicating exponential growth in the number of cases. This finding contrasts with the results obtained from $R_t - MSP$, where from 4 August 2020 and for over a month, values below one were observed, suggesting that the spread of the infection was under control. However, this did not align with the reality in Guayas during that period, as the virus continued to exceed containment measures, leading to exponential growth in the number of cases.

The discrepancies observed in both series highlight the importance of obtaining a unified, effective reproduction number, R_t that accurately reflects the true evolution of the pandemic in Guayas. To achieve this, we use the testing capacity indicator as a criterion for selection. If the testing capacity indicator falls below 1, it suggests that the results derived from the Health Ministry data may not be as reliable. In such cases, we opt for the effective reproduction number obtained from the Civil Registry data, $R_t - RC$. Conversely, if the PCR testing capacity indicator exceeds one, it indicates the credibility of the value of $R_t - MSP$, and thus we choose it as the preferred option. By applying this approach on a weekly basis, we obtain the evolution of a robust effective reproduction number for Guayas, as depicted in Figure 5.15.

In Guayas' case, $R_t - Robust$ exhibits changes in its behavior, shifting between $R_t - MSP$ and $R_t - RC$ on three specific dates: April 2, 2020, January 7, 2021, and July 8, 2021. We depict them with vertical red lines in Figure 5.15. In the case of Pichincha, Figure 5.16 shows the evolution of the reproduction number computed

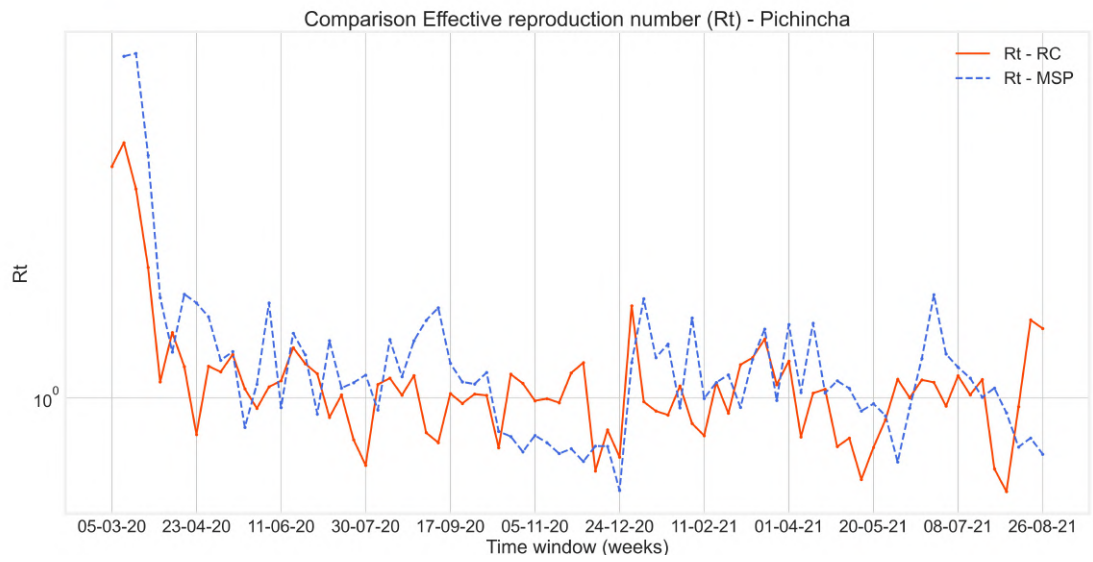

Figure 5.16: Evolution of the effective reproduction number in Pichincha computed with MSP and RC data from 5 March 2020 to 26 August 2021

with MSP and RC data. Different from Guayas' series, for Pichincha, in most of the cases, $R_t - MPS$ exhibits higher values compared with $R_t - RC$. Following the same procedure to combine the reproduction numbers taking into account both data sources, we aim to derive a comprehensive and accurate estimate of the effective reproduction number that captures the true dynamics of the pandemic in Pichincha. Figure 5.17 shows the result of this combination.

In this case, the robust R_t experiences a change in behavior on a single date. From the beginning of the study until June 25, 2020, the robust estimator is based just on $R_t - RC$ values, which is expected considering the low average PCR tests conducted during the pandemic outbreak. However, after this date, there has been a significant increase in the number of PCR tests. Consequently, from late June 2020 until the end of the study, the robust R_t is determined exclusively by $R_t - MSP$ values.

Remarks of the chapter

As final remarks on this chapter, we would like to comment on what follows:

- We present a robust methodology to calculate the evolution of the documented infected population in Pichincha and Guayas. Our approach is based on the optimal estimation of the parameters of the SARS-CoV-2 propagation model, accounting for uncertainty by using a variational data assimilation approach. Then, we solved the stochastic SEIR model with the computed parameters. Ad-

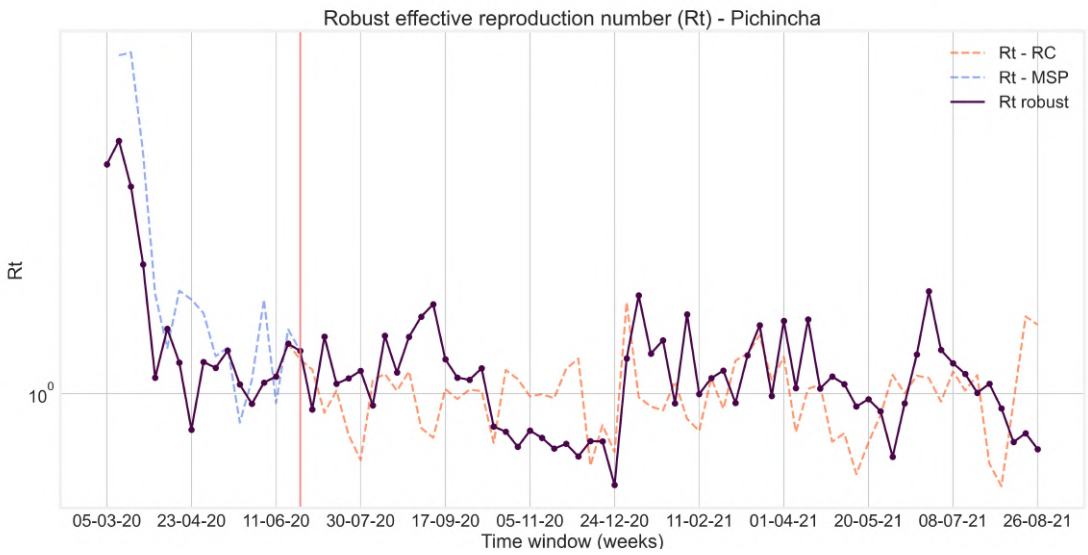

Figure 5.17: Evolution of the Robust R_t for Pichincha. The vertical line indicates the date when the robust estimator changes from $R_t - RC$ to $R_t - MSP$.

ditionally, we used two data sources to address the significant data uncertainty in the Ecuadorian context; as a result, we obtained two sets of solution vectors. The robust solution is computed as their weighted average.

- We consider that around one-third of cases were unreported. This value was taken as an average of the values presented in the extensive COVID-19 literature, available at the time of our study. While we acknowledge that adopting alternative, potentially more region-specific parameterizations for the reporting rate (as the ones showed in in [10]) could further refine the results of this study, a comprehensive investigation, including a full re-run and evaluation of the data assimilation system, would be required to quantify this impact. Such a detailed analysis is an important direction for future work.

- The number of PCR tests conducted in each province played a crucial role in determining the reliability of the solution variables obtained with both data sources. In Pichincha, where more PCR tests were conducted, greater weight was given to the data from the Public Health Ministry. Conversely, in Guayas, where testing capacity often fell below a critical threshold, the data from the Civil Registry was more reliable, and its contribution was greater on average.

- A comparative analysis was conducted between Pichincha and Guayas, which experienced different pandemic situations, particularly during the pandemic onset. To explain these differences, we explore various socioeconomic factors, revealing significant disparities between the studied provinces, such as notably higher

overcrowding rates in Guayas compared to Pichincha, as well as the different healthcare establishment types.

- This tailored approach provided a more accurate representation of the pandemic's evolution in each region and could be adapted for other Ecuadorian provinces with similar data availability. However, this analysis depends on the accuracy of the forecast of expected deaths, which could be biased if another extraordinary event affected mortality data from previous years. Additionally, incorporating different data sources, such as hospital mortality data, could further enhance the analysis.

- Our approach's main limitation is the assumption of no mobility between provinces. Our analysis will be more precise if we consider the spatial movement of COVID-19. However, mobility data was not available. Nevertheless, the isolated SEIR model produces accurate results since mobility between provinces was prohibited, at least during the first months of the pandemic in Ecuador. Likewise, it would be ideal to distinguish the excess mortality directly attributed to SARS-CoV-2 infection from that caused by non-related factors to understand the true impact of the pandemic. Unfortunately, there is no available data to make such a distinction. Nonetheless, by working with all-causes excess mortality, we can obtain a more reliable and comprehensive picture of the COVID-19 pandemic in Ecuador compared to using the official statistics from the Public Health Ministry.

- A significant strength of the methods developed in this study is their posterior combination, which results in robust and reliable outcomes. This robustness is achieved by considering the diversity of data sources. However, one of the data sources requires several weeks to be consolidated by the official Ecuadorian entities. As a result, we cannot create an online version of the robust result.

Conclusions and outlook

This thesis explores variational data assimilation from both theoretical and practical perspectives, addressing key challenges and providing contributions to each one. In what follows, we summarize the main findings of the research and discuss their broader implications while highlighting opportunities for future work.

Building on the theoretical results developed in Chapters 3 and 4, we conclude that *maximal parabolic regularity* provides a comprehensive framework for addressing variational data assimilation problems in infinite-dimensional settings. This approach suits the inherent challenges posed by pointwise-in-space observations and low-regularity initial conditions that, in addition to being constitutive elements of the problem, must hold simultaneously. Specifically, we addressed $4D$-VAR problems subject to linear and semilinear parabolic PDEs. Unlike previous related contributions that focus on distributed or boundary control, our work centers on controlling the initial condition.

The first main result of the theoretical part is the proof of the well-posedness of the parabolic linear state equation under the framework described above. We achieved the desired regularity for the state variable without imposing stronger assumptions on the initial condition, provided that the operator involved in the constraint satisfies the maximal parabolic regularity condition. In the context of the $4D$-VAR problem, imposing additional regularity on the initial condition to ensure continuity-in-space of the state variable is not desirable, as it would imply changing the natural L^2-norm framework of the data assimilation cost function. A key element in our analysis is the application of embedding results for real and complex interpolation spaces, which enable the transition to the target spaces: $L^\beta(\Omega)$ for the initial condition, with $\beta \in \left]d, \frac{2d}{d-2}\right[$ and $d = 2, 3$, standing for the problems dimension, and $L^{r'}(I; C(\bar{\Omega}))$ with $r' > 2$ for the state variable. We recall that before applying these embedding results, the maximal parabolic regularity of the operator allowed us to obtain a state variable in $\mathbb{W}_0^r$, given that the initial condition belongs to $(W^{-1,\beta}(\Omega), W_0^{1,\beta}(\Omega))_{1-\frac{1}{r},r}$.

It is important to emphasize that the pointwise nature of the observations (in space) introduces additional complexity, as it results in an adjoint equation with regular Borel measures on its right-hand side. As with the analysis of the state equation, we need to prove the well-posedness of the adjoint equation in appropriate function spaces. The

latter can be challenging, particularly due to the low regularity of the right-hand side. In the linear case, this problem can be addressed by using the fact that the maximal parabolic regularity of the operator A implies the maximal parabolic regularity of A^*.

The analysis of the semilinear $4D$-VAR problem is more complex. However, the regularity results obtained for the linear case provide a groundwork for achieving the same regularity in the semilinear setting. Addressing the well-posedness of the semilinear parabolic state equation requires first using classical existence results of weak and mild solutions. The desired regularity is then enhanced through a bootstrapping argument jointly with the regularity framework developed for the linear case. Using the same methodology, we establish the well-posedness of both the linearized and non-homogeneous linearized equations within the required function spaces.

Additionally, we observe that while the linearized equation for our specific problem has a zero right-hand side, the existence result for the non-homogeneous linearized equation is crucial to establish the maximal parabolic regularity of the non-autonomous operator $A + \mathbf{g}'(y(\cdot))$. This result is fundamental for proving the well-posedness of the adjoint equation in the appropriate function spaces. It is important to highlight that, unlike the autonomous case, where the maximal parabolic regularity of an operator directly extends to its adjoint (in the corresponding spaces), there is no analogous general result for non-autonomous operators. Consequently, in the non-autonomous case, each adjoint problem must be addressed through a detailed analysis of the equation itself. Conducting this analysis for our specific problem represents one of the main contributions of this thesis.

Our findings contribute to the mathematical literature on data assimilation by extending the analysis of $4D$-VAR problems to low-regularity spaces without compromising the natural framework of the problem. While second-order optimality conditions are beyond the scope of this manuscript, the results presented here have laid a strong foundation supporting their successful derivation aimed at fully characterizing optimal solutions in the semilinear case. Additionally, our work opens avenues for further exploration, including extending these results to nonlinear systems with more complex boundary conditions.

In the application problem addressed in Chapter 5, we employed variational data assimilation to model the evolution of the COVID-19 pandemic in Ecuador. Based on the work developed in this chapter, we conclude that variational data assimilation methods are particularly well-suited for addressing initial condition and parameter estimation problems when uncertainty is an inherent aspect of the system.

We developed a methodological framework consisting of several steps. The first one is choosing an adequate propagation model that captures the dynamics of virus propagation. We chose the SEIR (Susceptible-Exposed-Infectious-Recovered) compart-

mental model. Then, we used variational data assimilation to estimate the initial conditions and model parameters. The variational framework used in this study involves defining a cost functional that quantifies the discrepancy between the observed data and the model outputs, taking into account the data uncertainty through the error covariance matrices that must be built according to the data reliability, to then optimize this cost functional to find the best-fit parameters. Our approach integrated multiple data sources, including official COVID-19 statistics and excess mortality estimates, to mitigate the biases inherent in relying on a single dataset. Furthermore, a multimodel ensemble forecasting strategy was employed to combine the outputs from different data sources. By assigning greater weight to more reliable data, this approach provided a more comprehensive understanding of the pandemic's progression, particularly in the provinces of Pichincha and Guayas. The comparative analysis between these two provinces highlighted how geographical and demographic factors influence the spread of the virus, offering valuable insights for public health strategies.

Bibliography

[1] Adams & Fournier, *Sobolev Spaces*, Pure & Applied Mathematics series, Elsevier, 2003 (cited on pages: 43, 44, 46).

[2] Agoshkov & Ipatova, Solvability of the observation data assimilation problem in the three-dimensional model of ocean dynamics, *Differential Equations* 43 (2007), 1088–1100 (cited on page: 2).

[3] Alekseev, Tikhomirov & Fomin, *Optimal Control*, Springer Science & Business Media, 1987 (cited on pages: 109–112).

[4] Allen, A primer on stochastic epidemic models: Formulation, numerical simulation, and analysis, *Infectious Disease Modelling* 2 (2017), 128–142 (cited on page: 51).

[5] Amann, *Linear and Quasilinear Parabolic Problems: Volume I: Abstract Linear Theory*, Birkhäuser, Basel, 1995 (cited on pages: 45, 46, 48, 50).

[6] Amann, Linear parabolic problems involving measures, *Rev. R. Acad. Cien. Serie A. Mat.(RACSAM)* 95 (2001), 85–119 (cited on pages: 46, 50).

[7] Amann, Nonautonomous parabolic equations involving measures, *Journal of Mathematical Sciences* 130 (2005), 4780–4802 (cited on pages: 46–49, 89, 96, 98).

[8] Ambrosetti & Prodi, *A Primer of Nonlinear Analysis*, Cambridge University Press, 1995 (cited on page: 80).

[9] Arendt, Chill, Fornaro & Poupaud, Lp-maximal regularity for non-autonomous evolution equations, *Journal of Differential Equations* 237 (2007), 1–26 (cited on pages: 47, 91, 102).

[10] Aronna, Guglielmi & Moschen, Estimate of the rate of unreported COVID-19 cases during the first outbreak in Rio de Janeiro, *Infectious Disease Modelling* 7 (2022), 317–332 (cited on page: 144).

[11] Asch, Bocquet & Nodet, *Data Assimilation: Methods, Algorithms, and Applications*, SIAM, 2016 (cited on pages: 14, 16, 19, 20, 22, 27, 29, 32).

[12] Atkinson & Han, *Theoretical numerical analysis: A functional analysis framework*, Springer, 2007 (cited on page: 89).

[13] Bannister, A review of operational methods of variational and ensemble-variational data assimilation, *Quarterly Journal of the Royal Meteorological Society* 143 (2017), 607–633 (cited on pages: 14, 22).

[14] Bechtel & Egert, Interpolation theory for Sobolev functions with partially vanishing trace on irregular open sets, *Journal of Fourier Analysis and Applications* 25 (2019), 2733–2781 (cited on pages: 61, 64, 68).

[15] Bergh & Löfström, *Interpolation Spaces: An Introduction*, Springer, 1976 (cited on page: 45).

[16] Biegel & Lega, EpiCovDA: A mechanistic COVID-19 forecasting model with data assimilation, *ArXiv* (2021) (cited on page: 7).

[17] Bitsouni, Gialelis & Stratis, A model for the outbreak of COVID-19: Vaccine effectiveness in a case study of Italy, in: *International Scientific Conference (on) Modern Methods, Problems and Applications of Operator Theory and Harmonic Analysis*, Springer, 2020, 91–107 (cited on pages: 5, 105).

[18] Blayo, Bocquet, Cosme & Cugliandolo, *Advanced data assimilation for geosciences: Lecture notes of the LES Houches School of Physics: Special issue, June 2012*, OUP Oxford, 2014 (cited on page: 25).

[19] Bonifacius & Neitzel, Second order optimality conditions for optimal control of quasilinear parabolic equations, *Mathematical Control & Related Fields* 8 (2018), 1–34 (cited on pages: 4, 46, 58, 60, 63).

[20] Brauer, Mathematical epidemiology: Past, present, and future, *Infectious Disease Modelling* 2 (2017), 113–127 (cited on page: 54).

[21] Brezis, *Functional Analysis, Sobolev Spaces and Partial Differential Equations*, Springer Science & Business Media, 2010 (cited on pages: 68, 77, 101).

[22] Brockwell & Davis, *Introduction to time series and forecasting*, Springer, 2002 (cited on page: 126).

[23] Carrassi, Bocquet, Bertino & Evensen, Data assimilation in the geosciences: An overview of methods, issues, and perspectives, *Wiley Interdisciplinary Reviews: Climate Change* 9 (2018), e535 (cited on pages: 14, 15).

[24] Casas, Control of an elliptic problem with pointwise state constraints, *SIAM Journal on Control and Optimization* 24 (1986), 1309–1318 (cited on page: 57).

[25] Casas & Chrysafinos, Analysis and optimal control of some quasilinear parabolic equations, *Math. Control Relat. Fields* 8 (2018), 607–623 (cited on pages: 4, 58).

[26] Casas, Clason & Kunisch, Parabolic control problems in measure spaces with sparse solutions, *SIAM Journal on Control and Optimization* 51 (2013), 28–63 (cited on pages: 58, 60, 63).

[27] Casas, De Los Reyes & Tröltzsch, Sufficient second-order optimality conditions for semilinear control problems with pointwise state constraints, *SIAM Journal on Optimization* 19 (2008), 616–643 (cited on page: 73).

[28] Casas & Tröltzsch, Second order optimality conditions and their role in PDE control, *Jahresbericht der Deutschen Mathematiker-Vereinigung* 117 (2015), 3–44 (cited on page: 4).

[29] Castro & De Los Reyes, A bilevel learning approach for optimal observation placement in variational data assimilation, *Inverse Problems* (2019) (cited on pages: 2, 56, 63).

[30] Castro, De los Reyes, González-Andrade & Merino, Estimación de Parámetros para un Modelo del SARS-CoV-2 en Ecuador en Presencia de Incertidumbre, *Revista Politécnica* 47 (2021), 7–16 (cited on page: 107).

[31] Castro, De los Reyes & Neitzel, Analysis of Four-dimensional Variational Data Assimilation Problems in Low Regularity Spaces, *arXiv preprint 2303.00847v2* (2025) (cited on pages: 102, 103).

[32] Cevallos-Valdiviezo, Vergara-Montesdeoca & Zambrano-Zambrano, Measuring the impact of the COVID-19 outbreak in Ecuador using preliminary estimates of excess mortality, March 17–October 22, 2020, *International Journal of Infectious Diseases* 104 (2021), 297–299 (cited on pages: 6, 133).

[33] Chowell, Fitting dynamic models to epidemic outbreaks with quantified uncertainty: A primer for parameter uncertainty, identifiability, and forecasts, *Infectious Disease Modelling* 2 (2017), 379–398 (cited on page: 55).

[34] Chowell et al., The basic reproductive number of Ebola and the effects of public health measures: the cases of Congo and Uganda, *Journal of theoretical biology* 229 (2004), 119–126 (cited on page: 55).

[35] Clarke, *Functional analysis, calculus of variations and optimal control*, Springer, 2013 (cited on page: 114).

[36] Cuéllar et al., Excess deaths reveal unequal impact of COVID-19 in Ecuador, *BMJ Global Health* 6 (2021), e006446 (cited on page: 6).

[37] Daza-Torres, Capistrán, Capella & Christen, Bayesian sequential data assimilation for COVID-19 forecasting, *Epidemics* 39 (2022), 100564 (cited on page: 7).

[38] De Falco, Della Cioppa, Scafuri & Tarantino, Differential evolution to estimate the parameters of a SEIAR model with dynamic social distancing: the case of COVID-19 in Italy, in: *Data Science for COVID-19*, Elsevier, 2021, 75–90 (cited on pages: 5, 105).

[39] De los Reyes, *Numerical PDE-constrained optimization*, Springer, 2015 (cited on pages: 112, 114, 120, 129).

[40] Denk, An introduction to maximal regularity for parabolic evolution equations, in: *International Workshop on Nonlinear Partial Differential Equations for Future Applications*, Springer, 2017, 1–70 (cited on pages: 41, 45, 47).

[41] Diekmann, Heesterbeek & Metz, On the definition and the computation of the basic reproduction ratio R0 in models for infectious diseases in heterogeneous populations, *Journal of mathematical biology* 28 (1990), 365–382 (cited on page: 54).

[42] Diestel & Uhl, The Radon-Nikodym theorem for Banach space valued measures, *The Rocky Mountain Journal of Mathematics* 6 (1976), 1–46 (cited on page: 13).

[43] Diestel & Uhl, *Vector Measures*, American Mathematical Society, 1977 (cited on page: 68).

[44] Dirección General del Registro Civil, Identificación y Cedulación, Cifras Defunciones, 2021, (visited on 07/09/2021) (cited on page: 122).

[45] Disser, Meyries & Rehberg, A unified framework for parabolic equations with mixed boundary conditions and diffusion on interfaces, *Journal of Mathematical Analysis and Applications* 430 (2015), 1102–1123 (cited on pages: 4, 46).

[46] Disser, Ter Elst & Rehberg, Hölder estimates for parabolic operators on domains with rough boundary, *Annali della Scuola Normale Superiore di Pisa. Classe di scienze* 17 (2017), 65–79 (cited on pages: 4, 46).

[47] Disser, Ter Elst & Rehberg, On maximal parabolic regularity for non-autonomous parabolic operators, *Journal of Differential Equations* 262 (2017), 2039–2072 (cited on page: 48).

[48] Dondl & Zeinhofer, $L^p(I, C^\alpha(\Omega))$ Regularity for Diffusion Equations with Non-smooth Data, *Results in Mathematics* 78 (2023), 142 (cited on pages: 58, 63, 65).

[49] Dore, L^p regularity for abstract differential equations, in: *Functional Analysis and Related Topics, 1991: Proceedings of the International Conference in Memory of Professor Kôsaku Yosida held at RIMS, Kyoto University, Japan, July 29–Aug. 2, 1991*, Springer, 2006, 25–38 (cited on page: 47).

[50] Engbert, Rabe, Kliegl & Reich, Sequential data assimilation of the stochastic SEIR epidemic model for regional COVID-19 dynamics, *Bulletin of mathematical biology* 83 (2021) (cited on page: 7).

[51] Evans, *Partial differential equations*, American Mathematical Society, 2022 (cited on page: 34).

[52] Evensen, Vossepoel & Van Leeuwen, *Data assimilation fundamentals: A unified formulation of the state and parameter estimation problem*, Springer Nature, 2022 (cited on pages: 30, 55).

[53] Evensen et al., An international initiative of predicting the SARS-CoV-2 pandemic using ensemble data assimilation, *Foundations of Data Science* 3 (2021), 413–477 (cited on page: 7).

[54] Evensen, Sequential data assimilation with a nonlinear quasi-geostrophic model using Monte Carlo methods to forecast error statistics, *Journal of Geophysical Research: Oceans* 99 (1994), 10143–10162 (cited on page: 22).

[55] Evensen et al., *Data assimilation: the ensemble Kalman filter*, Springer, 2009 (cited on page: 22).

[56] Fabre, Puel & Zuazua, On the density of the range of the semigroup for semilinear heat equations, in: *Control and optimal design of distributed parameter systems*, Springer, 1995, 73–91 (cited on page: 84).

[57] Fattorini, *Infinite Dimensional Optimization and Control Theory*, Cambridge University Press, 1999 (cited on page: 84).

[58] Fernández-Naranjo et al., Statistical data-driven approach of COVID-19 in Ecuador: R0 and Rt estimation via new method, *Infectious Disease Modelling* 6 (2021), 232–243 (cited on page: 6).

[59] Frias-Martinez, Williamson & Frias-Martinez, An agent-based model of epidemic spread using human mobility and social network information, in: *2011 IEEE Third International Conference on social computing*, IEEE, 2011, 57–64 (cited on page: 52).

[60] Gajewski, Gröger & Zacharias, *Nichtlineare Operatorgleichungen und Operatordifferentialgleichungen*, Akademie-Verlag, Berlin, 1974 (cited on page: 47).

[61] Gallon, Bodies are being left in the streets in an overwhelmed Ecuadorian city, 2020, (visited on 05/24/2022) (cited on page: 131).

[62] El-Ghitany et al., Asymptomatic versus symptomatic SARS-CoV-2 infection: A cross-sectional seroprevalence study, *Tropical Medicine and Health* 50 (2022), 98 (cited on page: 125).

[63] Goldberg, Kampowsky & Tröltzsch, On NEMYTSKIJ Operators in Lp-Spaces of Abstract Functions, *Mathematische Nachrichten* 155 (1992), 127–140 (cited on pages: 75, 78, 80).

[64] Gröger, A $W^{1,p}$-estimate for solutions to mixed boundary value problems for second order elliptic differential equations, *Mathematische Annalen* 283 (1989), 679–687 (cited on page: 60).

[65] Helton & Davis, Latin hypercube sampling and the propagation of uncertainty in analyses of complex systems, *Reliability Engineering & System Safety* 81 (2003), 23–69 (cited on page: 127).

[66] Herzog, Meyer & Stötzner, Existence of solutions of a thermoviscoplastic model and associated optimal control problems, *Nonlinear Analysis: Real World Applications* 35 (2017), 75–101 (cited on pages: 4, 46, 49, 58, 102).

[67] Hömberg, Meyer, Rehberg & Ring, Optimal control for the thermistor problem, *SIAM Journal on Control and Optimization* 48 (2010), 3449–3481 (cited on pages: 96, 102).

[68] Hoppe, Meinlschmidt & Neitzel, Global-in-time solutions for quasilinear parabolic PDEs with mixed boundary conditions in the Bessel dual scale, *arXiv preprint arXiv:2303.04659* (2023) (cited on pages: 4, 58, 60, 63).

[69] Hoppe & Neitzel, Optimal control of quasilinear parabolic PDEs with state-constraints, *SIAM J. Control Optim.* 60 (2022), 330–354 (cited on pages: 4, 58, 63).

[70] Huff, The Radon-Nikodym property for Banach-spaces—a survey of geometric aspects, in: *North-Holland Mathematics Studies*, Elsevier, 1977, 1–13 (cited on page: 13).

[71] Hunter, Mac Namee & Kelleher, A comparison of agent-based models and equation-based models for infectious disease epidemiology (2018) (cited on page: 52).

[72] ICOVID CHILE, Testeo, 2020, (visited on 06/24/2023) (cited on page: 128).

[73] Instituto Nacional de Estadísticas y Censos (INEC), Registro estadístico de recursos y actividades de Salud, 2020 (cited on page: 133).

[74] Instituto Nacional de Estadísticas y Censos (INEC), Encuesta Nacional de Empleo, Desempleo y Subempleo, anual, 2022, (visited on 06/18/2023) (cited on page: 133).

[75] Kalnay, *Atmospheric Modeling, Data Assimilation and Predictability*, Cambridge University Press, 2003 (cited on pages: 14, 15).

[76] Keeling & Rohani, *Modeling infectious diseases in humans and animals*, Princeton University Press, 2011 (cited on pages: 52, 53).

[77] Kelley, *Iterative methods for Optimization*, SIAM, 1999 (cited on pages: 121, 129).

[78] Kermack & McKendrick, A contribution to the mathematical theory of epidemics, *Proceedings of the Royal Society of London. Series A, Containing papers of a mathematical and physical character* 115 (1927), 700–721 (cited on pages: 5, 51).

[79] Korn, Strong Solvability of a Variational Data Assimilation Problem for the Primitive Equations of Large-Scale Atmosphere and Ocean Dynamics, *Journal of Nonlinear Science* 31 (2021), 1–53 (cited on pages: 2, 3).

[80] Krishnamurti et al., Multimodel ensemble forecasts for weather and seasonal climate, *Journal of Climate* 13 (2000), 4196–4216 (cited on pages: 6, 128).

[81] Krumbiegel & Rehberg, Second order sufficient optimality conditions for parabolic optimal control problems with pointwise state constraints, *SIAM Journal on Control and Optimization* 51 (2013), 304–331 (cited on pages: 58–60, 63, 73, 91).

[82] Kung et al., Underestimation of COVID-19 mortality during the pandemic, *ERJ open research* 7 (2021) (cited on pages: 104, 133).

[83] Ladyzhenskaia, Solonnikov & Ural'ceva, *Linear and Quasi-linear Equations of Parabolic Type*, American Mathematical Soc., 1968 (cited on pages: 56, 75, 82, 84, 86, 90, 94).

[84] Le Dimet, Navon & Ştefănescu, Variational data assimilation: Optimization and optimal control, in: *Data Assimilation for Atmospheric, Oceanic and Hydrologic Applications (Vol. III)*, Springer, 2017, 1–53 (cited on page: 2).

[85] Le Dimet & Talagrand, Variational algorithms for analysis and assimilation of meteorological observations: theoretical aspects, *Tellus A: Dynamic Meteorology and Oceanography* 38 (1986), 97–110 (cited on pages: 1, 2, 29).

[86] Li et al., Substantial undocumented infection facilitates the rapid dissemination of novel coronavirus (SARS-CoV-2), *Science* 368 (2020), 489–493 (cited on pages: 5, 6, 105–107).

[87] Lorenzi & Rhandi, *Semigroups of bounded operators and second-order elliptic and parabolic partial differential equations*, CRC Press, 2021 (cited on page: 40).

[88] Lu et al., Estimating the early outbreak cumulative incidence of COVID-19 in the United States: three complementary approaches, *medRxiv* (2020) (cited on page: 104).

[89] Lunardi, *Interpolation theory*, Springer, 2018 (cited on pages: 42, 44, 45).

[90] Lunardi, *Analytic semigroups and optimal regularity in parabolic problems*, Springer Science & Business Media, 2012 (cited on pages: 38–40).

[91] Martinez & Sanz, *The theory of fractional powers of operators*, Elsevier, 2001 (cited on page: 61).

[92] Mata & Dourado, Mathematical modeling applied to epidemics: an overview, *Sao Paulo Journal of Mathematical Sciences* 15 (2021), 1025–1044 (cited on page: 53).

[93] Meinlschmidt, Meyer & Rehberg, Optimal control of the thermistor problem in three spatial dimensions, Part 1: Existence of optimal solutions, *SIAM Journal on Control and Optimization* 55 (2017), 2876–2904 (cited on pages: 4, 46, 58).

[94] Meinlschmidt, Meyer & Rehberg, Optimal control of the thermistor problem in three spatial dimensions, part 2: Optimality conditions, *SIAM Journal on Control and Optimization* 55 (2017), 2368–2392 (cited on pages: 4, 46, 58).

[95] Meinlschmidt & Rehberg, Hölder-estimates for non-autonomous parabolic problems with rough data, *Evolution Equations & Control Theory* 5 (2016), 147 (cited on pages: 4, 46, 58, 63).

[96] Meyer & Susu, Optimal control of nonsmooth, semilinear parabolic equations, *SIAM Journal on Control and Optimization* 55 (2017), 2206–2234 (cited on pages: 4, 46, 58, 59, 84, 86).

[97] MIDAS Coordination Center, MIDAS Online COVID-19 Portal, 2020, (visited on 04/29/2022) (cited on page: 124).

[98] Ministerio de Salud Pública del Ecuador, Informe epidemiológico de COVID-19, Ecuador 2021, December 07, 2021 (2021) (cited on page: 125).

[99] Ministerio Salud Pública Ecuador, Informe de Situación COVID-19 Ecuador, 2020, (visited on 06/10/2023) (cited on page: 131).

[100] Nadler et al., An epidemiological modelling approach for COVID-19 via data assimilation, *European Journal of Epidemiology* 35 (2020), 749–761 (cited on page: 7).

[101] Nikolai, Meyer, Kremsner & Velavan, Asymptomatic SARS Coronavirus 2 infection: Invisible yet invincible, *International Journal of Infectious Diseases* 100 (2020), 112–116 (cited on page: 125).

[102] Pazy, *Semigroups of Linear Operators and Applications to Partial Differential Equations*, Springer, 1983 (cited on pages: 34, 47, 51, 84).

[103] Peirlinck et al., Visualizing the invisible: The effect of asymptomatic transmission on the outbreak dynamics of COVID-19, *Computer Methods in Applied Mechanics and Engineering* 372 (2020), 113410 (cited on pages: 5, 105).

[104] Rao, Fournais, Moller & Stetkaer, *Complex analysis: An invitation. A Concise Introduction to Complex Function Theory*, World Scientific Publishing Company, 2015 (cited on pages: 38, 39).

[105] Raymond & Tröltzsch, Second order sufficient optimality conditions for nonlinear parabolic control problems with state constraints, *Discrete & Continuous Dynamical Systems-A* 6 (2000), 431 (cited on page: 73).

[106] Raymond & Zidani, Hamiltonian Pontryagin's principles for control problems governed by semilinear parabolic equations, *Applied Mathematics and Optimization* 39 (1999), 143–177 (cited on page: 4).

[107] Raymond & Zidani, Hamiltonian Pontryagin's principles for control problems governed by semilinear parabolic equations, *Applied Mathematics and Optimization* 39 (1999), 143–177 (cited on page: 57).

[108] Renardy & Rogers, *An introduction to partial differential equations*, Springer Science & Business Media, 2006 (cited on page: 37).

[109] Rhodes & Hollingsworth, Variational data assimilation with epidemic models, *Journal of theoretical biology* 258 (2009), 591–602 (cited on page: 55).

[110] Roubíček, *Nonlinear Partial Differential Equations with Applications*, Birkhäuser, 2013 (cited on pages: 42, 101).

[111] Rozante, Moreira, Godoy & Fernandes, Multi-model ensemble: technique and validation, *Geoscientific Model Development* 7 (2014), 2333–2343 (cited on page: 6).

[112] Sah et al., Asymptomatic SARS-CoV-2 infection: A systematic review and meta-analysis, *Proceedings of the National Academy of Sciences* 118 (2021), e2109229118 (cited on page: 125).

[113] Shutyaev, Solvability of the data assimilation problem in the scale of Hilbert spaces for quasilinear singularly perturbed evolutionary problems, *Russ. J. Numer. Anal. Math. Model* 12 (1997) (cited on pages: 2, 3).

[114] Simon, Compact sets in the space $L^p(0,T;B)$, *Annali di Matematica pura ed applicata* 146 (1986), 65–96 (cited on page: 87).

[115] Skaggs & Kabala, Recovering the release history of a groundwater contaminant, *Water Resources Research* 30 (1994), 71–79 (cited on page: 57).

[116] Sun & Crook, Dynamical and microphysical retrieval from Doppler radar observations using a cloud model and its adjoint. Part I: Model development and simulated data experiments, *Journal of the Atmospheric Sciences* 54 (1997), 1642–1661 (cited on page: 57).

[117] Triebel, *Interpolation Theory, Function Spaces, Differential Operators*, Nortn Holland, Amsterdam, 1978 (cited on pages: 42–46, 64).

[118] Tröltzsch, *Optimal Control of Partial Differential Equations*, American Mathematical Soc., 2010 (cited on pages: 4, 66, 75, 77–79, 82, 84, 89, 91, 95).

[119] Warner, *Numerical Weather and Climate Prediction*, Cambridge University Press, 2010 (cited on page: 14).

[120] Yang, Gui & Xiong, Comparison of clinical characteristics of patients with asymptomatic vs symptomatic coronavirus disease 2019 in Wuhan, China, *JAMA network open* 3 (2020), e2010182–e2010182 (cited on page: 125).

[121] Yu et al., Characteristics of asymptomatic COVID-19 infection and progression: a multicenter, retrospective study, *Virulence* 11 (2020), 1006–1014 (cited on page: 125).

[122] Zeidler, *Nonlinear functional analysis and its applications: II/A: linear monotone operators*, Springer Science & Business Media, 1990 (cited on page: 89).

[123] Zemkoho, A basic time series forecasting course with Python, in: *Operations Research Forum*, Springer, 2022 (cited on page: 123).

[124] Zibell, Coronavirus en Ecuador: el drama de Guayaquil, que tiene más muertos por covid-19 que países enteros y lucha a contrarreloj para darles un entierro digno, 2020, (visited on 06/10/2023) (cited on page: 131).

[125] Zowe & Kurcyusz, Regularity and stability for the mathematical programming problem in Banach spaces, *Applied Mathematics and Optimization* 5 (1979), 49–62 (cited on pages: 4, 67, 69, 99).